REPORT DOCUMENTATION PAGE

Form Approved
OMB No. 0704-0188

1. AGENCY USE ONLY *(Leave blank)*	2. REPORT DATE	3. REPORT TYPE AND DATES COVERED
	23.Aug.00	DISSERTATION

4. TITLE AND SUBTITLE
DIGITAL CONTROLLER DESIGN FOR ALIASED SAMPLED-DATA SYSTEMS

5. FUNDING NUMBERS

6. AUTHOR(S)
MAJ HANSEN DAVID S

7. PERFORMING ORGANIZATION NAME(S) AND ADDRESS(ES)
BRIGHAM YOUNG UNIVERSITY

8. PERFORMING ORGANIZATION REPORT NUMBER
CY00365

9. SPONSORING/MONITORING AGENCY NAME(S) AND ADDRESS(ES)
THE DEPARTMENT OF THE AIR FORCE
AFIT/CIA, BLDG 125
2950 P STREET
WPAFB OH 45433

10. SPONSORING/MONITORING AGENCY REPORT NUMBER

11. SUPPLEMENTARY NOTES

12a. DISTRIBUTION AVAILABILITY STATEMENT
Unlimited distribution
In Accordance With AFI 35-205/AFIT Sup 1

12b. DISTRIBUTION CODE

13. ABSTRACT *(Maximum 200 words)*

DISTRIBUTION STATEMENT A
Approved for Public Release
Distribution Unlimited

20000921 065

14. SUBJECT TERMS	15. NUMBER OF PAGES
	272
	16. PRICE CODE

17. SECURITY CLASSIFICATION OF REPORT	18. SECURITY CLASSIFICATION OF THIS PAGE	19. SECURITY CLASSIFICATION OF ABSTRACT	20. LIMITATION OF ABSTRACT

DIGITAL CONTROLLER DESIGN FOR ALIASED SAMPLED-DATA SYSTEMS

by

David S. Hansen

A dissertation submitted to the faculty of

Brigham Young University

in partial fulfillment of the requirements for the degree of

Doctor of Philosophy

Department of Mechanical Engineering

Brigham Young University

August 2000

ABSTRACT

DIGITAL CONTROLLER DESIGN FOR

ALIASED SAMPLED-DATA SYSTEMS

David S. Hansen

Department of Mechanical Engineering

Doctor of Philosophy

Many of the dynamic systems in use today consist of an analog plant controlled by a digital controller. Design of these digital controllers assumes a system with no aliasing, and most, if not all, current design methods employ means to assure no aliasing is present. The drawbacks to these methods are unobservable and/or uncontrollable high frequency modes.

This research effort provides a means to design a digital controller for systems with aliased modes. A model is developed in which both continuous and discrete portions of a sampled-data system are included. From this model, the unique digital controller function that will excite the analog plant is found. Moreover, as a result of the discrete-to-continuous manner of the model, the sample period allowing aliasing becomes a

design parameter. Sampling frequencies providing improved response are determined and responses at these frequencies are explored.

With aliasing allowed in the discrete-to-continuous system, stability for some systems is actually introduced and improved over the same systems in which aliasing is not allowed, as evidenced by increased gain margins and improved time domain responses.

A deadbeat response controller is designed using proportional-integral control by placing one pole of a second-order system at the optimal position of the origin in the z-plane. The response of this controller is such that the desired position is obtained within a single sample period. Robustness of this controller is examined with favorable results.

In a fourth-order system in which one mode is aliased, control of the aliased mode is accomplished simply by selecting the sample rate correctly. The resulting effects of the aliased mode are negligible, and design of the controller for the non-aliased mode follows traditional theory.

Disturbance rejection for both the second-order and fourth-order systems was examined and found to be excellent for disturbances with frequencies below that of the sampler. These systems were unable to follow input or reject disturbances with frequencies greater than that of the sampler. Experiments on electric circuits matched the predicted model.

BRIGHAM YOUNG UNIVERSITY

GRADUATE COMMITTEE APPROVAL

of a dissertation submitted by

David S. Hansen

This dissertation has been read by each member of the following graduate committee and by majority vote has been found to be satisfactory.

6/2/00	
Date	Craig C. Smith, Chair
6/2/00	
Date	Randal W. Beard
6/2/00	
Date	Mark S. Evans
6/2/2000	
Date	Timothy W. McLain
6/5/2000	
Date	Scott D. Sommerfeldt

BRIGHAM YOUNG UNIVERSITY

As chair of the candidate's graduate committee, I have read the dissertation of David S. Hansen in its final form and have found that (1) its format, citations, and bibliographical style are consistent and acceptable and fulfill university and department style requirements; (2) its illustrative materials including figures, tables, and charts are in place; and (3) the final manuscript is satisfactory to the graduate committee and is ready for submission to the university library.

6/5/2000
Date

Craig C. Smith
Chair, Graduate Committee

Accepted for the Department

Craig C. Smith
Graduate Coordinator

Accepted for the College

Douglas M. Chabries
Dean, College of Engineering and Technology

ACKNOWLEDGMENTS

First and foremost I wish to express my gratitude to my Heavenly Father. It is His blessings that brought me here, that helped with inspiration, that sustained me in times of trial and, of course, happiness. Truly, the glory of God is intelligence, and this effort has taught me how little I know, and how omniscient He truly is.

Next, to Dr. Smith: a man whom I've grown to greatly admire. Thank you for you many hours of patient instruction, your special and significant insights to this research effort, your professionalism, and most of all for your true friendship.

To the professionals of my dissertation committee: Dr. McLain, Dr. Beard, Dr. Evans, and Dr. Sommerfeldt—thanks for added knowledge, different tacks of thought, needed encouragement, and the constant prodding to do better. And thanks for not failing me because of my jokes…

To office friends and colleagues: Chris Bailey, Alan Raines, Ben and Alisa Henrie, Tim Hakala, and Jason Dahl. Thanks for the chance to vent frustrations, for friendship, for encouragement, and for helping me beyond my abilities. Jason and Tim—I couldn't have done it without you.

To the folks at the Air Force Academy: Thanks for trusting in me enough to send me. I guess now I'm coming back and you're the ones that are stuck with me.

To my extended family, I wish to express gratitude for all you've done. Mom and Dad, I wouldn't be here if you hadn't taught me well. You've stood behind me in trials and successes. My success is yours.

Finally and most importantly, thanks go to my family. Kids, you're the best I could want. Thanks for putting up with the grumpy days. But above all to my eternal mate, Lisa: without you I'm lost in the jungle that is this world. I'm so happy we're forever, for I'll love you that long, and more. You're my best friend. This dissertation is as much yours as it is mine. I dedicate it to you.

TABLE OF CONTENTS

LIST OF TABLES

LIST OF FIGURES

CHAPTER ONE. INTRODUCTION

1.0 BACKGROUND

As computers have become the norm in use for control of analog systems, much research has been conducted into methods of digital control of these systems. Many of the dynamic systems in which control is utilized consist of an analog plant controlled by a digital controller (computer).

Several methods are currently employed to design digital controllers [3]. All these methods, however, assume a system with no aliasing, ignore the continuous response between samples, and ignore the computational delay—each assuming one can sample and compute as fast as is necessary. A brief review of these design methods will follow.

1.1 Current Digital Controller Design

One of the easiest design methods to understand is that of emulation. Emulation involves designing the controller in the continuous (s-plane) domain using traditional root locus or frequency response design methods, and then mapping the controller design from the continuous domain into the discrete (z-plane) domain. Several methods for the mapping have been developed. Included in these methods are numerical integration methods, the zero-pole matching method, and hold equivalent methods [3:187-208, 215-222]].

Another method of designing digital controllers involves direct design by the root locus methods in the z-plane. Performance specifications familiar in the s-plane are translated into the z-plane, and the mechanics of root locus plotting introduced by Evans remain the same. This method requires a complete discretization of the model prior to any design [3:222-234].

Design in the digital domain is also accomplished using frequency response function methods. However, the effects of the sampling and zero-order hold make a computer necessary for the design. The simple hand-plotting techniques for continuous systems no longer hold true in the discrete domain. Interpretations of phase and gain margins are also more difficult, causing the need for more analysis [3:234-264].

Both emulation and direct digital domain design can be used in state space design, as well. Additionally, other methods such as LQR optimal control, Kalman filters, and Luenberger observers are powerful tools in the design of digital controllers using state space design methods [3:270-351].

As mentioned above, all these digital design methods make assumptions as to the necessary sample rate, as well as the time between sampling, computation, and control output. Sample rates of 20 to 30 times the system natural frequencies must be employed in most cases. Moreover, computation time is generally assumed to be as fast as necessary in order for it to be neglected in the design of the controller. Physical systems, however, may make such assumptions invalid.

1.2 ALIASING

In sampled-data systems, where the plant is continuous and the controller is digital, a digitization or sampling of the analog plant must be performed. One well-observed effect of sampling analog data is the ambiguity that occurs when a signal of high frequency is sampled at a low frequency. Shannon's well-know sampling theorem [1] states that any signal whose frequency components are greater than one-half the sampling frequency, known as the folding or Nyquist frequency [2], will be *aliased* to a lower frequency.

These aliased frequencies will become indistinguishable from the system's response in the lower frequency range.

Aliasing causes errors in the characterization of the system or plant. These errors can be severe if the sampled signal contains enough high-frequency components. Because of the sampling operation, the signal's high frequency components will not be correctly identified. In fact, the high-frequency content will incorrectly appear as lower-frequency components in the sampled signal. A simple example will demonstrate this:

Suppose one wishes to sample a 10 Hertz signal. If samples are taken every 0.0833 seconds (f_s = 12 Hz) the sampled signal will appear as a sine wave of only 2 Hertz, as shown in figure 2.2. The 10 Hertz signal has been aliased to a 2 Hertz signal by the sampling operation. This is an example of aliasing of a pure sinusoidal signal. Aliasing of a pure sinusoid can also be thought of as a "folding" operation. The explanation of this follows.

Figliola and Beasley [18:273] define the Nyquist frequency as

$$f_N = \frac{f_s}{2} \quad . \qquad [1.1]$$

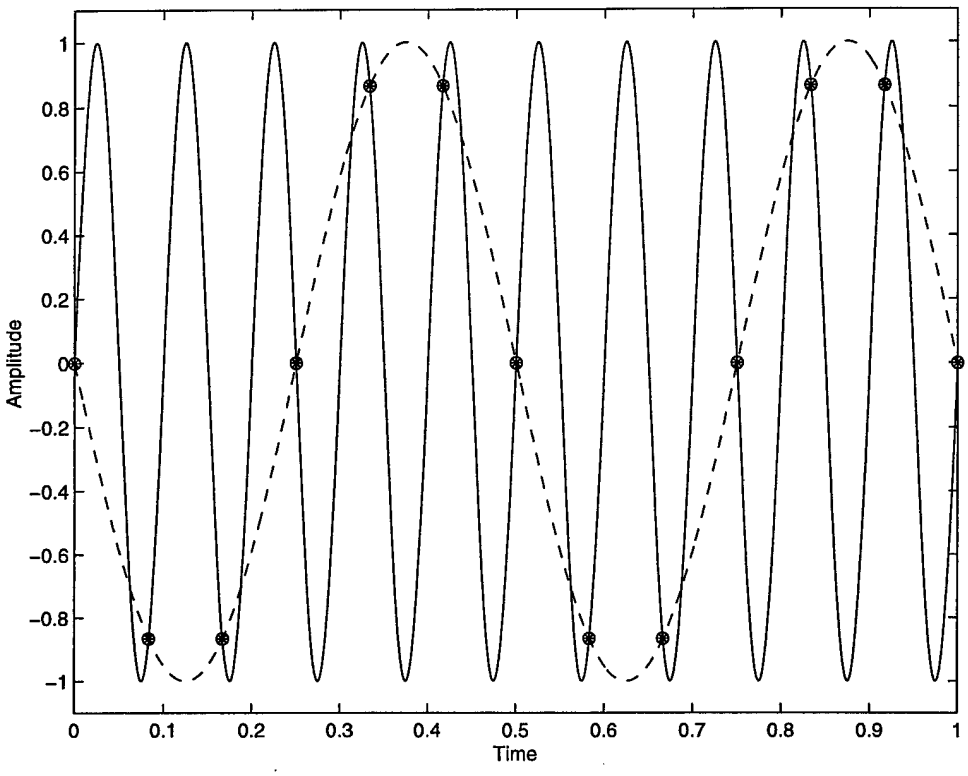

Figure 1.1 Aliasing of 10 Hz Signal

Any content in the signal above the Nyquist frequency will be aliased and will falsely appear as frequency components of the signal below the Nyquist frequency. The Nyquist frequency is also known as the folding frequency since, in the frequency domain, aliased frequencies can be thought of as having been folded back at that frequency and superimposed on the signal at lower frequencies. This is illustrated for the simple example given above in figure 1.2.

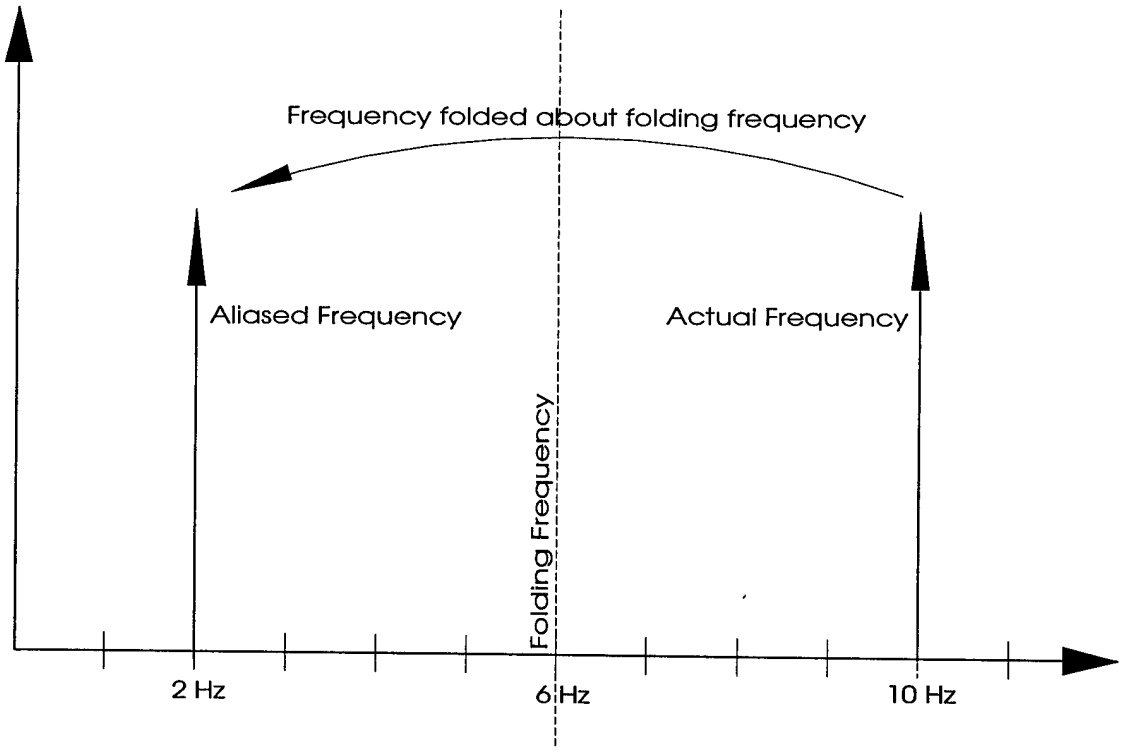

Figure 1.2 Aliasing Shown as Folding in Frequency Domain

Recall the sampling frequency was 12 Hz, so the folding frequency is 6 Hz. The frequency band from dc (f = 0) to the folding frequency ($f = f_s/2$) is known as the *primary band.* Any frequency components above the Nyquist frequency will fold as many times as necessary to be within the primary band. Thornhill & Smith [19:7.7-7.11] and Figliola & Beasley [18:273-275] offer excellent examples of this folding technique and its aid in visualizing aliasing.

Likewise, aliasing of signals not purely sinusoidal can be thought of as this same folding operation. The component of the signal found above the folding frequency is folded back

to its corresponding frequency within the primary band and added to the components of frequency already present there. Based on the band from which the frequency component is folded, a complex conjugation might also be necessary. This folding operation is linear, and the aliased FRF, given the original FRF is linear, remains linear. Durney offers an excellent analysis of this operation in his thesis [6:15-18].

One current practice used to avoid aliasing is to precede the sampling operation with low pass filters. This will remove the spectral content above the Nyquist frequency, rendering these modes unobservable. Another practice is to smooth the output of the controller such that the high frequency components are not excited. One drawback to these methods, however, is that these modes thus become uncontrollable.

One may also avoid aliasing errors by sampling at a rate greater than twice the largest frequency content present in the system response. This, however, requires a greater knowledge of the system to be controlled, and may require expensive hardware to sample at the required frequencies. In other cases it may simply be impossible or undesirable.

Kuo [4:21] states that a signal can be completely defined, even if sampled at less than twice the folding frequency, if the derivatives of the signal are also sampled at the sampling instants. The downside to this is an increase in the number of sensors needed to characterize the signal, or the difficulty associated with determining the derivatives.

In physical systems there may be a need to control modes that would be rendered either unobservable or uncontrollable by filters. Cost limitations always impact the number of sensors or the speed of those sensors or the hardware necessary to interpret their output. Aliasing at times is unavoidable and may even be the desirable alternative for some of the reasons mentioned above. This research effort proposes to re-examine aliased systems and determine some basic means and methods for designing control systems for such aliased systems.

1.3 Previous Research in Aliasing

Very little research has been found in the area of aliasing. This must be due, in a large part, to the assumptions mentioned above regarding sampling rates and low-pass filters. However, a few efforts have been completed in this direction. They are briefly summarized here.

Ehrlich, Taussig, and Abramovitch [5] introduce a method to determine the dynamics of a continuous-time, linear, time-invariant (LTI) system to frequencies well beyond the Nyquist frequency. Given a stable closed-loop configuration, using single-frequency inputs, and measuring the input and output spectral amplitudes using a spectrum analyzer, they identify the open-loop plant transfer function of the LTI system, Gp(jw), from the closed-loop response. They take the aliased transfer function and divide its normalized

spectrum by the normalized spectrum of the zero-order hold function to give an estimate of the discrete-time closed-loop transfer function. The natural frequency of the system of their example is four times the sampling frequency. The effects of the zero-order hold on aliasing are demonstrated and used in their research as they will be in this research effort.

Durney [6] demonstrates that a robot controller's on-board hardware and sensors can be effectively used to identify the system's dynamics, thus allowing for on-line control law design. In his work, he develops a model for aliased frequency response functions (AFRF) and shows that, given an original linear plant, these AFRFs are also linear. The linearity of the AFRF will be used in this research effort.

Kang and Yang [8] examine the effects of time delay in stabilization of noncollacted control of beam vibrations. In their research, they show the effects on stability of frequency folding when there is aliasing. They introduce a controller phase plot folded at the Nyquist frequency and show that it is possible to stabilize the infinite number of modes introduced by sampling. This research revisits the infinite modes introduced by sampling and develops root locus methods for design with respect to these infinite modes.

Yang and Hu [7] develop further Kang and Yang's controller phase plot, and analytically show they can control aliased modes. If the aliased mode lies within the folded phase plot, the aliased mode will be stabilized, and hence, controllable. The idea of controlling aliased modes is developed more thoroughly in this research. Furthermore, a drawback to

their research is that, other than stability, other system response characteristics cannot be obtained from the phase plots.

Sims [9] presents the use of aliased frequency response functions in controller design. His work shows AFRFs can predict closed-loop stability, and AFRFs are useful tools in the design of controllers implemented without smoothing or antialias filters, actually showing improved performance over such systems. Sims shows that systems performance can actually be improved at times with aliased systems, a fact which also becomes evident in this research effort.

Dormido, Lopez-Rodriguez, Fdez-Marron, and Aranda [10] present a method of plotting a root locus using the sample period as the parameter of interest. While not directed specifically at aliasing, their results led to the use of the sample period as a design parameter in the aliased systems of this research effort.

Lyman [10a] further develops the method of root locus plotting using the sample period as the parameter of interest. He allows aliasing and determines its affect on the z-plane root locus of the systems. He further examines the effects of time delay on these root loci plots. His root locus method is useful in designing controllers of sampled-data systems. His work is directly applicable to this research effort, as the effects of aliasing and sample period selection on the root loci of the mixed continuous and discrete systems of this research is used extensively.

1.4 Related Research

Although not directly related to efforts on designing controllers for systems in which aliasing is allowed, much current research is being conducted in areas of peripheral interest to this research effort. Some of these efforts are summarized below.

Wang, Wang, and Lee [33] explore the effects of sampling time on the higher-order digitizations used to convert a continuous system into the discrete domain. The two higher-order digitizations include the Madwed and Boxer-Thaler methods [34]. Comparisons are made between these digitizations and the Tustin method. They introduce the z-plane root locus based on sample period, which they call the "polynomial root locus," for all three digitization methods. Stability is determined by the unit circle in the z-plane. Additionally they developed a new method to transform the system to the w-plane, allowing use of the Routh-Hurwitz stability criterion of a continuous system in the determination of the maximum sample time.

Diduch and Doraiswami [35] perform a study on the influence of the sample period on a system in which the controller is a simple servomechanism. They look at how the sample period affects both the sensitivity of the design and the performance of the system. Their simulations show that the performance of the closed-loop system degrades monotonically with the sample period, leading to the obvious conclusion that a sample period of zero is

optimal. They also demonstrate a decrease in robustness and an increase in sensitivity with an increase in the sample period.

Hirata and Powell [36] examine the effects of sample rate on broadband disturbance rejection in digital control systems. They show that the selection of the correct sample rate has a great effect on the system's ability to reject disturbances. They show that with a sample rate as low as eight times the closed-loop bandwidth there is a 50% degradation in the discrete system's disturbance rejection in comparison to a continuous controller. Hirata also discusses peaks found in the cost survey of a linear quadratic Gaussian (LQG) approach used to evaluate performance [37:43-47]. These peaks occur at integer fractions of twice the natural frequency of the systems he researched. He states that at these frequency ratios the systems he studies, in particular the mass-spring-mass system, are uncontrollable, since their cost functions peak quite sharply. In this dissertation, however, at these frequency ratios the systems prove to be controllable given the fact they include damping. As damping approaches zero, the cost of controlling at these frequency ratios do indeed rise drastically.

Kranc introduced the concept of analysis of multirate feedback systems in 1957 [27]. He developed a general technique that extended the z-transform methods to sampled-data systems in which "synchronized switches" did not operate with the same sampling frequency as the overall system. This method could be used to examine system output

between sampling instants by introducing a sampler operating at a rate greater than that of the system.

Tornero, Gu, and Tomizuka [23] analyze multi-rate controllers that update the controller output faster than the measurement sampling frequency by an integer factor. The systems they control are continuous and the controller is discrete with a zero-order hold. As a result of the multi-rate controller the control input becomes oscillatory. They theorize, however, that the multi-rate controller may enable stability of a system that is unstable with a single-rate controller.

Tangirala, Li, Patwardhan, Shah, and Chen [24] also examine multi-rate controllers in which the controller receives input at a greater frequency than the output. They, however, introduce the concept of lifting techniques [25] in which a fast-rate signal is mapped to a slow-rate signal with an increased dimensionality, and inverse lifting techniques in which the mapping is from a lifted signal to a fast-rate one. They demonstrate that this discrete lifting will introduce intersample ripples in the outputs of the closed-loop multi-rate systems if the steady-state gains of the lifted models are non-uniform. If the gains are identical, however, there are no oscillations of the outputs. They additionally show that a fast-rate integrator will eliminate these oscillations no matter what the gains are.

Cavicchi [26] introduces the concept of a phase-root locus and the resulting stability measures than can be examined from this plot. Cavicchi develops the phase-root locus as

the dual of the conventional root locus, it being a plot of the closed-loop pole movement as phase is added to the open-loop transfer function. The phase-root locus, plotted together with the traditional root locus, allow the s-plane to be used to determine robustness, perform transient design, and aid in stability analysis.

Diduch and Doraiswami [38] show that when unmodeled process dynamics are included in the analysis, an increased sample time may actually improve the robustness of an optimally designed sampled-data system. This is because, with the inclusion of the unmodeled dynamics, the mapping of the uncertainty from the continuous to the discrete domain shrinks or contracts as the sample period is increased. This would tend to indicate that stability may be increased with an increase in sample period as shown in this dissertation.

Braslavsky, Middleton, and Freudenberg [39] introduce a frequency domain lifting technique to analyze what they call hybrid systems—systems in which they wish to examine intersample behavior. They demonstrate the application of their technique to the stability robustness of an LTI and non-LTI system.

Much has been researched with respect to the effects of time delay on the stability of systems. Perhaps the "grand-daddy" of this research effort is that presented by Tsypkin [28]. He derived stability conditions for systems in which the feedback is delayed. His development allowed simplification of such systems.

Other research into the effects of time delay include the work done by Lyman [12] on root loci with time delay as the parameter of variation. He verifies, based on the root loci plots, Tsypkin's three types of behavior: stability for all delay, stability to a critical value of delay, and a finite alternation between stability and instability as delay increases.

Other research in time delay effects includes stability criteria introduced by Hou and Ali [29], compensation methods for computational delay by Rattan [30] and Ovaska and Vainio [31], and the effects of zeros in digital control systems in which computational time delay is present by Hara, Kondo, and Katori [32].

1.5 Dissertation Outline

This research effort begins by developing a model for a system in which the effects of aliasing on continuous output can be examined. The model, then, will consist of discrete and continuous portion. Due to this mixed nature, examination of the system poles and zeros must occur in a common plane. The s-plane is valid for examination of the continuous roots of the system and the z-plane is valid for examination of the discrete roots of the system, but neither is completely accurate for examination of discrete and continuous roots together.

A new plane for examination of these poles and zeros is first introduced: the s*-plane. This plane allows for examination of the continuous poles and zeros with their locations determined as they are in the traditional s-plane. Discrete poles and zeros and transformed to the primary band of the s*-plane from the z-plane and repeated infinitely into every other band formed according to sample rate.

A model of a mixed discrete and continuous system is developed next; this model is contrary to the strictly discrete or continuous models used for common study of sampled-data systems. In the model developed here, the plant will be a continuous plant and the controller will be a discrete controller. Input will be restricted to discrete input only. The systems studied in this research effort, then, are sampled-data systems in which the input and feedback are discrete, but the output is continuous.

For this model to be valid it must equal a discrete system in the limit as sampling period increases, and it must equal a continuous system in the limit as sampling period goes to zero. Limit analysis shows this to indeed be the case. In strictly discrete or continuous systems, the open-loop poles of the plant are cancelled by a set of the system's closed-loop zeros, allowing for placement of the closed-loop poles to enable control. This research shows this to be the case for the mixed discrete and continuous system under consideration, allowing control of the continuous plant with the discrete controller.

With the model developed and the s*-plane introduced, the effects of aliasing on classical measures of stability such as the root loci and frequency response function plots are investigated, with a determination of acceptable aliasing regions introduced. Design methods using root locus tools are extended from the traditional methods of non-aliased system design. The impulse and step responses of these systems are examined, as well as how well these systems follow a sinusoidal input. The ability of these aliased control systems to follow a sinusoidal input is poor unless the frequency of the sine wave is less than the sampling frequency.

This research effort includes only second- or fourth-order, linear, time-invariant systems. First, a second-order plant with no zeros is examined and a relationship between sampling frequency and root loci locations is developed. Sampling frequencies are found which actually introduce stability with increased aliasing. A deadbeat response of the closed-loop system is developed using simple proportional-integral control, with the response settling to the final values within one sample period. This deadbeat controller requires very accurate knowledge of the controlled system's natural frequency and damping ratio. Robustness is examined and found to be adequate. Disturbance rejection is also examined. It was found the system can reject step disturbances within one sample period of the feedback of the disturbance to the controller. This system does not have the ability to reject broadband disturbances.

A simple fourth-order plant with no zeros is investigated next. The high-frequency mode of this plant is aliased, and the effects of this high-frequency are minimized by allowing aliasing. Again, the increased aliasing actually improves response. With the effects of the aliased high-frequency mode minimized, the design of control for the low-frequency mode follows traditional design methods. Again, very accurate information of the aliased mode's natural frequency and damping ratio are required. Robustness and disturbance rejection results were similar to those of the second-order system.

The contribution of the research effort is easy to determine. As a result of the research, aliasing becomes acceptable in certain design regions; indeed, aliasing caused by a slow sample rate even becomes a design parameter, introducing stability and allowing the control of the high-frequency aliased modes. In areas where aliasing is unavoidable, the development of these design tools will become very valuable. The limitation to this method is its inability to follow high-frequency inputs or reject high frequency disturbances. If, however, the input and disturbances are at frequencies below the sampler, this method provides an excellent means to control aliased modes.

CHAPTER TWO. THEORY

2.0 INTRODUCTION

In this chapter we develop the basic theory and model for the study of systems in which aliasing is allowed. This development depends on the reader's understanding of Laplace transforms, z-transforms, complex logarithms, root locus plots, the sampling operation and the definition of an ideal sampler, and the effects of a zero-order hold on a plant. A brief review of these principles can be found in Appendix A.

This chapter begins with the introduction of the s*-plane, a plane in which both the continuous and discrete poles and zeros can be examined. With the introduction of the s*-plane and a basic understanding of sampling, aliasing, and the zero-order hold, the model used for examination of aliased systems can now be developed. Here the model consists of both discrete and continuous parts, and is thus named a discrete-to-continuous system. From this model, a discrete-to-continuous transfer function is derived. The model is examined in the limits as the sample period goes to zero and infinity and found

to reduce to the continuous and discrete system, respectively. For control of the closed-loop discrete-to-continuous system to occur, the open-loop poles must be cancelled by a set of the closed-loop zeros. This is found to be the case for the mixed system. And finally, prior to plotting the s*-plane root locus, an examination is made of the origins of the closed-loop poles and zeros and the effects of the sample period on these roots.

2.1 THE S*PLANE

Traditionally, root locus analysis has been performed in the s- or Laplace domain for continuous systems and in the z-domain for discrete systems. In this research effort, however, examination will be of a system containing both discrete and continuous portions in the transfer function. Transforming the continuous poles and zeros to the discrete domain, although mathematically possible, means little in terms of design with slow sample rates. Conversely, transforming the discrete poles and zeros to the s-plane means little since these discrete poles and zeros are repeated infinitely due to the sampler. To have a common plane in which to examine both the continuous and discrete poles and zeros, we will introduce the s*-plane. It's development follows.

The mapping from the s-domain to the z-domain is common, and tables included in most digital control theory texts [1, 31, 32, 33] have s-domain as well as z-domain forms of basic time functions, allowing the transform from the s-domain to the z-domain. A word

of caution is in order however. When transforming from the s-domain to the z-domain one must ensure the system to be mapped is in pole-residue form—the tables are constructed based on this fact. A z-transform (Appendix A) of the poles and zeros using

$$z = e^{sT_s} \qquad [2.1]$$

would map the zeros to different locations than finding the pole-residue form, performing the z-transform, and then recombining to calculate the zero locations. In other words, poles map using Equation 2.1, but zeros do not! The reason for this will be explored later.

The mapping from the s-plane to the z-plane is a many-to-one mapping. The reason for this follows: The s-plane is first divided into infinitely many bands of "height" ω_s, as shown in Figure 2.1. The primary band extends from $\omega = -\frac{\omega_s}{2}$ to $\omega = +\frac{\omega_s}{2}$.

Using the relation of Equation 2.1 the points 1, 2, 3, 4, and 5 are mapped to the z-plane. Corresponding points are shown in Figure 2.2.

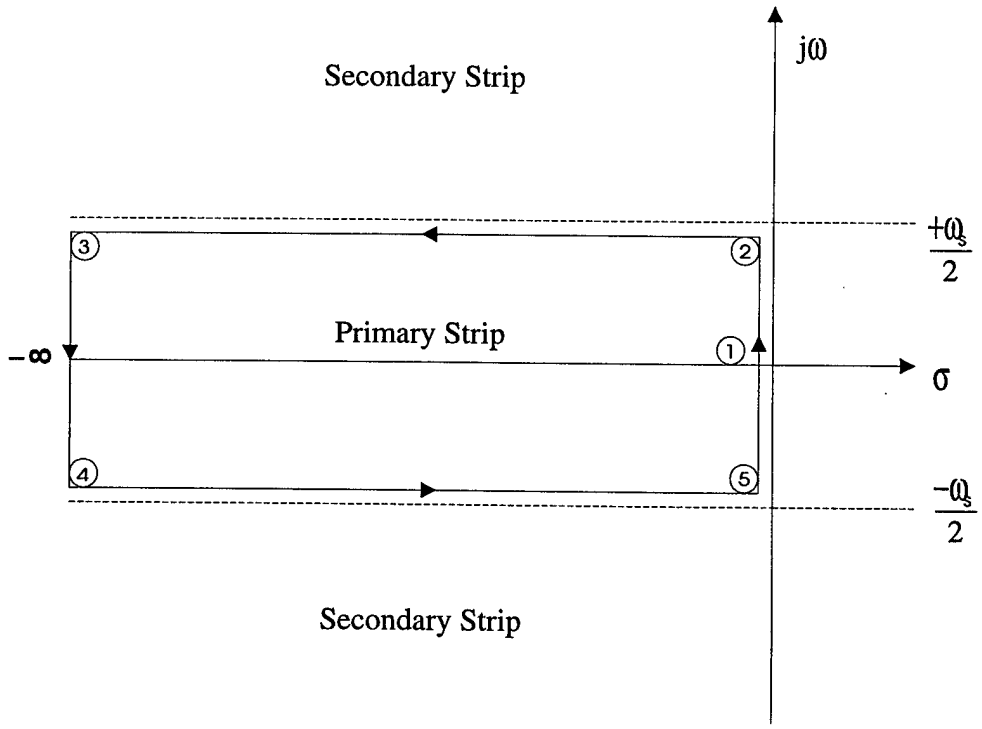

Figure 2.1 The S-Plane

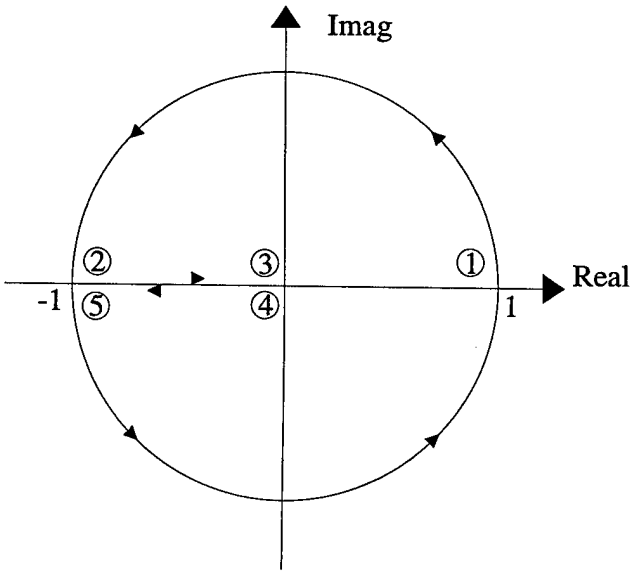

Figure 2.2 The Z-Plane

Since

$$e^{(s+jn\omega_s)T_s} = e^{sT_s}e^{jn\omega_s T_s} = e^{sT_s} = z \qquad [2.2]$$

each of the complementary bands extending from $-\frac{\omega_s}{2}$ to $-\frac{3\omega_s}{2}$, from $+\frac{\omega_s}{2}$ to $+\frac{3\omega_s}{2}$, and so forth, map to the same location in the z-plane. Thus, this mapping is a many-to-one mapping. This fact also explains the non-uniqueness of the inverse z-transform. In performing this inverse z-transform, one cannot define to which band the mapping should occur—it is a one-to-many mapping. The mapping from the z-plane to the s*-plane, however, will account for this fact.

With the above mentioned caution of transformations using the pole-residue form it is relatively straightforward to translate from the s-plane into the z-plane, and no difficulties are encountered with the sample period, T_s. In transforming from the z-plane to the s*-plane, however, because of the one-to-many mapping, there exist multiple bands to which the z-plane poles can be mapped. Additionally when considering pole-zero or pole-residue form, one must know what form is invoked by performing the inverse z-transform.

An inverse z-transform of the pole-residue form of $F(z)$ gives the equation for $f(kT_s)$, which may or may not equal $f^*(t)$ because of it's non-uniqueness (see Equation A.14).

Taking the inverse z-transform of $F(z)$ to the s*-plane provides the pole-residue form of $F^*(s)$, if the poles and residues of $\mathcal{Z}^{-1}\{F(z)\}$ are mapped to the primary band and repeated in every band infinitely. The infinite sum of these poles and residues would then provide the pole-zero form of $F^*(s)$.

The easier way of obtaining this pole-zero form, however, is to simply map the zeros and poles from the z-plane to the s*-plane using the inverse relation of Equation 2.1:

$$s = \frac{1}{T_s}\ln(z) \quad . \qquad [2.3]$$

Once the poles and residues are combined into the poles and zeros in the z-plane, the infinite sum is already accomplished because of the many-to-one mapping that occurs in the transform from the s-plane to the z-plane. These z-plane poles and zeros are then mapped to the primary band of the s*-plane using Equation 2.3, and repeated infinitely to produce the pole-zero form of $F^*(s)$.

This infinite repetition to produce the pole-zero form of F*(s) is the result calculating the logarithm of a complex number (Appendix A). Because of the nature of calculating the argument of z, the mapping from the z-plane to the s*-plane is a one-to-many mapping. Each of the poles and zeros mapped from the z-plane to the principal or primary band in

the s*-plane is repeated infinitely to every other band at intervals of $jn\omega_s$, where $n = 0, \pm 1, \pm 2, \ldots$.

The difference between the mapping of the pole-residue form and the pole-zero form is a direct result of aliasing. In the limit as T_s goes to zero, the width of the primary band in the imaginary axis direction becomes infinite. Thus, the effect of the poles and residues does not overlap across bands, and the infinite sum, which produces the pole-zero form, equates to the infinite product of that pole-zero form. As T_s goes to zero, the pole-zero and the pole-residue forms become the same. As T_s increases, however, the "tails" of the poles and residues cross the band boundaries, adding to the effects of the poles and residues of other bands, and the infinite sum has to include these influences. Thus, as aliasing increases the location of the zeros will move, and the poles and zeros found by mapping the poles and residues using Equation 2.3 will not produce the same zero locations as mapping the poles and zeros unless the infinite summation is performed.

One may notice the similarity in concept of mapping from the z-plane to the s*-plane as the bilinear transformation made to map the unit circle from the z-plane to the imaginary axis of the w-plane [34:225-230]. This w-plane mapping allows the use of the continuous forms of the Routh-Hurwithz criterion and Bode techniques in the examination of a discrete system. The difference here, however, is that the w-plane mapping is a one-to-one mapping and, as such, does not allow for the examination of aliasing that the s*-plane

mapping, a one-to-many mapping, does. Perhaps a mapping closer to that of the s*-plane would be that one found from using the modified z-transform [33]

2.2 Model Development

The model for this research effort is shown below in Figure 2.3. Parameters resulting from discrete components are designated by the asterisk (*); therefore, the sampled version of the output signal in the frequency domain, $C(s)$, is designated as $C*(s)$.

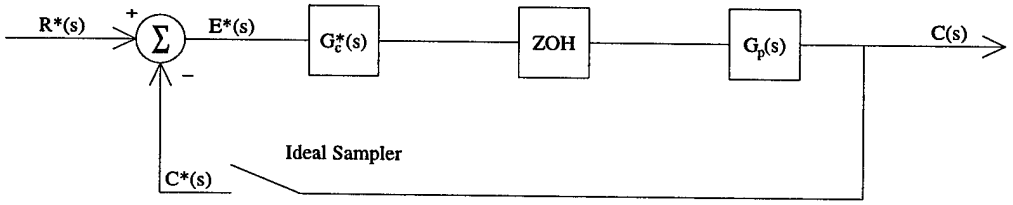

If (ZOH)*(G_p(s)) = H(s), then

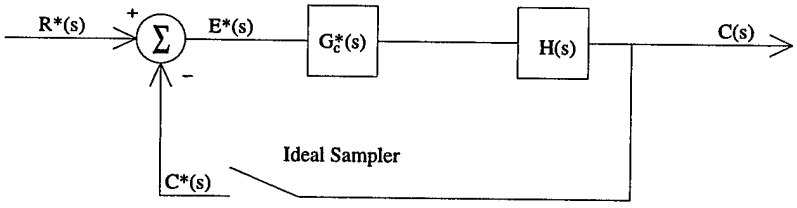

Figure 2.3 Sampled-Data System Model

The input to the sampled-data system will be restricted to change only at the sample instants, hence the input is shown as $R^*(s)$. The zero-order hold, $ZOH(s)$, and the plant, $G_p(s)$, will be combined into a function called $H(s)$. The control law, implemented by the computer, is discrete and is designated as $G_c^*(s)$.

The following two relations can be derived from Figure 2.3:

$$C(s) = G_c^*(s)H(s)E^*(s) \qquad [2.4]$$

$$E^*(s) = R^*(s) - C^*(s) \qquad [2.5]$$

Substituting Equation 2.5 into Equation 2.4 gives

$$\begin{aligned} C(s) &= G_c^*(s)H(s)[R^*(s) - C^*(s)] \\ &= G_c^*(s)H(s)R^*(s) - G_c^*(s)H(s)C^*(s) \end{aligned} \qquad [2.6]$$

Applying the sampling relationship (Equation A.18, Appendix A) to Equation 2.6 to find an expression for the sampled version of $C(s)$ gives

$$\begin{aligned} C^*(s) &= [G_c^*(s)H(s)R^*(s) - G_c^*(s)H(s)C^*(s)]^* \\ &= G_c^*(s)H^*(s)R^*(s) - G_c^*(s)H^*(s)C^*(s) \end{aligned} \qquad [2.7]$$

Collecting like terms and solving for $C^*(s)$ gives

$$C^*(s) = \frac{H^*(s)G_c^*(s)}{1+H^*(s)G_c^*(s)} R^*(s) \quad . \qquad [2.8]$$

Substituting Equation 2.8 into Equation 2.6:

$$C(s) = \left\{ G_c{}^*(s)H(s) - G_c{}^*(s)H(s)\left[\frac{H^*(s)G_c{}^*(s)}{1+H^*(s)G_c{}^*(s)} \right] \right\} R^*(s)$$

$$= G_c{}^*(s)H(s)\left[1 - \frac{H^*(s)G_c{}^*(s)}{1+H^*(s)G_c{}^*(s)} \right] R^*(s)$$

$$= G_c{}^*(s)H(s)\left[\frac{1+H^*(s)G_c{}^*(s) - H^*(s)G_c{}^*(s)}{1+H^*(s)G_c{}^*(s)} \right] R^*(s)$$

$$C(s) = \left[\frac{G_c{}^*(s)H(s)}{1+G_c{}^*(s)H^*(s)} \right] R^*(s) \quad . \qquad [2.9]$$

Equation 2.9 suggests a discrete-to-continuous transfer function in the form of continuous output over discrete input:

$$\frac{C(s)}{R^*(s)} = \frac{G_c^*(s)H(s)}{1+G_c^*(s)H^*(s)} = F^*(s)H(s). \qquad [2.10]$$

Systems having both discrete and continuous signals are traditionally known as sampled-data systems. Such systems have been studied extensively. However, examination has been in either the digital (discrete) or continuous domain. Here, the discrete and continuous domains are examined together. The discrete-to-continuous transfer function of Equation 2.10 includes both the continuous (typically aperiodic) and the discrete (periodic) frequency components, and as such is not a transfer function in the classical sense of the term. The frequency response function (FRF) corresponding to this discrete-to-continuous transfer function will be examined below. The FRF of the sampled-data transfer function will be termed a *discrete-to-continuous frequency response function* (DCFRF).

A DCFRF for the system discussed earlier (ω_n = 100 rad/sec, ξ = 0.01) is plotted below in Figure 2.4 for a sampling frequency of ω_s = 90 rad/sec. The DCFRF includes only proportional control, with $G_c^*(s) = 0.1$. Examination of Figure 2.4 clearly shows the effects of aliasing, sampling, and the zero-order hold (ZOH).

Although typical intuition cannot be applied to the DCFRF, several results can be seen in Figure 2.4. The aliasing effect can be seen as the resonant frequency is folded about the folding frequency (ω_f = 45 rad/sec). All frequency components above 45 rad/sec are folded into the primary band ($-45 < \omega < 45$). Sampling effects are seen in the repetition of the primary band characteristics at multiples of the sampling frequency. And finally,

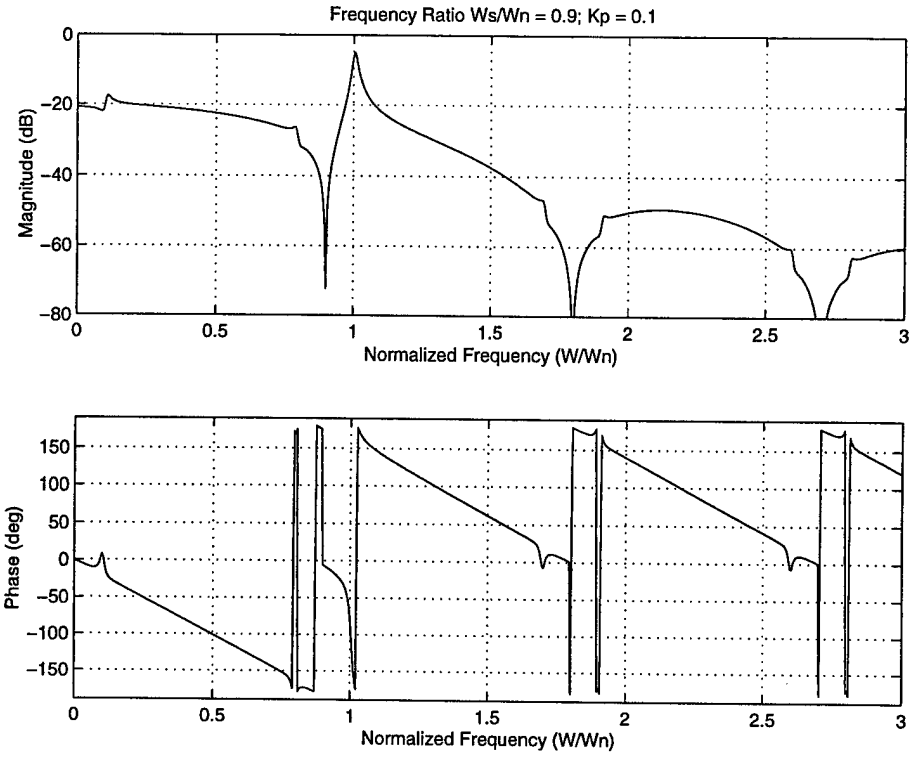

Figure 2.4 Discrete-to-Continuous Frequency Response Function at $\omega_s = 90$ rad/sec

the effects of the ZOH can be seen as the magnitude decreases while frequency increases, and with the magnitude plot going to zero at integer multiples of the sampling frequency.

The discrete-to-continuous impulse response for this system is shown in Figure 2.5. Sampling points in time are shown by the asterisks, and the continuous output of the sampled-data system is the solid line. Here, the aliased mode of the sampled system is easily observable, as is the natural response of the system. It appears that between sample

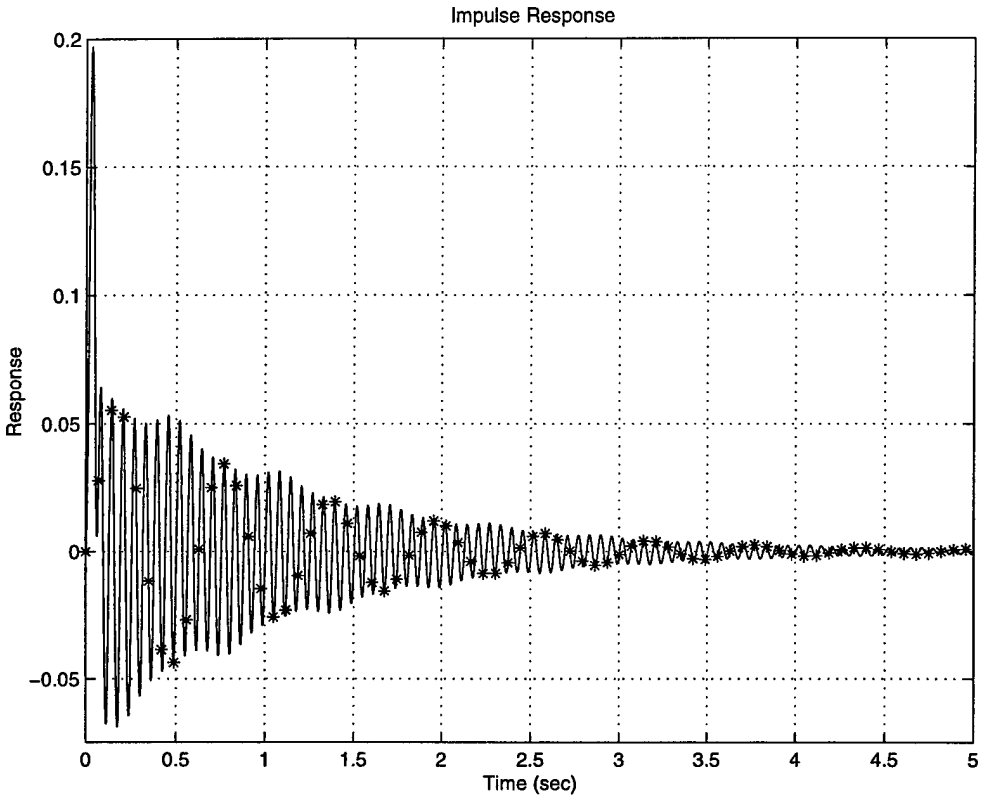

Figure 2.5 Impulse Response of Aliased Sampled-Data System at $\omega_s = 90$ rad/sec

periods the continuous system responds at its open-loop undamped natural frequency. This will indeed be shown to be the case later on.

In this dissertation, we will primarily be concerned with the unique $F^*(s)$, and as such will be using the inverse z-transform of the pole-zero form of $F(z)$. Traditionally, poles

and zeros are mapped to a primary band existing between $s = \frac{-\omega_s}{2}$ and $s = \frac{\omega_s}{2}$. For our analysis, however, we are also interested in the poles and zeros that are repeated at $\pm j\omega_s$ intervals infinitely throughout the s-plane and their effect on the continuous response. Therefore, any plot of the root locus in the s*-plane includes these repeated poles and zeros.

Recall that the transform of $F(z)$ from the z-plane to the s-plane using the inverse z-transform method gives one of an infinite number of functions $F(s)$ that will describe the function $f(t)$ only at the sample instants. The unique transform of $F(z)$ to $F^*(s)$, however, gives the unique function, which is also the $F(s)$ function that will excite the analog plant, $G_p(s)$. The plant is only excited at the sample points with impulses input into the zero-order hold. The $F^*(s)$, then is the only appropriate controller function.

As explained before, the unique form of $F^*(s)$ which represents a discrete time function is periodic in frequency. The plant $H(s)$, pre-multiplied by the zero-order hold, is aperiodic in frequency and represents a continuous time function. When $H(s)$ is multiplied by $F^*(s)$, then, the resulting output of our system will become aperiodic in frequency and continuous in time.

2.3 DISCRETE-TO-CONTINUOUS SYSTEM IN SAMPLE PERIOD LIMITS

The equation for the discrete-to-continuous transfer function is defined in Equation 2.10. This equation should reduce to the continuous transfer function in the limit as the sample period, T_s, goes to zero. The following shows this is indeed the case.

Recall $H(s)$ is defined as the plant, $G_p(s)$, multiplied by the zero-order hold:

$$H(s) = \frac{1 - e^{-sT_s}}{s} G_p(s) \quad . \qquad [2.11]$$

The limit, then, as the sample period goes to zero is

$$\lim_{T_s \to 0} \frac{H(s)}{T_s} = \lim_{T_s \to 0} \frac{1 - e^{-sT_s}}{sT_s} G_p(s) = \frac{1-1}{0} G_p(s) = \frac{0}{0} \quad . \qquad [2.12]$$

Applying L'Hopital's rule gives

$$\lim_{T_s \to 0} \frac{H(s)}{T_s} = \lim_{T_s \to 0} \frac{se^{-sT_s}}{s} G_p(s) = \frac{s}{s} G_p(s) = G_p(s) \quad . \qquad [2.13]$$

Now examine the $H^*(s)$ term of the denominator of $\frac{C(s)}{T_s R^*(s)}$. For our system, the ZOH is included with the plant

$$H(s) = ZOH(s)G_p(s) \quad . \qquad [2.14]$$

Since

$$ZOH(s) = \frac{1 - e^{-sT_s}}{s} \qquad [2.15]$$

the resulting product of the zero-order hold and plant is

$$H(s) = \frac{1 - e^{-sT_s}}{s} \frac{N_p(s)}{D_p(s)} \quad , \qquad [2.16]$$

and, using the equation for a sampled signal, Equation A.16,

$$H^*(s) = \frac{1}{T_s} \sum_{n=-\infty}^{\infty} \frac{1 - e^{-(s+jn\omega_s)T_s}}{s + jn\omega_s} \frac{N_p(s + jn\omega_s)}{D_p(s + jn\omega_s)} . \qquad [2.17]$$

Expanding the exponential term in the numerator gives

$$e^{-(s+jn\omega_s)T_s} = e^{-sT_s}e^{-jn\omega_s T_s} \quad . \qquad [2.18]$$

The relationship between the sample time and the sample frequency is

$$\omega_s = \frac{2\pi}{T_s} \quad , \qquad [2.19]$$

so

$$e^{-jn\omega_s T_s} = e^{-jn\frac{2\pi}{T_s}T_s} = e^{-j2n\pi} = 1 \quad , \quad \text{for n = integer} \quad . \qquad [2.20]$$

Substituting this into Equation 2.17, the equation for $H^*(s)$, gives

$$H^*(s) = \frac{1-e^{-sT_s}}{T_s} \sum_{n=-\infty}^{\infty} \frac{N_p(s+jn\omega_s)}{(s+jn\omega_s)D_p(s+jn\omega_s)} \quad . \qquad [2.21]$$

Looking at the limit of the summation:

$$\lim_{T_s\to 0}\sum_{n=-\infty}^{\infty}\frac{N(s+jn\omega_s)}{(s+jn\omega_s)D(s+jn\omega_s)}=\left[\begin{array}{l}\cdots+\dfrac{N_p\left(s-\dfrac{j2\pi}{0}\right)}{\left(s-\dfrac{j2\pi}{0}\right)D_p\left(s-\dfrac{j2\pi}{0}\right)}+\dfrac{N_p(s)}{sD_p(s)}\\ +\dfrac{N_p\left(s+\dfrac{j2\pi}{0}\right)}{\left(s+\dfrac{j2\pi}{0}\right)D_p\left(s+\dfrac{j2\pi}{0}\right)}+\cdots\end{array}\right]$$

$$\lim_{T_s\to 0}\sum_{n=-\infty}^{\infty}\frac{N_p(s+jn\omega_s)}{(s+jn\omega_s)D_p(s+jn\omega_s)}=\cdots+0+\frac{N_p(s)}{sD_p(s)}+0+\cdots=\frac{1}{s}G_p(s) \qquad [2.22]$$

The zeros of the infinite summation term occur because the order of the denominator of the plant will always be greater than or equal to the order of the numerator (physical realizability). Thus with the zero-order hold term, the order of the denominator terms will always be at least one greater than that of the numerator, causing the limit to be $\frac{1}{\infty}$, which is zero.

The limit of the non-summation term is

$$\lim_{T_s\to 0}\frac{1-e^{-sT_s}}{T_s}=\frac{1-1}{0}=\frac{0}{0}\ , \qquad [2.23]$$

so L'Hopital's rule must be applied:

$$\lim_{T_s \to 0} \frac{1 - e^{-sT_s}}{T_s} = \lim_{T_s \to 0} \frac{se^{-sT_s}}{1} = s \quad . \qquad [2.24]$$

Therefore,

$$\lim_{T_s \to 0} H^*(s) = s\frac{1}{s} G_p(s) = G_p(s) \quad , \qquad [2.25]$$

which is the expected result.

Finally, examine the controller, $G_c^*(s)$. For the sake of comparison to the continuous case, assume $G_c^*(s)$ is simply the ideally sampled version of $G_c(s)$, the inverse mapping of the controller $G_c(z)$.

In this case

$$G_c^*(s) = \frac{1}{T_s} \sum_{n=-\infty}^{\infty} G_c(s + jn\omega_s) \quad . \qquad [2.26]$$

Following the same reasoning as before, in the limit as the sample period goes to zero this approaches the continuous controller, $G_c(s)$:

$$\lim_{T_s \to 0} G_c{}^*(s) = G_c(s) \qquad [2.27]$$

Looking, then, at the limit as the sample period goes to zero, one can see that the discrete-to-continuous transfer function equals the continuous transfer function:

$$\lim_{T_s \to 0} \frac{C(s)}{T_s R^*(s)} = \lim_{T_s \to 0} \frac{G_c{}^*(s)\dfrac{H(s)}{T_s}}{1 + G_c{}^*(s)H^*(s)} = \frac{G_c(s)G_p(s)}{1 + G_c(s)G_p(s)} \qquad [2.28]$$

Now, examine the limit of the discrete-to-continuous transfer function as the sample period approaches infinity. Begin by examining the numerator term, $H(s)$

$$\lim_{T_s \to \infty} \frac{H(s)}{T_s} = \lim_{T_s \to \infty} \frac{1 - e^{-sT_s}}{sT_s} G_p(s) = \frac{1-0}{\infty} G_p(s) = 0 \qquad [2.29]$$

This will be the limit of the entire discrete-to-continuous transfer function, if the denominator terms do not also equal zero. The limit of $H^*(s)$ is

$$\lim_{T_s\to\infty} H^*(s) = \lim_{T_s\to\infty} \frac{1-e^{-sT_s}}{T_s} \sum_{n=-\infty}^{\infty} \frac{N_p(s+jn\omega_s)}{(s+jn\omega_s)D_p(s+jn\omega_s)} \qquad [2.30]$$

$$= \frac{1-0}{\infty} \lim_{T_s\to\infty} \sum_{n=-\infty}^{\infty} \frac{N_p(s+jn\omega_s)}{(s+jn\omega_s)D_p(s+jn\omega_s)} = 0$$

Because the limit of the term is zero, the limit of the denominator term of the continuous-to-discrete transfer function equals 1, and

$$\lim_{T_s\to\infty} \frac{C(s)}{T_s R^*(s)} = \frac{0}{1} = 0 \qquad [2.31]$$

This result is expected. As the sample period goes to infinity, the loop is never closed, never allowing the controller to input to the system, and the system response is zero.

2.4 Cancellation of The Open-Loop Poles by The Zeros from The Closed-Loop System

With a strictly continuous or discrete system, the process which allows its control once the loop is closed is that fact that the open loop poles will be canceled by the closed loop zeros, allowing for the placement of the closed loop poles in desired locations for desired system response. This fact will be shown below. This is also the case with the discrete-to-continuous system of this research effort. The mathematical proof of this fact follows.

Suppose, in the continuous domain, the plant is defined by

$$G_p(s) = \frac{N_p(s)}{D_p(s)} \quad , \qquad [2.32]$$

and a controller defined by

$$G_c(s) = \frac{N_c(s)}{D_c(s)} \quad . \qquad [2.33]$$

If the loop is closed with negative feedback the resulting transfer function is

$$\frac{C(s)}{R(s)} = \frac{G_c(s)G_p(s)}{1 + G_c(s)G_p(s)}, \qquad [2.34]$$

where $C(s)$ is the output and $R(s)$ is the input. Using Equations 2.32 and 2.33 in Equation 2.34 gives

$$\frac{C(s)}{R(s)} = \frac{\frac{N_c(s)}{D_c(s)}\frac{N_p(s)}{D_p(s)}}{1 + \frac{N_c(s)}{D_c(s)}\frac{N_p(s)}{D_p(s)}} \quad , \qquad [2.35]$$

which after some algebraic manipulation, and before any cancellation, becomes

$$\frac{C(s)}{R(s)} = \frac{N_c(s)N_p(s)D_c(s)D_p(s)}{D_c(s)D_p(s)[D_c(s)D_p(s) + N_c(s)N_p(s)]} \quad . \qquad [2.36]$$

Zeros are those factors for which the numerator equals zero. Likewise, poles are those factors for which the denominator equals zero. Notice that by closing the loop we have caused a pole-zero cancellation—the zeros found from the term $D_p(s)$ in the numerator cancel the poles of the same form in the denominator. When one thinks this through, this indeed must occur if we wish to control the system: the open loop poles must be rendered inactive by this cancellation to allow control, or movement of the poles, through design of the controller. The resulting system is

$$\frac{C(s)}{R(s)} = \frac{N_c(s)N_p(s)}{D_c(s)D_p(s) + N_c(s)N_p(s)} \quad . \qquad [2.37]$$

In the discrete domain the analysis is identical, with each "s" in Equation 2.32 through Equation 2.37 replaced with a "z". Thus, the results are the same: to control a discrete system, the discrete open loop poles must be cancelled, with new pole placement (and thus system control) occurring through design of the controller.

The question that must next be answered is whether this same pole-zero cancellation occurs in the mixed continuous-discrete system of this research. The following proof shows that, indeed, this cancellation occurs. Given a function, F(s), the definition for its sampled version is given as [7:19]

$$F^*(s) = \frac{1}{T_s} \sum_{n=-\infty}^{\infty} F(s + jn\omega_s) \quad , \qquad [2.38]$$

given the order of the system's numerator is less than the order of its denominator, which is true for all real systems. Recall $H^*(s)$, the sampled version of $H(s)$, was found to be

$$H^*(s) = \frac{1 - e^{-sT_s}}{T_s} \sum_{n=-\infty}^{\infty} \frac{N_p(s + jn\omega_s)}{(s + jn\omega_s) D_p(s + jn\omega_s)} \quad . \qquad [2.39]$$

Finding a common denominator of the term within the summation sign gives

$$H^*(s) = \frac{1 - e^{-sT_s}}{T_s} \frac{\sum_{n=-\infty}^{\infty} \left\{ N_p(s + jn\omega_s) \prod_{m=-\infty}^{m \neq n}^{\infty} \left[(s + jm\omega_s) D_p(s + jm\omega_s) \right] \right\}}{\prod_{n=-\infty}^{\infty} \left[(s + jn\omega_s) D_p(s + jn\omega_s) \right]} \quad . \qquad [2.40]$$

Assuming a similar form for the sampled version of the controller gives

$$G_c^*(s) = \frac{1}{T_s} \frac{\sum_{n=-\infty}^{\infty} \left[N_c(s + jn\omega_s) \prod_{m=-\infty}^{m \neq n}{}^{\infty} D_c(s + jm\omega_s) \right]}{\prod_{n=-\infty}^{\infty} D_c(s + jn\omega_s)} , \qquad [2.41]$$

where the controller includes no zero-order hold.

The equation for the discrete-to-continuous transfer function is

$$\frac{C(s)}{T_s R^*(s)} = \frac{G_c^*(s) \frac{H(s)}{T_s}}{1 + G_c^*(s) H^*(s)} . \qquad [2.42]$$

Substituting the equations for $G_c^*(s)$, $H(s)$, and $H^*(s)$ into Equation 2.42 gives

$$\frac{C(s)}{T_s R^*(s)} = \frac{\left(\frac{1}{T_s}\right) \left(\frac{\sum_{n=-\infty}^{\infty} N_c(s + jn\omega_s) \prod_{m=-\infty}^{m \neq n}{}^{\infty} D_c(s + jm\omega_s)}{\prod_{n=-\infty}^{\infty} D_c(s + jn\omega_s)} \right) \left(\frac{1 - e^{-sT_s}}{sT_s} \right) \left(\frac{N_p(s)}{D_p(s)} \right)}{\left[1 + \left(\frac{1}{T_s}\right) \left(\frac{\sum_{n=-\infty}^{\infty} N_c(s + jn\omega_s) \prod_{m=-\infty}^{m \neq n}{}^{\infty} D_c(s + jm\omega_s)}{\prod_{n=-\infty}^{\infty} D_c(s + jn\omega_s)} \right) \left(\frac{1 - e^{-sT_s}}{T_s} \right) \left(\frac{\sum_{n=-\infty}^{\infty} N_p(s + jn\omega_s) \prod_{m=-\infty}^{m \neq n}{}^{\infty} (s + jm\omega_s) D_p(s + jm\omega_s)}{\prod_{n=-\infty}^{\infty} (s + jn\omega_s) D_p(s + jn\omega_s)} \right) \right]}$$

[2.43]

which, after algebraic manipulation gives

$$\frac{C(s)}{T_s R^*(s)} = \frac{\left(1-e^{-sT_s}\right)\left(N_p(s)\right)(num1)(num2)}{sD_p(s)(den1+den2)} \qquad [2.44]$$

where

$$num1 = \sum_{n=-\infty}^{\infty} N_c(s+jn\omega_s) \prod_{m=-\infty}^{m\neq n}{}^{\infty} D_c(s+jm\omega_s) \quad , \qquad [2.45]$$

$$num2 = \prod_{n=-\infty}^{\infty} (s+jn\omega_s) D_p(s+jn\omega_s) \quad , \qquad [2.46]$$

$$den1 = T_s{}^2 \left(\prod_{n=-\infty}^{\infty} D_c(s+jn\omega_s) \right) \left(\prod_{n=-\infty}^{\infty} (s+jn\omega_s) D_p(s+jn\omega_s) \right) \text{, and} \qquad [2.47]$$

$$den2 = (1-e^{-sT_s}) \left(\sum_{n=-\infty}^{\infty} N_c(s+jn\omega_s) \prod_{m=-\infty}^{m\neq n}{}^{\infty} D_c(s+jm\omega_s) \right) \left(\sum_{n=-\infty}^{\infty} N_p(s+jn\omega_s) \prod_{m=-\infty}^{m\neq n}{}^{\infty} D_p(s+jm\omega_s) \right) \qquad [2.48]$$

Notice, however, that the n = 0 term in the $num2$ term will cancel the $sD_p(s)$ from the denominator:

$$\frac{C(s)}{T_s R^*(s)} = \frac{\left(1 - e^{-sT_s}\right)\left(N_p(s)\right)(num1)(num3)}{(den1 + den2)} \qquad [2.49]$$

where

$$num3 = \sum_{n=-\infty}^{n\neq 0}{}^{\infty}(s + jn\omega_s)D_p(s + jn\omega_s) \quad . \qquad [2.50]$$

Thus, one set of discrete zeros will always cancel the open-loop continuous poles from the plant, allowing for design of the control for the discrete-to-continuous system.

2.5 Root Locus Development

The root locus of a system may be plotted in one of two domains—the continuous (s- or Laplace domain) or the discrete (z-domain). Because of the peculiar nature of the discrete-to-continuous system developed here, however, the root loci will by nature be "mixed," containing both continuous and discrete portions. It is advantageous to first calculate poles and zeros in the appropriate domain then combine these poles and zeros from both domains into the Laplace domain.

To begin examination of the root loci plots, the discrete-to-continuous transfer function previously introduced will be rewritten to reflect the domain in which calculations will initially be performed:

$$\frac{C(s)}{T_s R^*(s)} = \frac{C(s)}{T_s R(z)} \qquad [2.51]$$

or

$$\frac{\frac{1}{T_s} G_c^*(s) H(s)}{1 + G_c^*(s) H^*(s)} = \frac{\frac{1}{T_s} G_c(z) H(s)}{1 + G_c(z) H(z)} = \frac{G_c(z) \frac{ZOH(s)}{T_s} G_p(s)}{1 + G_c(z) H(z)} \qquad [2.52]$$

The starred quantities are the periodic versions of the sampled time function in the s-domain. For example, the sampled form of a function $f(t)$ is $f^*(t)$, which is a series of impulses at the sample points, has a value of zero between sample points, and is continuous. Recall that $H(z)$ is the z-transform of the plant $G_p(s)$ with a zero-order hold applied. Therefore, $H^*(s)$ is the periodic version of the function $H(s)$ which gives the same values as $H(z)$ at the sample instants.

Suppose each of the pieces of this transfer function is split into numerator and denominator terms:

$$G_c(z) = \frac{G_c num(z)}{G_c den(z)} \quad , \qquad [2.53]$$

$$\frac{ZOH(s)}{T_s} = \frac{1 - e^{-sT_s}}{sT_s} \quad , \qquad [2.54]$$

$$G_p(s) = \frac{G_p num(s)}{G_p den(s)} \quad \text{, and} \qquad [2.55]$$

$$H(z) = \frac{Hnum(z)}{Hden(z)} \quad . \qquad [2.56]$$

Substituting these back into Equations 2.51 and 2.52:

$$\frac{C(s)}{T_s R(z)} = \frac{\frac{G_c num(z)}{G_c den(z)} \frac{1 - e^{-sT_s}}{sT_s} \frac{G_p num(s)}{G_p den(s)}}{1 + \frac{G_c num(z)}{G_c den(z)} \frac{Hnum(z)}{Hden(z)}} \quad . \qquad [2.57]$$

Following algebraic manipulation Equation [2.57] becomes

$$\frac{C(s)}{T_s R(z)} = \left[\frac{G_c num(z) Hden(z)}{G_c num(z) Hnum(z) + G_c den(z) Hden(z)} \right] \left[\frac{(1 - e^{-sT_s}) G_p num(s)}{(sT_s) G_p den(s)} \right] \quad . \qquad [2.58]$$

This equation, then, becomes the basis for determining pole and zero locations.

2.5.0 Zeros

The zeros of Equation 2.58 will be located where the numerator terms equate to zero. These zeros will consist of four sets of zeros from the following components of the discrete-to-continuous transfer function: 1) the zero-order-hold numerator, 2) the continuous plant numerator, 3) the discrete controller numerator, and 4) the discrete plant denominator.

The zeros found from the zero-order-hold numerator are defined by the equation

$$1-e^{-sT_s}=0 \qquad [2.59]$$

in the s-plane. The solution to Equation 2.59 gives

$$s=0\pm jn\omega_s \qquad n=0,1,2,\ldots \qquad [2.60]$$

This corresponds to one zero at $z=1$ in the z-plane, which is fixed regardless of the sample period, T_s. In the s*-plane the zero-order-hold produces zeros starting at $s=0$ and repeated every ω_s in both the positive and negative directions along the imaginary

axis. A change in the sample period, T_s, will only change the spacing along the imaginary axis of these zeros.

The continuous plant numerator will introduce zeros at the solutions to the equation

$$G_p num(s) = 0 \qquad [2.61]$$

Locations of these zeros in the s*-plane are fixed, given the equation of the plant is fixed. These zeros, since they are from the continuous plant, do not exist in the z-plane.

The discrete controller numerator will produce zeros in the z-plane according to the solution of the equation

$$G_c num(z) = 0 \qquad [2.62]$$

These zeros may be placed anywhere in the z-plane according to classical design theory with the only restriction being physical realizability, which gives the condition that

$$\text{Order}\left(G_c num(z)\right) \leq \text{Order}\left(G_c den(z)\right) \qquad [2.63]$$

The zeros, once the controller is designed, are fixed in the z-plane with no dependence on the sample period, T_s. In the s*-plane the zeros can be found by transforming the z-plane zeros by

$$s = \frac{1}{T_s}\ln(z) \quad , \qquad [2.64]$$

giving their location in the principal band. This transformation will be explained in a later paragraph. These zeros are then repeated at $jn\omega_s$ intervals for $n = 0, \pm 1, \pm 2, \ldots$ Sample period only changes the spacing of these zeros in the imaginary axis direction.

The zeros found from the discrete plant denominator are found from the solution of the equation

$$Hden(z) = 0 \qquad [2.65]$$

In the z-plane these correspond to the location of the open-loop poles of the plant transformed according to

$$z = e^{sT_s} \quad , \qquad [2.66]$$

so their locations are sample period dependent. Just like the controller zeros, they are transformed to the s*-plane and repeated in the imaginary axis direction at $jn\omega_s$ intervals. Because they are sample period dependent in the z-plane, they are sample period dependent in the s-plane, in addition to the sample period dependence of the spacing of repeated zeros in the imaginary axis direction. Notice these zeros are located at precisely the same location they were at before the z-transformation, only now they are repeated in every band.

A summary of the location of the zeros is presented in table 2.1 below.

Table 2.1 Summary of Zero Locations

Zero name	Found from...	Z-plane T_s Dependence?	S*-Plane T_s Dependence?
1. ZOH Numerator	$1-e^{-sT_s}=0$	No	Yes
2. $G_p(s)$ Numerator	$G_p num(s)=0$	N/A	No
3. $G_c(z)$ Numerator	$G_c num(z)=0$	No	Yes
4. H(z) Denominator	$Hden(z)=0$	Yes	Yes

2.5.1 Poles

The poles of Equation 2.58 will be located where the denominator terms equate to zero. These will consist of three sets of poles from the following components of the discrete-to-continuous transfer function: 1) the zero-order-hold denominator, 2) the continuous plant

denominator, and 3) the combined term involving both numerator and denominator terms from both the discrete controller and discrete plant.

The single pole from the zero-order-hold denominator is found from solving the equation

$$sT_s = 0 \qquad [2.67]$$

giving

$$s = 0 \qquad [2.68]$$

This pole in the s*-plane is located at the origin and cancels the zero from the zero-order-hold located there. It is sample period, T_s, independent in the s*-plane, and has no real meaning by transforming to the z-plane.

The locations of the continuous plant denominator poles come from the solution of the equation

$$G_p den(s) = 0 \qquad [2.69]$$

The locations of these poles are the locations of the open loop plant poles, and the locations do not move, given the equation of the plant is fixed.

Poles from the combined term are found by solving the equation

$$G_c num(z)Hnum(z) + G_c den(z)Hden(z) = 0 \qquad [2.70]$$

Locations of these poles in the z-plane are dependent both upon the controller design as well as the sample period, T_s, because of the discretization of the plant, $G_p(s)$, which gives the locations of the $Hnum(z)$ and $Hden(z)$ terms. The locations in the s*-plane are determined by the transform of Equation 2.70 to the s*-plane using the inverse of Equation 2.67, and repeated in the imaginary axis direction at $jn\omega_s$ intervals. Because they are sample period dependent in the z-plane, they are sample period dependent in the s*-plane, in addition to the sample period dependence of the spacing of repeated poles in the imaginary axis direction.

A summary of the location of the poles is presented in table 2.2 below.

Table 2.2 Summary of Pole Locations

Pole name	Found from…	Z-plane T_s Dependence?	S*-Plane T_s Dependence?
1. ZOH Denominator	$sT_s = 0$	N/A	No
2. $G_p(s)$ Denominator	$G_p den(s) = 0$	N/A	No
3. Combined Term	$G_c den(z) Hden(z) + G_c num(z) Hnum(z) = 0$	Yes	Yes

2.6 Chapter Two Summary

In this chapter, the s*-plane was introduced. The s*-plane is the plane that allows analysis of the discrete and continuous pieces of the sampled-data system together. The model of the discrete-to-continuous system and its related equations were developed. The model consists of discrete and continuous portions. In the limits as the sample period goes to zero and infinity the model reduces to its continuous and discrete counterparts, respectively. A set of the discrete closed-loop controller zeros was determined to cancel the continuous open-loop poles, allowing for control of the discrete-to-continuous system. The origins of the mixed system zeros and poles and the effects of the sample period on these roots were examined and determined. With the theoretical development complete, examination of the effects of aliasing on the design of the discrete-to-continuous system can now begin.

CHAPTER THREE. SECOND-ORDER SYSTEM DESIGN WITH ALIASING – PROPORTIONAL CONTROL

3.0 INTRODUCTION

With the tools and model developed for the discrete-to-continuous system, design issues will now be addressed. First, the generalized root locus for the system is developed and the locations of the poles in the gain limited is examined. The second-order plant is introduced and its z-transform performed. The effect of the sample time on the zero-gain root locus is determined. Using a simple proportional gain for the discrete controller (P-control), the effects of different sampling rates that allow aliasing of the system are examined. Comparison between root loci, frequency response functions, impulse and step responses, and responses to sinusoidal inputs is made to a system with the same controller gain sampled at a fast sample rate to avoid aliasing. A sampling rate equal to the damped natural frequency of the second-order system is found to give excellent response and an optimal gain for this system with P-control is found. Robustness of this system is investigated.

3.1 ROOT LOCUS PRELIMINARIES

With the additional allowance of aliasing in the system, the sample period or time as it introduces aliasing now becomes a design parameter. One must also examine the effects of the design in the s*-plane, the plane in which poles and zeros incorporate both the continuous plant and the discrete controller.

For convenience in design, Equation 2.58, is repeated:

$$\frac{C(s)}{T_s R(z)} = \left[\frac{G_c num(z) Hden(z)}{G_c num(z) Hnum(z) + G_c den(z) Hden(z)}\right]\left[\frac{(1-e^{-sT_s})G_p num(s)}{(sT_s)G_p den(s)}\right] . \quad [3.1]$$

Now letting the controller be written as in Equation 2.53, but with a controller gain, K:

$$G_c(z) = K\frac{G_c num(z)}{G_c den(z)} \quad [3.2]$$

Grouping all the terms in Equation 3.1 which are functions of z and substituting Equation 3.2, define $F(z)$:

$$F(z) = \frac{KG_c num(z) Hden(z)}{KG_c num(z) Hnum(z) + G_c den(z) Hden(z)} \quad [3.3]$$

Finally, recalling the zero-order-hold times the plant is defined as $H(s)$, Equation 3.1 can now be written as

$$\frac{C(s)}{T_s R(z)} = F(z)\frac{H(s)}{T_s} \qquad [3.4]$$

Using Equations 3.2 and 3.3, the controller design will be accomplished in the digital or z-domain. However, the effects on the overall discrete-to-continuous transfer function must be examined as well. Therefore, the effects of z-plane controller design will be combined with the continuous plant effects in the s*-plane.

3.2 Root Loci at Gain Limits

Since the root loci in both the z- and s*-planes will be plotted, determination of trends as the gain of Equation 3.3 approaches zero and infinity needs to be made.

For the z-domain, in the limit as K approaches zero, the poles of $F(z)$ will approach the roots of $G_c den(z)$ and $Hden(z)$. Likewise, in the limit as K approaches infinity, the poles of $F(z)$ will approach the roots of $G_c num(z)$ and $Hnum(z)$. As in either the continuous or discrete cases, then, the poles of the root locus begin at the open-loop pole locations and migrate toward the open-loop zeros of the system. Notice, however, that this migration of the discrete poles is not toward the open-loop zeros of the continuous

system $Hnum(s)$, but toward the open-loop zeros of the discrete or sampled version of the plant $Hnum(z)$.

These results transform to the s*-plane as well, using the transformation of Equation 2.64. In other words, the root locus of the closed-loop system begins at the open-loop pole locations, found from $G_c * den(s)$ and $H * den(s)$, and migrate toward the open-loop zeros found from $G_c * num(s)$ and $H * num(s)$. In this case, however, the location of the poles from $Hden(s)$ and $H * den(s)$ are the same, even though the zeros of $Hnum(s)$ and $H * num(s)$ are different.

The root locus in the s*-plane will therefore include the following poles and zeros:

1. The poles and zeros from the continuous plant $G_p(s)$. These poles and zeros are stationary and will not move based on either controller gain or sample period selections.

2. The zeros from the zero-order-hold. These zeros will not move based on controller gain, but will repeat at intervals dependent upon T_s as described in chapter three.

3. The single pole of the zero-order-hold. It remains fixed at $s^* = 0$, but is always cancelled by one of the zeros of the zero-order hold which is at the same location.

4. The zeros from the numerator of the mixed term of the controller $F(z)$ transformed to the s*-plane ($F^*(s)$). These zeros will not move based on controller gain. In the s*-plane, they are located at the location of the open-loop poles of $H(s)$ and repeated at intervals dependent upon T_s as described in chapter three.

5. The poles from the denominator of the mixed term of the controller $F(z)$ transformed to the s*-plane ($F^*(s)$). These poles begin at the location of the open-loop poles and move toward the location of the open-loop zeros of $H^*(s)$, which, again, is different than $H(s)$.

3.3 THE SECOND-ORDER PLANT

Before determining the effect of sample period on the discrete-to-continuous system of the model developed in chapter three, the characteristics of a simple second-order plant will be examined.

Consider a plant that is lightly damped with two poles of the form

$$G_p(s) = \frac{\omega_n{}^2}{s^2 + 2\zeta\omega_n s + \omega_n{}^2} \quad . \qquad [3.4]$$

Easily recognizable are the locations of the poles in the s-plane:

$$s_{pole1,2} = \frac{-2\zeta\omega_n \pm \sqrt{(2\zeta\omega_n)^2 - 4\omega_n{}^2}}{2} = -\omega_n\left(\zeta \pm \sqrt{\zeta^2 - 1}\right) \quad . \qquad [3.5]$$

Note that for damping less than $\zeta = 1.0$ these poles are a complex conjugate pair.

Labeling these poles $-p_1$ and $-p_2$, Equation 3.4 can be rewritten as

$$G_p(s) = \frac{\omega_n{}^2}{(s + p_1)(s + p_2)} \quad . \qquad [3.6]$$

Using partial fraction expansion on Equation 3.6, divided by s in preparation for its z-transform with the zero-order hold applied, gives

$$\frac{G_p(s)}{s} = \omega_n{}^2\left(\frac{a_0}{s} + \frac{a_1}{s + p_1} + \frac{a_2}{s + p_2}\right) \quad , \qquad [3.7]$$

where

$$a_0 = \frac{1}{p_1 p_2} \quad , \tag{3.8}$$

$$a_1 = \frac{1}{p_1(p_1 - p_2)} \quad \text{, and} \tag{3.9}$$

$$a_2 = -\frac{1}{p_2(p_1 - p_2)} \quad . \tag{3.10}$$

Taking the z-transform of the plant, including the zero-order hold gives

$$Z\{G_p(s)\} = (1 - z^{-1})Z\left\{\frac{G_p(s)}{s}\right\} = (1 - z^{-1})Z\left\{\omega_n{}^2\left(\frac{a_0}{s} + \frac{a_1}{s + p_1} + \frac{a_2}{s + p_2}\right)\right\}$$

$$Z\{G_p(s)\} = (1 - z^{-1})\omega_n{}^2\left(\frac{a_0}{1 - z^{-1}} + \frac{a_1}{1 - e^{-p_1 T_s} z^{-1}} + \frac{a_2}{1 - e^{-p_2 T_s} z^{-1}}\right) \quad , \tag{3.11}$$

which, following algebraic manipulation, becomes

$$Z\{G_p(s)\} = H(z) = \frac{c_1 z + c_2}{(z + b_1)(z + b_2)} \quad , \tag{3.12}$$

where

$$b_1 = -e^{-p_1 T_s} \quad , \qquad [3.13]$$

$$b_2 = -e^{-p_2 T_s} \quad , \qquad [3.14]$$

$$c_1 = \omega_n{}^2 (a_0 - a_1 b_1 - a_2 b_2) \, , \text{ and} \qquad [3.15]$$

$$c_2 = \omega_n{}^2 (a_0 b_1 b_2 - a_1 b_2 - a_2 b_1) \quad . \qquad [3.16]$$

This system, then, becomes the basis for the designs to follow.

3.4 Design of a Proportional Controller Using Sample Period as a Design Parameter

Since the system consists of a mixture of continuous and discrete parts, it is advantageous to determine the effect of sample period T_s on the location of the poles and zeros in the z-plane, and the effect of these locations on the response of the system. Thus, the sample period T_s, or sample frequency ω_s, becomes a design parameter.

For the design to follow, the controller will be strictly proportional control,

$$G_c(z) = G_c^*(s) = K_p \quad . \qquad [3.17]$$

Solving for $F(z)$, the combined term of Equation 3.3,

$$F(z) = \frac{K_p(z+b_1)(z+b_2)}{K_P(c_1 z + c_2) + (z+b_1)(z+b_2)} \quad , \qquad [3.18]$$

where b_1, b_2, c_1, and c_2 are as defined in Equations 3.13 through 3.16. After algebraic manipulation, this equation becomes

$$F(z) = \frac{K_p(z+b_1)(z+b_2)}{z^2 + d_1 z + d_2} \quad , \qquad [3.19]$$

where

$$d_1 = K_p c_1 + b_1 + b_2 \quad , \text{and} \qquad [3.20]$$

$$d_2 = K_p c_2 + b_1 b_2 \quad . \qquad [3.21]$$

When the gain K_p is set to zero the poles of Equation 3.19 are located at $-b_1$ and $-b_2$, which also correspond to the locations of the open-loop poles, were they transformed to the z-plane. Plotting the location of these poles, referred to as zero-gain poles, as sample period T_s is varied produces Figure 3.1 below. For purposes of non-dimensionalization let $\overline{T_s} = T_s\omega_n$ and plot for changing $\overline{T_s}$. The value of damping was set to $\zeta = 0.1$.

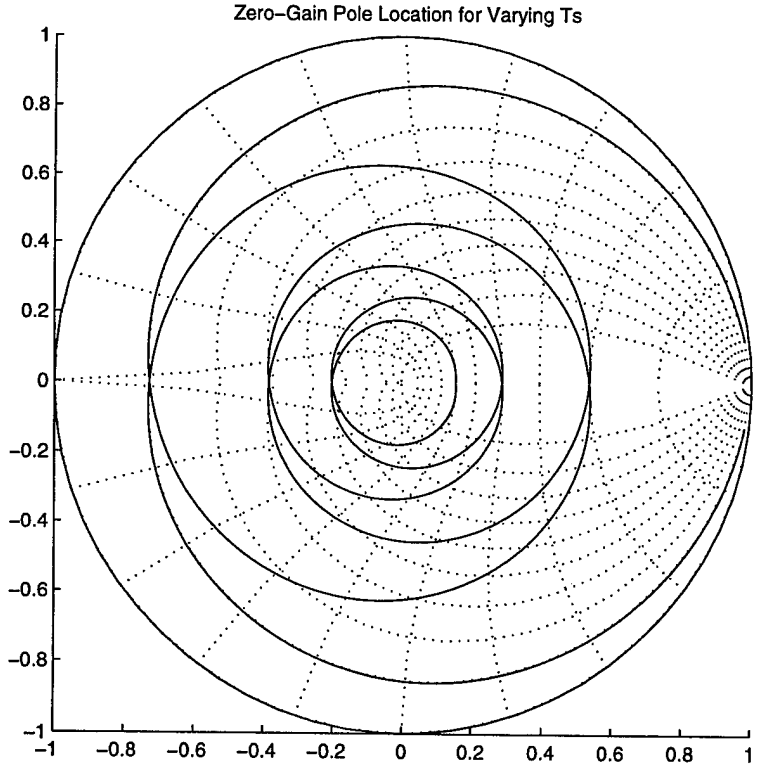

Figure 3.1 $\overline{T_s}$ Root Locus of Zero-Gain Poles in Z-Domain

In the z-plane, as $\overline{T_s}$ increases the locations of the zero-gain poles move in a logarithmic spiral inward from $z=1$ at $\overline{T_s}=0$ toward $z=0$ at $\overline{T_s}=\infty$. In the s*-plane, a relationship exists between the crossings of the real axis and the location of the infinitely repeated plant poles within the bands. This relationship will be explored further later.

In examining Figure 3.1, one may question if, given the need for allowing aliasing, there exist locations within the z-plane where the discrete-to-continuous system response is more desirable than other locations. In other words, given aliasing, can the designer select a sample period that will produce better results than by selecting some other sample period? To examine this, we will look at several classic tools used to evaluate designs, including root loci in both the z- and s*-planes, magnitude and phase plots of frequency response functions, and continuous and discrete responses to an impulse, step, and sinusoidally varying inputs. The proportional controller of Equation 3.17 will be employed with gain $K_p=0.15$ to ensure stability. Examination of this simple system will aid in seeing some trends otherwise not seen as clearly.

To non-dimensionalize the plots to follow, define the frequency ratio (FR) as

$$FR=\frac{\omega_s}{\omega_d} \quad , \qquad [3.22]$$

where ω_d is the damped natural frequency:

$$\omega_d = \omega_n \sqrt{1-\zeta^2} \quad . \qquad [3.23]$$

For comparison purposes of the aliased system, Figures 3.2 through 3.5 are plots of the system for $FR = 50$, where the discrete portion of Equation 3.19 is basically continuous—i.e., no aliasing is present. Notice from Figure 3.2 the limited amount of

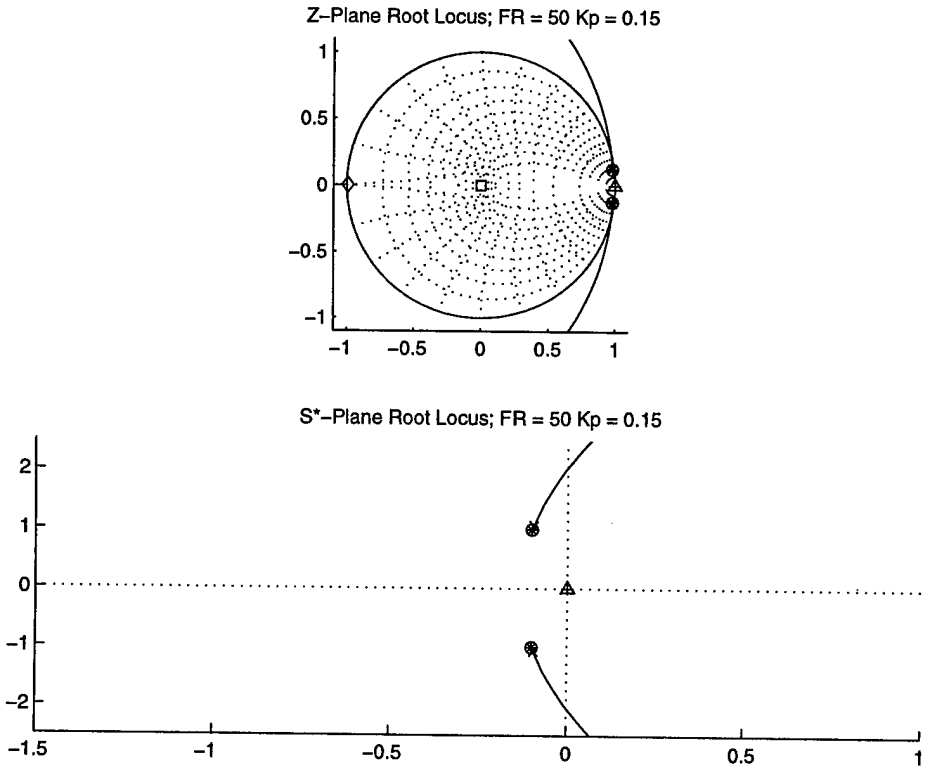

Figure 3.2 Root Loci for FR = 50, K_p = 0.15

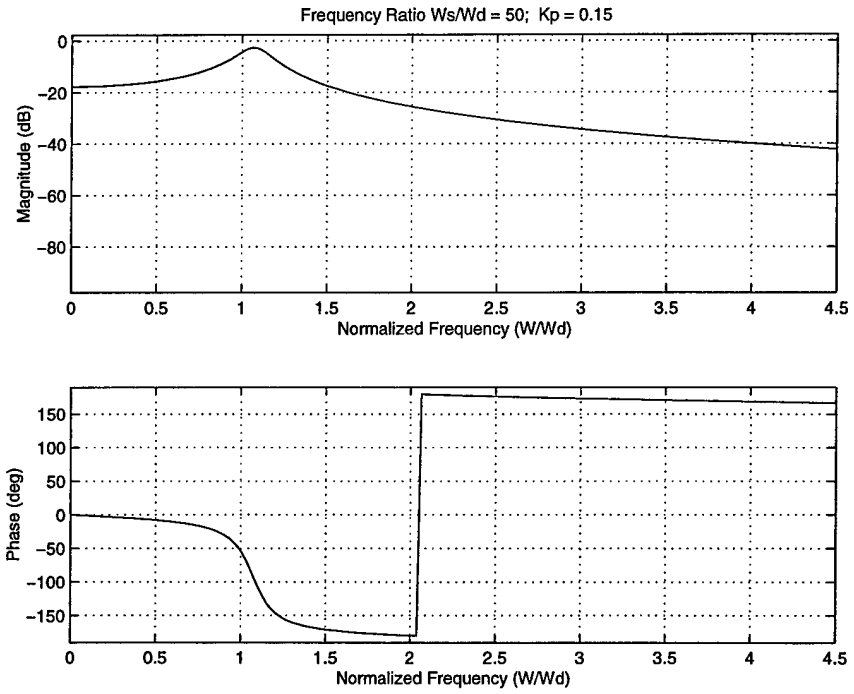

Figure 3.3 Frequency Response Function Plot for FR = 50, $K_p = 0.15$

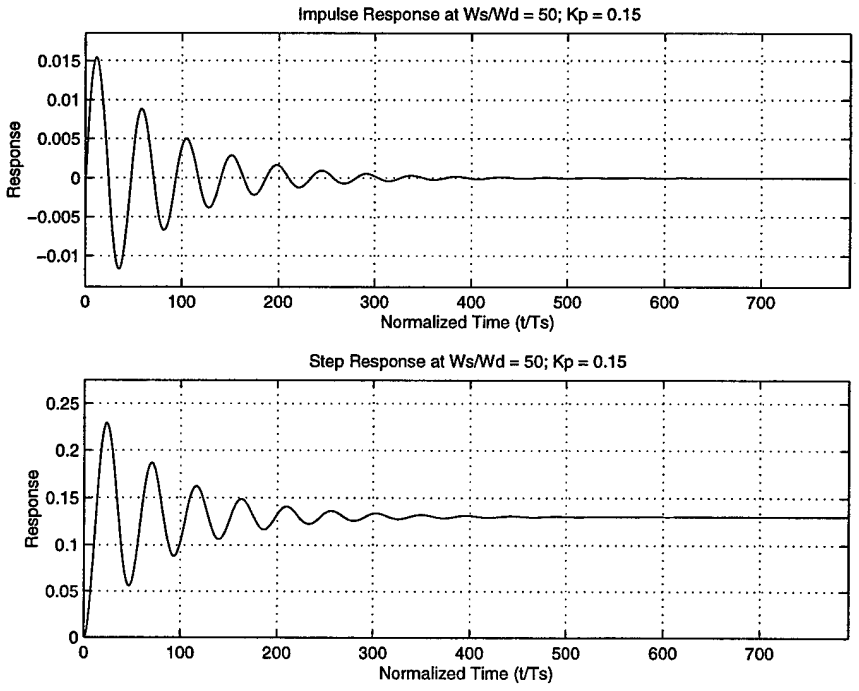

Figure 3.4 Impulse and Step Responses for FR = 50, $K_p = 0.15$

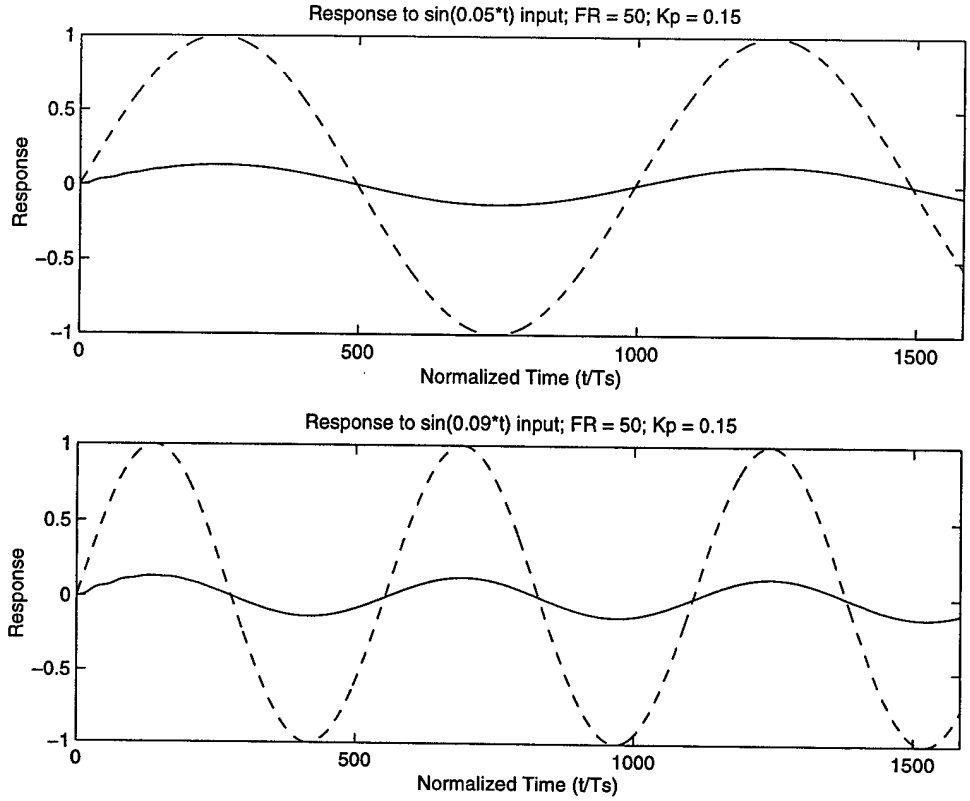

Figure 3.5 Response to Sinusoidal Inputs for FR = 50, $K_p = 0.15$

gain before instability occurs. Figure 3.3 shows the classical frequency response function plot of a second-order system, with a magnitude peak at the plant natural frequency along with the phase passing through -90° at that point, as well. The impulse and step responses of the system are shown in Figure 3.4, showing the characteristics of the lightly damped system. Finally, Figure 3.5 shows how well the closed-loop system responds to the sinusoidal inputs shown as dashed lines.

Figures 3.6 through 3.9 show the root loci for varying FR, and thus varying T_s. These correspond to frequency ratios of $\frac{2}{1.0}$, $\frac{2}{1\frac{1}{3}}$, $\frac{2}{1\frac{2}{3}}$, and $\frac{2}{2.0}$, which are even steps of frequency ratios around the second loop of Figure 3.1.

The symbols for these root loci are as follows. The triangle and plus symbols represent the zeros and pole, respectively, of the zero-order hold. The square and asterisks represent the zeros and poles, respectively, of the continuous plant, $G_p(s)$. Although in reality these do not exist in the z-plane, they are shown there for clarity. The diamond represents the zero of the $H(z)$. Again, this term does not exist in the s*-plane, but is shown there for clarity. The circles and "x's" respectively represent the zeros and poles at the given gain of the mixed term $F(z)$ or $F^*(s)$, which includes the controller and the discretized plant with the zero-order hold. The solid line represents the locus of the poles of the mixed term for all values of K_p. Finally, in the s*-plane the dashed lines represent the "band" boundaries, which equate to multiples of the folding frequency. Thus, $-\frac{\omega_s}{2}$ to $+\frac{\omega_s}{2}$ represents the primary band, $-\frac{3\omega_s}{2}$ to $-\frac{\omega_s}{2}$ and $+\frac{\omega_s}{2}$ to $+\frac{3\omega_s}{2}$ represent the secondary band, and so on.

With the sampling rate such that the frequency ratio is 2.0 the damped natural frequency is located at the folding frequency, and the entire z-plane root locus lies on the negative real axis. The plots of the system root loci for this frequency ratio are shown in

Figure 3.6. A gain of $K_p = 0.15$ was selected to ensure stability, and one can see that, although they are close to the stability boundaries, the poles of Figure 3.6 do indeed lie within the stability boundaries of the unit circle in the z-plane and the negative left-half plane in the s*-plane.

The entire root locus lies entirely upon the real axis in the z-plane. Although not easily discernable, the zero from $H(z)$, and therefore $H^*(s)$, lie directly on top of the zeros of $F(z)$ and the open-loop poles of $G_p(s)$. Thus, one of the poles of $F(z)$ does not move at all, a phenomenon that will be discussed later. The remaining pole moves from the closed-loop zero toward infinity, as predicted by gain limit analysis.

Additionally, one can graphically see here, as well as in Figures 3.7 through 3.9, the proof that one set of the closed-loop zeros cancels the open-loop poles, as proved mathematically in chapter three (Equation 2.49), in both the z-plane and s*-plane root loci. In the s*-plane, the open-loop poles, closed-loop zeros, and the zeros of $H(z)$ all lie on the band boundaries: the frequencies corresponding to multiples of the folding frequency. A frequency ratio of $FR = 2.0$, then, causes the entire root locus to lie on the real axis of the z-plane and on band boundaries of the s*-plane.

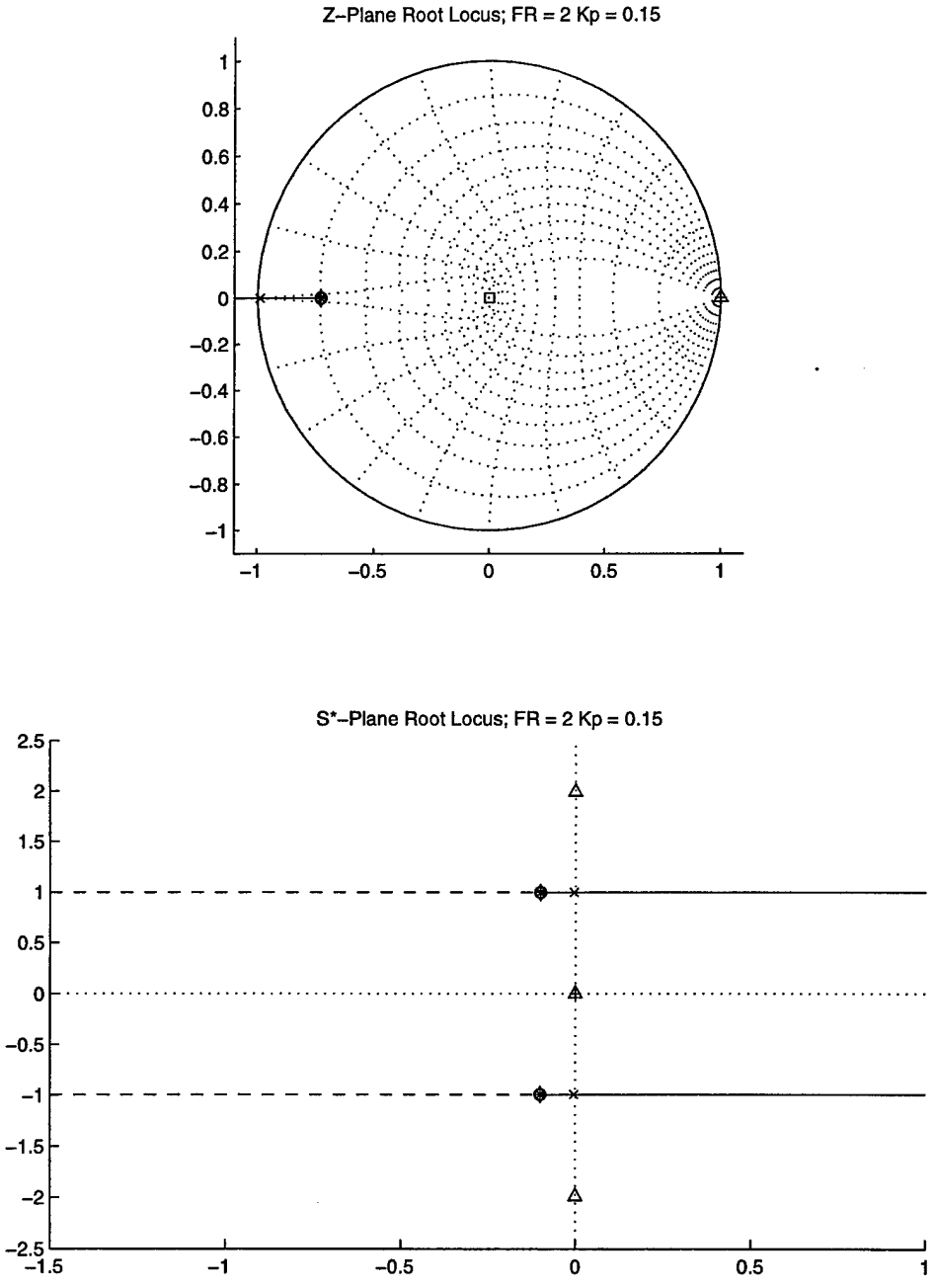

Figure 3.6 Root Locus – FR = 2.0, $K_p = 0.15$

One last thing to recognize about Figure 3.6 is the limited amount of gain allowed before the stability boundary is reached. With this small gain, however, the closed-loop pole has moved quite a distance from the closed-loop zeros. Both these facts speak to the robustness of this design.

Figures 3.7 and 3.8 show the root loci for frequency ratios of 1.5 and 1.2, values of frequency ratios that "move" the location of the zero-gain poles around the second loop of Figure 3.1. Notice in the s*-plane the open-loop poles fall between the boundaries of the secondary bands, indicating that aliasing is occurring. If there were no aliasing, these poles would remain within the primary band. As further and further aliasing occurs, these poles will move to bands further and further from the primary band. Moreover, as the frequency ratio decreases (sample period increases) the size of all the bands decreases, in effect "moving" the open-loop poles, and hence the zero-gain poles, to different locations within the bands. One may note these poles are moving toward the center of the band, which corresponds to multiples of the sampling frequency.

Further examination of the s*-plane root loci show that, indeed, the closed-loop poles begin at the location of the closed-loop zeros—the zeros of $F(z)$ are correspondingly the open-loop poles of $G_p(s)$—and migrate toward the open-loop zeros of $H(z)$.

Another effect of increasing the sampling period identifiable from the Figures is that of the decreasing effect of the gain K_p, since the poles, given the same gain of $K_p = 0.15$,

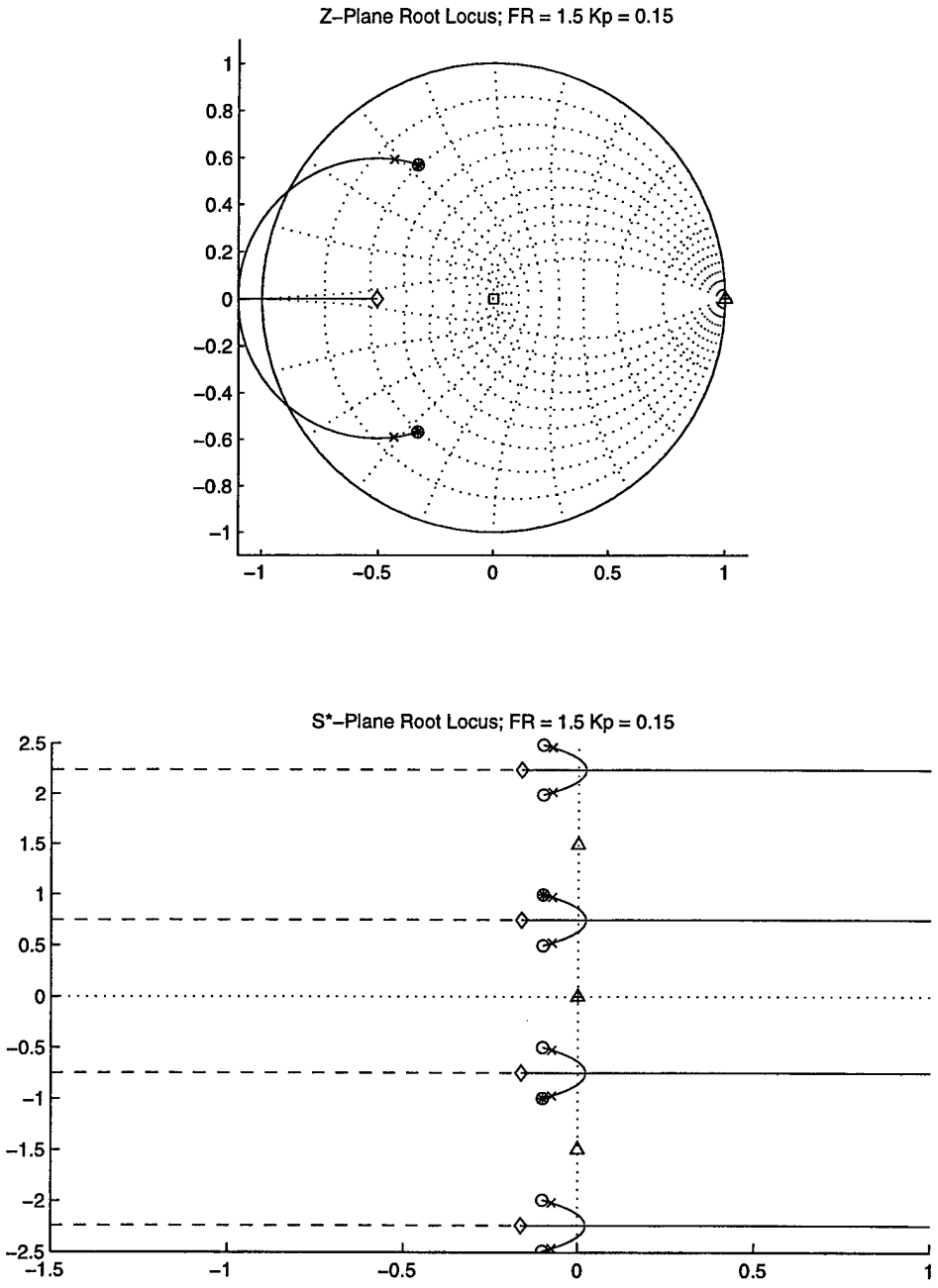

Figure 3.7 Root Locus – FR = 1.5, $K_p = 0.15$

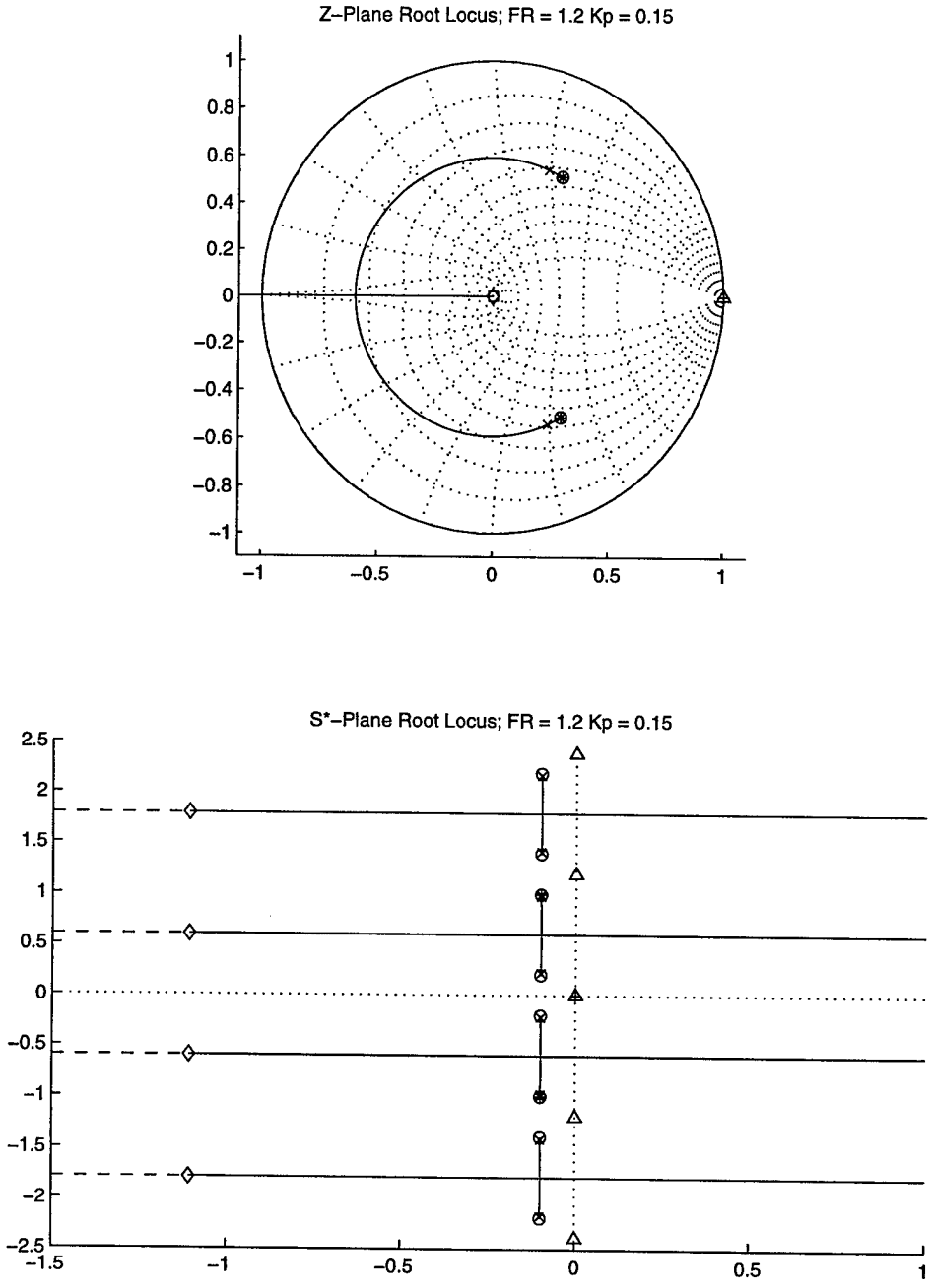

Figure 3.8 Root Locus – FR = 1.2, $K_p = 0.15$

move less and less distance from the closed-loop zeros. This would tend to indicate an increased robustness with increased aliasing! This fact will be explored further later.

Finally, Figure 3.9 shows the root loci for a frequency ratio of 1.0. Notice the similarities between these root loci and the root loci of Figure 3.6. The entire root locus lies on the real axis in the z-plane. Here again, one of the closed-loop poles lies directly on top of one of the closed loop zeros, and remains at the location of the open-loop zero of $H(z)$.

The mathematics behind this stationary pole follow: recall the definition of $H(z)$ of Equation 3.12, repeated here for clarity:

$$H(z) = \frac{c_1 z + c_2}{(z + b_1)(z + b_2)} \quad , \qquad [3.24]$$

where b_1, b_2, c_1, and c_2 are as defined in Equations 3.13 through 3.16. At the frequency ratios of interest, $FR = \frac{2}{1.0}$ and $FR = \frac{2}{2.0}$, the entire root locus lies on the real axis.

In this case,

$$b_1 = b_2 = b \quad . \qquad [3.25]$$

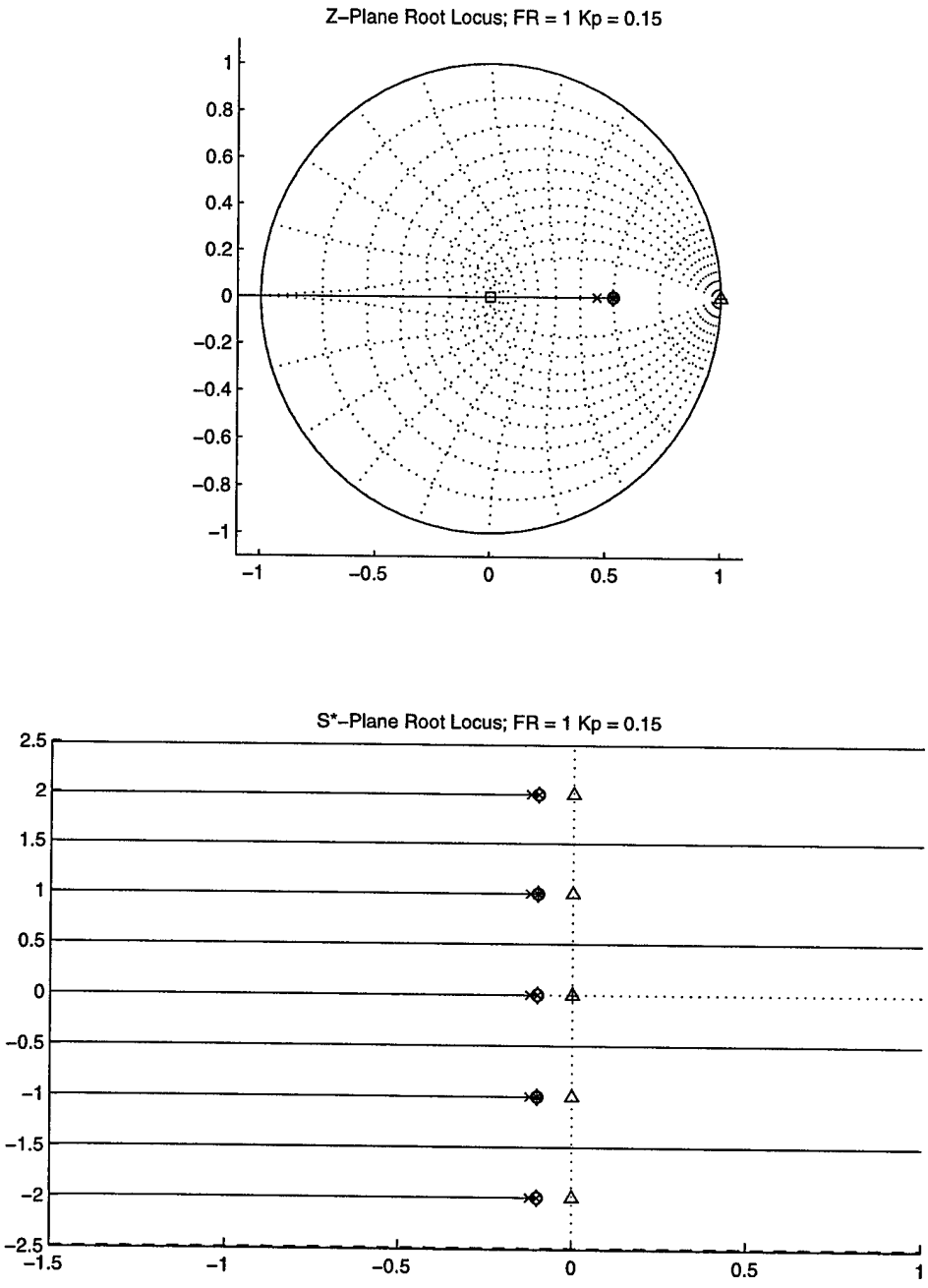

Figure 3.9 Root Locus – FR = 1.0, $K_p = 0.15$

The zero of $H(z)$ is found from setting the numerator term of Equation 3.24 equal to zero:

$$zero = \frac{-c_2}{c_1} = 0 = \frac{\omega_n{}^2(a_1 b + a_2 b - a_0 b^2)}{\omega_n{}^2(a_1 b + a_2 b - a_0)} \quad . \qquad [3.26]$$

Equation 3.26 is easily simplified using a relationship found from Equations 3.8 through 3.10:

$$a_1 + a_2 = -a_0 \quad . \qquad [3.27]$$

Substituting Equation 3.27 into Equation 3.26 and canceling gives:

$$zero = \frac{(a_1 + a_2 - a_0 b)b}{a_1 b + a_2 b - a_0} = \frac{(-a_0 - a_0 b)b}{-a_0 b - a_0} = b \quad , \qquad [3.28]$$

which from Equation 3.19 is the value of the closed-loop zeros. Hence, the open-loop zero of $H(z)$ is located at the same point as the closed-loop zeros and the open-loop poles, and one of the closed-loop poles remains at this point.

The motion of the other closed-loop poles, however, is somewhat different in this case since the closed-loop zeros are located together on the positive real axis. Because of this, the second closed-loop pole will travel through the point $z = 0$, which corresponds to the

pole moving through infinity in the s*-plane. At that point, a shift occurs because of the nature of the natural logarithm of a complex number (chapter two). As z approaches $z = 0$ from the negative side of the real axis, its natural logarithm has an argument equal to π. Once z crosses to the positive side of the real axis, the argument of its natural logarithm equals 0. This fact is seen in the s*-plane as the pole travels toward $-\infty$ along the band boundaries, corresponding to an argument of π, then "returns" from $-\infty$ along the mid-band line, corresponding to an argument of 0. Hence, in the s*-plane, the second pole travels toward $-\infty$ along the mid-band line then returns along the band boundary. This mid-band to band boundary "jumping" will occur anytime the zero of $H(z)$ lies on the positive real axis of the z-plane.

Finally, recall the s*-plane root loci for the system in which $FR = \frac{2}{1.0}$ was entirely on the line separating bands, the lines corresponding to multiples of the folding frequency. Similarly here the open-loop poles, the closed-loop zeros, and the zero of $H^*(s)$ with its accompanying closed-loop pole all lie on the mid-band line: the line corresponding to multiples of the sampling frequency. One can see that unique things occur when the root loci lie on these lines.

These unique things occur at specific frequency ratios. The frequency ratios of interest correspond to the real axis crossings of the zero-gain root locus of Figure 3.1. The crossings of the real axis occur at multiples of the frequency ratio defined by the following equation:

$$FR_{crossing} = \frac{2}{n} \quad , \qquad n = 1,2,3,\ldots \qquad [3.29]$$

In the z-plane, if n of Equation 3.29 is odd the root locus lies entirely on the negative real axis. The zero of $H(z)$ lies on top of the open-loop poles and the closed-loop zeros, which are all located at the same spot. One of the closed-loop poles also lies at this point, since it starts at the closed-loop zero and travels to the open-loop zero of $H(z)$. Additionally, the other pole travels along the negative real axis toward infinity, the other zero of $H(z)$. Since both closed-loop zeros are located on the negative real axis, neither pass through the point $z = 0$.

If n is even, the entire root locus lies partially on the positive and partially on the negative real axis. Again, the zero of $H(z)$ lies on top of the open-loop poles and the closed-loop zeros, and, with one of the closed loop poles, all are located at the same spot. The other pole travels along the real axis toward infinity, passing through the point $z = 0$.

These same trends are evident in the s*-plane. However, if n of Equation 3.29 is odd, the open-loop poles, closed-loop zeros, and closed-loop poles are all located on band boundaries, corresponding to integer multiples of the folding frequency. If n is even, however, the open-loop poles and closed-loop zeros are located on the mid-band line, corresponding to integer multiples of the sampling frequency. The one traveling pole will also move toward infinity along this mid-band line, but return along the band boundary line.

Movement of the open-loop poles within the bands of the s*-plane is also dependent upon the frequency ratio. This "movement" is a measure of how much the poles are aliased. Traditionally, aliasing has been thought of as the folding and addition of components of the frequency response when these components are not equal to zero outside of the folding frequency. Here, however, we wish to discuss the aliasing of poles, or the movement outside of the primary band of the poles causing the response. This type of aliasing will hereafter be referred to as "pole-aliasing." When thinking of pole-aliasing, think of the poles transformed from the z-plane to the s*-plane and repeated infinity through all bands.

Little aliasing as defined traditionally is present for frequency ratios much greater than $FR = 2.0$, the aliasing boundary according to Nyquist. At this boundary, however, aliasing is already occurring, unless the signal is a pure sinusoid. Before this boundary, pole-aliasing does not occur. These frequency ratios correspond to the first half-loop of Figure 3.1 from $z = 1$ to the point it meets the negative real axis. The open-loop poles are located within the primary band for these frequency ratios as well. At $FR = 2.0$, the open-loop poles lie on the boundary between the primary and secondary bands. This is the boundary for pole-aliasing.

As the frequency ratio is decreased, the open-loop poles move farther into the secondary band. These changes correspond to traveling along the second loop of Figure 3.1 until the positive real axis is reached at a frequency ratio of $FR = 1.0$. At this point, the open-loop poles are located in the exact middle of the frequency band. Now as the frequency

ratio is decreased, corresponding to the third loop of Figure 3.1, the poles travel again toward the band boundary and will reach it when the frequency ratio is $FR = 0.67$. The special characteristics of the response at the frequency ratios of Equation 3.29 will continue to be seen through the remaining plots and examined in greater detail below.

Figures 3.10 through 3.13 show the magnitude and phase plots of the discrete-to-continuous frequency response functions of the system for the same frequency ratios. The effects of aliasing are clearly discernable in these plots. Figure 3.10, corresponding to a frequency ratio of 2.0, shows the dominant peak of the damped natural frequency located at the folding frequency. The effect of the zero-order hold can be seen at multiples of the sampling frequency, $\frac{\omega_s}{\omega_d} = 2,4,\ldots$. Notice that as the frequency ratio decreases, the aliasing becomes prevalent in the additional peaks seen in the magnitude plots. Finally, in Figure 3.13 see the disappearance of any peak in the magnitude plot of the system with frequency ratio equal to 1.0. It appears that by selecting a correct sampling frequency, a response cancellation occurs. This is indeed the case, as will be shown later.

Finally, examination of the phase plots of Figures 3.10 through 3.13 shows that increased aliasing tends to linearize the phase plots. The phase plot of Figure 3.13 seems much more linear than the phase plot of Figure 3.10, although this is also a function of the gain margin differences.

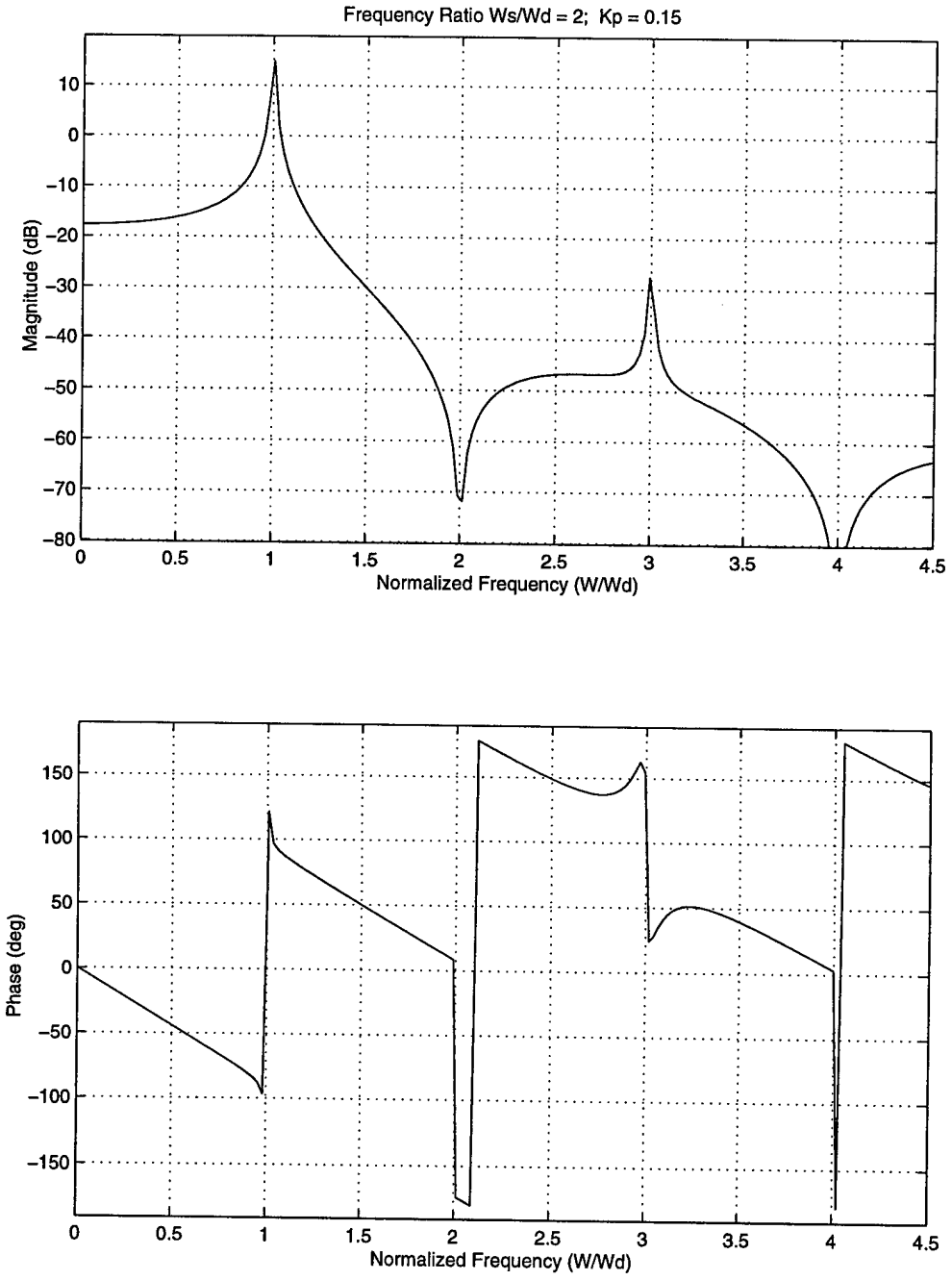

Figure 3.10 Frequency Response Function Plot – FR = 2.0, $K_p = 0.15$

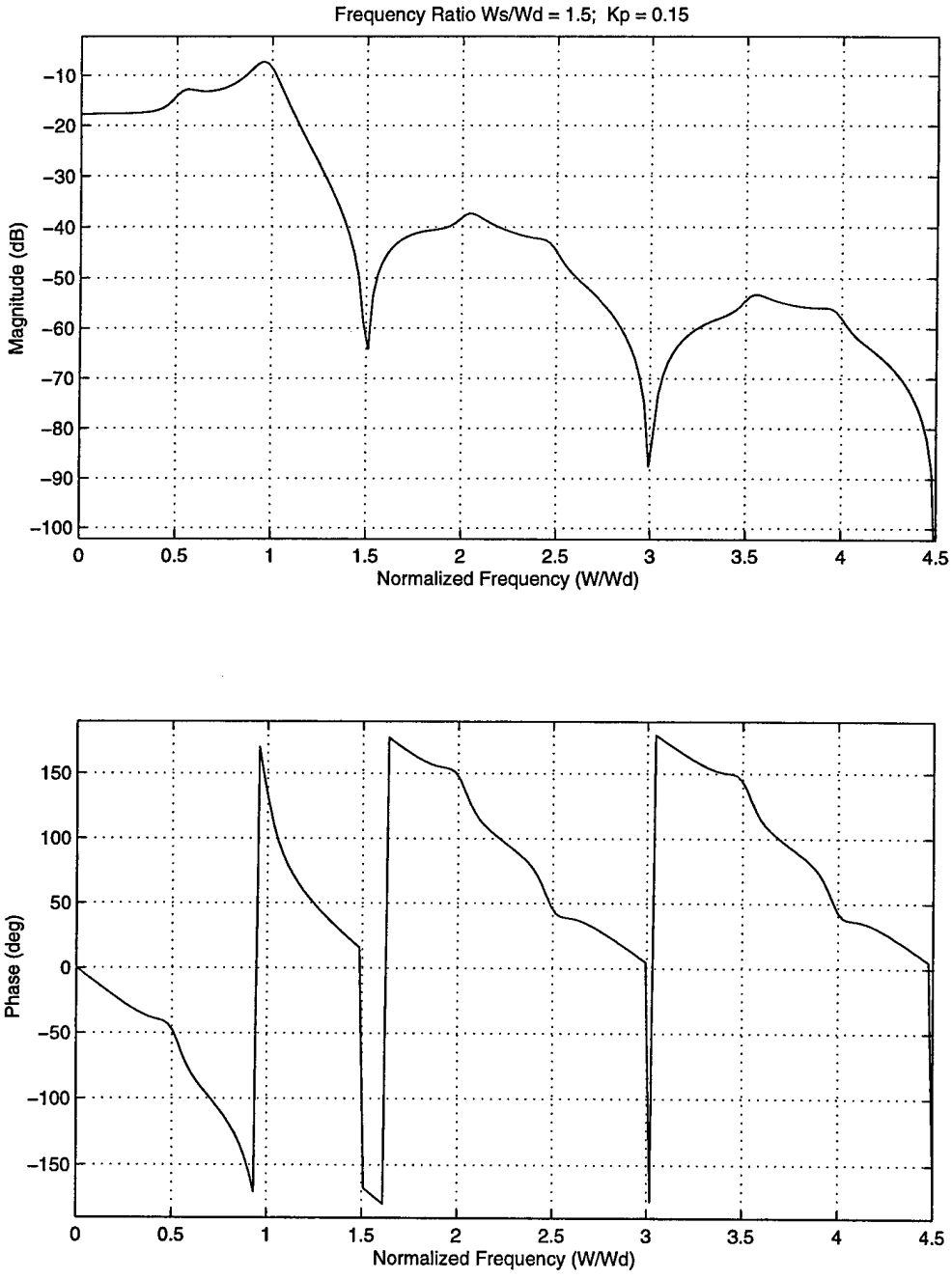

Figure 3.11 Frequency Response Function Plot – FR = 1.5, $K_p = 0.15$

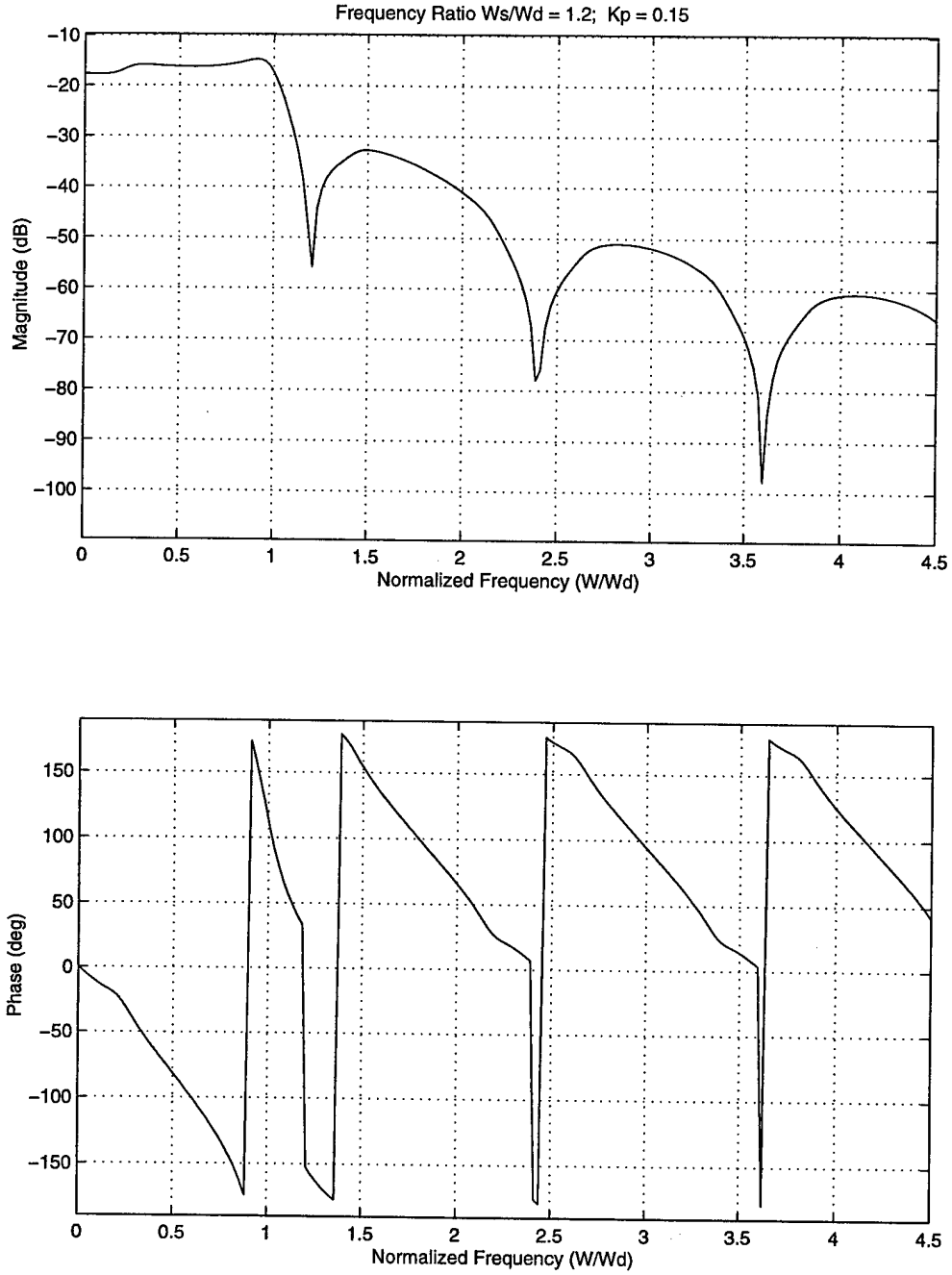

Figure 3.12 Frequency Response Function Plot – FR = 1.2, $K_p = 0.15$

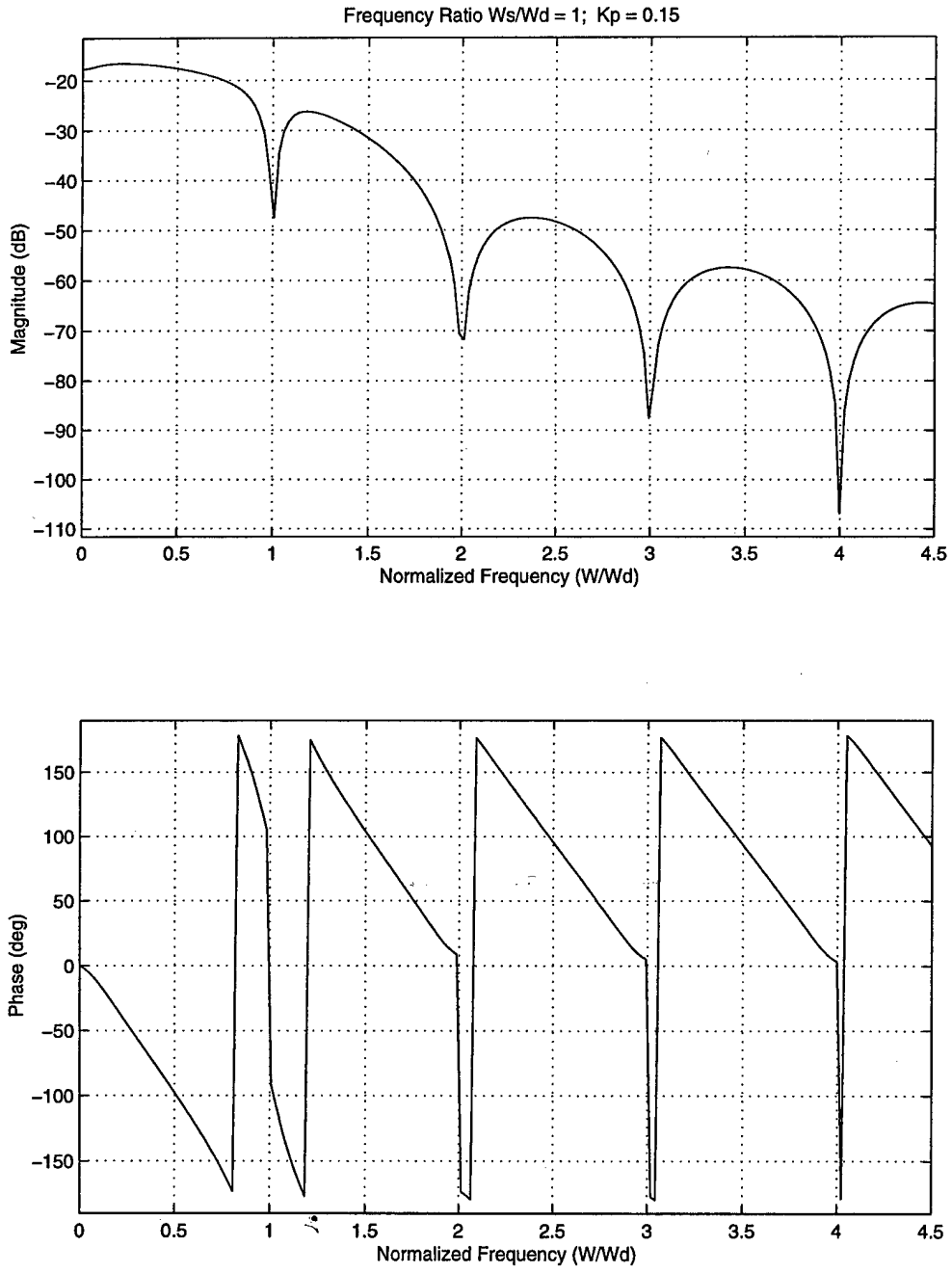

Figure 3.13 Frequency Response Function Plot – FR = 1.0, $K_p = 0.15$

Figures 3.14 through 3.17 show the impulse and the step responses for the frequency ratio changes of the systems represented by root loci in Figures 3.10 through 3.13. Here the solid line represents the response of the continuous plant (or continuous output). The asterisks represent the discrete response, or the response the controller sees. Responses here show the same trends visible in the root loci and frequency response function plots.

Figure 3.14 shows the responses of the system with a frequency ratio of 2.0. Based on a location of the poles in the z-plane root locus the response of the discrete system should be a lightly damped sinusoidal response, which is indeed the case. For both the impulse and step responses, the response is much worse than the "continuous" responses of Figure 3.3. The magnitude of the initial pulse of the impulse response is greater by a factor of almost 20. Although the magnitude of the step response is only slightly larger, the number of oscillations to obtain its final value is very much greater.

As the frequency ratio decreases in Figures 3.15 through 3.17, both impulse and step responses improve. Note the magnitudes of the responses' initial "pulses" remain the same, but the normalized settling time improves greatly. Additionally, discrete responses (dashed lines) are as would be predicted given the pole locations in the z-plane [33:351-353]. The continuous responses, however, are those of the continuous

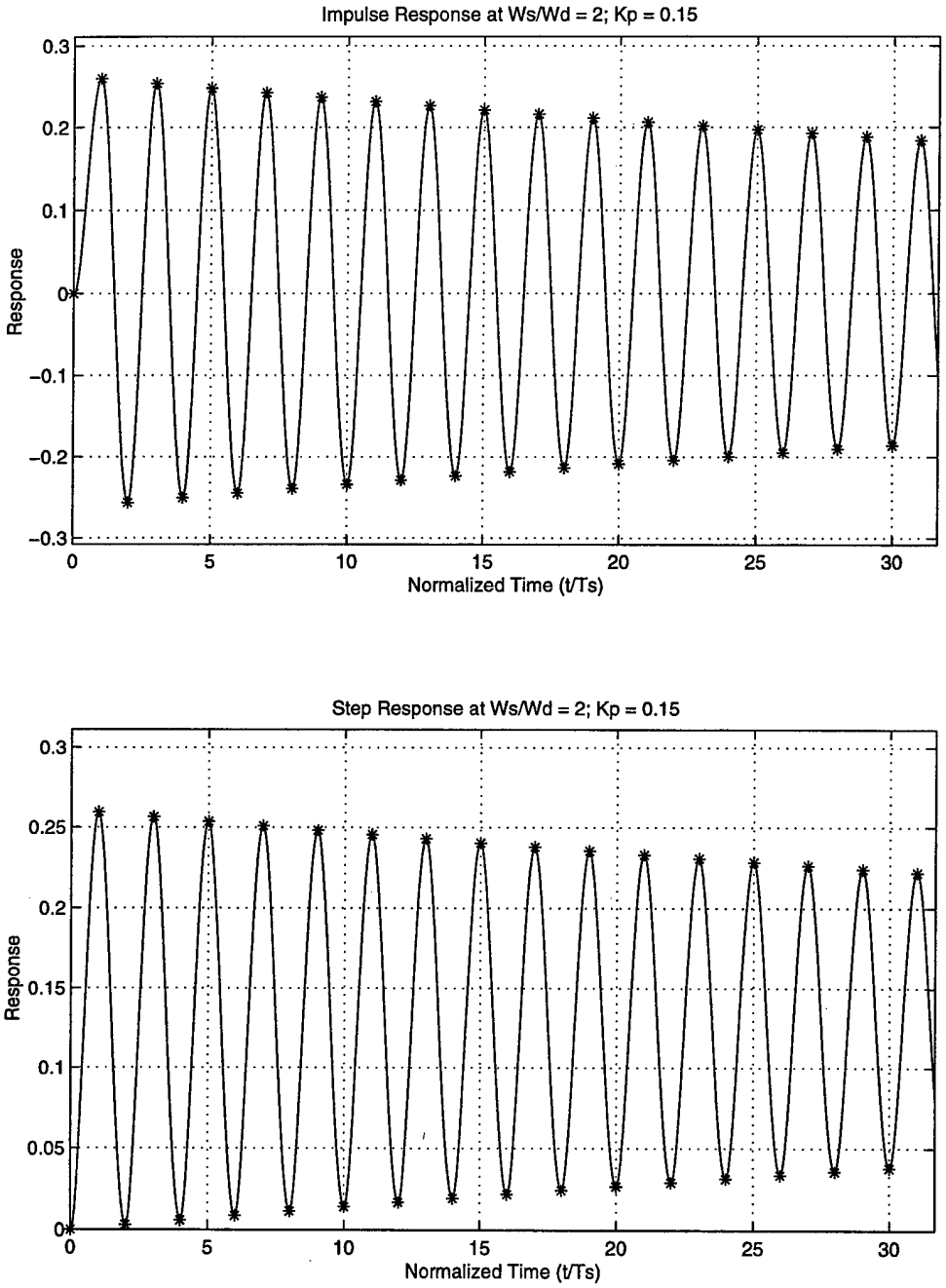

Figure 3.14 Impulse and Step Responses – FR = 2.0, $K_p = 0.15$

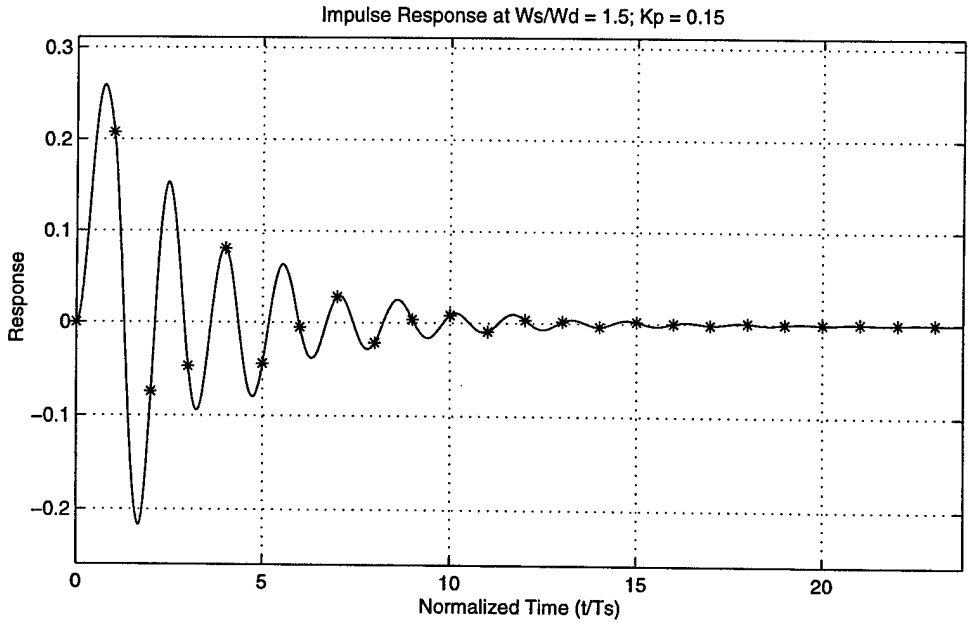

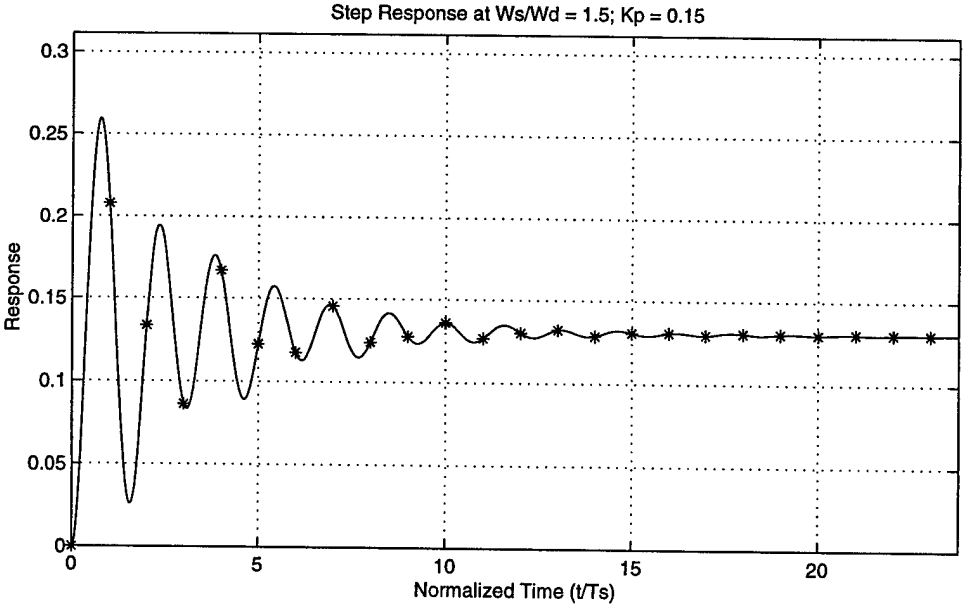

Figure 3.15 Impulse and Step Responses – FR = 1.5, $K_p = 0.15$

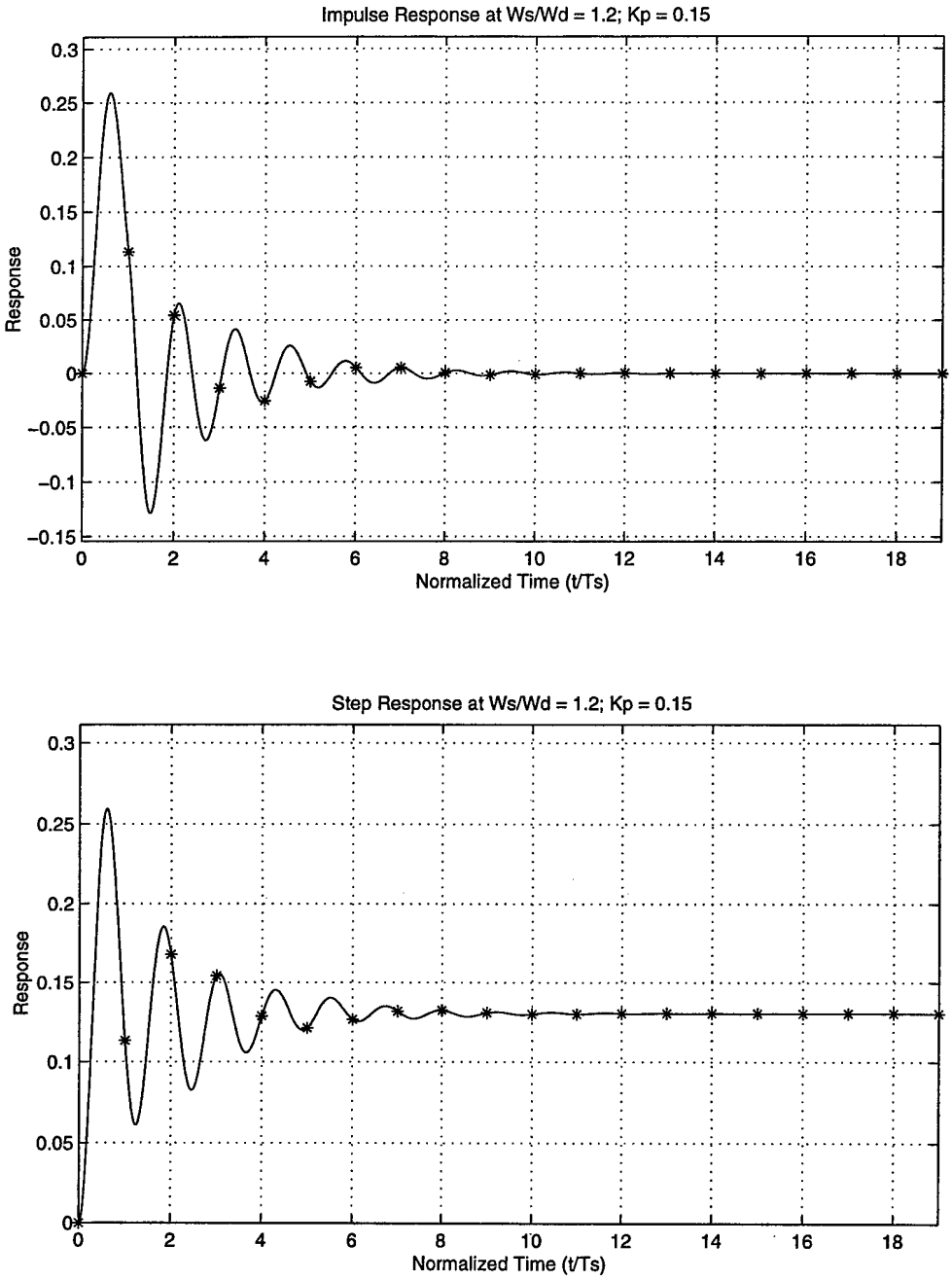

Figure 3.16 Impulse and Step Responses – FR = 1.2, $K_p = 0.15$

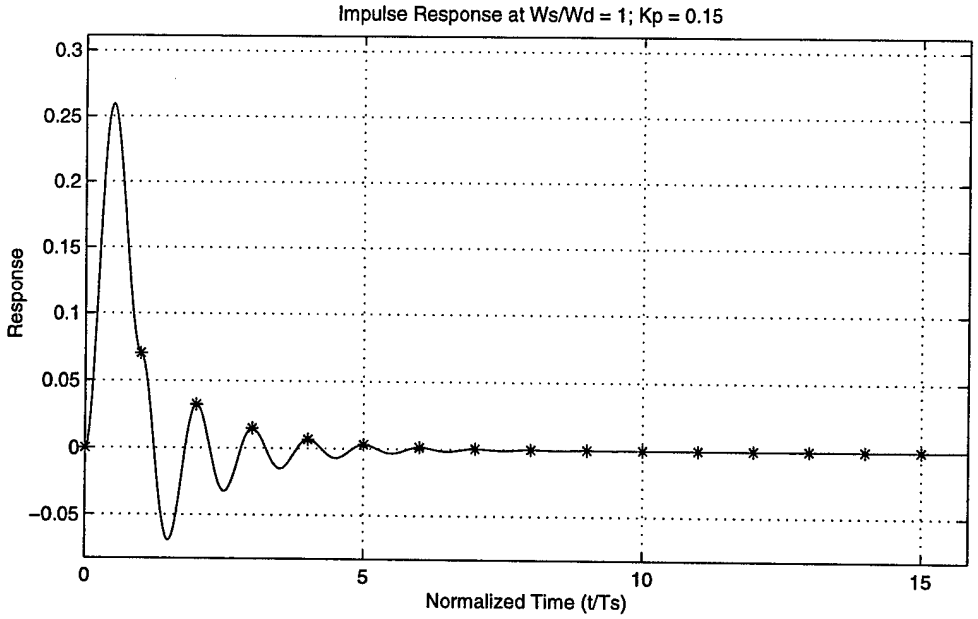

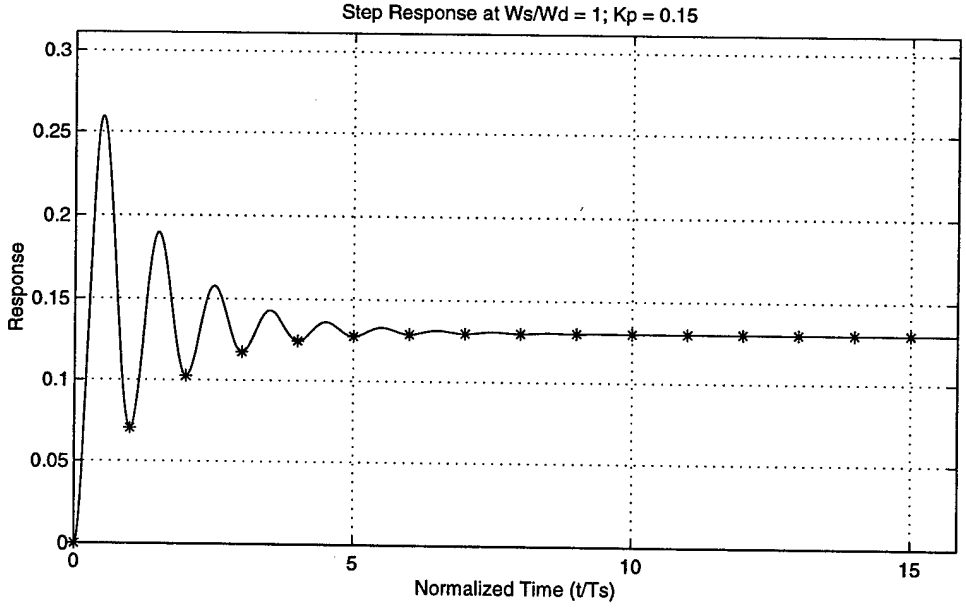

Figure 3.17 Impulse and Step Responses – FR = 1.0, $K_p = 0.15$

plant. In both cases, the continuous response is that of step inputs at the sample periods with the added initial conditions caused because of previous plant response.

The continuous response, then, is the open-loop response of the plant to a step input with the given initial conditions. This open-loop response is the damped sinusoidal response given from the open-loop poles located where they are in the s*-plane. How can this be, given these poles are essentially cancelled by one set of closed-loop zeros?

This phenomenon appears to be similar to Gibb's phenomenon [35:740-741]. In taking an infinite Fourier series of a function, a "ringing" appears at the discontinuity produced by truncating the series. Taken one step farther, if one term were eliminated from this series, the result would be a sinusoid of the frequency of the eliminated term. This is illustrated for the following. The Fourier series for a square wave is given as

$$f(x)=\frac{2}{\pi}\sum_{n=1}^{\infty}\frac{1-(-1)^n}{n}\sin(nx) \qquad [3.30]$$

This equation is plotted in Figure 3.18 with 200 (essentially ∞) terms included. It is plotted again in Figure 3.19 with the tenth term missing. The result is the sine wave superimposed on the square wave. The absence of the term in the infinite sum makes the presence of the term in the response.

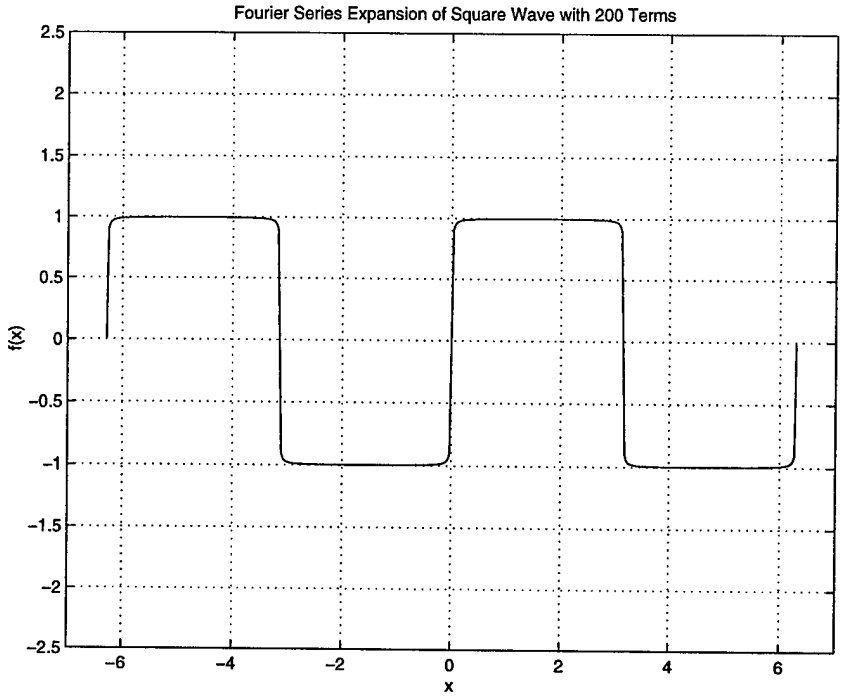

Figure 3.18 Fourier Series of a Square Wave

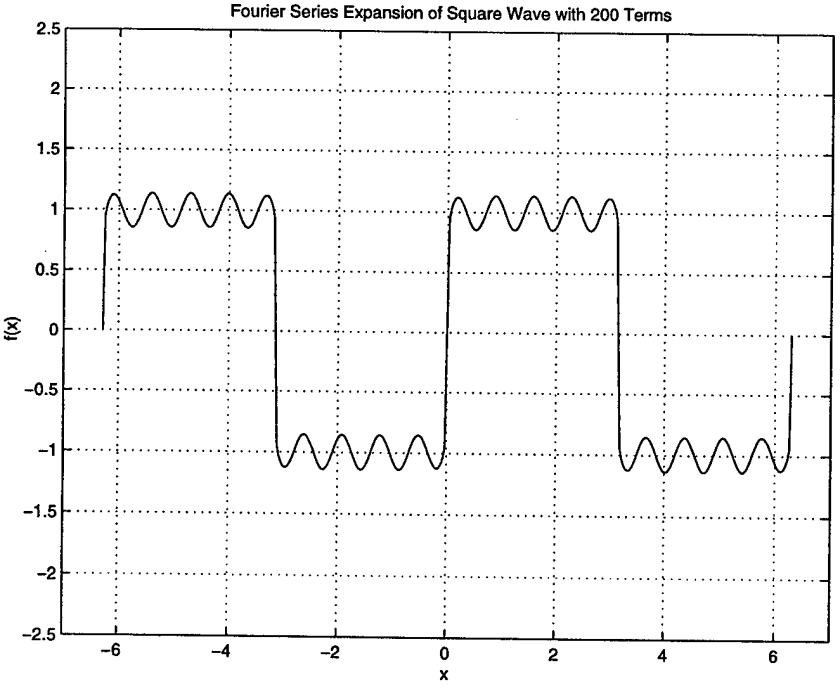

Figure 3.19 Fourier Series of a Square Wave With One Missing Term

Similarly, with the closed-loop zeros repeated infinitely in the s*-plane their effect is to "eliminate" the frequency at that point. When these zeros are cancelled by the open-loop poles, the effect is to eliminate all the harmonics of that frequency, except that one which will show up in the continuous response of the system.

Examining Figures 3.14 through 3.17 show the effect changing the sample period has on the continuous response. It is also easy to see that certain frequency ratios give better responses than others. Indeed, frequency ratios corresponding to $FR = \frac{2}{n}$ for $n = even$ give better response than those in which $n = odd$. These correspond to closed-loop zeros located on the positive real axis in the z-plane, with the corresponding location of these zeros on the mid-band line in the s*-plane.

Figure 3.20 shows a comparison of the impulse and step responses of the discrete-to-continuous system at the frequency ratios discussed above. Notice that by slowing the sample rate one may actually improve the system response, a fact opposite to common practice of improving response by sampling faster.

The fact that the continuous response between samples is that of the open-loop plant is more easily seen as the sample rate is further decreased, thus allowing more aliasing.

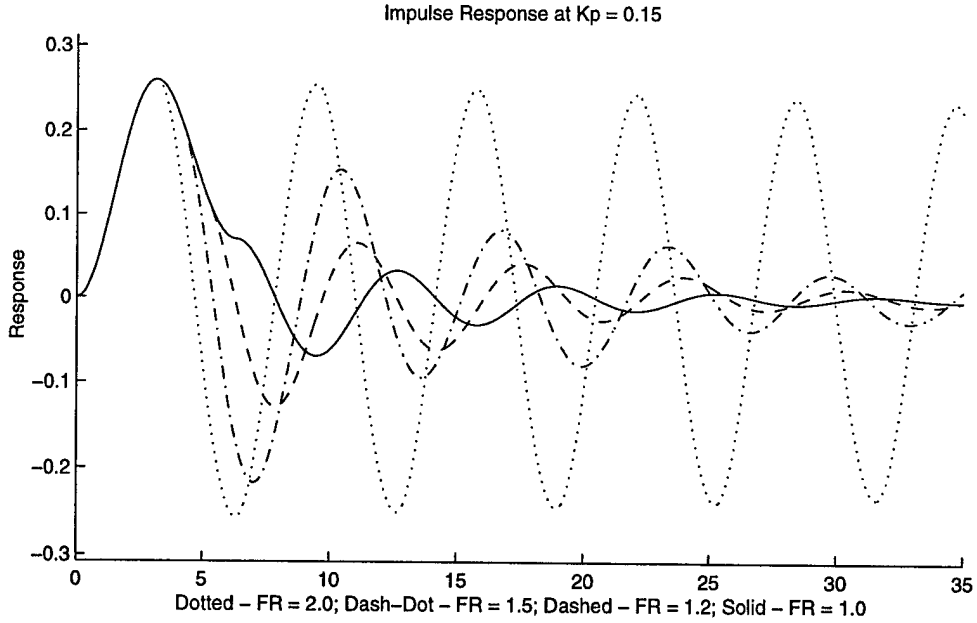

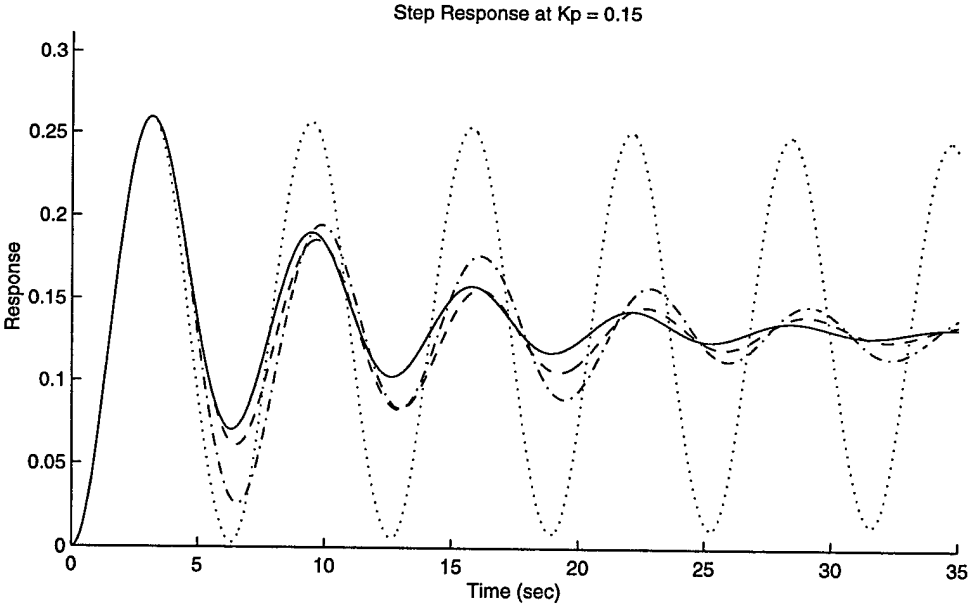

Figure 3.20 Comparison of Impulse and Step Responses for Varying Sample Rate

Figure 3.21 shows the responses of the discrete-to-continuous system when the frequency ratio is set to $FR = \frac{2}{6.0}$, corresponding to open-loop poles located in the quaternary band. Easily discernable in the impulse and step responses are three cycles of the open-loop response between sample periods. Thus as stated before, the continuous response consists of a series of step responses, given the initial conditions which correspond to the open-loop's response at the sample period. Since the controller has no capability of controlling between sample periods, this free response of the system will always be present with no possibility of control between sample periods.

Figures 3.22 through 3.25 show the response of the discrete-to-continuous system to two different frequency sine waves. The discrete response remains essentially unchanged from the "continuous" (or non-aliased) case of Figure 3.5, while the continuous response seems to worsen for the smaller frequency ratios. One can see the increased magnitude of the continuous response as the frequency ratio decreases from $FR = 2.0$ to $FR = 1.0$.

The sinusoidal responses show the drawback of allowing aliasing. The controller can only control the system at the sample periods. It can do nothing for the continuous response between samples. The continuous output between sample periods, as discussed before, is the damped natural response of the open-loop plant. Nothing can be done to control this response with an aliased discrete-to-continuous system, and the responses of the system to sinusoidal input seen in Figures 3.22 through 3.25 again reaffirm this.

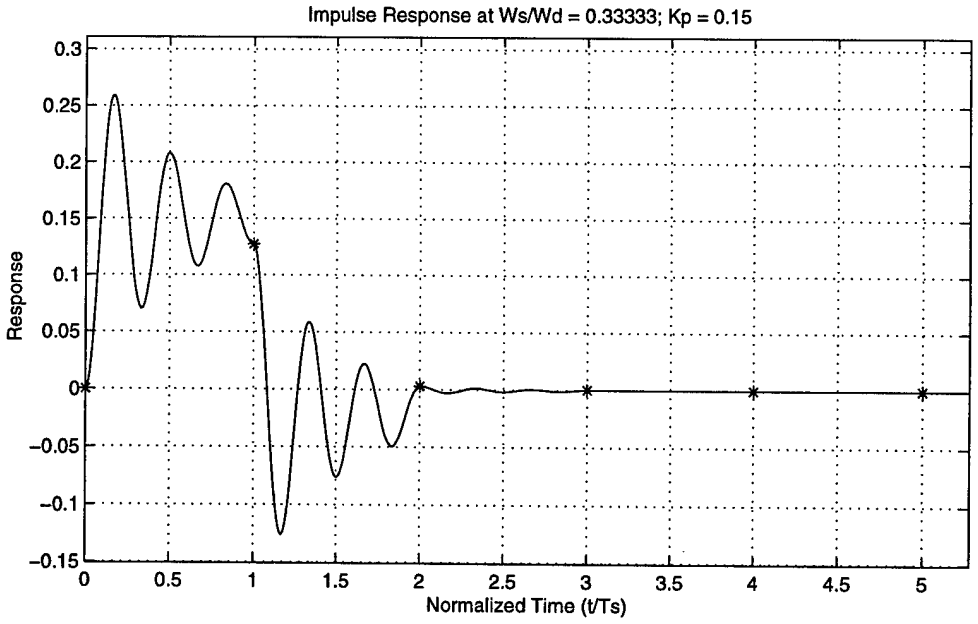

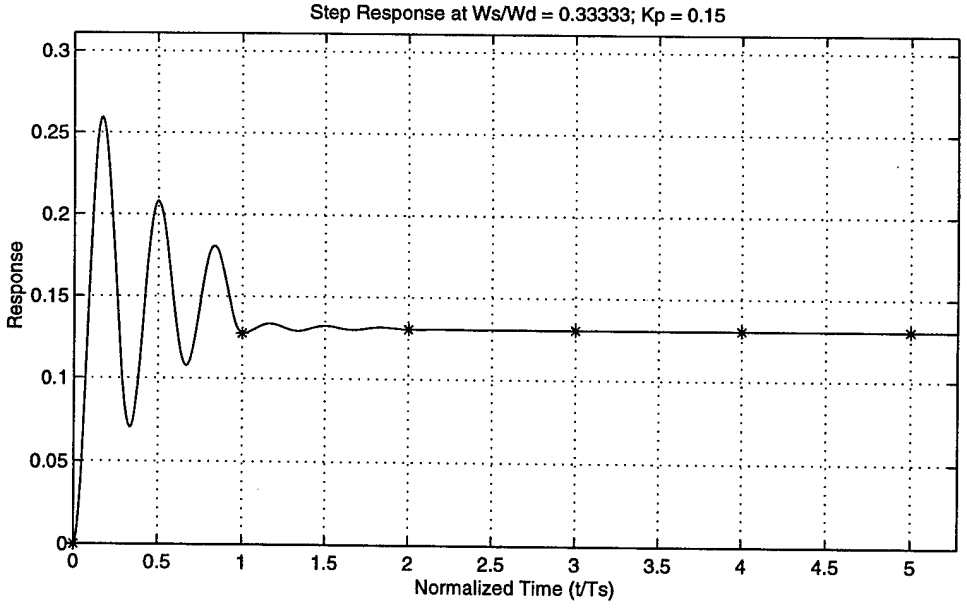

Figure 3.21 Impulse and Step Responses – FR = 0.33, $K_p = 0.15$

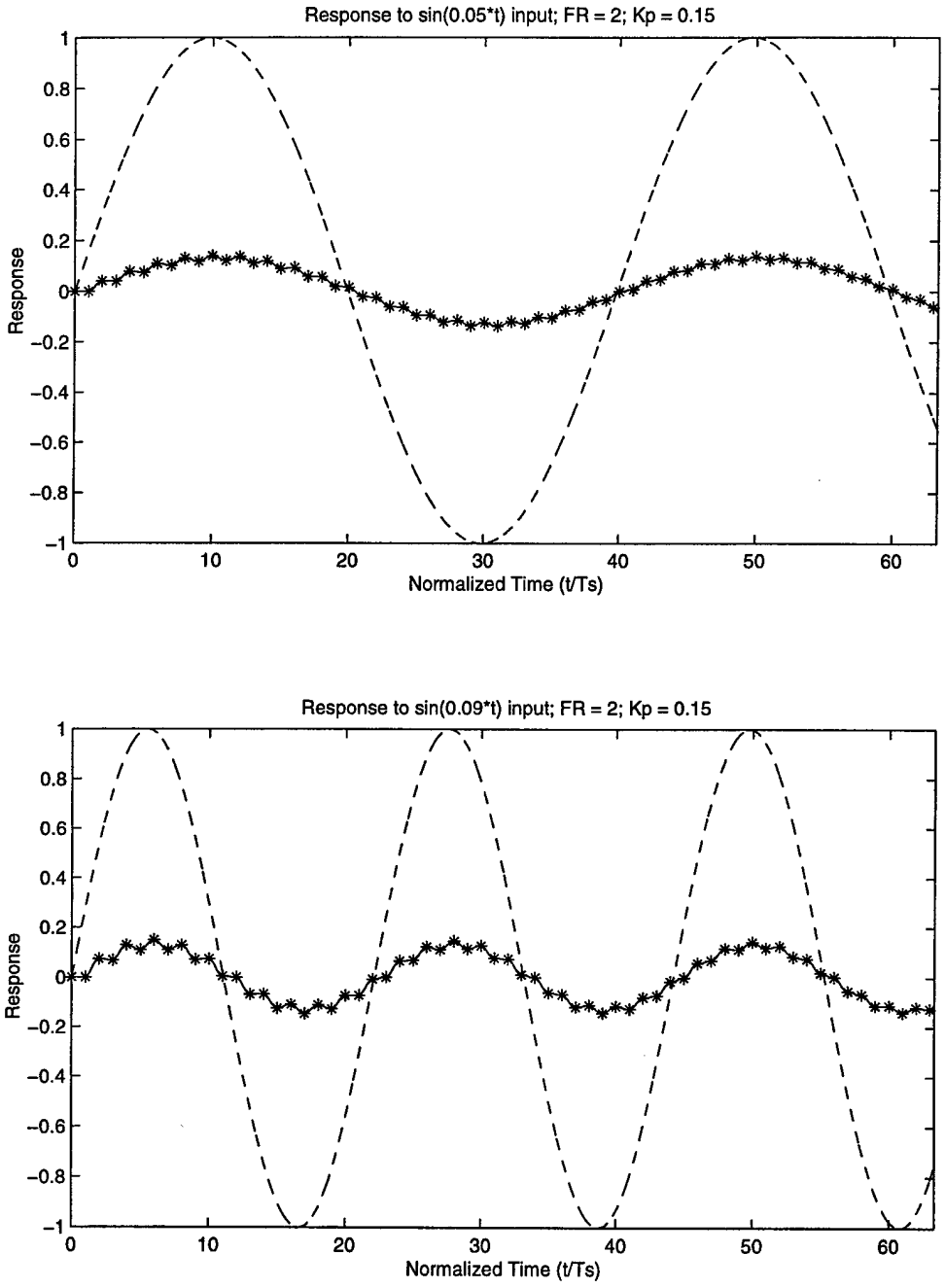

Figure 3.22 Sinusoidal Responses – FR = 2.0, $K_p = 0.15$

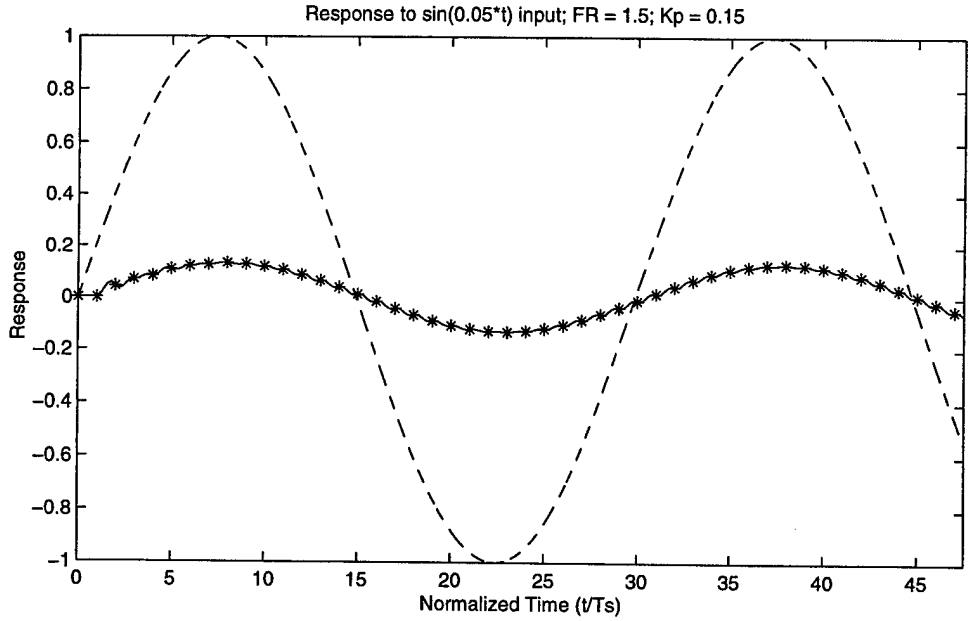

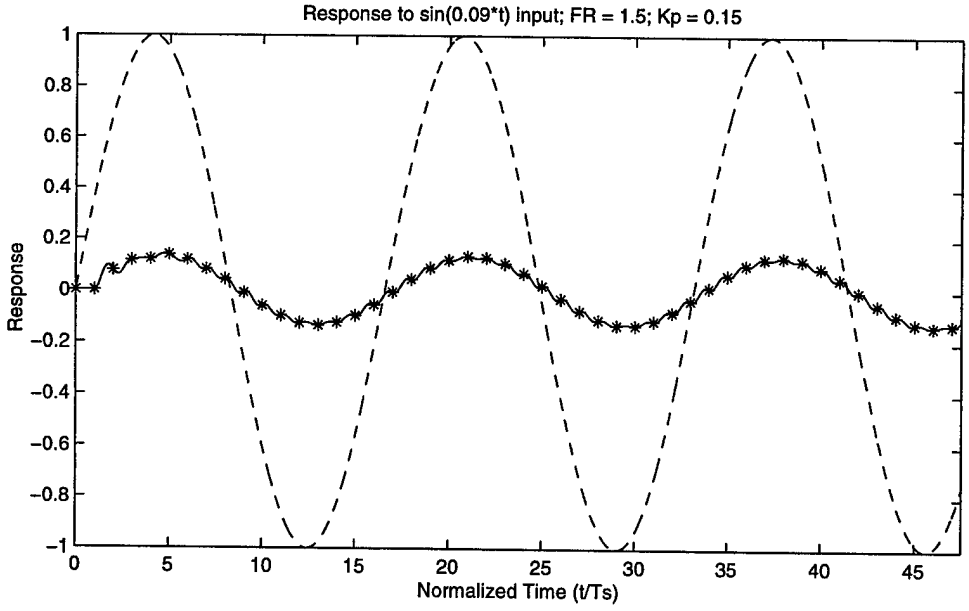

Figure 3.23 Sinusoidal Responses – FR = 1.5, $K_p = 0.15$

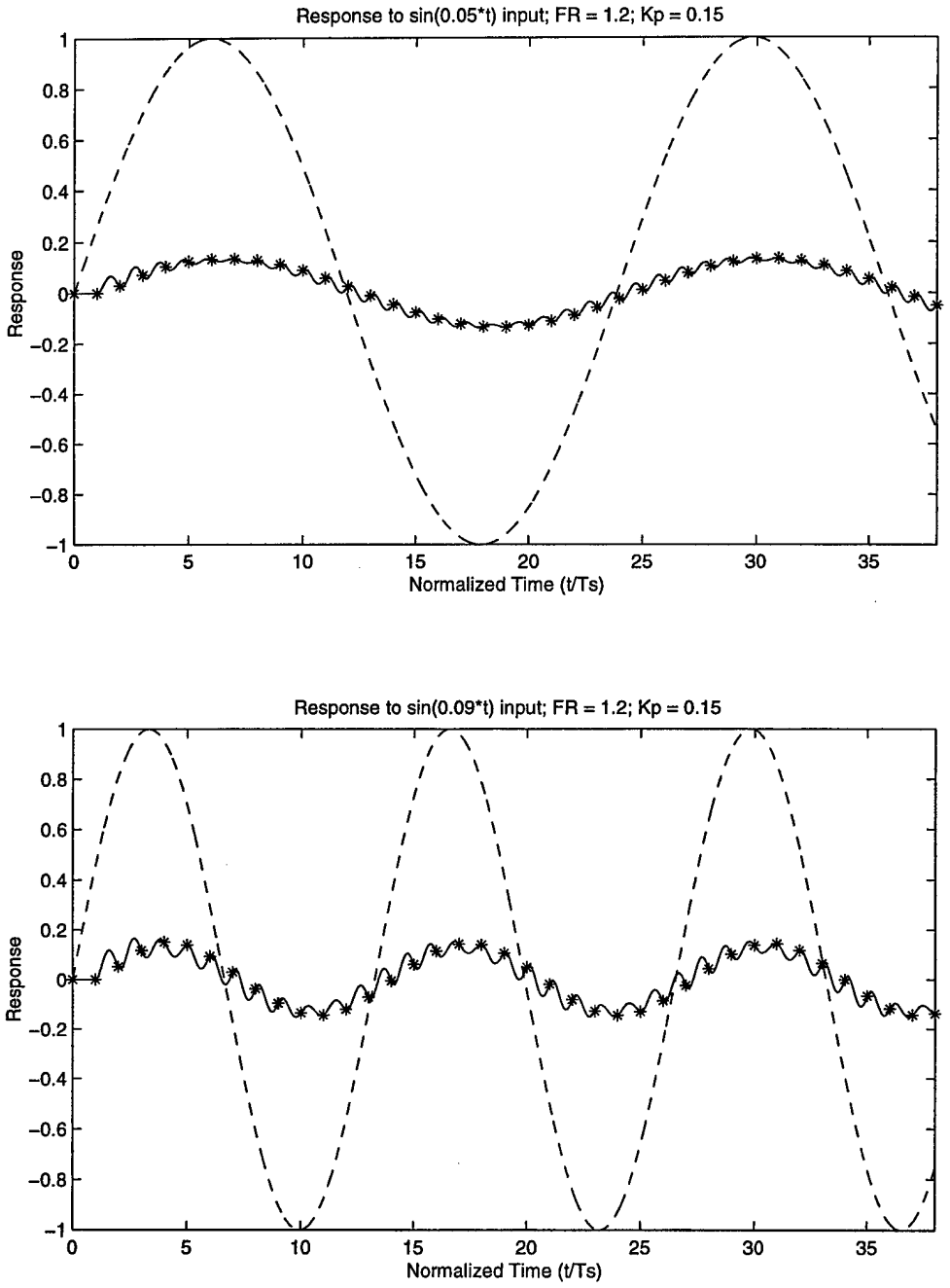

Figure 3.24 Sinusoidal Responses – FR = 1.2, $K_p = 0.15$

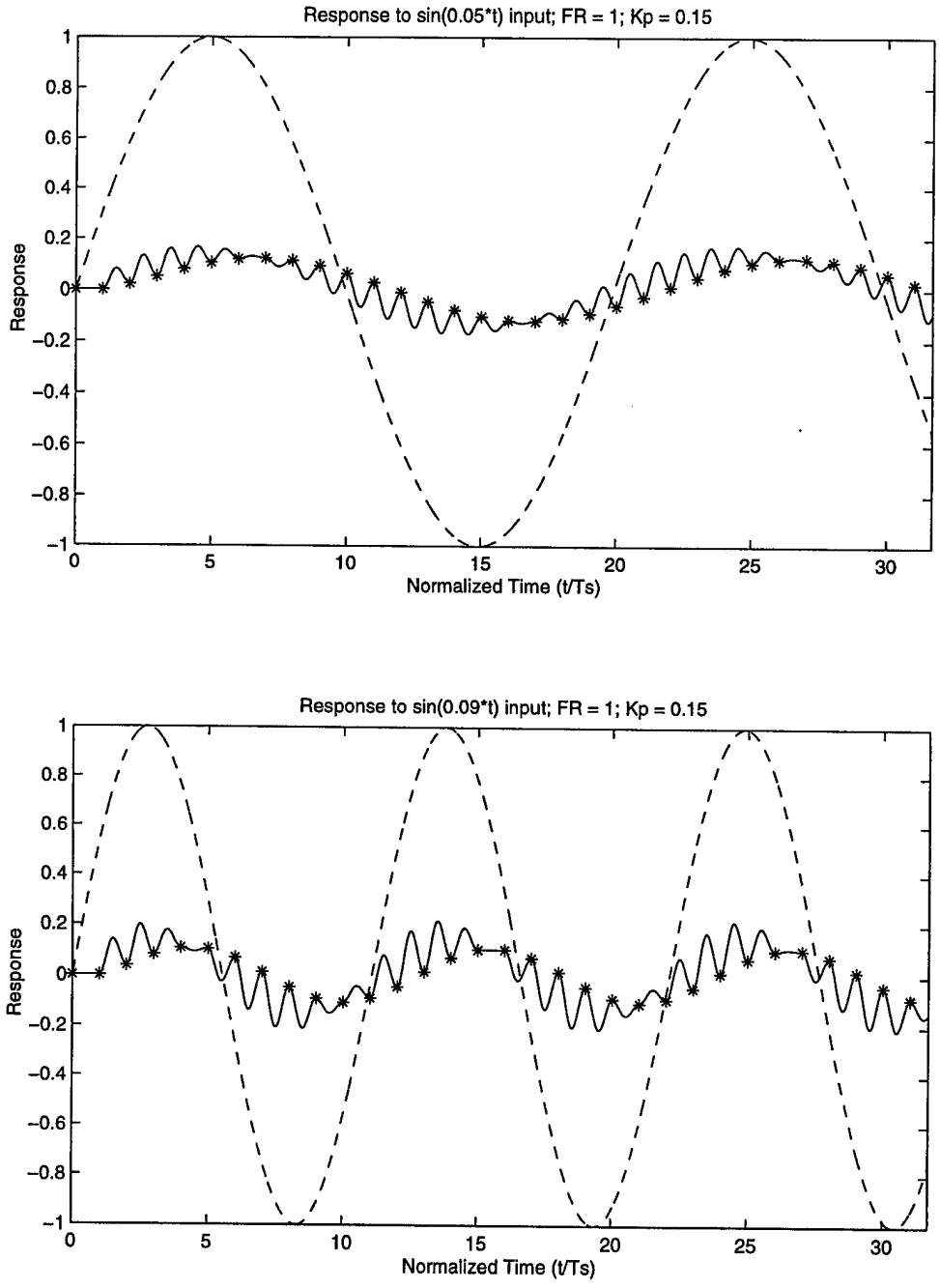

Figure 3.25 Sinusoidal Responses – FR = 1.0, $K_p = 0.15$

3.5 Optimal Proportional Controller Design at FR = 1.0

With the preliminary examination of sample period effects on the discrete-to-continuous system with proportional control complete, it is obvious that, indeed, the designer who must allow aliasing can judiciously select a sample rate that will improve performance. Particularly, the sample rates such that $FR = \frac{2}{n}$, $n = even$, give superior results to those in which the sample rates are such that $n = odd$. In both cases the entire root loci lie entirely on the real axis in the z-plane. However, only when $n = even$ does the root locus lie partially on the positive real axis. Additionally, in the s*-plane for these cases the root loci lie on either the band boundaries or the mid-band line, with $n = even$ equating to lying on the mid-band line and giving the better response. Also, in the frequency domain the frequency response function plots show that when $n = even$ the sampling to damped natural frequency ratio is such that the zeros of the zero-order hold are located at the same frequencies as the damped natural frequency, another reason for improved response.

The drawback when aliasing is allowed is the controller has no control over system response between sample periods, as discussed earlier. The more aliasing allowed in the system, the more the system will respond between sample periods.

Given the restraints above, it appears the best possible sample time, giving that aliasing must be allowed, is that which will make the frequency ratio equal to 1.0. This allows for

the benefits from allowing $n = even$ and avoids the pitfalls of open-loop system response for too many system periods. With this in mind, a further exploration of the discrete-to-continuous system will be made at $FR = \frac{2}{2.0} = 1.0$.

As discussed earlier, the discrete response follows what is expected from classical theory (see [1:126]). With this in mind, then, a pole located on the positive real axis of the z-plane (but within the unit circle) should produce an exponentially decaying response, similar to an overdamped system. This was indeed the case, as examination of Figure 3.17 demonstrates. A pole on the negative real axis should cause exponentially decaying oscillations, similar to an underdamped system. Again this was the case, shown in Figure 3.14 for a $FR = 2.0$. Will this, however, still be the case when $FR = 1.0$ if the one moving pole were placed there? Theory also predicts that a pole placed at the origin of the z-plane will produce a "deadbeat" response [36:598-601]. Again, this needs to be investigated for the case when aliasing is allowed and $FR = 1.0$.

Begin by placing the one moving pole at $z = -1$. This should correspond to a non-decaying oscillatory response of the discrete system. To find the value of the gain that will do this, use the denominator of Equation 3.19, setting the poles equal to $z = -1$ since that is where one pole is to be placed, and $z = -b$ since one sits on top of the closed-loop zeros:

$$(z+1)(z+b) = z^2 + d_1 z + d_2 \quad . \qquad [3.31]$$

Expanding the left-hand side of Equation 3.31 and substituting the values of d_1 and d_2, Equations 3.20 and 3.21, into the right-hand side of Equation 3.31 gives

$$z^2 + (b+1)z + b = z^2 + (K_p c_1 + 2b)z + (K_p c_2 + b^2) \quad . \qquad [3.32]$$

This gives two equations from which K_p may be found:

$$b + 1 = K_p c_1 + 2b \quad , \text{and} \qquad [3.33]$$

$$b = K_p c_2 + b^2 \quad . \qquad [3.34]$$

Solving Equation 3.33 for K_p:

$$K_p = \frac{1-b}{c_1} \quad . \qquad [3.35]$$

Solving Equation 3.34 for K_p:

$$K_p = \frac{b(1-b)}{c_2} \quad . \qquad [3.36]$$

These equations appear to give different results until one solves for the ratio of $\frac{c_2}{c_1}$ from Equations 3.15 and 3.16, setting $b_1 = b_2 = b$ since $FR = \frac{2}{n}$:

$$\frac{c_2}{c_1} = \frac{\omega_n{}^2(a_0 b^2 - a_1 b - a_2 b)}{\omega_n{}^2(a_0 - a_1 b - a_2 b)} = b \quad . \qquad [3.37]$$

Substituting this result into either Equation 3.35 or 3.36 shows the equivalency of these two equations. Setting the value of K_p as given in Equation 3.35 or 3.36 produces the results of Figures 3.26 and 3.27. These plots, a set of root loci and the impulse and step responses, are for the same values of ω_n and ξ as previously.

Examination of Figure 3.26 shows that the single non-stationary root is located on the stability boundary in both the z-plane and the s*-plane. In both planes, this fact would predict a non-damped oscillatory behavior. Looking at Figure 3.27 shows this to be the case, both the discrete and continuous portions of the response show this oscillatory response. The continuous response shows the aperiodic nature, however, resulting from the combination of the discrete and continuous systems.

Comparison of Figure 3.27 with Figure 3.14 shows that the response can be driven to the extreme edge of stability where non-damped oscillations occur. Notice the oscillation of the control effort, shown as the dashed-dot line of Figure 3.27. Furthermore, comparing

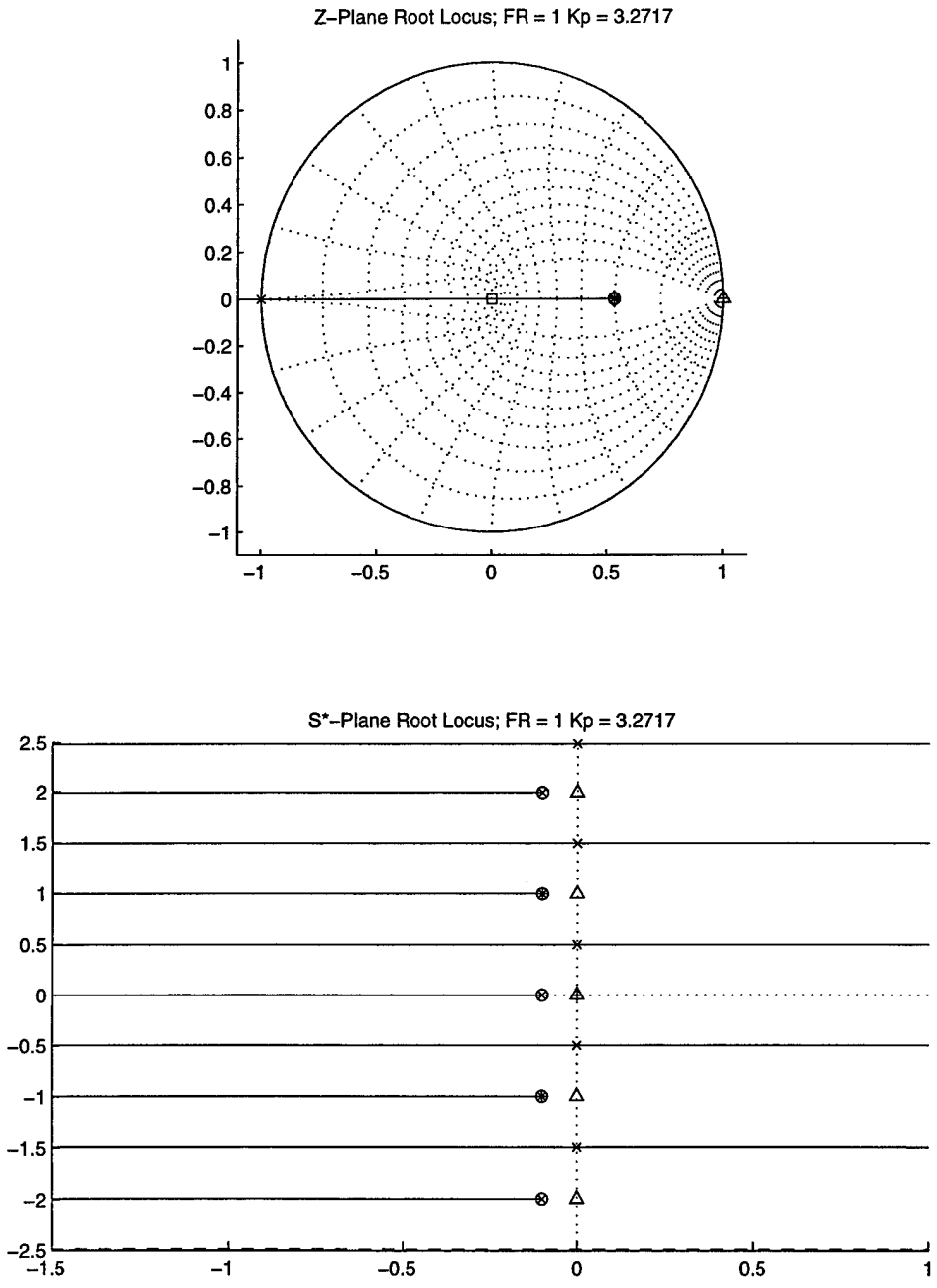

Figure 3.26 Root Loci for FR = 1.0 With Non-Stationary Pole at $z = -1$

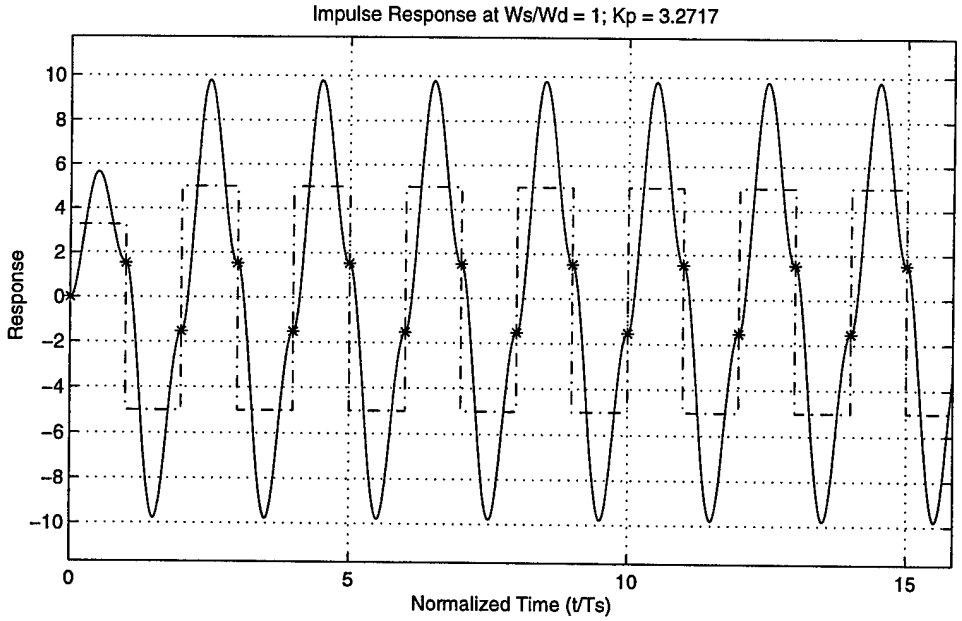

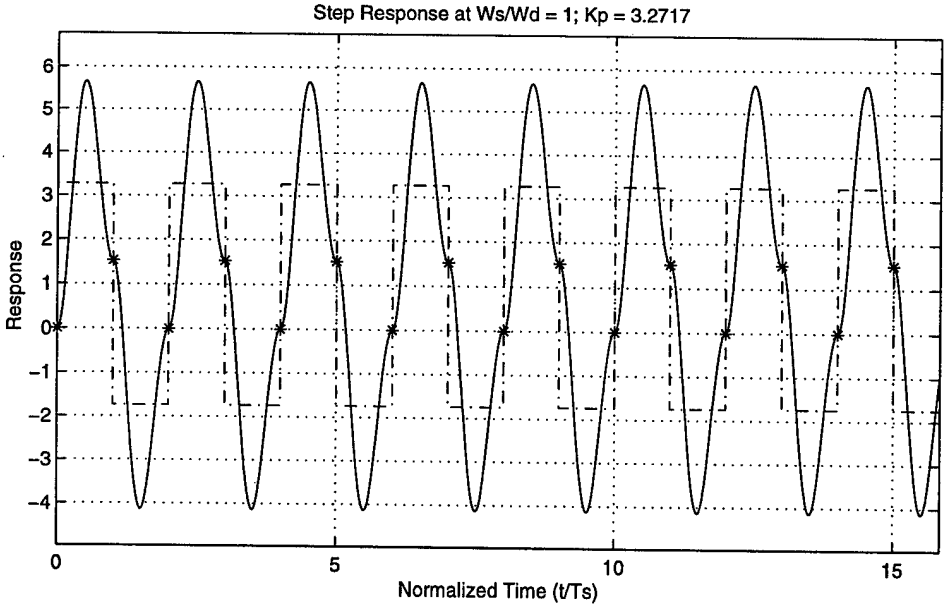

Figure 3.27 Impulse and Step Responses for FR = 1.0
with Non-Stationary Pole at $z = -1$

magnitudes of response, it would appear the case in which $FR = 1.0$ is worse, until one considers the magnitude increase in the gain between the two cases.

The final case of interest when $FR = 1.0$ is that of the system when the non-stationary pole is located at $z = 0$. Equation 3.31 is rewritten with this condition:

$$(z+0)(z+b) = z^2 + d_1 z + d_2 \quad . \qquad [3.38]$$

Solving this as before gives the value of the gain sought for:

$$K_p = -\frac{b}{c_1} = -\frac{b^2}{c_2} \quad . \qquad [3.39]$$

Figures 3.28 and 3.29 show the results. The z-plane root locus of Figure 3.28 shows the non-stationary root is located at $z = 0$, as desired. This root cannot be seen on the s*-plane root locus since it, and all the band-repeated roots, are located at negative infinity.

Perhaps most interesting are the results shown in the impulse and step responses of Figure 3.29. Not only does the discrete response show the deadbeat response predicted by root location in the z-plane, but the continuous response is a deadbeat response as well. The impulse shows a step "up" during the first sample period with a step "down"

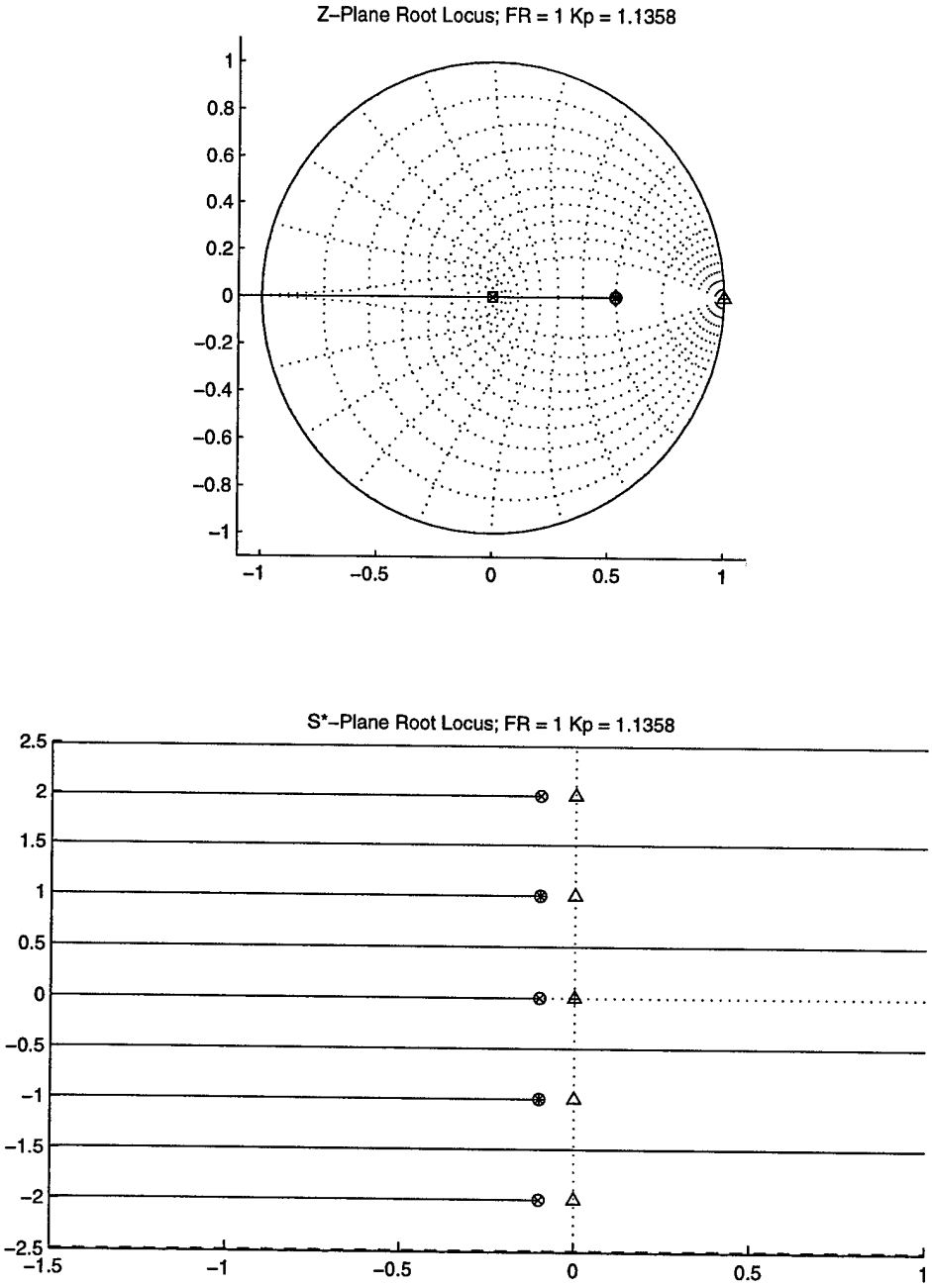

Figure 3.28 Root Loci for FR = 1.0 With Non-Stationary Pole at $z = 0$

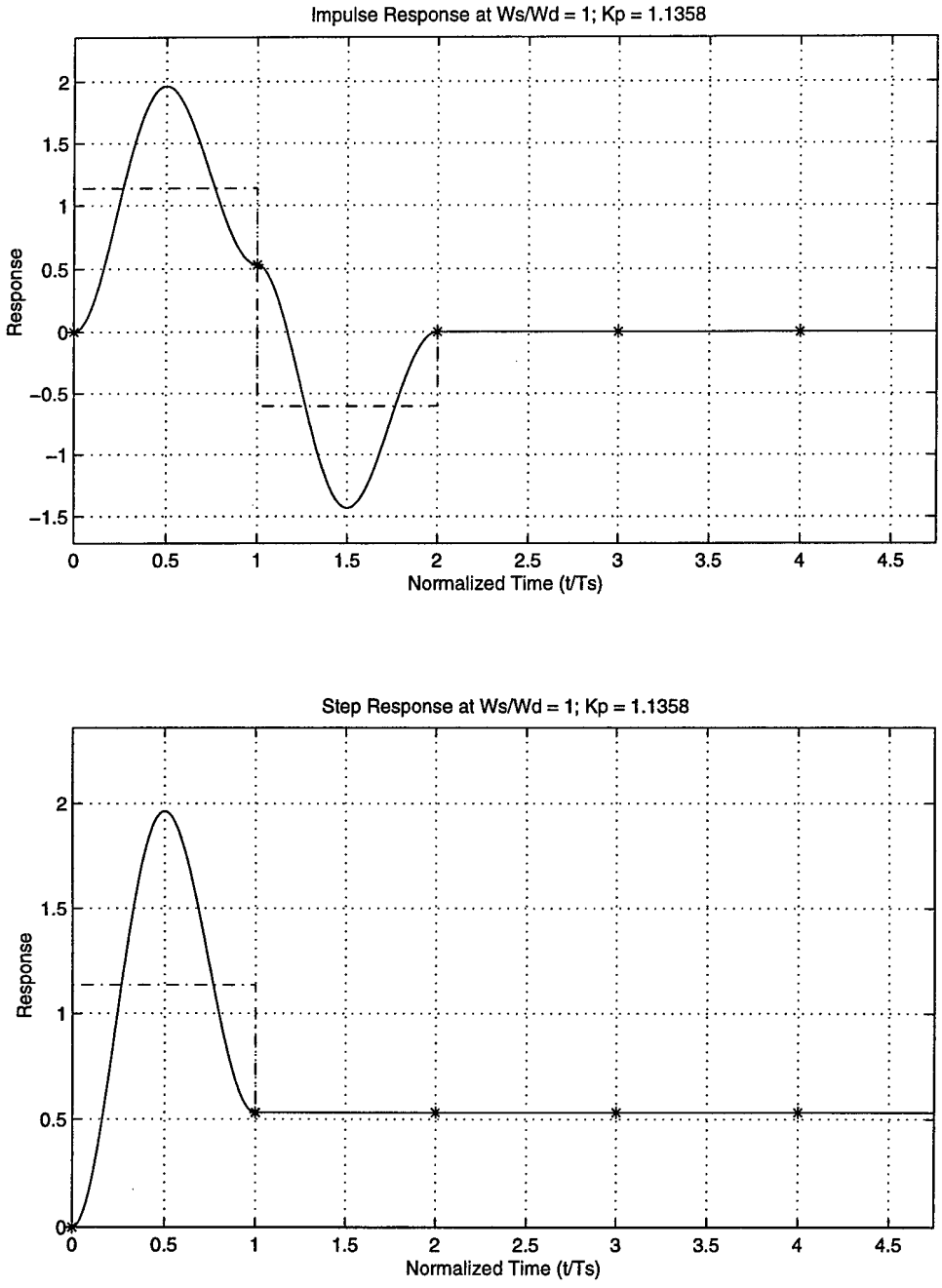

Figure 3.29 Impulse and Step Responses for FR = 1.0 with Non-Stationary Pole at $z = 0$

during the second period. This down-step is exactly equal, but opposite, to the up-step. In other words, the continuous response of the second sample period is equal and opposite to the continuous response of the first time period, causing the deadbeat response seen. The control effort for this response is plotted as the dash-dot lines of Figure 3.29. For the impulse response, the control effort of the second sample period is exactly equal and opposite to the control effort of the first sample period. For the step response, the control effort does not oscillate in any way, and is not large in magnitude. Similarly, here, the step response only takes one sample period to obtain the final value of the step with no oscillations whatsoever after the initial time period.

An interesting note made by Astrom and Wittenmark [38:254-255] is one of the drawbacks of traditional deadbeat controllers. They mention that the magnitude of the control signal increases with a decreasing sample period, thus giving the deadbeat controller a bad reputation. An examination of the deadbeat controller here shows very little control effort is required. By allowing aliasing, a pure deadbeat response is obtained much easier. With aliasing, the response of the system is not forced to a much greater level than the system's own natural response. Here, advantage is taken of that natural response and used for simple and elegant control. This is contrary to control required for deadbeat response without allowed aliasing.

Research continues in the area of deadbeat controllers. Some recent works include [39], [40], [41], [42], and [43].

To answer concerns as to the robustness of this system, examine parameters that may change, affecting the response of the discrete-to-continuous system. Begin first by again examining Equation 3.39. Recall b is defined as

$$b = -e^{-pT_s} \qquad [3.40]$$

for the case of $FR = 1.0$. One can easily see from Equations 3.4 and 3.6 that

$$p_1 p_2 = \omega_n^{\,2} \qquad [3.41]$$

when $FR = 1.0$. Given this fact, the exponent from Equation 3.40 becomes

$$p_1 T_s = p_1 \frac{2\pi}{\omega_d} = p_1 \frac{2\pi}{\omega_n \sqrt{1-\zeta^2}} = \frac{2\pi p_1}{\sqrt{(p_1 p_2)1-\zeta^2}} = p_2 T_s = \frac{2\pi p_2}{\sqrt{(p_1 p_2)1-\zeta^2}} \quad . \qquad [3.42]$$

Since the terms for the poles are interchangeable in Equation 3.42, the term b becomes independent of the plant's natural frequency at this frequency ratio. Equation 3.15 gives the definition for c_1, and using Equations 3.8 through 3.10 in Equation 3.15 leaves

$$c_1 = \omega_n^{\,2}\left[\frac{1}{p_1 p_2} - \frac{b}{p_1(p_1 - p_2)} + \frac{b}{p_2(p_1 - p_2)}\right] , \qquad [3.43]$$

which, following algebraic manipulation becomes

$$c_1 = \omega_n^2\left[\frac{p_1 - p_2 - bp_2 + bp_1}{p_1 p_2 (p_1 - p_2)}\right] = \omega_n^2\left[\frac{(p_1 - p_2)(1+b)}{\omega_n^2 (p_1 - p_2)}\right] = 1 + b \quad . \qquad [3.44]$$

Substituting Equations 3.44 and 3.40 into Equation 3.39:

$$K_p = \frac{-b}{1+b} \quad . \qquad [3.45]$$

Equation 3.45 along with Equation 3.42 show K_p for the deadbeat response is dependent only on the damping ratio ξ, and not the undamped natural frequency. The model for this deadbeat response, therefore, is dependent on the undamped natural frequency (or damped natural frequency since $\omega_d = \omega_n\sqrt{1-\zeta^2}$) and the damping ratio for calculation of the needed sampling frequency, and the damping ratio for calculation of the proportional gain K_p. Robustness, then, will be examined for changes in these two parameters.

Figure 3.30 shows plots of the impulse and step responses to changes in the natural frequency. If the natural frequency of the open-loop plant were to change, or were incorrect from the modeling, the frequency ratio would change as a result, since

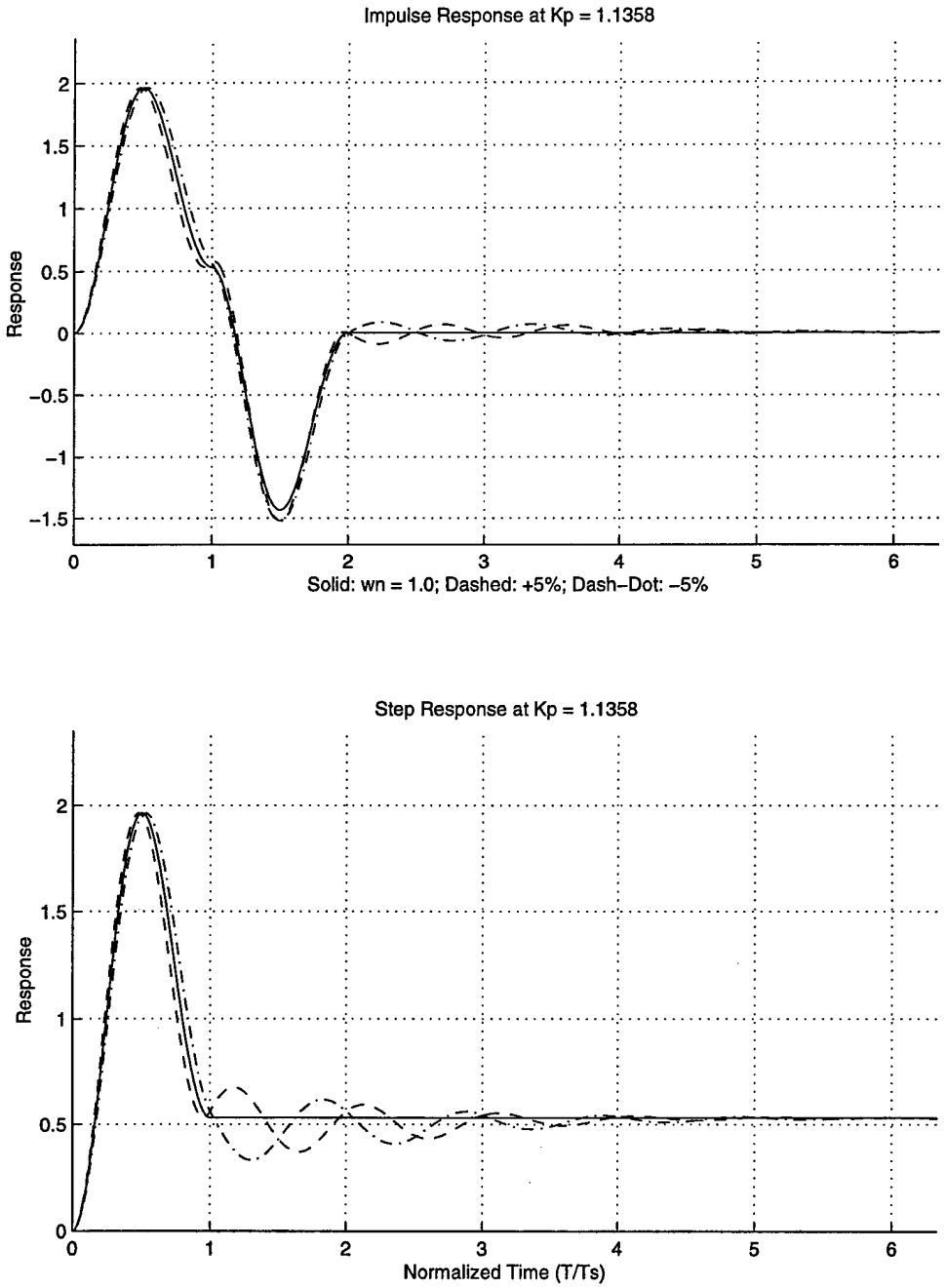

Figure 3.30 Robustness Comparison for Change in Natural Frequency

$$FR = \frac{\omega_s}{\omega_n \sqrt{1-\zeta^2}} \quad . \qquad [3.46]$$

Figure 3.30 shows comparisons for a $\pm 5\%$ change in the natural frequency.

Finally, Figure 3.31 shows comparisons for a $\pm 5\%$ change in the damping ratio, which again affects the FR according to Equation 3.46, as well as the correct proportional gain for the deadbeat response according to Equation 3.45.

Figures 3.30 and 3.31 demonstrate the robustness of this system. The most extreme changes occur with changes in the natural frequency of the open-loop plant. However for this case, even with a change of $\pm 5\%$, a large variation in a parameter, the system step response settles to a final value within six sample periods. The change in responses of the system with changes in the natural frequency is greater than for changes in K_p (or damping).

These changes of the system response from the optimal value demonstrate one of the classical problems with deadbeat systems—the cancellation of a desired frequency requires accurate knowledge of the frequency. Without this accuracy it becomes difficult to cancel the mode. Given the accuracy of the system model, however, this type of deadbeat response is difficult to match with conventional methods.

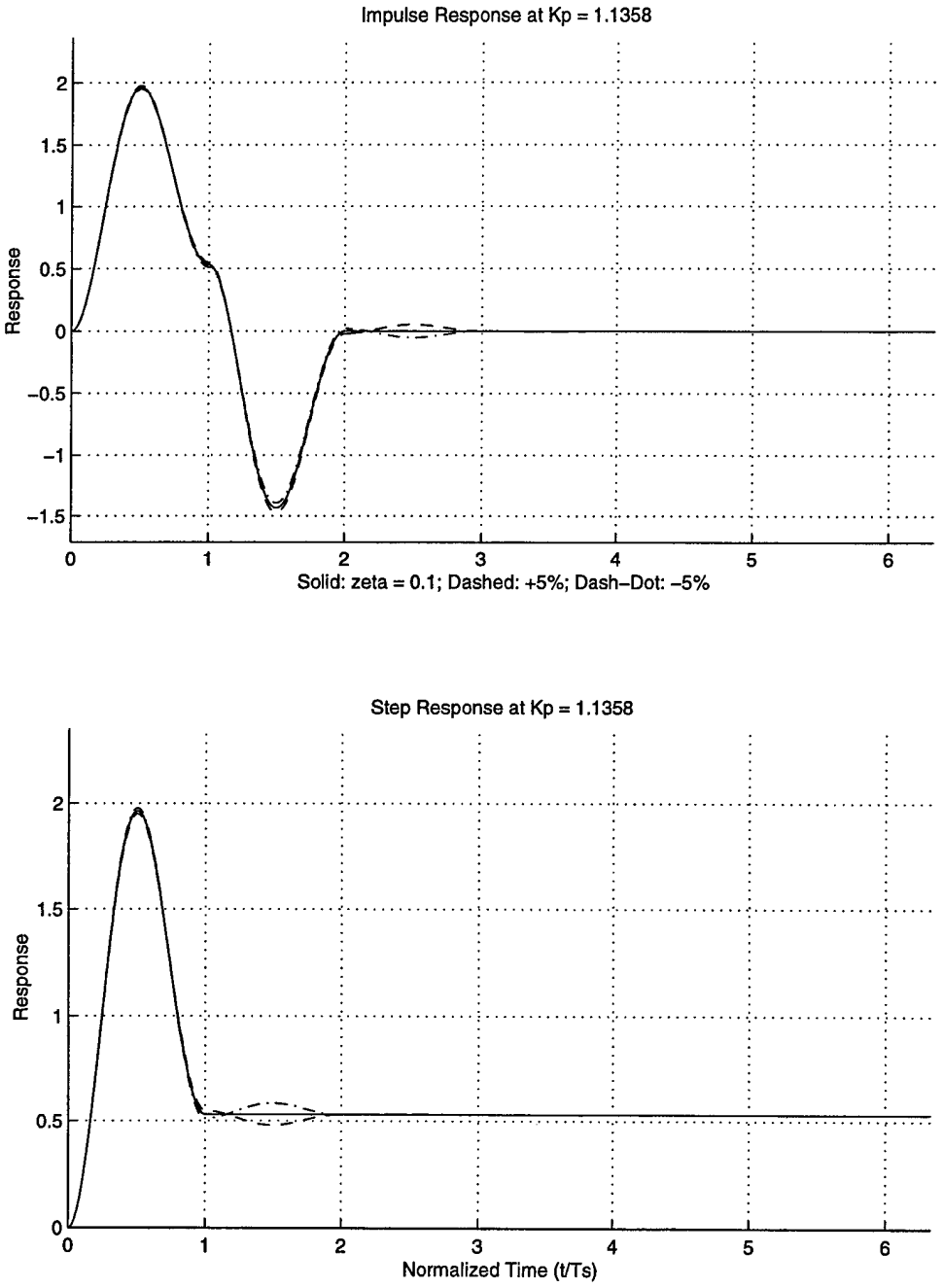

Figure 3.31 Robustness Comparison for Change in Damping Ratio

As is always the case with a control system consisting of proportional control only, the steady-state error is perhaps unacceptable. Traditionally, this error is taken care of by introducing an integrator. The next chapter will examine such a system to try and achieve comparable results as the proportional controller, but without the steady-state error seen here.

3.6 Chapter Three Summary

In chapter Three the root locus for the discrete-to-continuous system was developed and the movement of the poles in the gain limits for the system were examined. They were found to start at the locations of the closed-loop discrete zeros, which correspond to the open-loop continuous poles, and move toward the locations of the open-loop zeros of H*(s). A second-order system with proportional control only was developed and examined at different frequency ratios allowing aliasing. The frequency ratio of $FR = \frac{2}{n}$ was found to cause the entire z-plane root locus to lie on the real axis, as well as fixing one of the z-plane plant poles. When n is odd, part of the root locus lies on the positive real axis and one can place the non-stationary pole at the origin. This produces a deadbeat step response with a simple control effort contrary to tradition deadbeat controllers. It was seen that the system with aliasing will not follow a sinusoidal input very well, giving a limitation of this model—the frequency of the input must be lower than the frequency of the sampler.

CHAPTER FOUR. SECOND-ORDER SYSTEM DESIGN WITH ALIASING – PROPORTIONAL-INTEGRAL CONTROL

4.0 INTRODUCTION

As introduced in chapter three, the sample period turns out to be a powerful tool in the design of a discrete-to-continuous control system with a proportional controller in which aliasing is present. The deadbeat response seen in Figure 3.29 is an attractive design goal for certain applications, given that the steady-state error could be reduced. Here, the search for such a system will begin, starting with an examination of the integral controller and moving on to the proportional-integral controller. Comparison between root loci, frequency response functions, impulse and step responses, and responses to sinusoidal inputs will again be examined. Again, the frequency ratio allowing for the best response with aliasing present is found to be $FR = 1.0$. A deadbeat controller with zero steady-state error is designed, and robustness and disturbance rejection for this controller is examined.

4.1 Design of an Integral Controller Using Sample Period As a Design Parameter

Similar to the investigation of the proportional controller in chapter three, here examine the behavior of the integral controller as sample period changes. The integral controller is defined by

$$G_c(z) = \frac{K_i z}{z-1} \quad . \qquad [4.1]$$

Solving for $F(z)$ from Equation 3.3 gives

$$F(z) = \frac{K_i z(z+b_1)(z+b_2)}{K_i z(c_1 z + c_2) + (z-1)(z+b_1)(z+b_2)} \quad , \qquad [4.2]$$

where the constants are as defined previously in Equations 3.13 through 3.16. This equation becomes

$$F(z) = \frac{K_i z(z+b_1)(z+b_2)}{z^3 + d_1 z^2 + d_2 z + d_3} \quad , \qquad [4.3]$$

where

$$d_1 = K_i c_1 + b_1 + b_2 - 1 \quad , \qquad [4.4]$$

$$d_2 = K_i c_2 + b_1 b_2 - b_1 - b_2 \quad \text{, and} \qquad [4.5]$$

$$d_3 = -b_1 b_2 \quad . \qquad [4.6]$$

When K_i is equal to zero the poles of Equation 4.3 are located at $z = 1$, $-b_1$, and $-b_2$, which correspond to the pole of the controller and the poles of the open-loop plant, were they transformed to the z-plane. At $K_i = \infty$ the poles move to $z = 0$, $-\infty$, and $-\frac{c_2}{c_1}$, the location of the controller zero and the zeros of $H(z)$. This is as expected.

For comparison purposes, the discrete-to-continuous system consisting of the second-order plant of chapter three (Equation 3.6) and the controller of Equation 4.1 with a frequency ratio of $FR = 50$ is used for Figures 4.1 through 4.4. These correspond to plots in which no aliasing is present—i.e., a system for which traditional design methods would be used. A very low gain of $K_i = 0.01$ is used for stability. Notice the very small gain margin of this system, a direct result of using an integral controller by itself.

Now allow aliasing as before in chapter three. The frequency ratio, for non-dimensionalization, will again be as defined in Equation 3.22. Figures will be presented for frequency ratios of $FR = \frac{2}{1.0}$, $\frac{2}{1\frac{1}{3}}$, $\frac{2}{1\frac{2}{3}}$, and $\frac{2}{2.0}$.

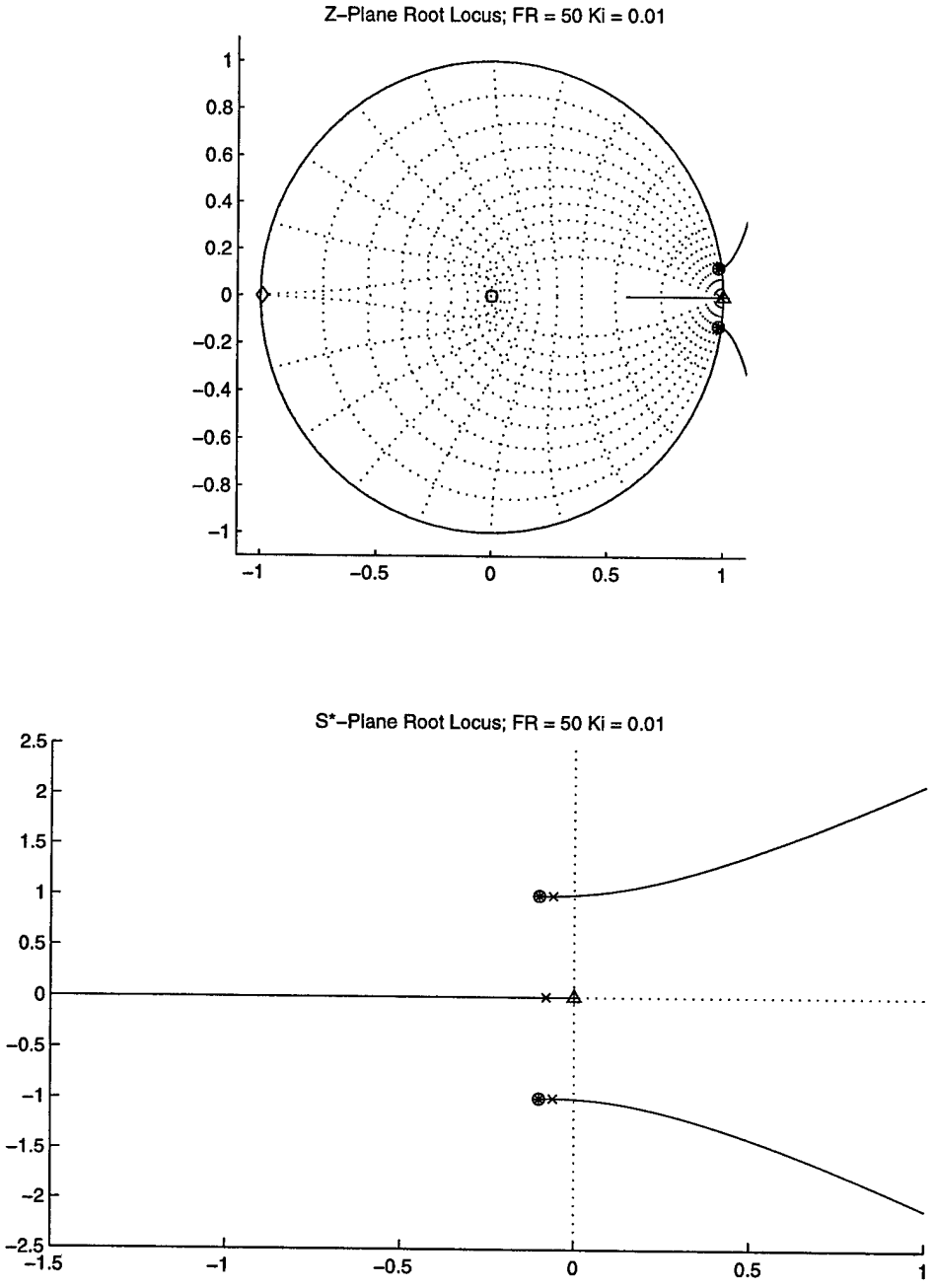

Figure 4.1 Root Loci for FR = 50, $K_i = 0.01$

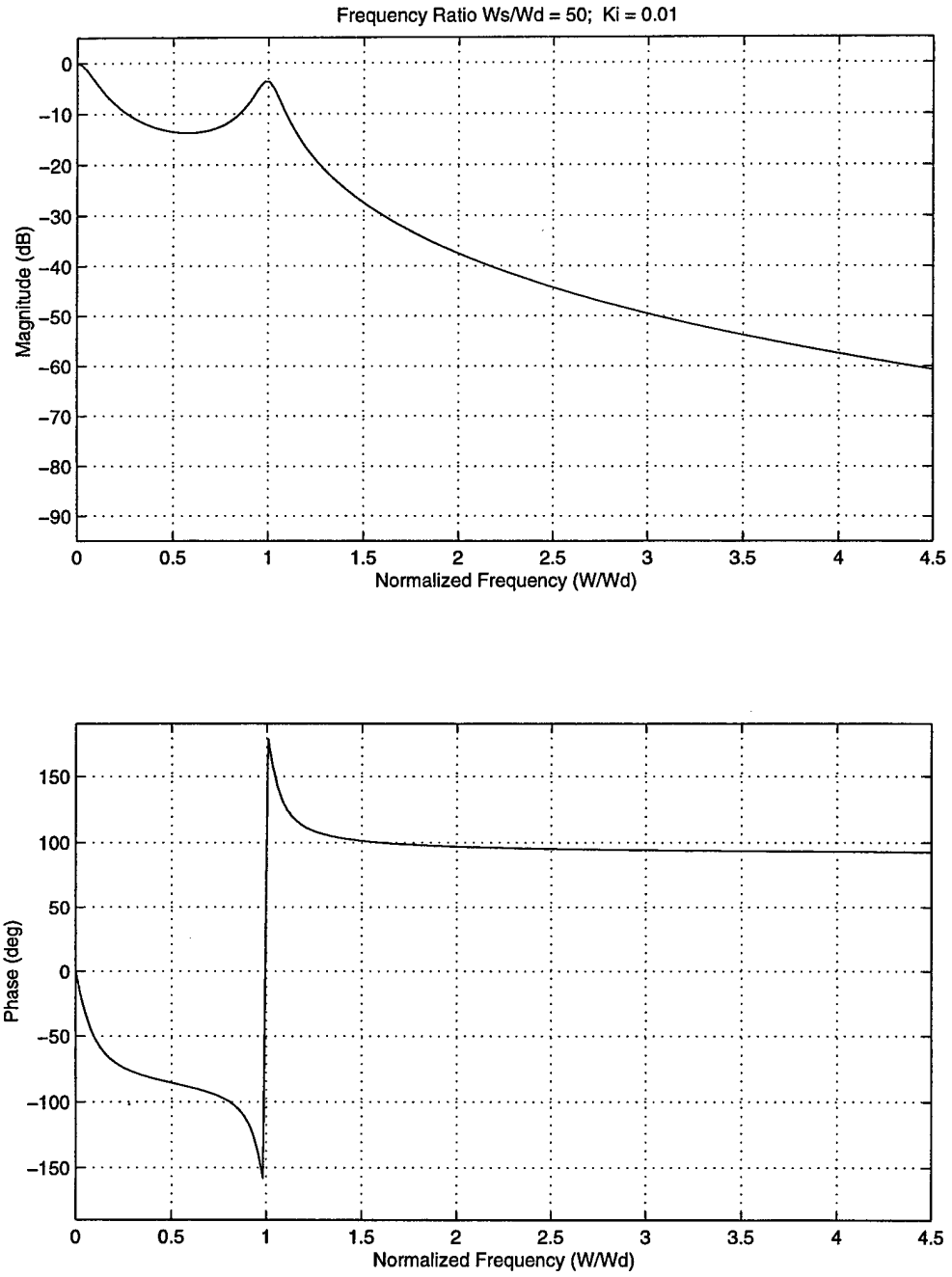

Figure 4.2 Frequency Response Function Plot for FR = 50, $K_i = 0.01$

Figure 4.3 Step and Impulse Responses for FR = 50, K_i = 0.01

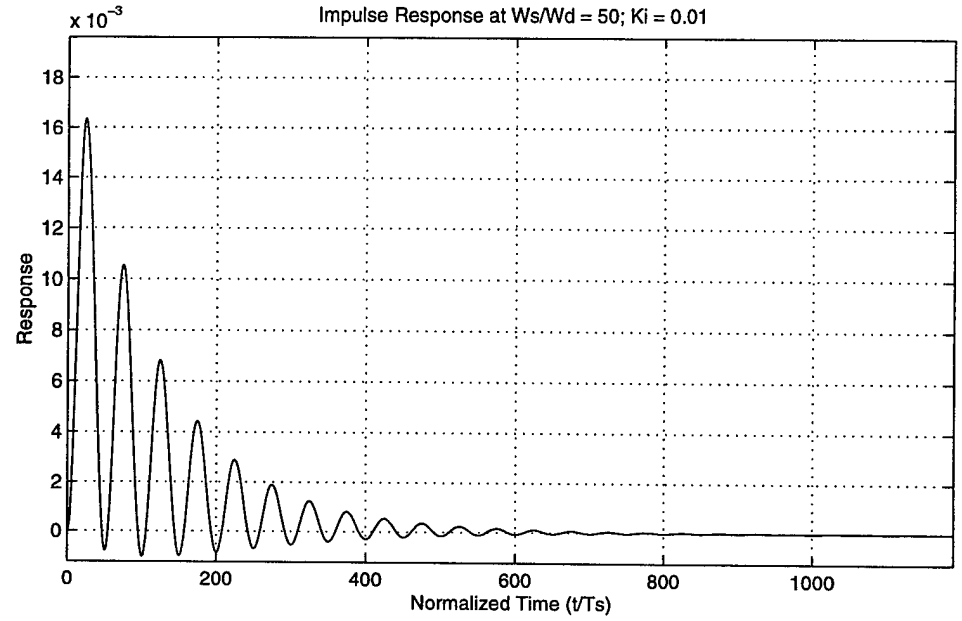

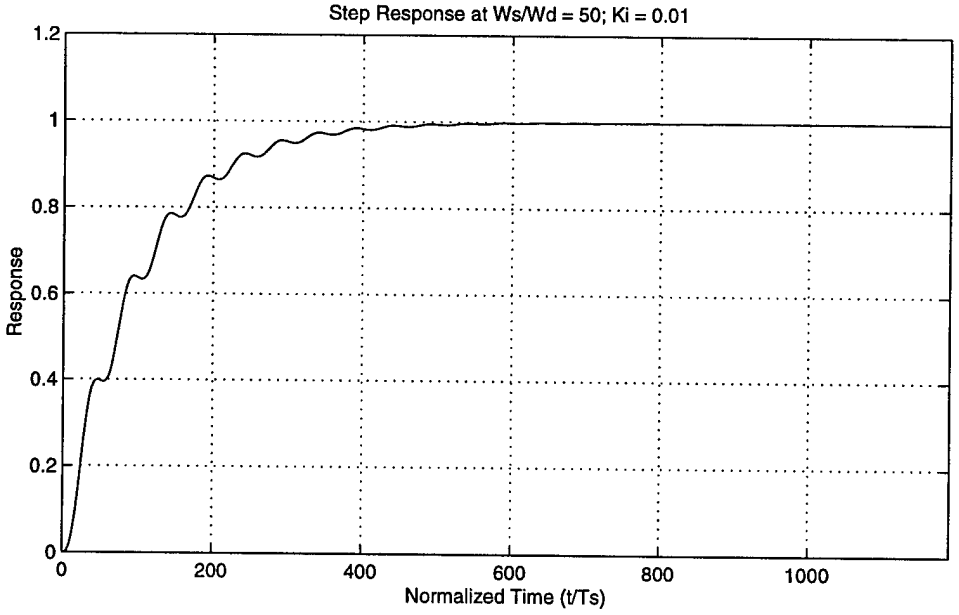

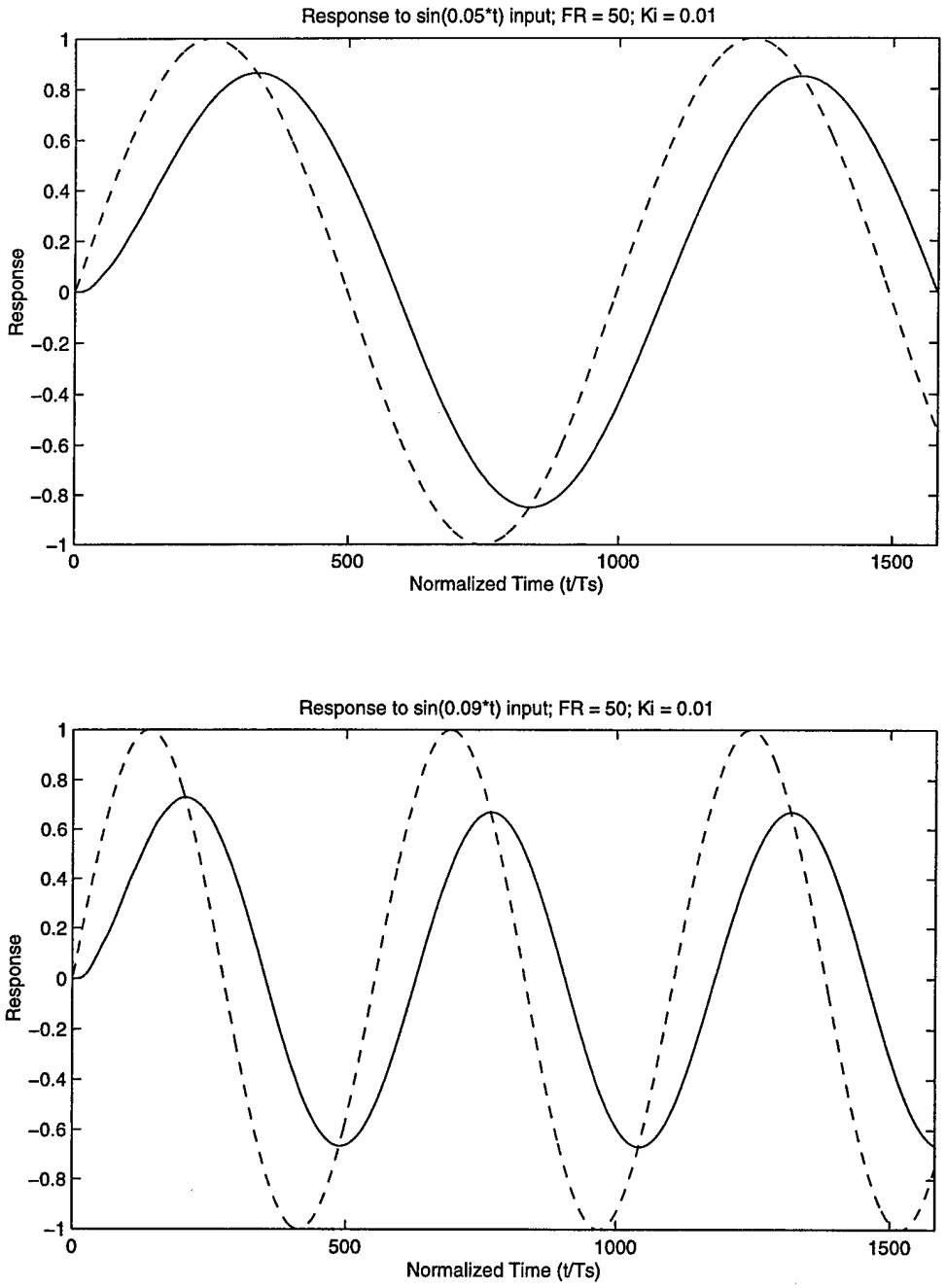

Figure 4.4 Response to Sinusoidal Inputs for FR = 50, $K_i = 0.01$

Figures 4.5 through 4.8 show the root loci plots for the discrete-to-continuous second-order system with an integral controller. Recall the definition of symbols on the plots: triangle and plus – zero-order hold zeros and pole, square and asterisks – plant zeros and poles, diamond – pole of $H(z)$, and circles, "x's" and solid line – zeros and poles of $F(z)$. Notice the increase in allowable gain before the stability boundaries are crossed. Again, by slowing the sample rate, stability is introduced, contrary to current design practices.

Figure 4.5 shows the entire root locus for a frequency ratio of $FR = 2.0$ lies entirely on the real axis of the z-plane. Similar to that of the proportional controller, it is different, however, in that a portion of it lies on the negative real axis, and another portion lies on the positive real axis. The portion that lies on the positive real axis consists of a pole that begins at $z = 1$, the open-loop controller pole location, and moves toward $z = 0$, the open-loop controller zero location. This portion of the root locus lies entirely within the stability range. The portion that lies on the negative real axis consists of one pole fixed at the location of the zeros of $F(z)$ found from the denominator of $H(z)$ and one pole that travels toward negative infinity. Once this pole passes $z = -1$, the system goes unstable.

The portion of the z-plane root locus that lies on the positive axis corresponds to the portion of the s*-plane root locus that lies on the mid-band line. These poles start at $s^* = 0$ and move toward negative infinity, the point corresponding to $z = 0$. The other non-stationary poles starts at the values of s* corresponding to the zeros of $F^*(s)$ and move along the band boundaries to infinity.

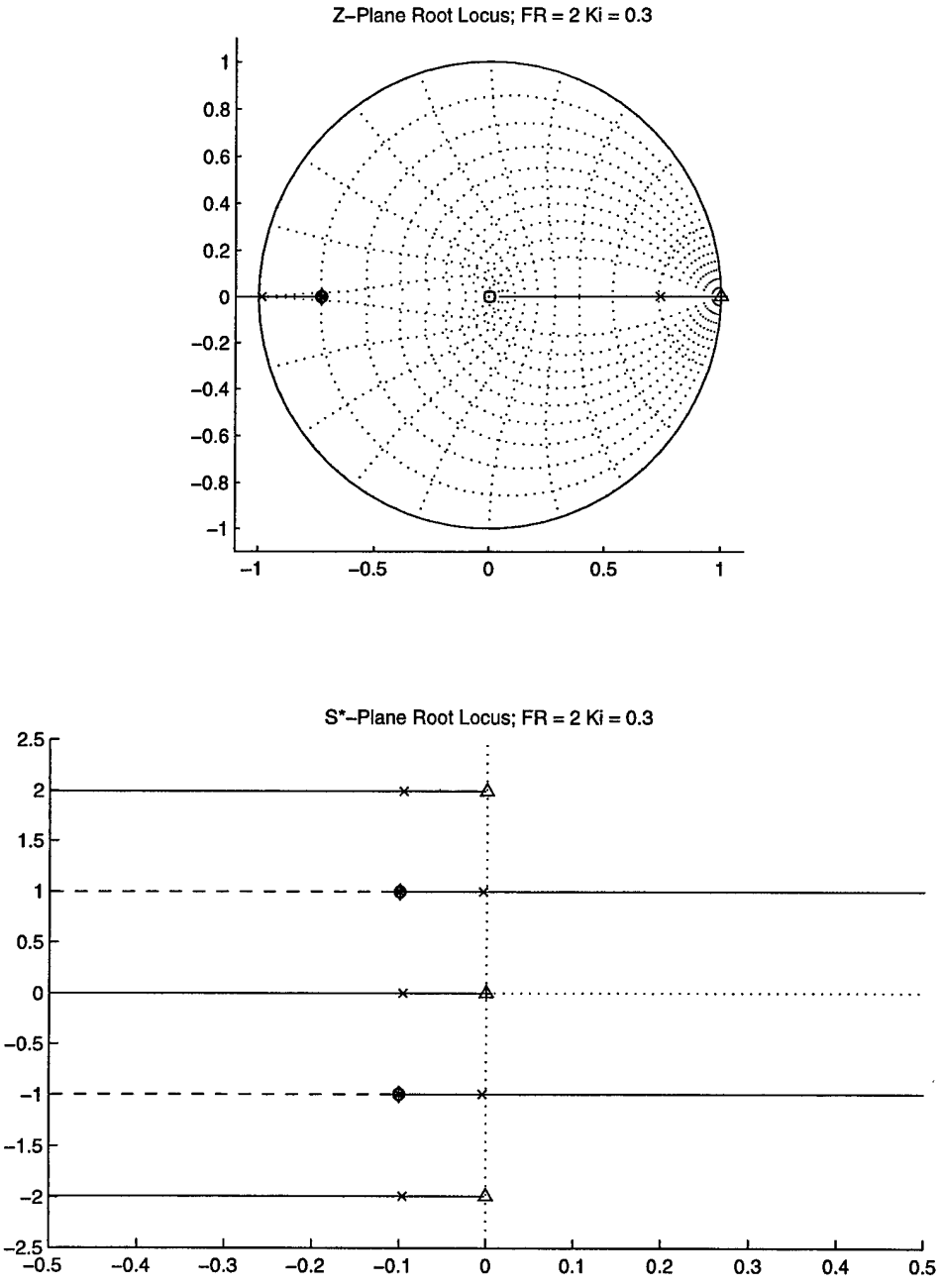

Figure 4.5 Root Loci for FR = 2.0, $K_i = 0.3$

Figures 4.6 and 4.7 show the root loci for frequency ratios of $FR = \frac{2}{1\frac{1}{3}}$ and $\frac{2}{1\frac{2}{3}}$, respectively. Here, there is no stationary pole, and the same general trends are observed.

Figure 4.8 shows the root loci for the special frequency ratio of $FR = 1.0$. Note the unique nature of these root loci, even though there are similarities of characteristics with the like root loci of the system with proportional control of Figure 3.9. At this frequency ratio one pole remains fixed at the location of the zeros of $F(z)$ found from the denominator term of $H(z)$ (see Equation 3.3). The second pole starts at these zeros and travels toward the pole that starts at $z = 1$, the controller pole location, and travels toward the second pole. Once these poles meet, they travel in a circle of constant radius around the zero found at the origin, meet at the real axis, and then split, with one pole traveling toward negative infinity and the other traveling toward $z = 0$, the location of the controller zero.

This constant radius circle in the z-plane corresponds to a constant value of the real part of the locus in the s*-plane. This can be seen as the change of only the imaginary portion of the root on the locus in the s*-plane of Figure 4.8. These repeated roots in the s*-plane travel to the band boundaries, where they "meet" the root coming from the adjacent band, then separate with one traveling to negative infinity and the other traveling to the location of the zero of $H(z)$ transformed to the s*-plane and repeated infinitely.

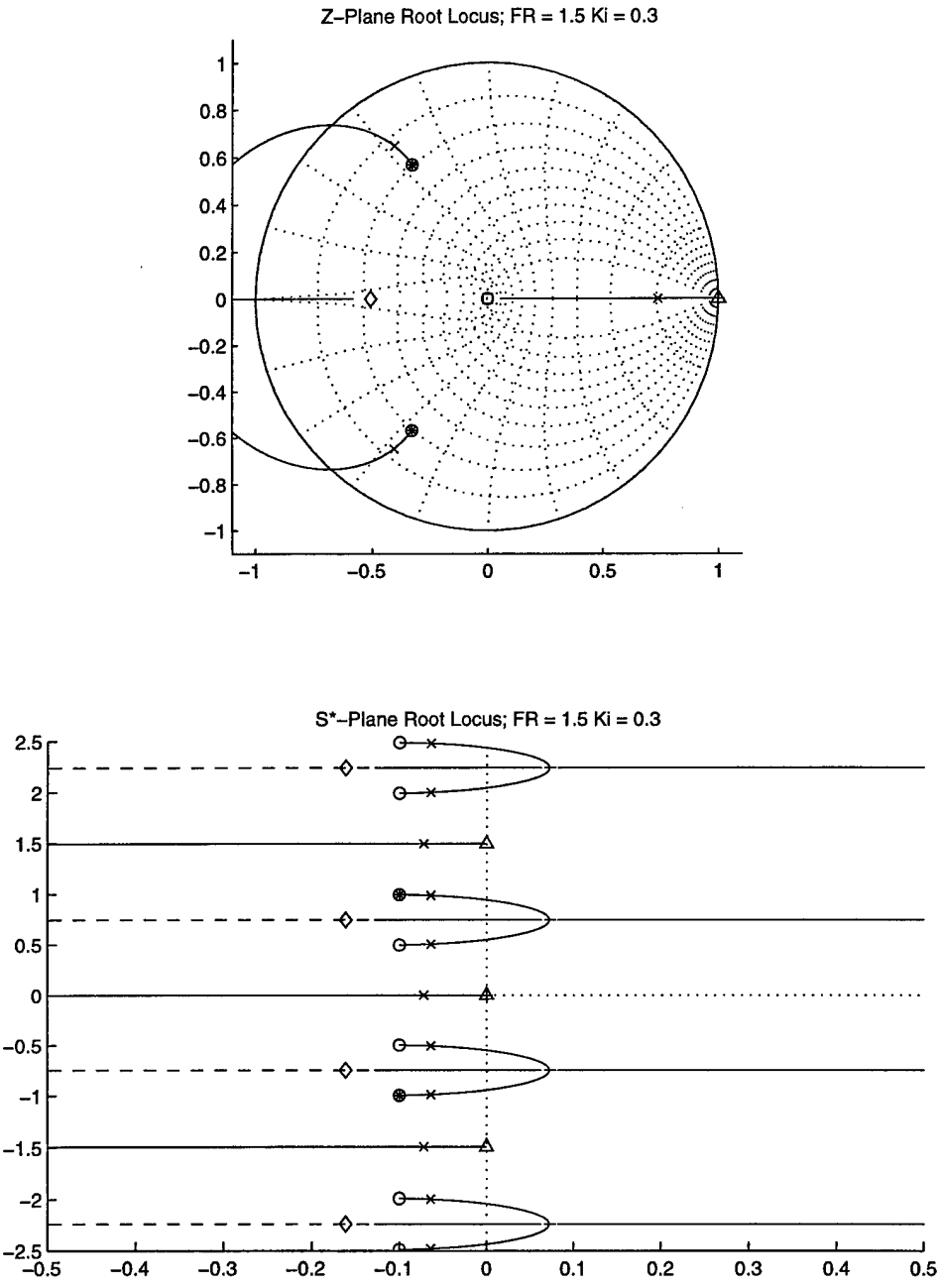

Figure 4.6 Root Loci for FR = 1.5, K_i = 0.3

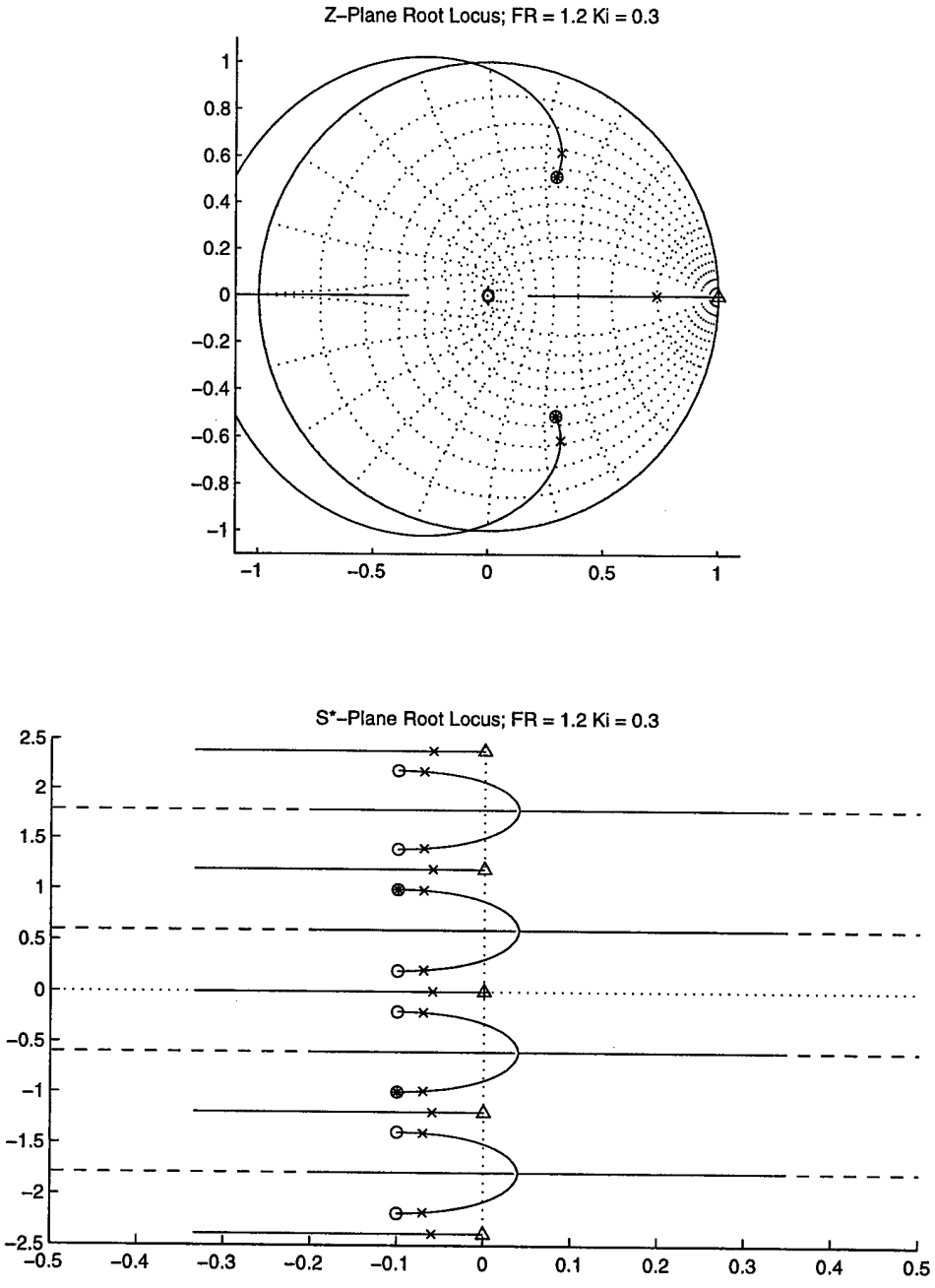

Figure 4.7 Root Loci for FR = 1.2, $K_i = 0.3$

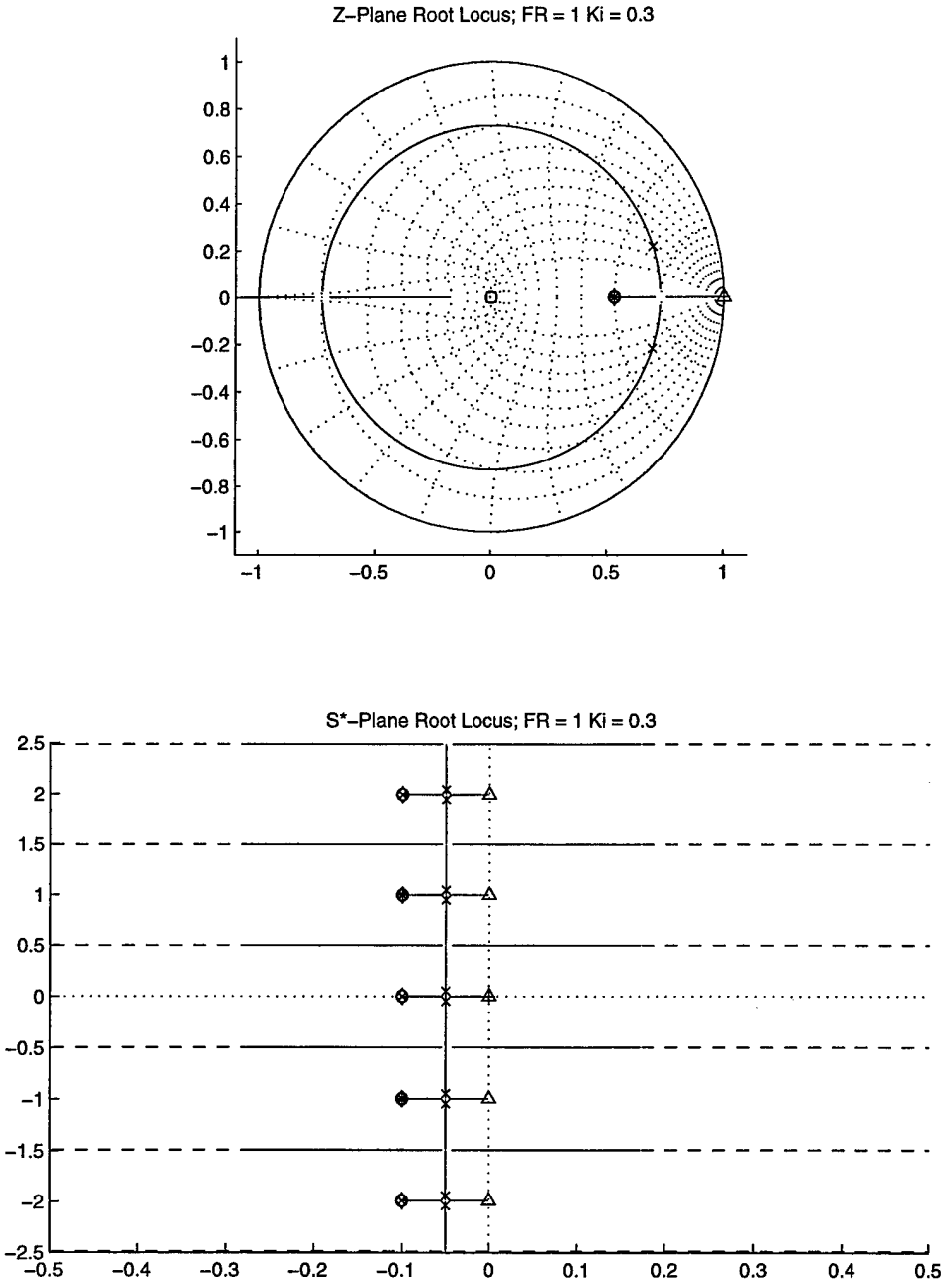

Figure 4.8 Root Loci for FR = 1.0, K_i = 0.3

Figures 4.9 through 4.12 show the frequency response function magnitude and phase plots of the second-order discrete-to-continuous system with integral control. Similar trends to those discussed in chapter three for the proportional controller can be observed here.

Figures 4.13 through 4.16 show the impulse and step responses of the system at the frequency ratios defined above. Again, the discrete responses follow the response predicted by the location of the poles in the z-plane. The response at a frequency ratio of $FR = 1.0$ is much better behaved than that at a frequency ratio of $FR = 2.0$. The step response at $FR = 1.0$, however, does not appear to be the best of the four frequency ratios—the step response at $FR = 1.5$ seems to be best overall. A comparison of these responses is plotted in Figure 4.17.

Figures 4.18 through 4.21 show the responses of the second-order discrete-to-continuous system to sinusoidal inputs. Unlike those for the proportional controller, differences can be seen when integral control is employed. Here, there is a definite degradation of performance as the sample rate decreases.

Looking now at the case where $FR = 1.0$, as with the proportional controller, an optimal gain will be calculated. It would seem this gain would be such that the non-stationary poles are at the same location in the z-plane, meeting on the positive z-axis. Calling this

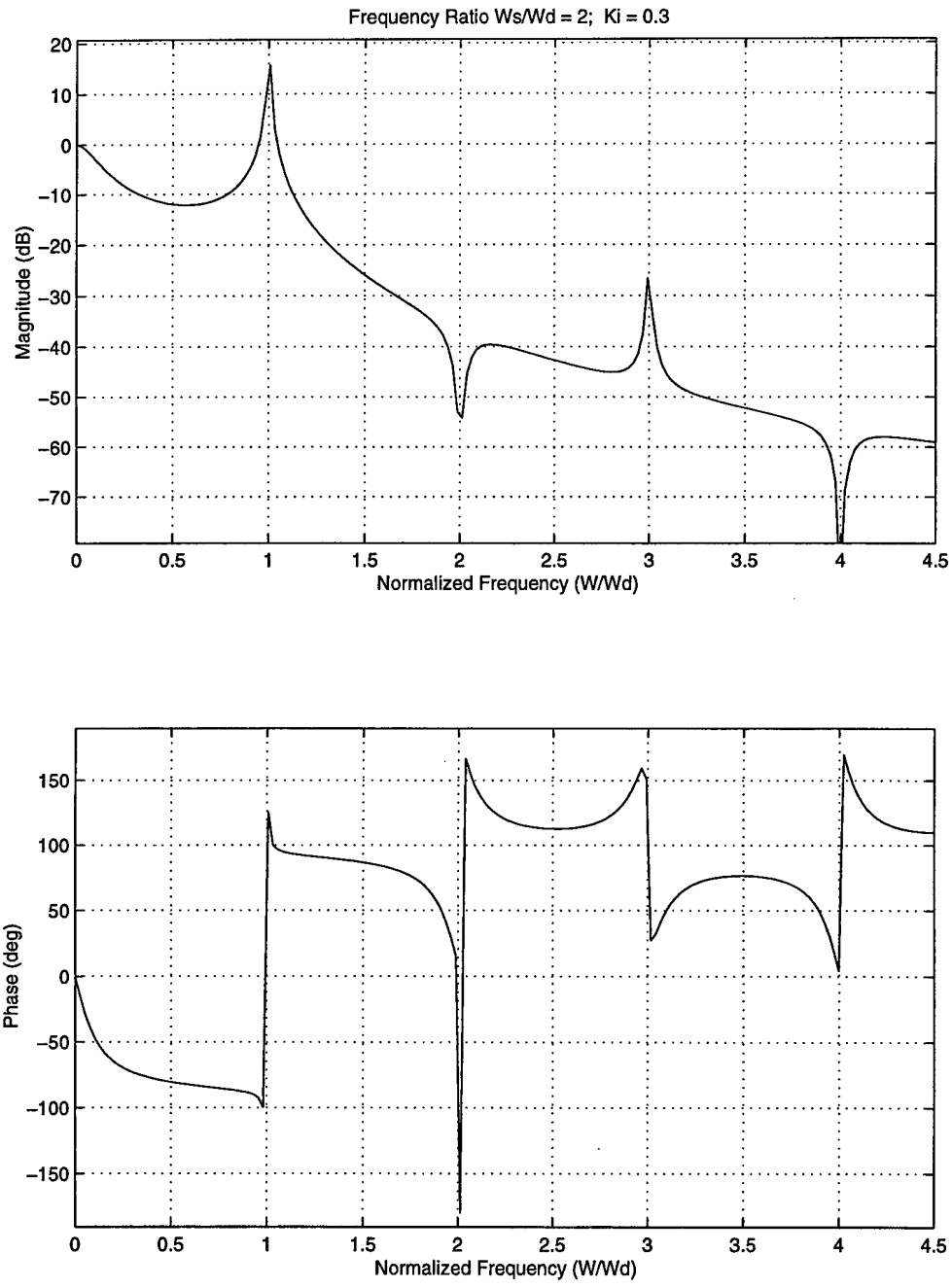

Figure 4.9 Frequency Response Function Plot – FR = 2.0, $K_i = 0.3$

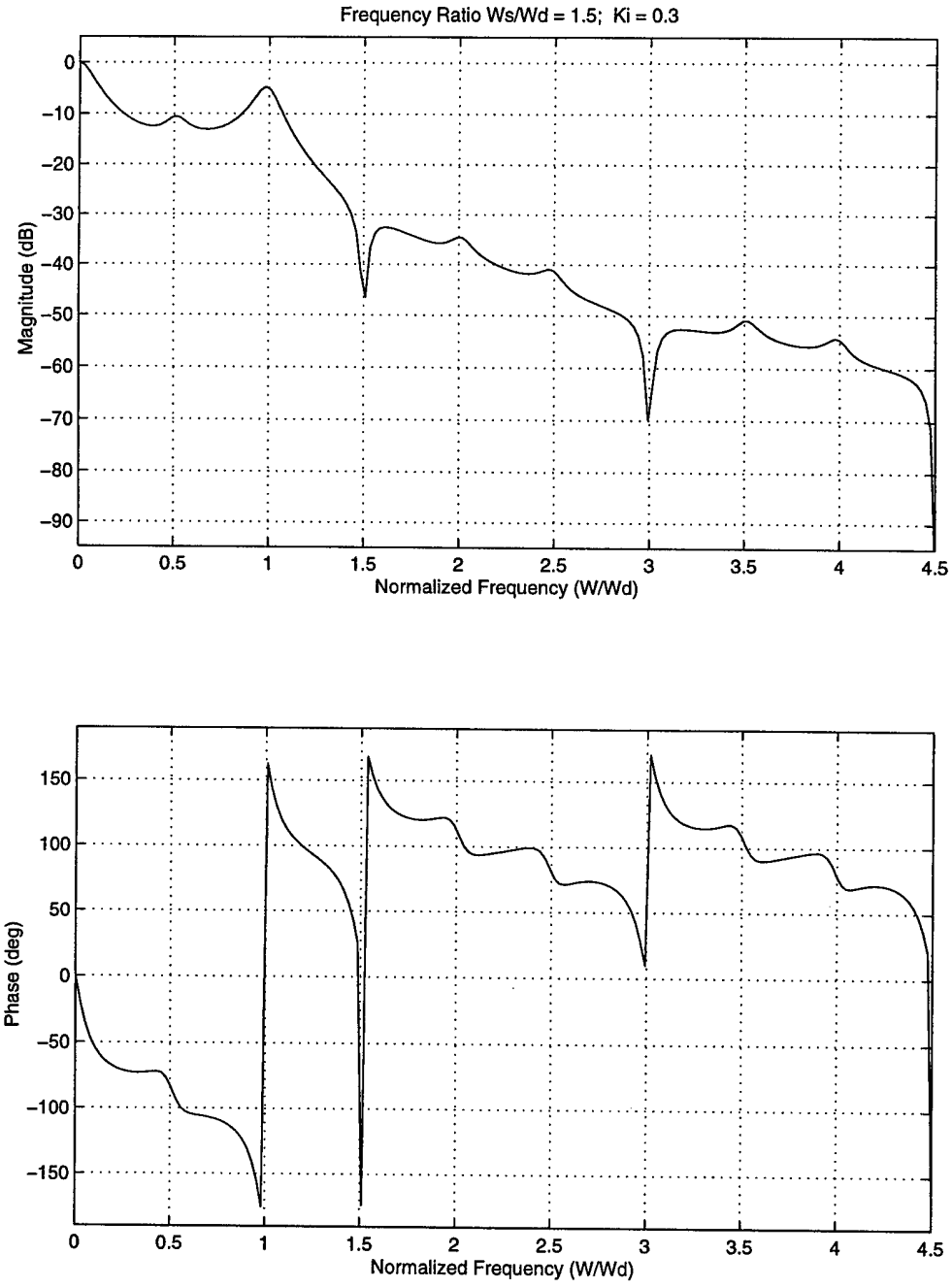

Figure 4.10 Frequency Response Function Plot – FR = 1.5, $K_i = 0.3$

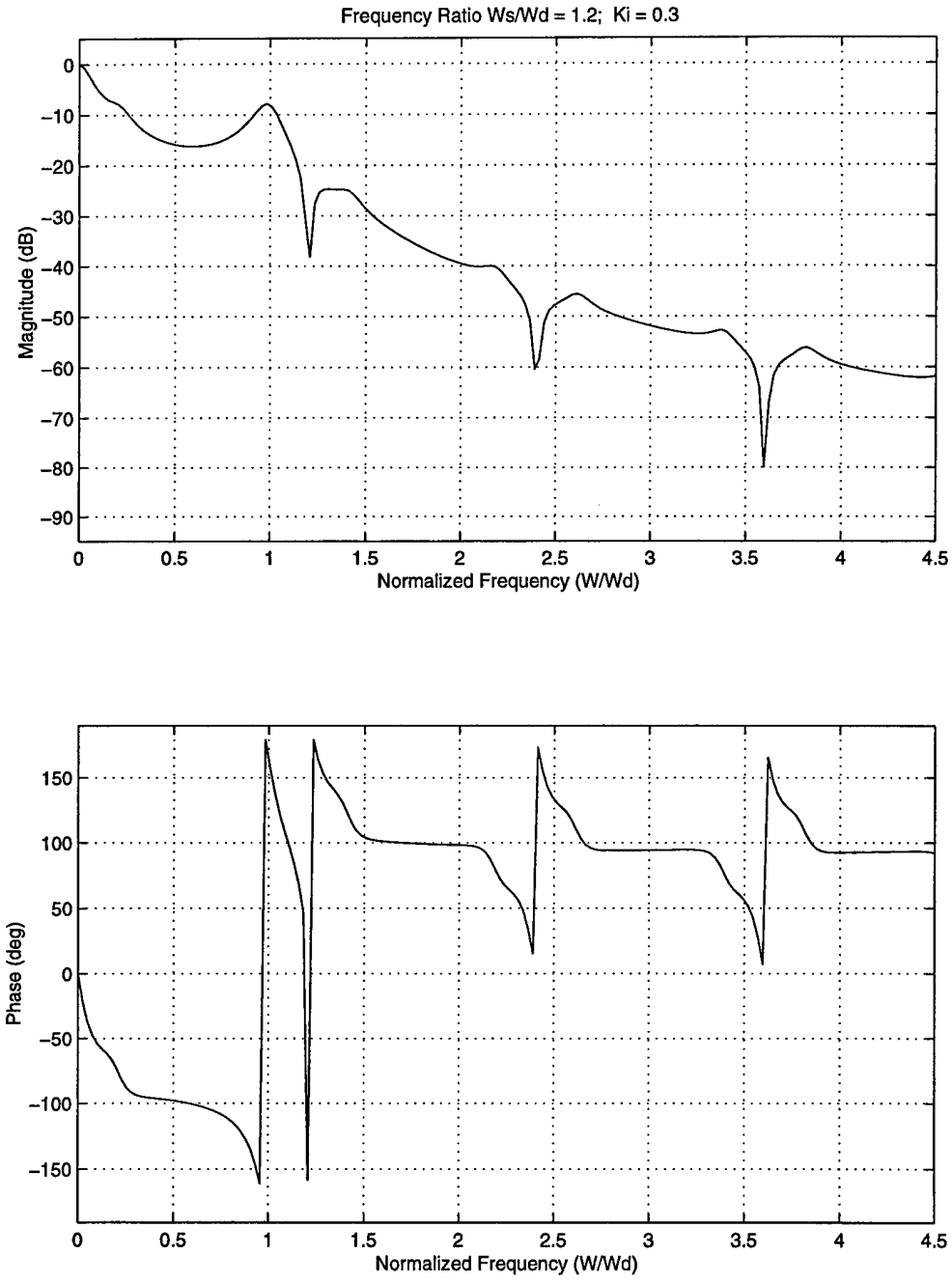

Figure 4.11 Frequency Response Function Plot – FR = 1.2, $K_i = 0.3$

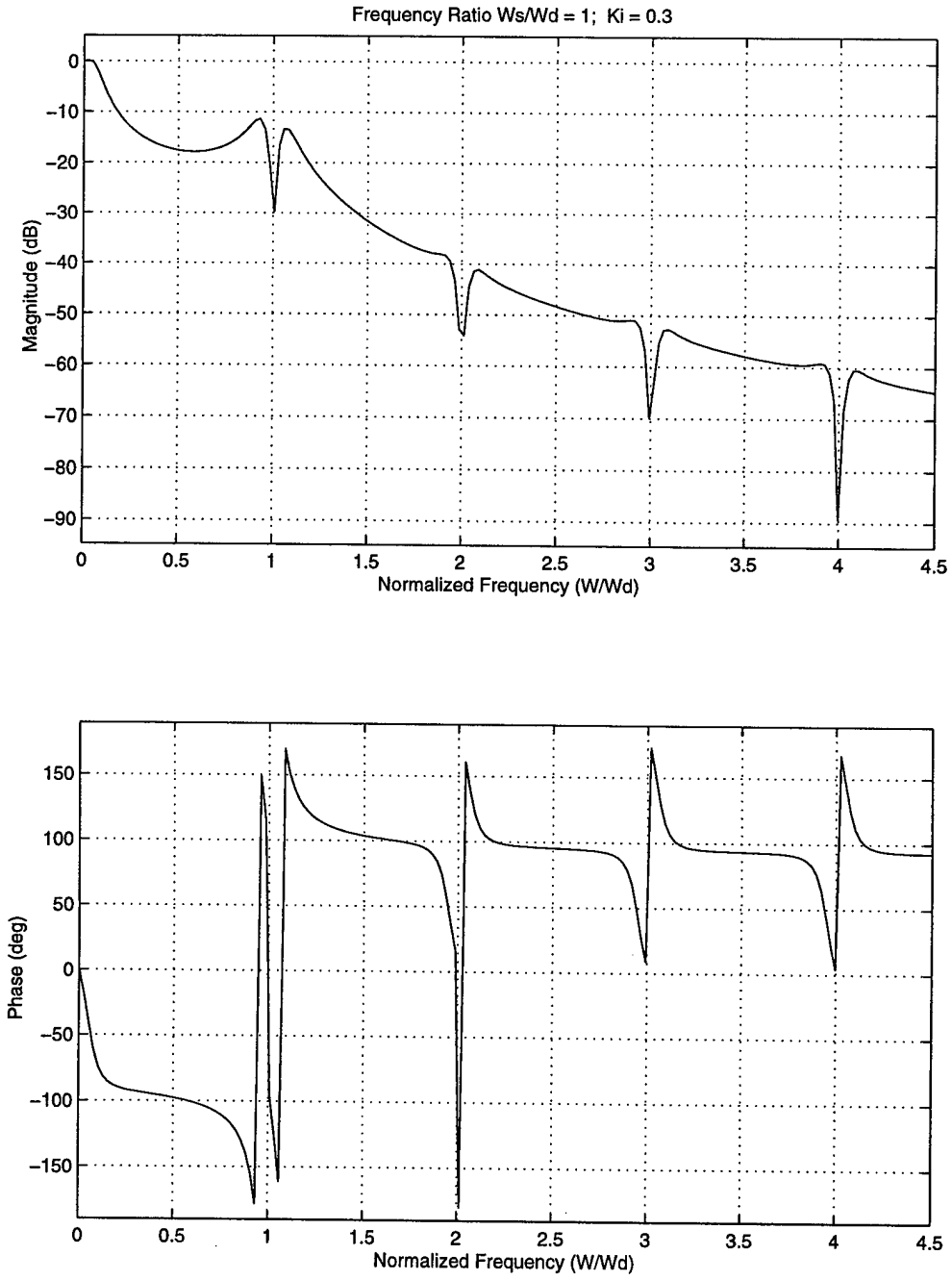

Figure 4.12 Frequency Response Function Plot – FR = 1.0, $K_i = 0.3$

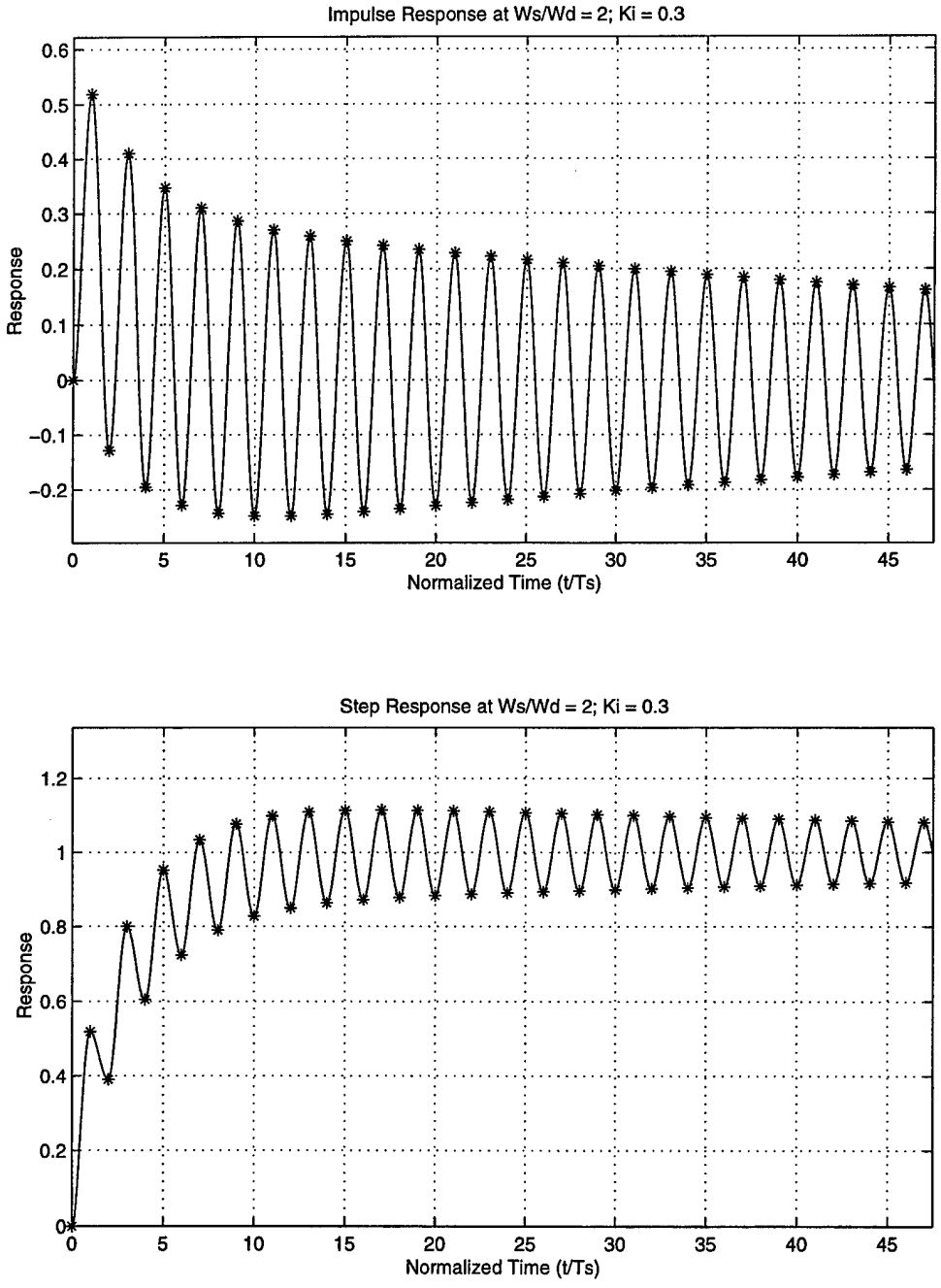

Figure 4.13 Impulse and Step Responses – FR = 2.0, $K_i = 0.3$

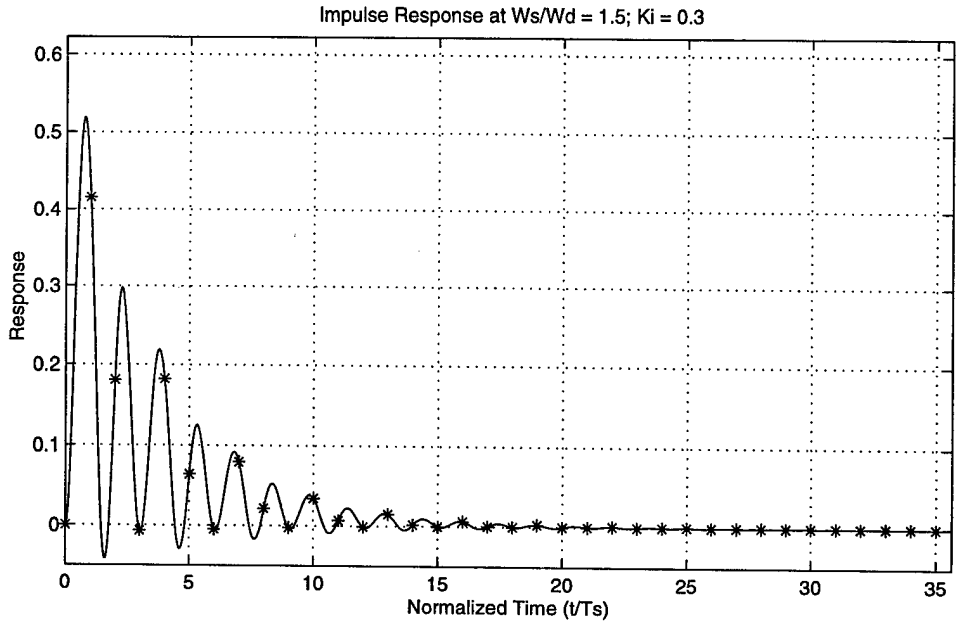

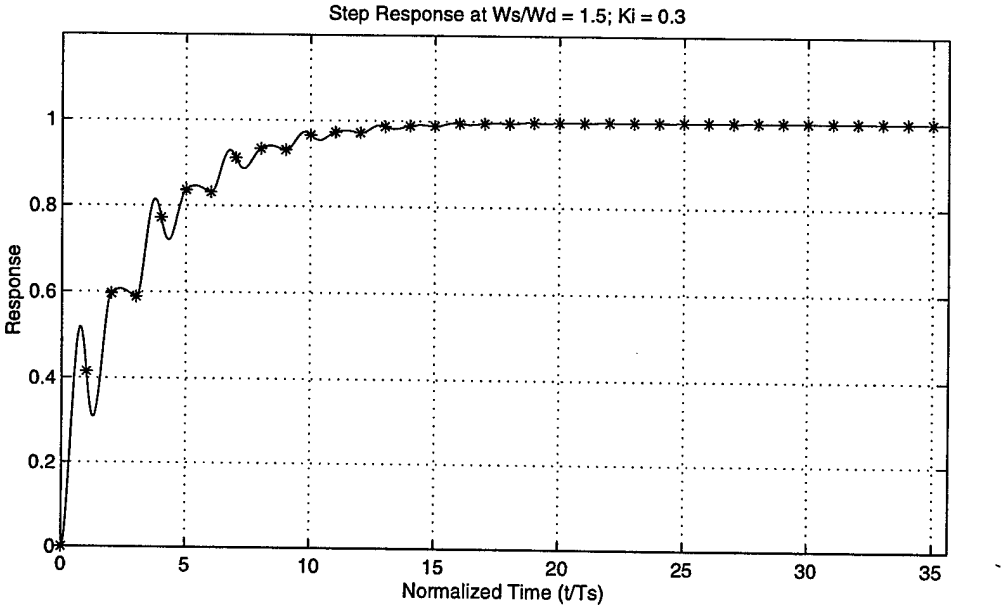

Figure 4.14 Impulse and Step Responses – FR = 1.5, $K_i = 0.3$

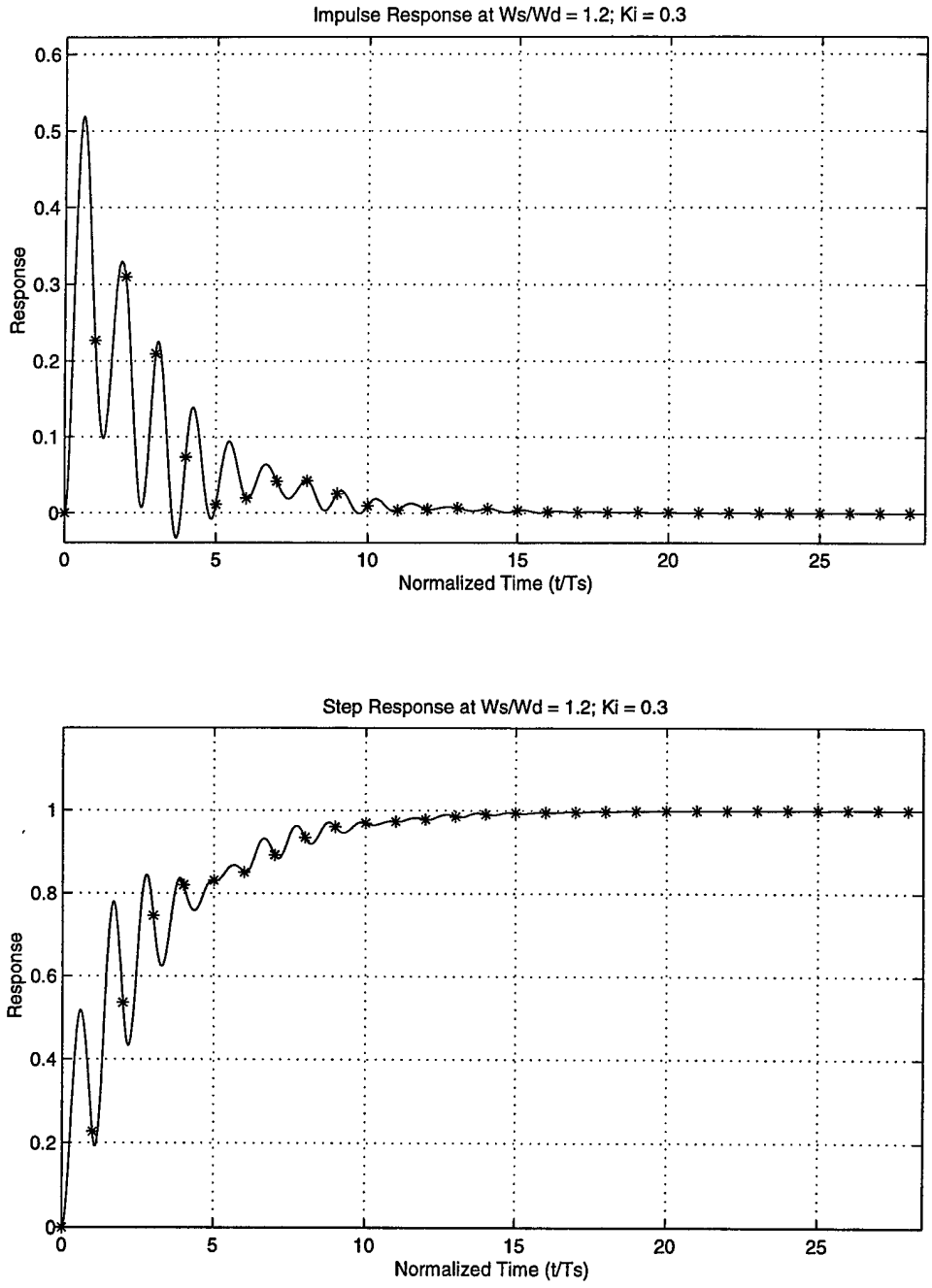

Figure 4.15 Impulse and Step Responses – FR = 1.2, $K_i = 0.3$

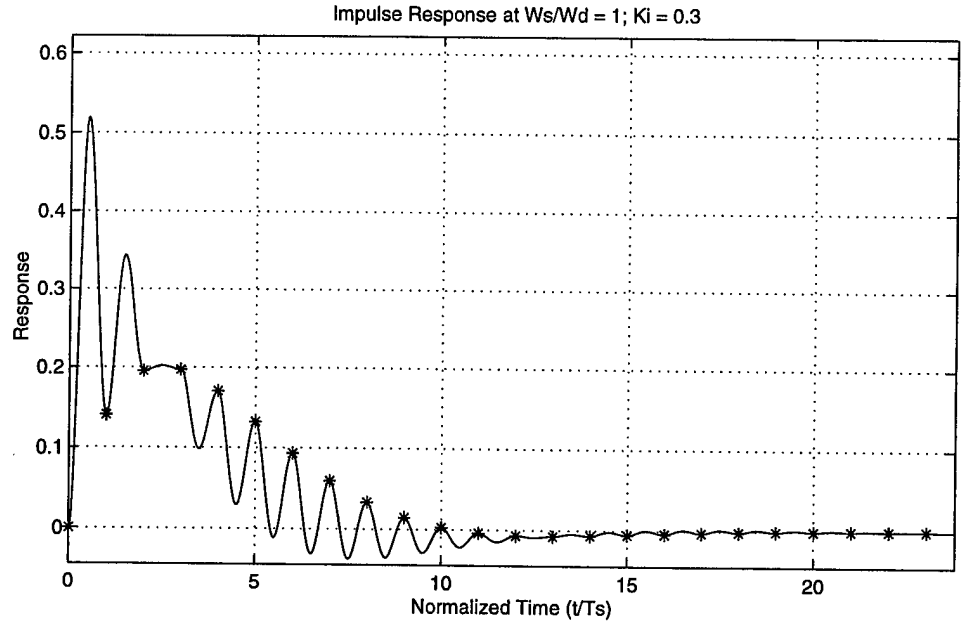

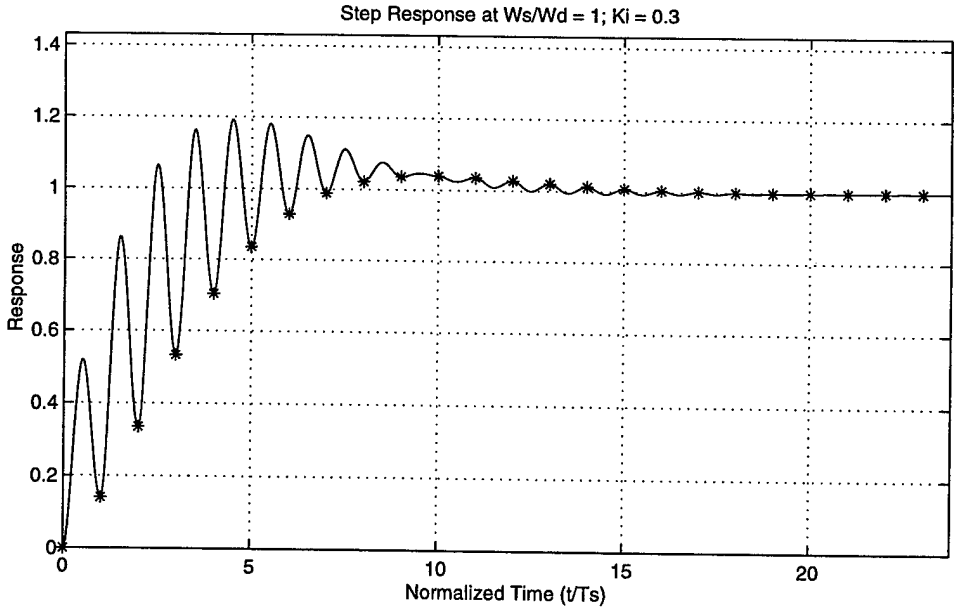

Figure 4.16 Impulse and Step Responses – FR = 1.0, $K_i = 0.3$

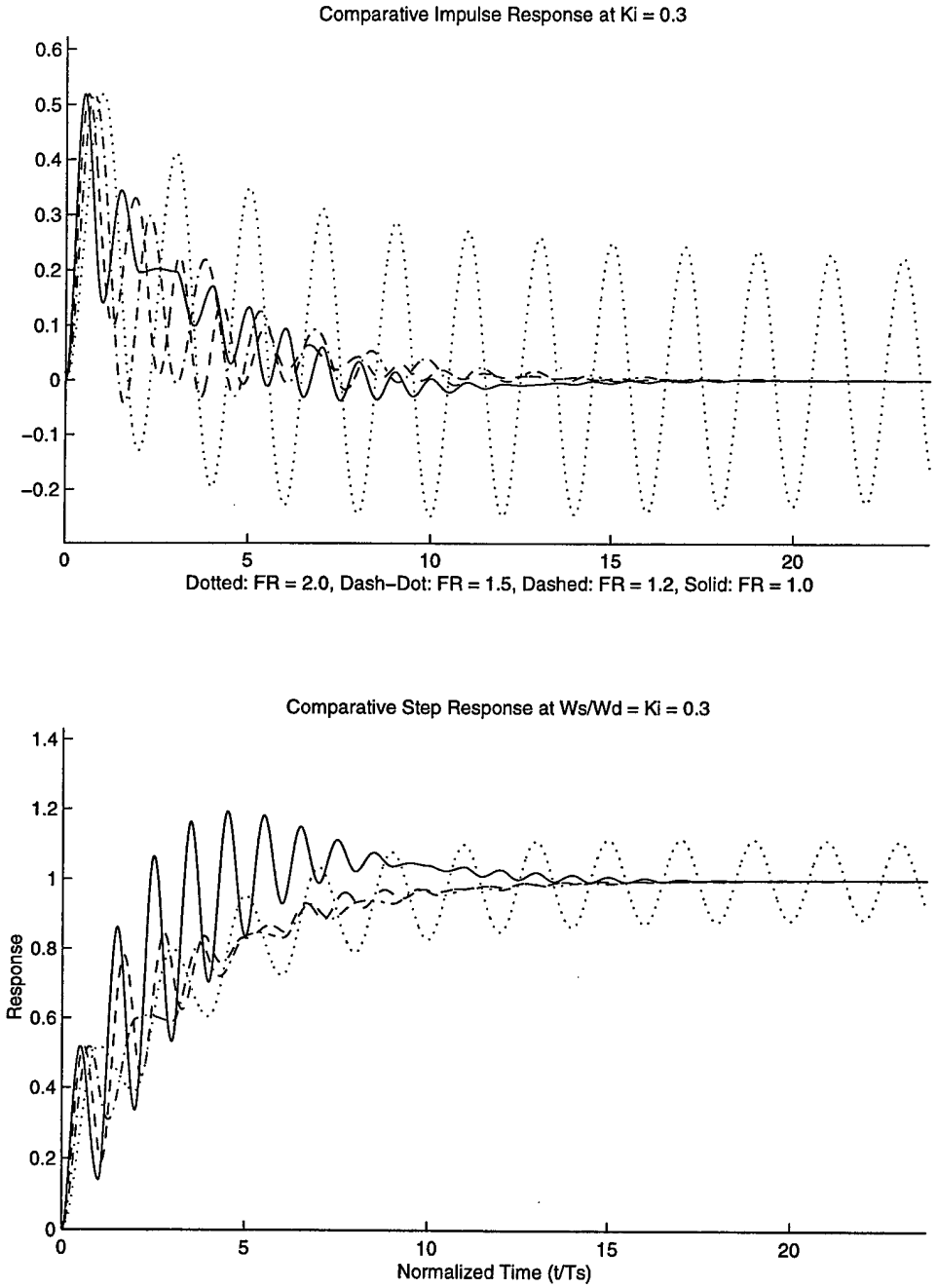

Figure 4.17 Comparison of Impulse and Step Responses for Varying Sample Rate

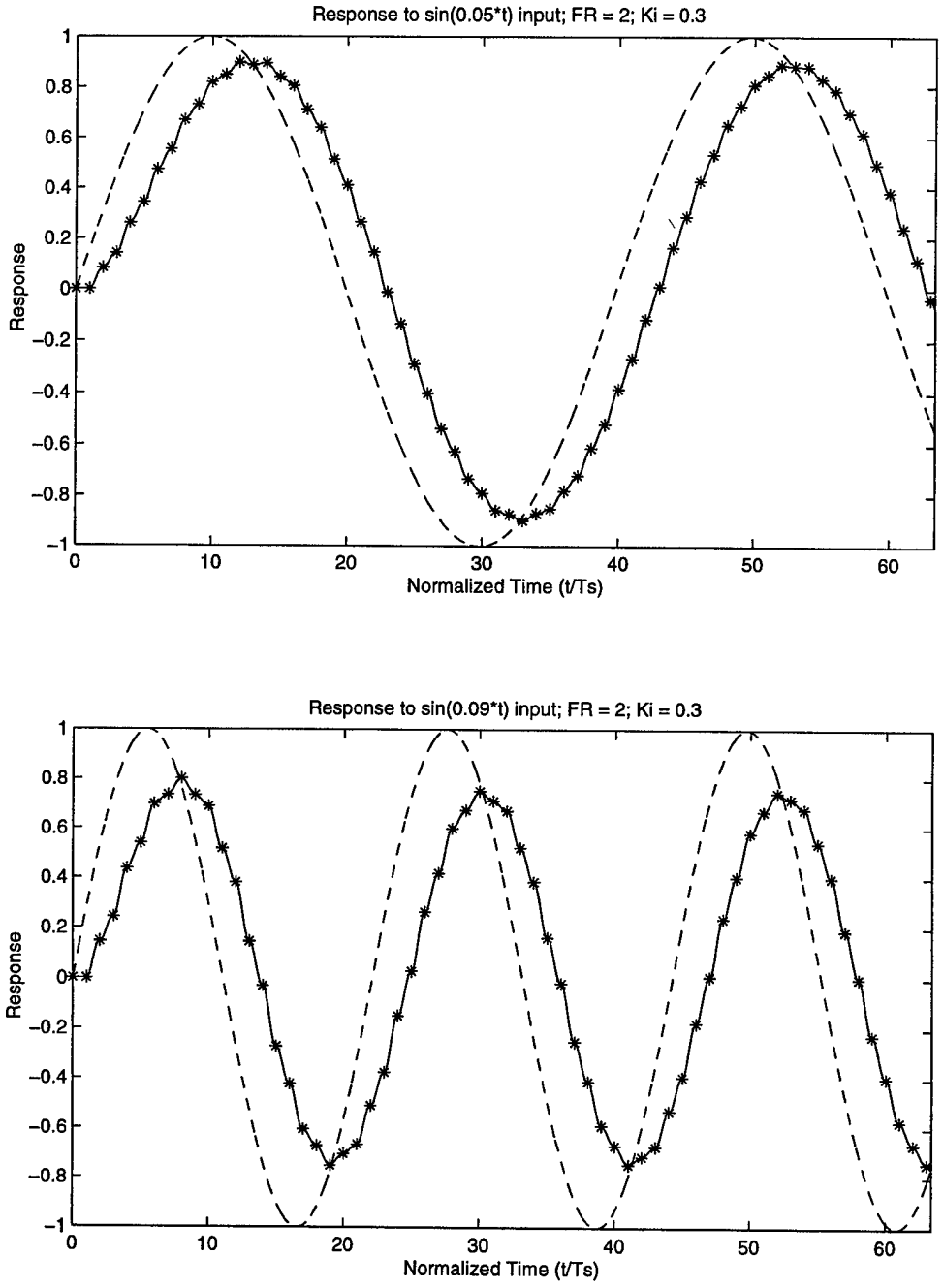

Figure 4.18 Sinusoidal Responses – FR = 2.0, $K_i = 0.3$

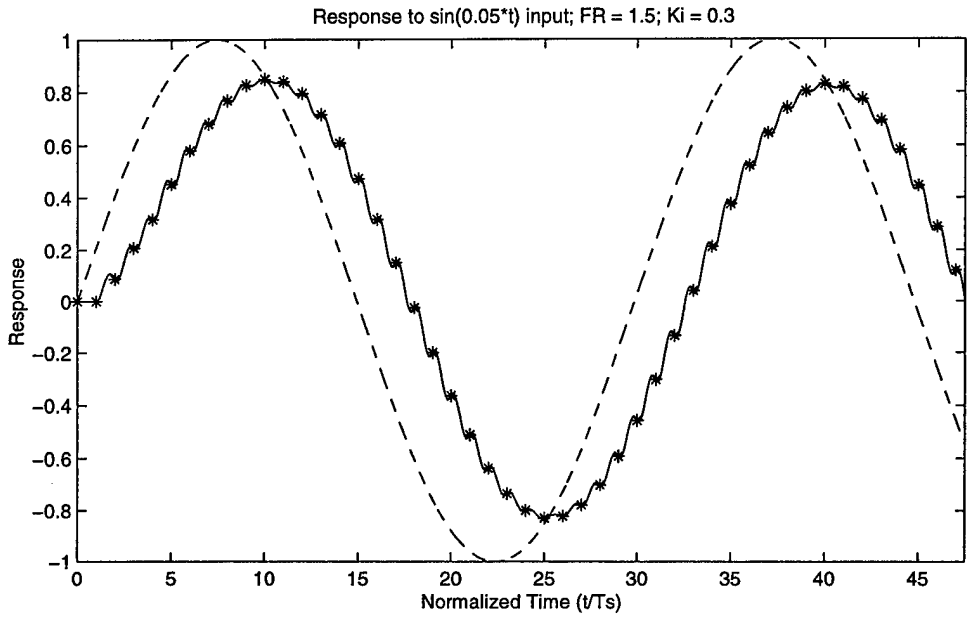

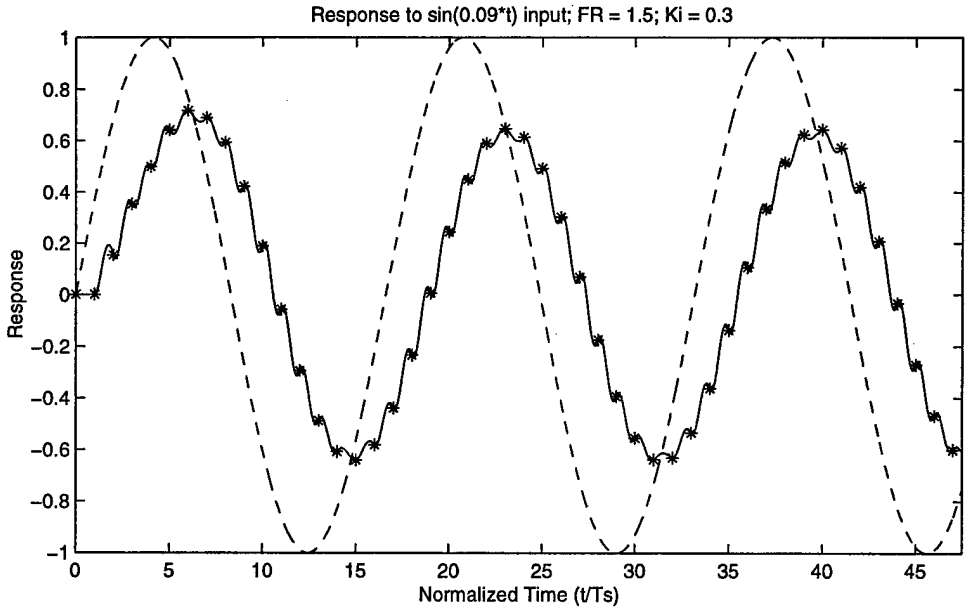

Figure 4.19 Sinusoidal Responses – FR = 1.5, $K_i = 0.3$

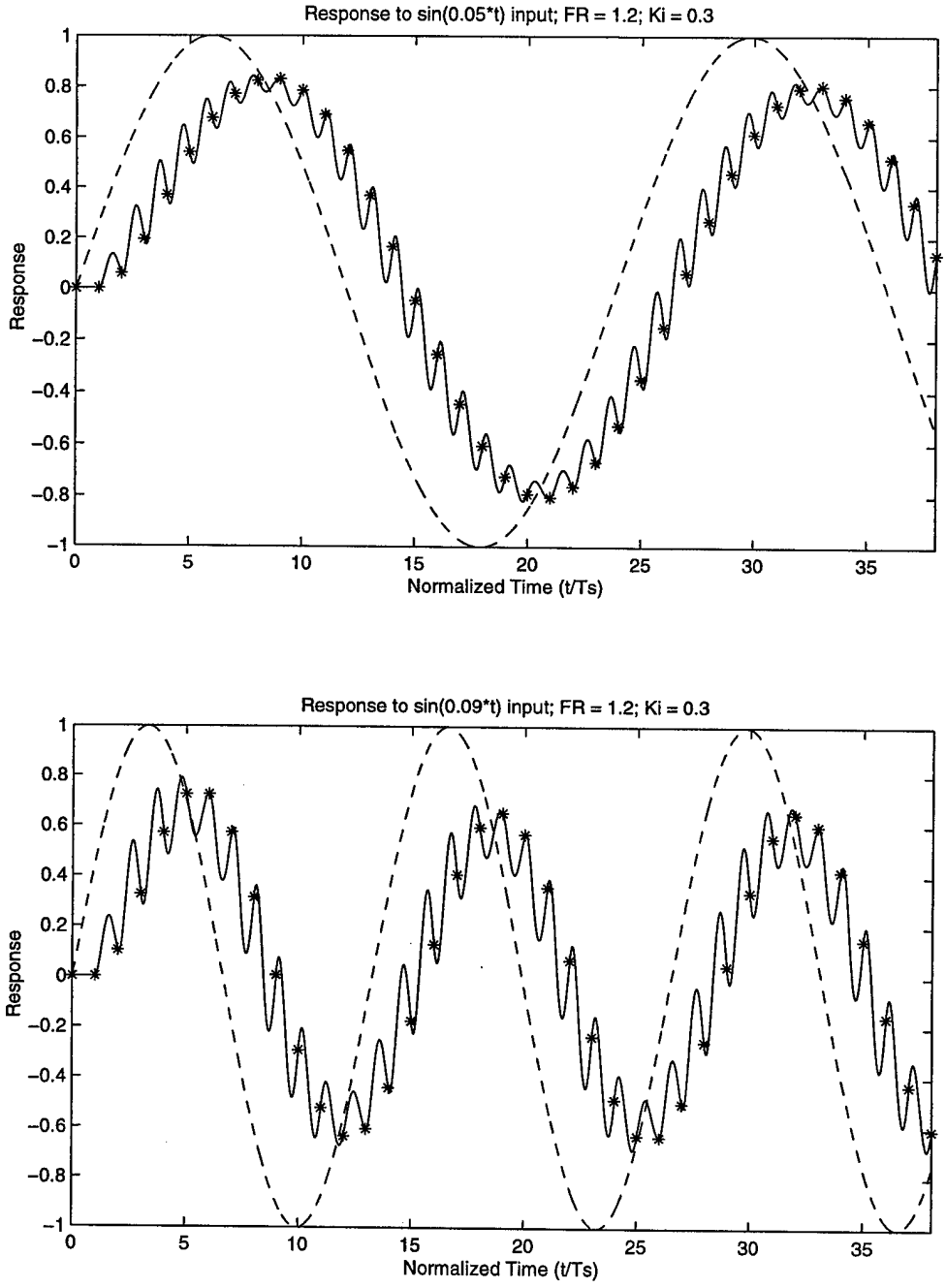

Figure 4.20 Sinusoidal Responses – FR = 1.2, $K_i = 0.3$

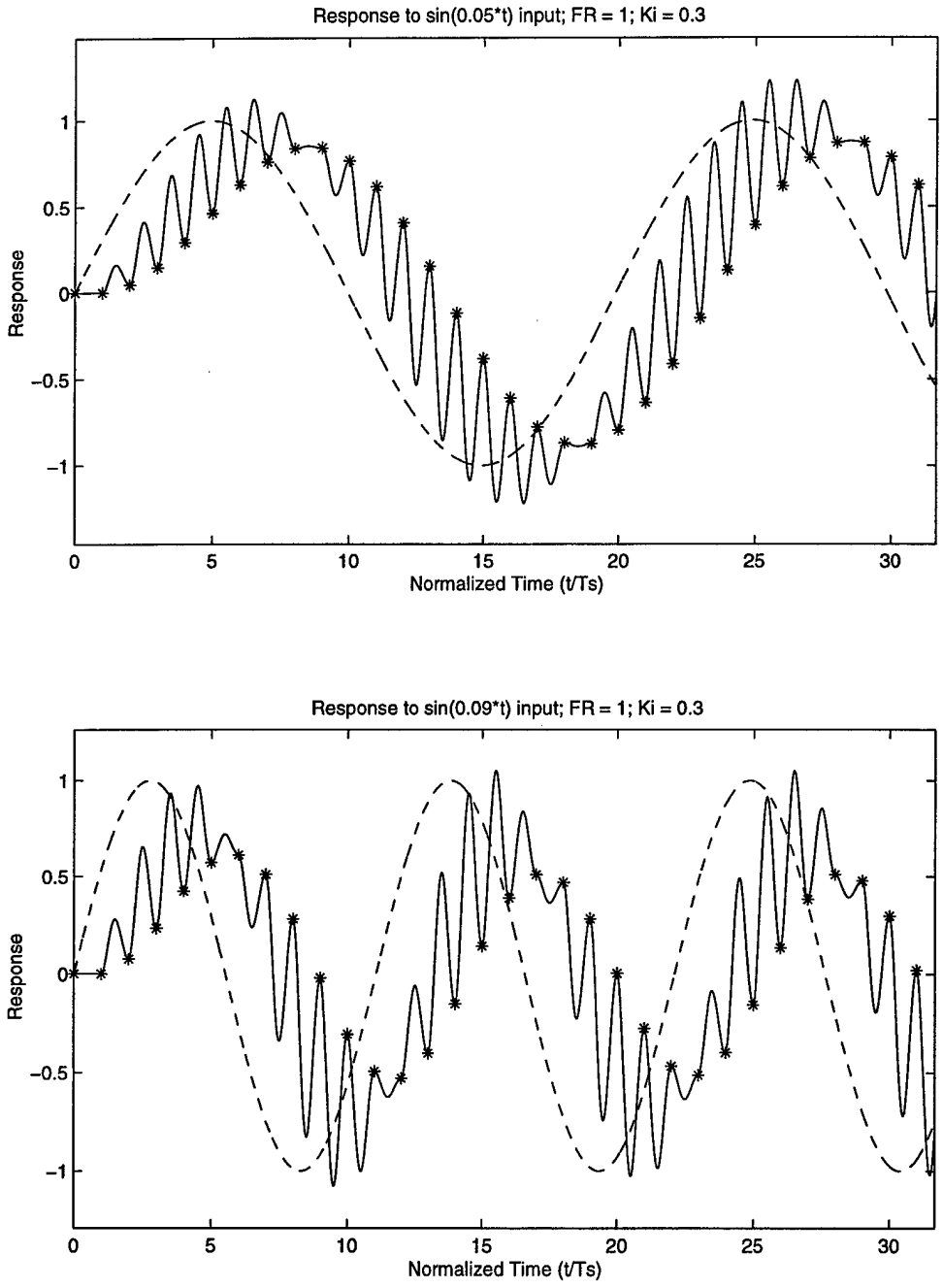

Figure 4.21 Sinusoidal Responses – FR = 1.0, $K_i = 0.3$

location on the z-axis b_3, and recalling that $b_1 = b_2 = b$, the denominator of Equation 4.3 may be set equal to the desired location of the poles:

$$(z - b_3)^2 (z + b) = z^3 + d_1 z^2 + d_2 z + d_3 \quad . \qquad [4.7]$$

Substituting in the values of Equations 4.4 through 4.6 and performing the multiplication gives

$$z^3 + (b - 2b_3) z^2 + (b_3{}^2 - 2bb_3) z + bb_3{}^2 = z^3 + (K_i c_1 + 2b - 1) z^2 + (K_i c_2 + b^2 - 2b) z - b^2 \quad . \qquad [4.8]$$

Equating same-order terms of Equation 4.8 gives three equations with the two unknowns, b_3 and K_i:

$$b - 2b_3 = K_i c_1 + 2b - 1 \quad , \qquad [4.9]$$

$$b_3{}^2 - 2bb_3 = K_i c_2 + b^2 - 2b \quad , \text{ and} \qquad [4.10]$$

$$bb_3 = -b^2 \quad . \qquad [4.11]$$

Solving Equation 4.11 for b_3 gives

$$b_3 = \sqrt{-b} \quad . \qquad [4.12]$$

Substituting Equation 4.12 into Equation 4.9 and solving gives

$$K_i = \frac{1 - b - 2\sqrt{-b}}{c_1} \quad . \qquad [4.13]$$

Substituting Equations 4.12 and 4.13 into Equation 4.10, and recalling Equation 3.37 ($c_2 = bc_1$) gives independent proof of correct solution for the two unknowns.

Figures 4.22 and 4.23 are the plots of the root loci and impulse and step responses when K_i is as given in Equation 4.13. Examination of Figure 4.22 shows placement of the poles is as desired. Figure 4.23 shows a much improved impulse response, the best of the previous plots, and a step response with no discrete overshoot. Again, this step response is not the "best" when compared to Figures 4.14 and 4.15. No results such as deadbeat response for the proportional controller, then, are seen here, though this was not expected.

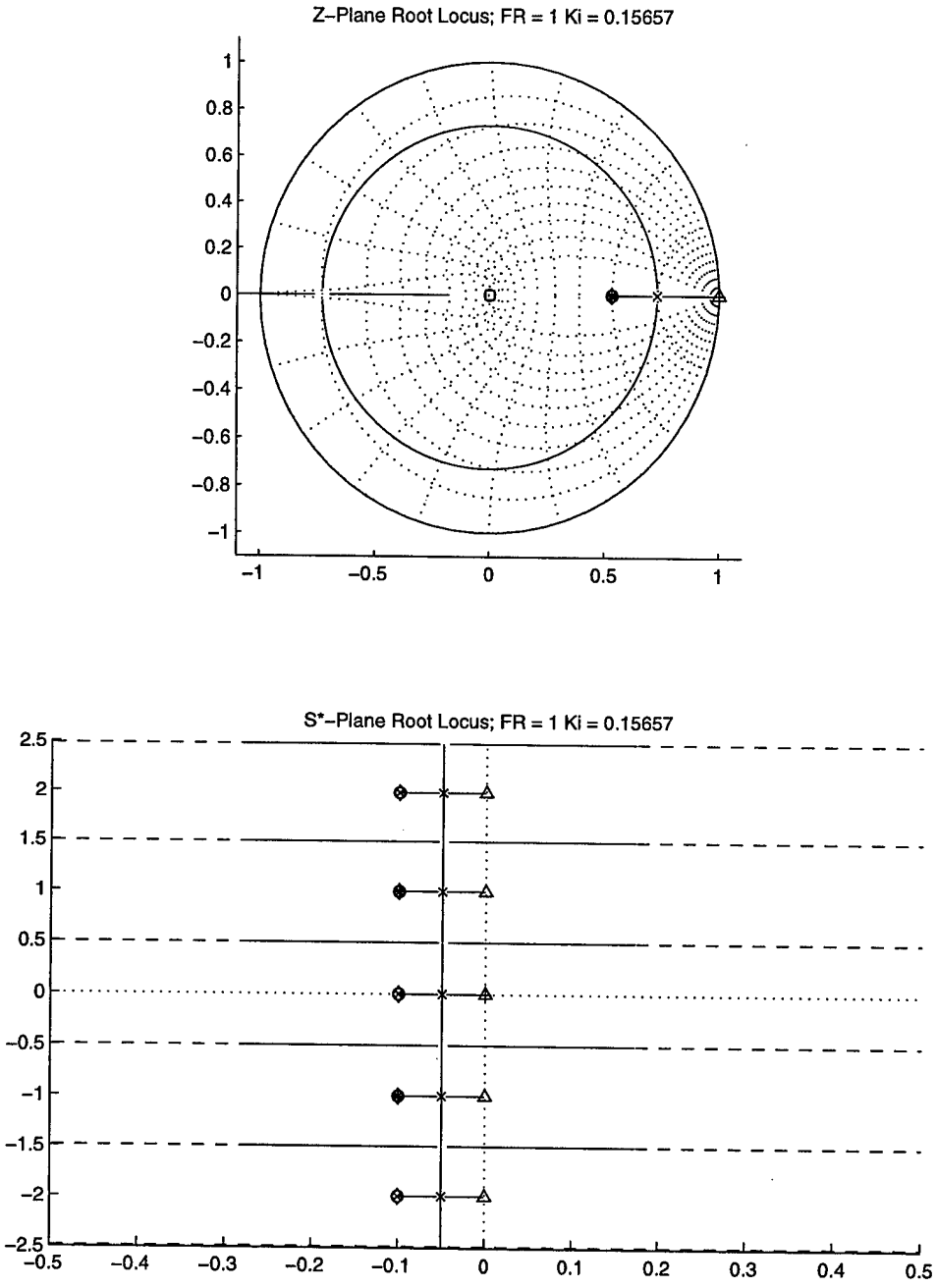

Figure 4.22 Root Loci for FR = 1.0, $K_i = 0.15657$

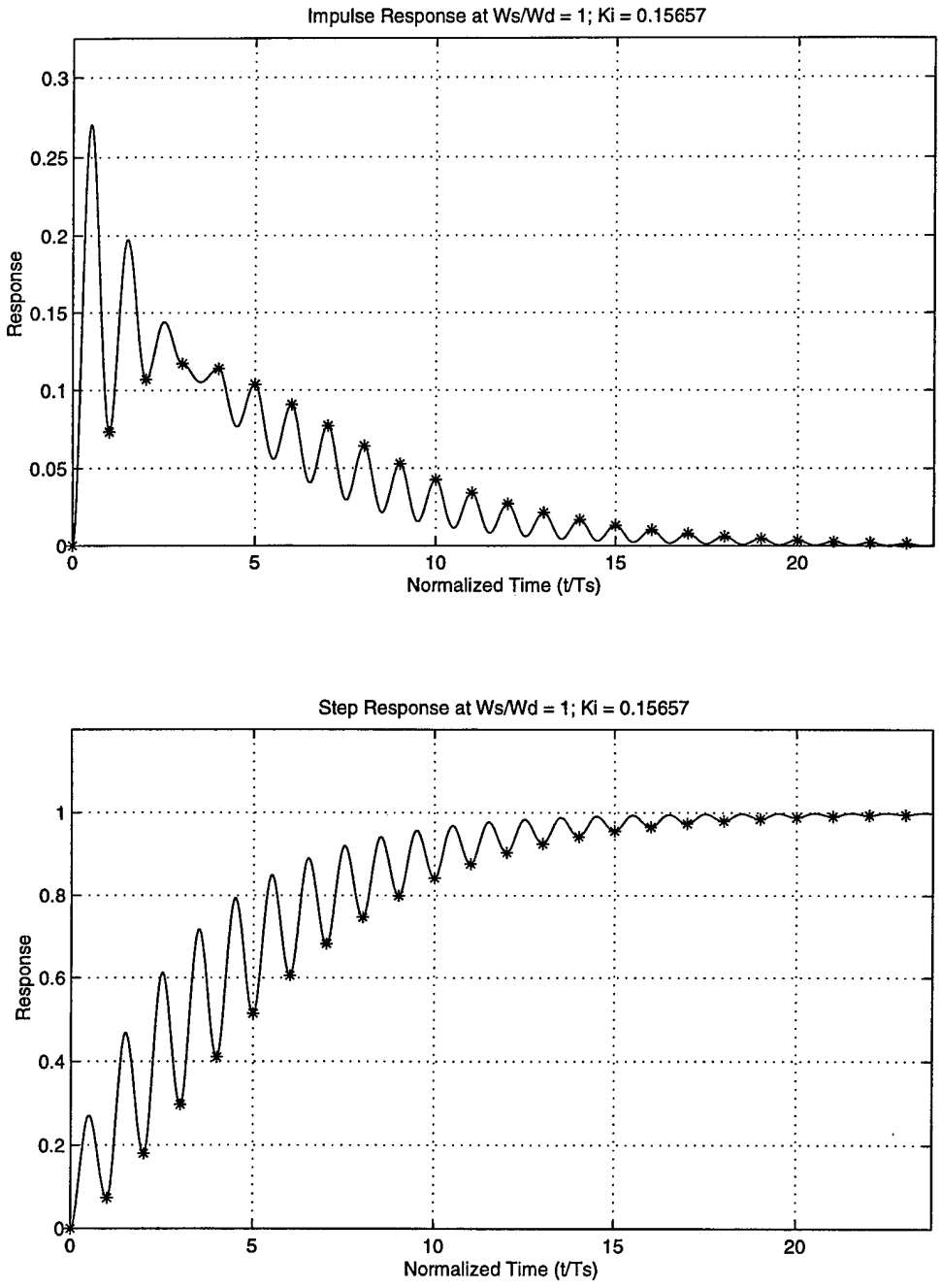

Figure 4.23 Impulse and Step Responses – FR = 1.0, $K_i = 0.15657$

4.2 Design of a Proportional-Integral Controller at FR = 1.0

Having a firmer understanding of the integral controller in which aliasing is allowed now allows the design of a proportional-integral (PI) controller in which aliasing is allowed. The plant used in this design will again be the second-order plant of Equation 3.4. The controller, for PI control is defined as

$$G_c(z) = K_p + K_i \frac{z}{z-1} = \frac{(K_p + K_i)z - K_p}{z-1} \quad . \qquad [4.14]$$

Using this in Equation 3.3 and solving for $F(z)$ gives

$$F(z) = \frac{[(K_p + K_i)z - K_p](z+b_1)(z+b_2)}{[(K_p + K_i)z - K_p](c_1 z + c_2) + (z-1)(z+b_1)(z+b_2)} \quad , \qquad [4.15]$$

and again the constants b_1, b_2, c_1, and c_2 are defined in Equations 3.13 through 3.16. Multiplying the denominator gives

$$F(z) = \frac{[(K_p + K_i)z - K_p](z+b_1)(z+b_2)}{z^3 + d_1 z^2 + d_2 z + d_3} \quad , \qquad [4.16]$$

where

$$d_1 = (K_p + K_i)c_1 + b_1 + b_2 - 1 \quad , \tag{4.17}$$

$$d_2 = (K_p + K_i)c_2 - K_p c_1 + b_1 b_2 - b_1 - b_2 \quad , \text{and} \tag{4.18}$$

$$d_3 = -K_p c_2 - b_1 b_2 \quad . \tag{4.19}$$

Since the deadbeat response is the aim here, select the frequency ratio of $FR = 1.0$ and the gain of the proportional portion of the controller to be equal to that which gives the deadbeat response:

$$K_p = -\frac{b}{c_1} \quad . \tag{4.20}$$

To begin, suppose the gain for the integral portion of the controller is as found in Equation 4.13. Figures 4.24 and 4.25 show the root loci and impulse and step responses for these values of the gain. Examination of Figure 4.24 shows the two "plant" poles located on top of the zeros as expected and the integrator pole close to the point $z = 1$. This seems to be causing the slow integrator response seen in the step response of Figure 4.25. Here again, the control is shown as the dash-dot line. The impulse response appears to be deadbeat, but closer examination shows small oscillations for many sample

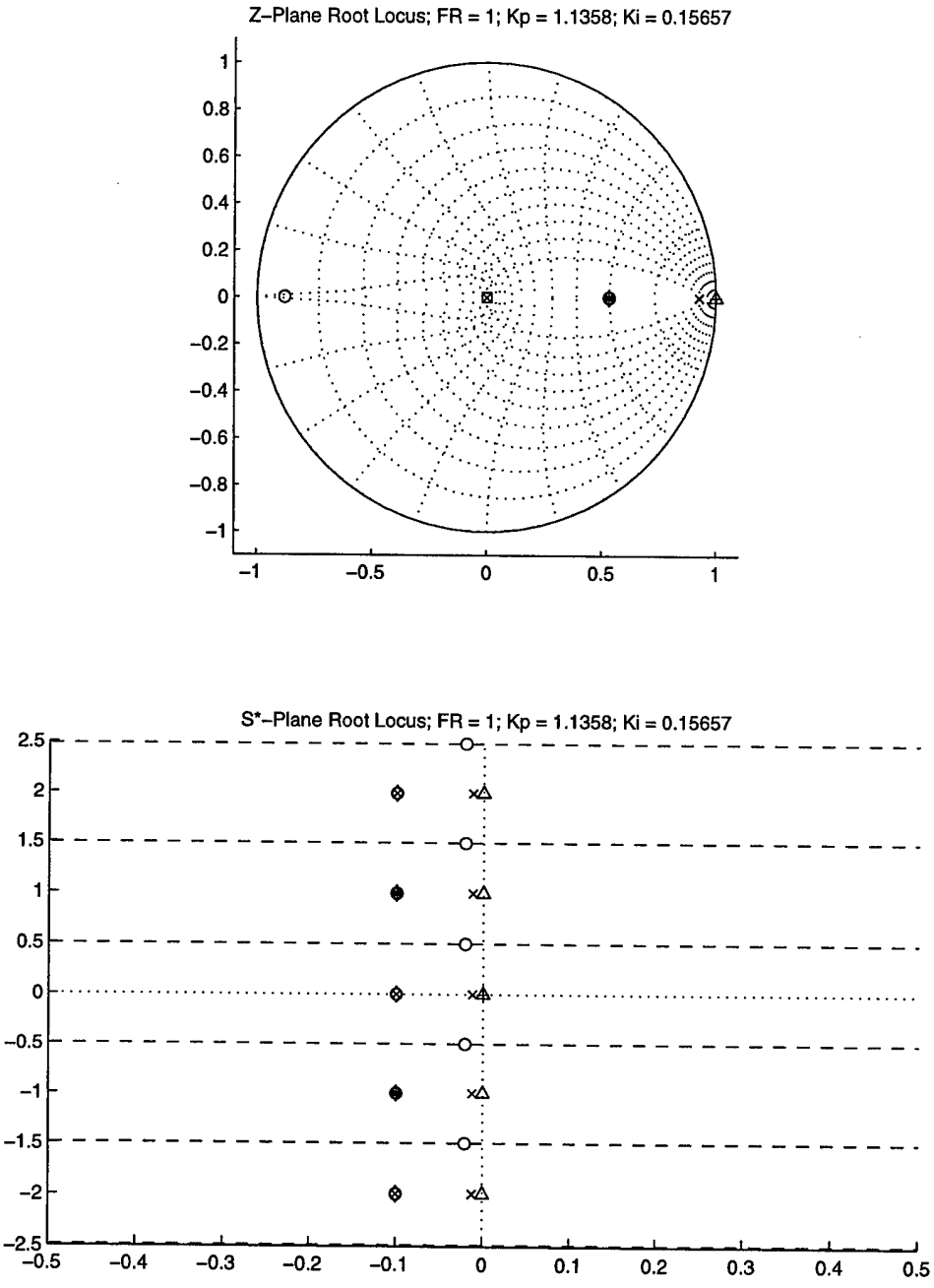

Figure 4.24 Root Loci – FR = 1.0, $K_p = 1.1358$, $K_i = 0.15657$

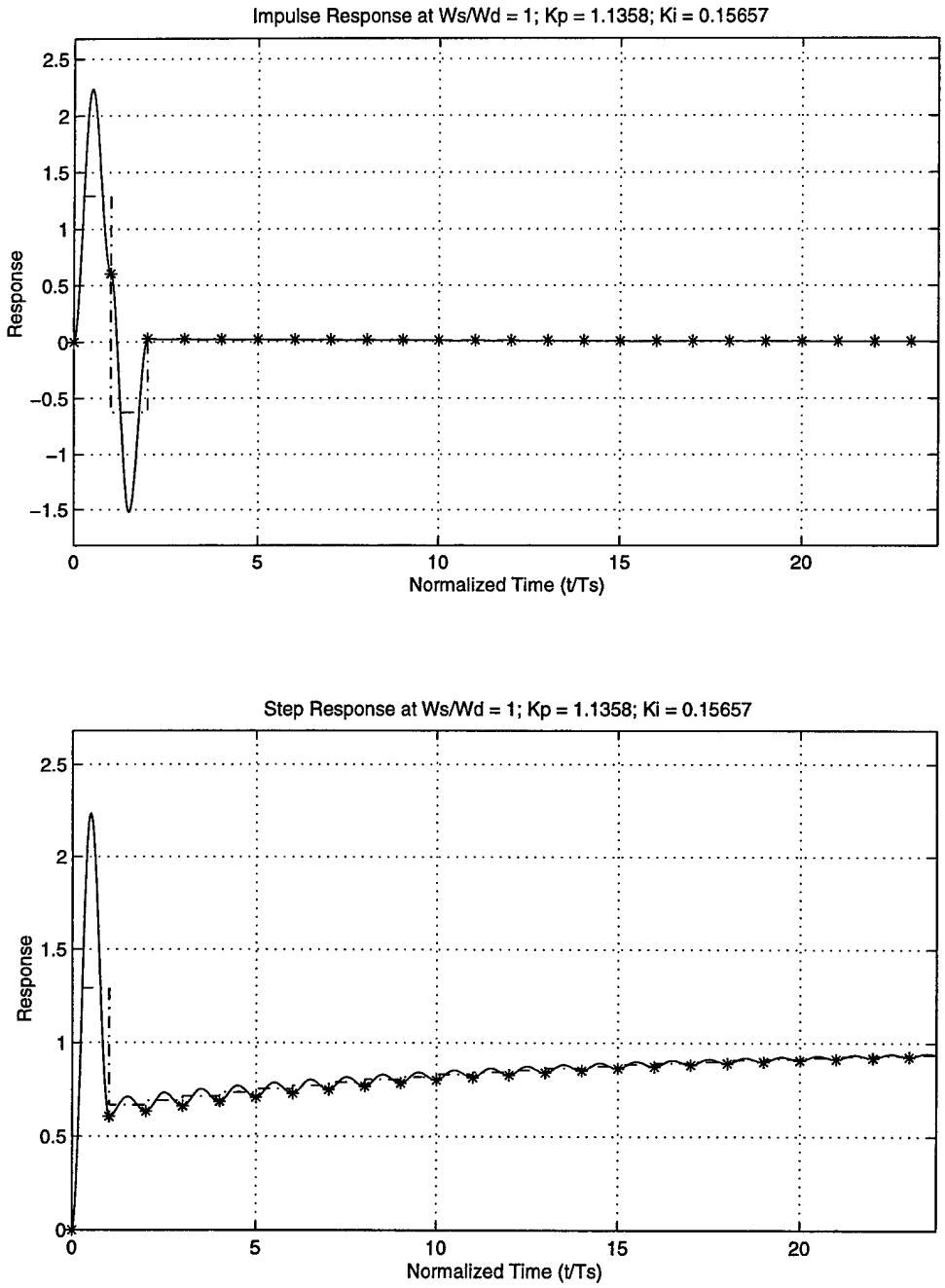

Figure 4.25 Impulse and Step Responses – FR = 1.0, K_p = 1.1358, K_i = 0.15657

periods. The step response shows the characteristics of the deadbeat response, but with the addition of the integrator, this response is no longer deadbeat.

To try and increase the integrator response, place the pole for the integrator closer to $z=0$, but with it remaining on the positive axis. To place it directly at $z=0$ the denominator of $F(z)$ must be

$$z^2(z+b)=z^3+d_1z^2+d_2z+d_3 \quad . \qquad [4.21]$$

Using Equations 4.17 through 4.19 in Equation 4.21 and solving for the values of K_p and K_i gives

$$K_p=-\frac{b}{c_1} \quad , \qquad [4.22]$$

which is the same as it was for the deadbeat response (Equation 3.39) and

$$K_i=\frac{1}{c_1} \quad . \qquad [4.23]$$

Figures 4.26 and 4.27 show the results of using these gains. Two roots are indeed placed at $z=0$ corresponding to $s^*=-\infty$, with the third root placed at the location of the zeros

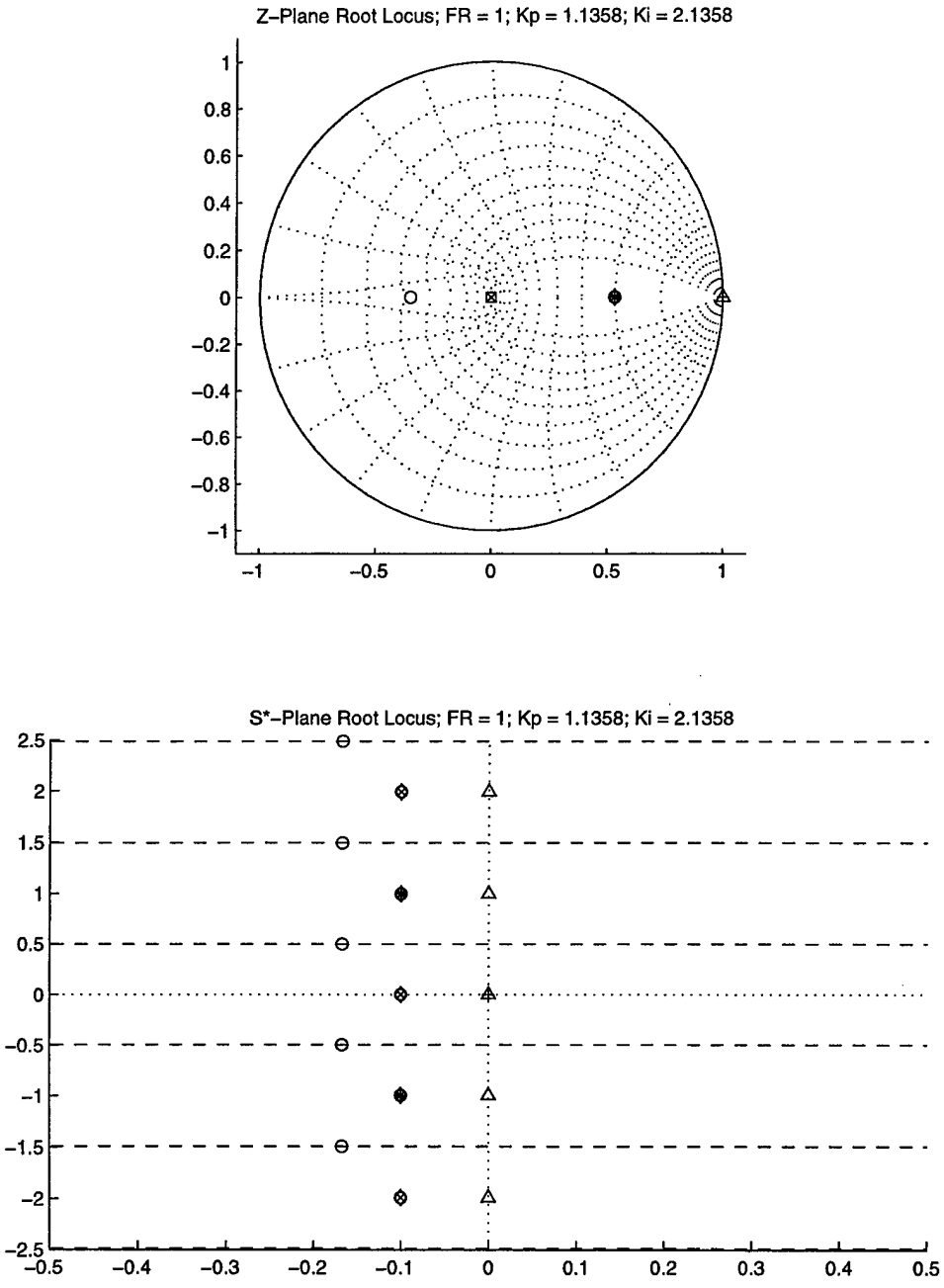

Figure 4.26 Root Loci – FR = 1.0, K_p = 1.1358, K_i = 2.1538

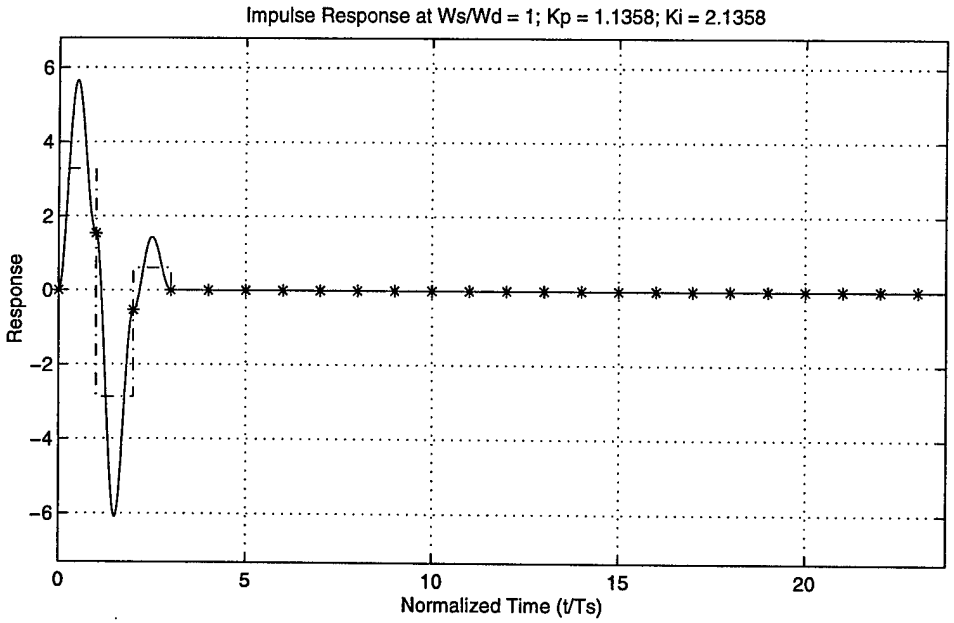

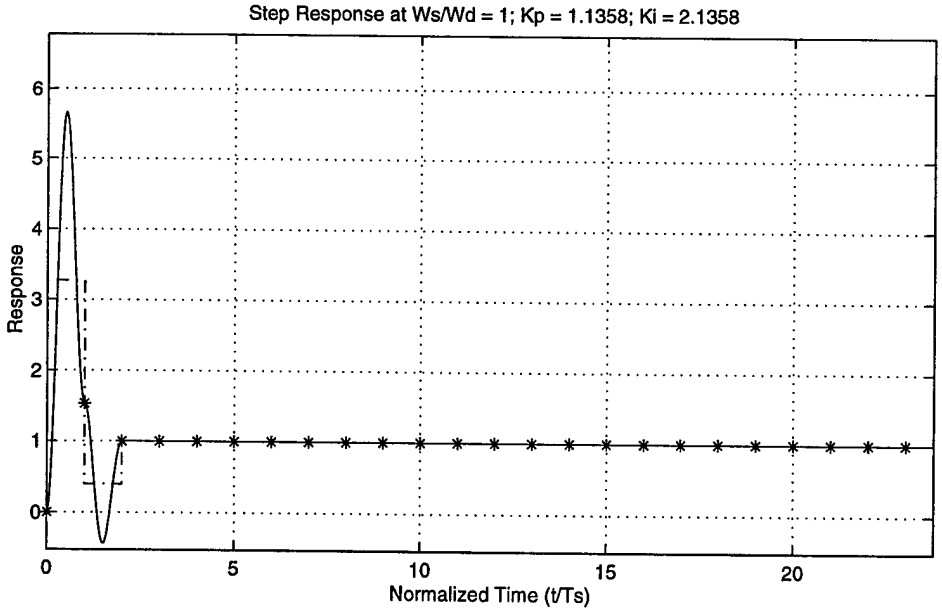

Figure 4.27 Impulse and Step Responses – FR = 1.0, $K_p = 1.1358$, $K_i = 2.1358$

found from the denominator term of $H(z)$. As a result, the response is closer to the sought-after deadbeat response. The impulse response returns to zero following the third sample period, and the step response is at a value of one after two sample periods. Overshoot increases by quite a lot in this case. Control effort is also plotted.

Perhaps placing the pole on the location of the other stationary pole will give better response. This zero is located at

$$z = -b \quad . \qquad [4.24]$$

Equation 4.21 now becomes

$$z(z+b)^2 = z^3 + d_1 z^2 + d_2 z + d_3 \quad , \qquad [4.25]$$

and the solution process yields

$$K_p = -\frac{b}{c_1} \quad \text{, and} \qquad [4.26]$$

$$K_i = \frac{(c_1 + c_2)b}{c_1 c_2} \quad . \qquad [4.27]$$

Equation 4.27 simplifies with the following. Recall Equation 3.15, repeated here for clarity:

$$c_1 = \omega_n^{\,2}(a_0 - a_1 b_1 - a_2 b_2) \quad . \qquad [4.28]$$

But, at $FR = 1.0$, $b_1 = b_2 = b$ and Equation 4.28 becomes

$$c_1 = \omega_n^{\,2}[a_0 - b(a_1 + a_2)] \quad . \qquad [4.29]$$

Since $a_1 + a_2 = -a_0$ (see Equations 3.8 through 3.10) Equation 4.29 becomes

$$c_1 = \omega_n^{\,2}(a_0 + b a_0) = a_0 \omega_n^{\,2}(1+b) \quad . \qquad [4.30]$$

From Equation 3.8, $a_0 = \dfrac{1}{p_1 p_2} = \dfrac{1}{\omega_n^{\,2}}$, so

$$c_1 = 1 + b \quad . \qquad [4.31]$$

Likewise

$$c_2 = c_1 b = b(1+b) \quad . \qquad [4.32]$$

Substituting Equation 4.31 and 4.31 into Equation 4.27 gives

$$K_i = \frac{(c_1 + c_2)b}{c_1 c_2} = \frac{[1 + b + b(1+b)]b}{(1+b)b(1+b)} = 1.0 \quad . \qquad [4.33]$$

Using the values of K_p from Equation 4.26 and $K_i = 1.0$, Figure 4.28 shows the placement of the poles and controller zero. Notice the location of the controller zero exactly opposite the zeros found from the denominator of $H(z)$ in the z-plane. In the s*-plane, these zeros all lie at the same real value in the $j\omega$ direction. Two poles are located at these zeros with the third pole at $z = 0$ or $s^* = -\infty$.

Figure 4.29 shows the desired deadbeat response in both the impulse and step responses. Control effort is also plotted with the dash-dot line. There is a large amount of overshoot in both cases. However, the response is truly deadbeat, and with the addition of the integrator, the final desired value of both the impulse and step is attained with no oscillations. Additionally, control effort to attain this response is simple and not overly large. This method of design, then, produces some exciting possibilities for control.

In examining the impulse response, one can see that the sample rate is such that the response resulting from the unit impulse at time $t = 0$, actually a step function to the continuous system once the zero-order hold is applied, is exactly equal and opposite to the impulse resulting from the impulse returning to zero at time $t = T_s$. The correct selection of the sample period allows this "phasing" of the response and its affect on the control effort. This method of control is reminiscent of the idea behind input shaping.

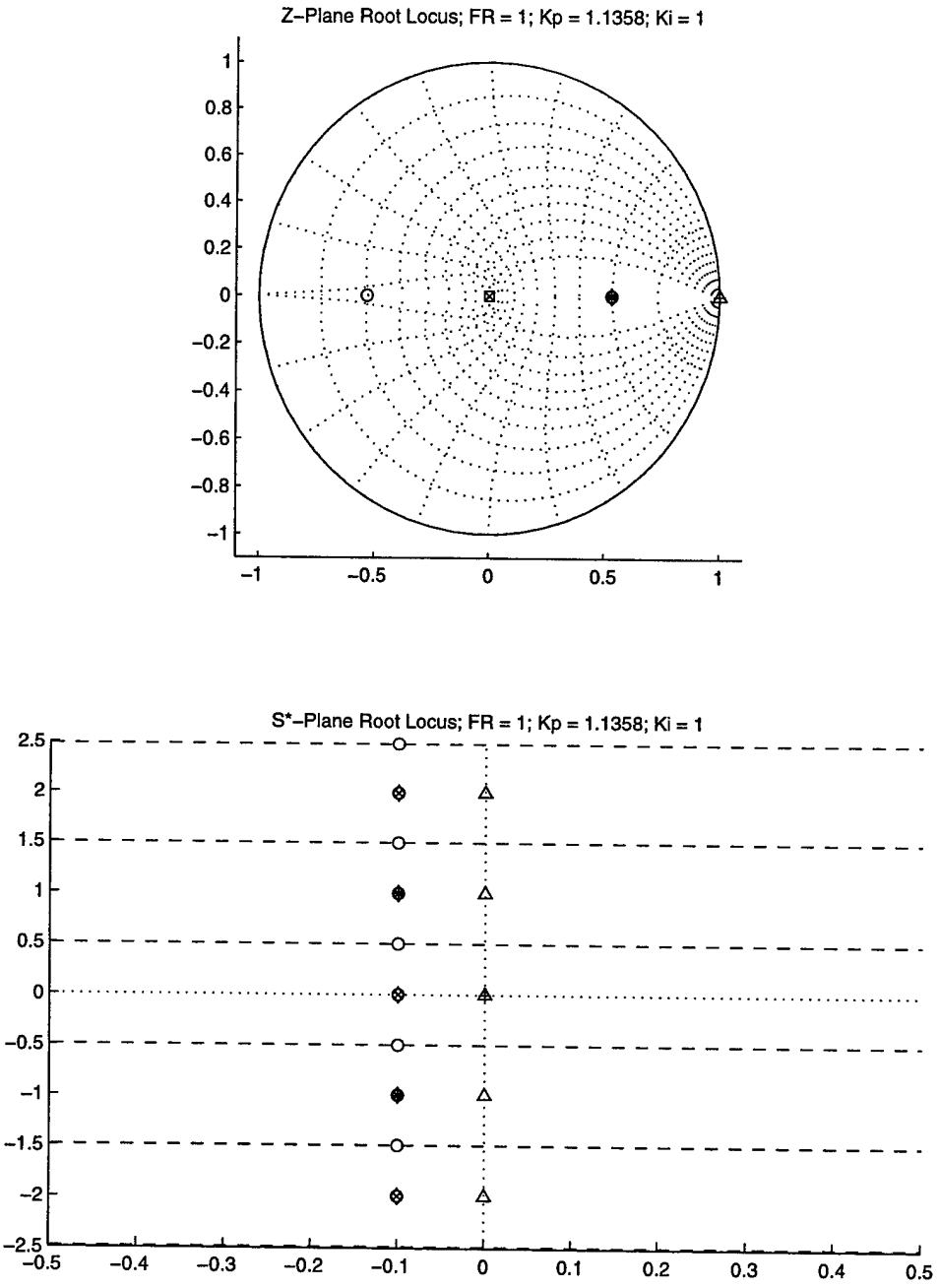

Figure 4.28 Root Loci – FR = 1.0, K_p = 1.1358, K_i = 1.0

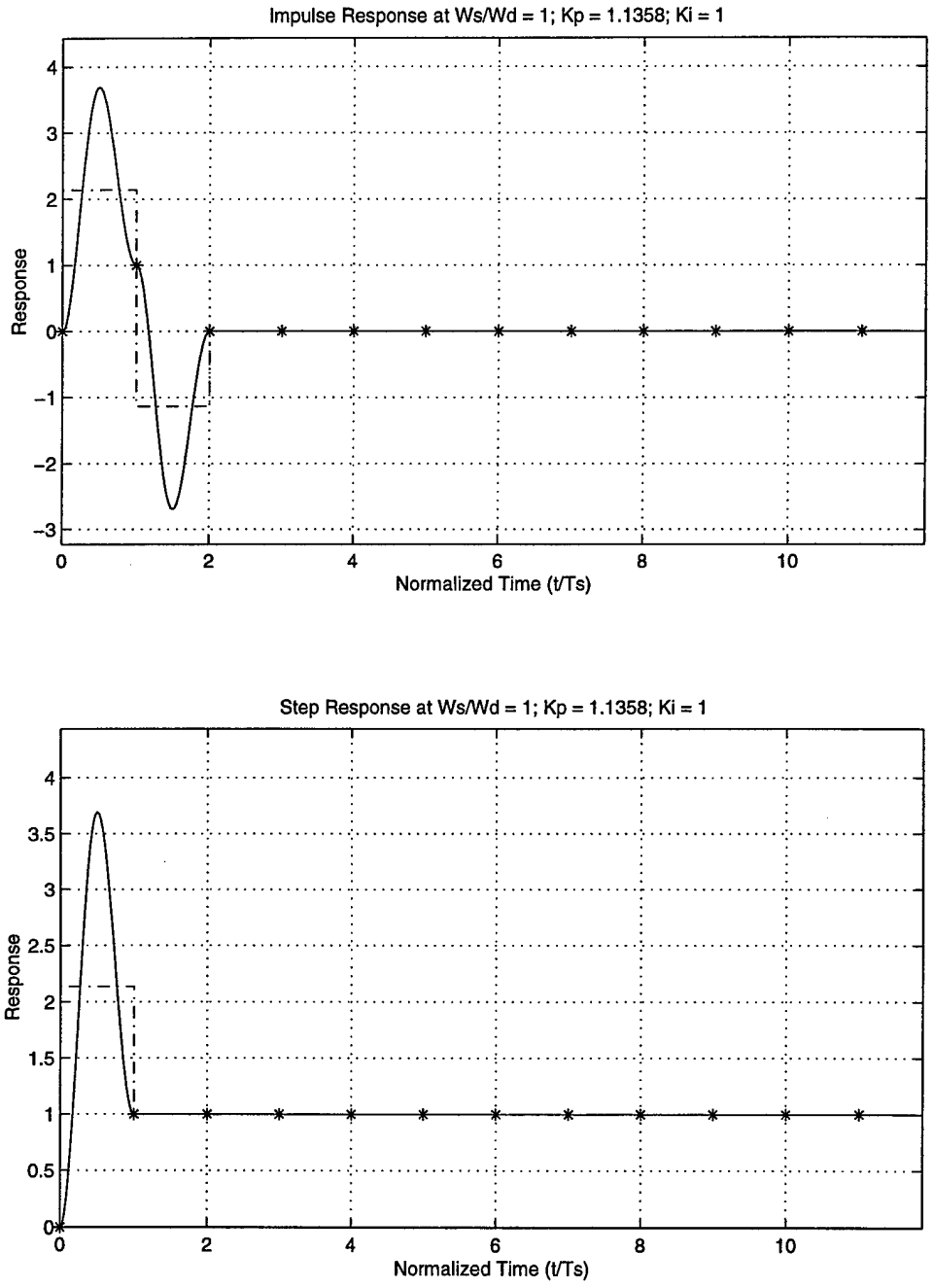

Figure 4.29 Impulse and Step Responses – FR = 1.0, K_p = 1.1358, K_i = 1.0

Currently much work is being accomplished on a method of control called input or command shaping, including the recent examples cited here [44], [45], [46], [47], and [48]. Input shaping is a feedforward technique used to eliminate vibration from the system under control. It consists of convolving a sequence of impulses with the desired command to the system, with the resulting shaped input used to drive the system. This input effectively cancels the vibrating poles regardless of the desired system input. One can see the similarities between input shaping and the results of the simple PI-controller of this dissertation.

Examining the response of the deadbeat system found above to a sinusoidal input shows again the limitation of such a system. Figure 4.30 shows the response to a sinusoid with frequencies lower than the sampling frequency. The controller is able to follow the input adequately at the discrete points, with the overshoot seen in the deadbeat controller coming between each sample period. Figure 4.31 shows the response of the system when the inputs frequencies are greater than the sampling frequency. Here, the controller cannot follow the input signal. Further showing of the limitation of this controller—input frequencies cannot be greater than that of the sampler.

Robustness of this system is again examined for five percent changes in the system parameters. Figure 4.32 plots the impulse and step responses as the natural frequency is varied, and Figure 4.33 plots the responses for changes in the damping ratio. Results of

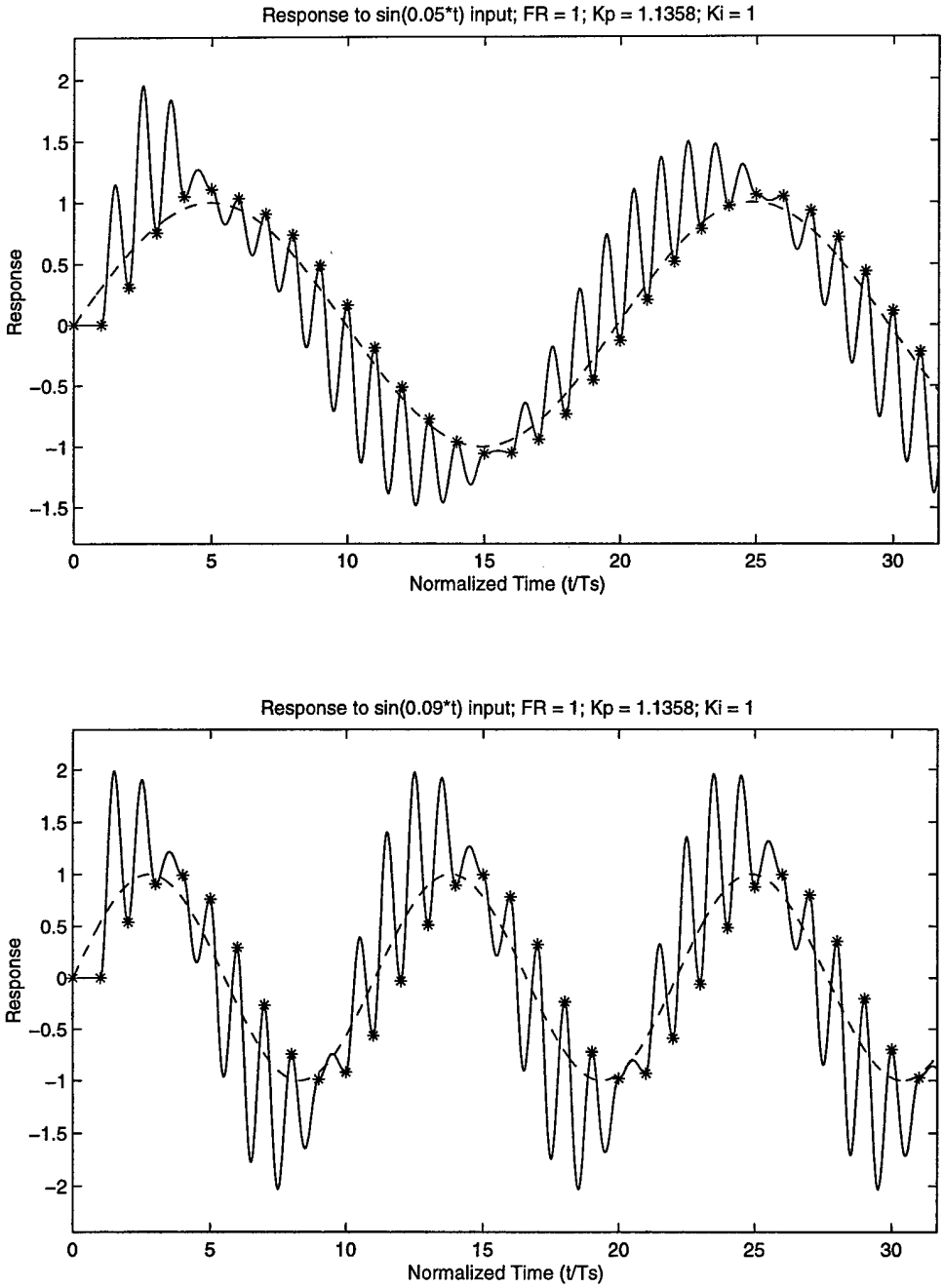

Figure 4.30 Response to Sinusoidal Inputs at Low Frequencies

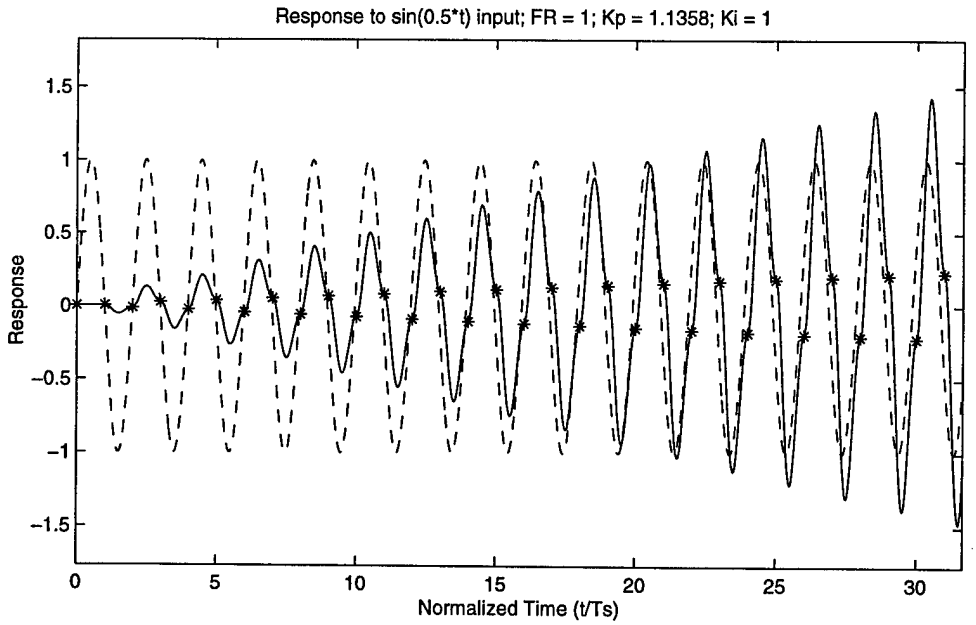

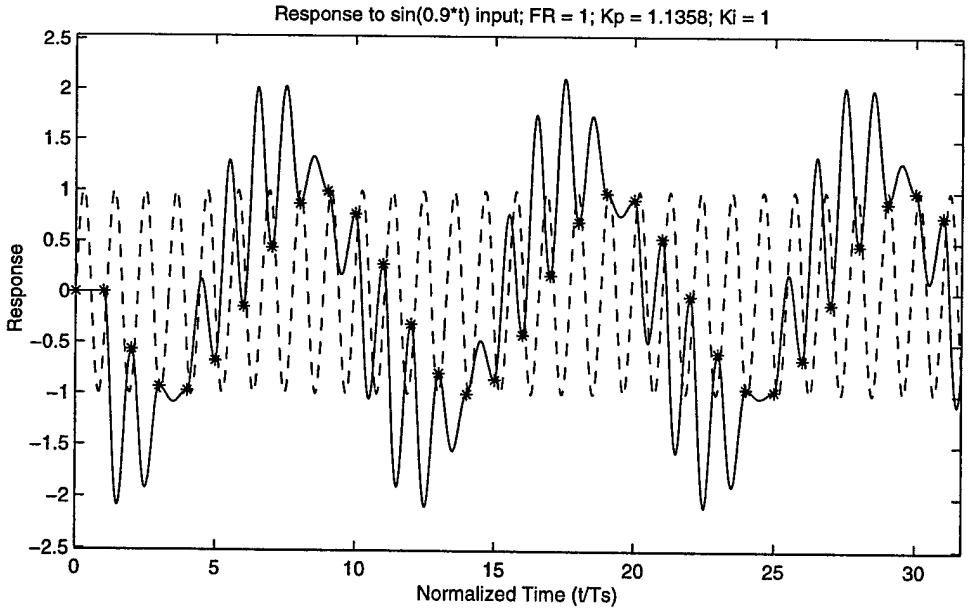

Figure 4.31 Response to Sinusoidal Inputs at High Frequencies

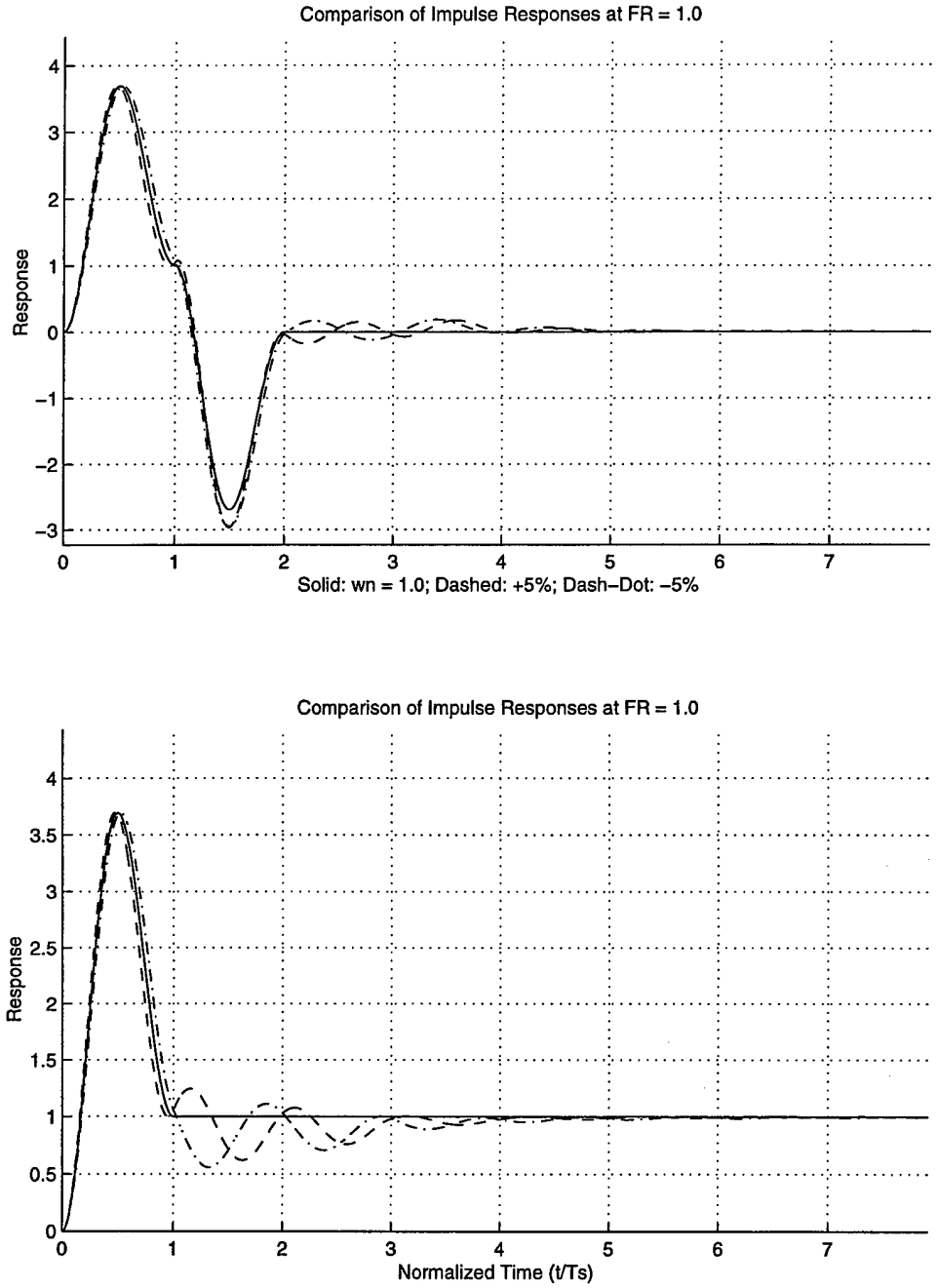

Figure 4.32 Robustness Comparisons for Change in Natural Frequency, $K_i = 1.0$

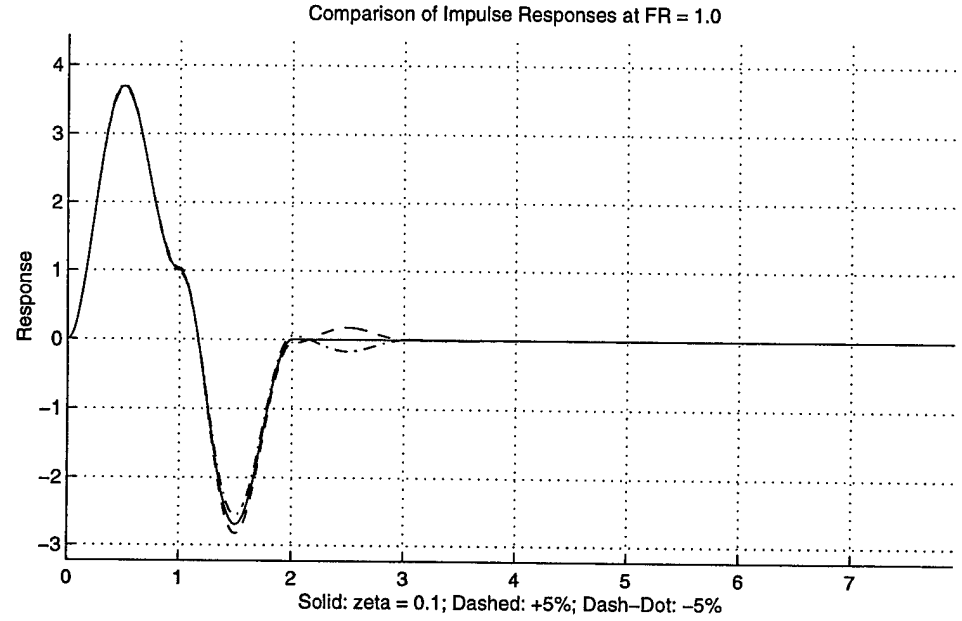

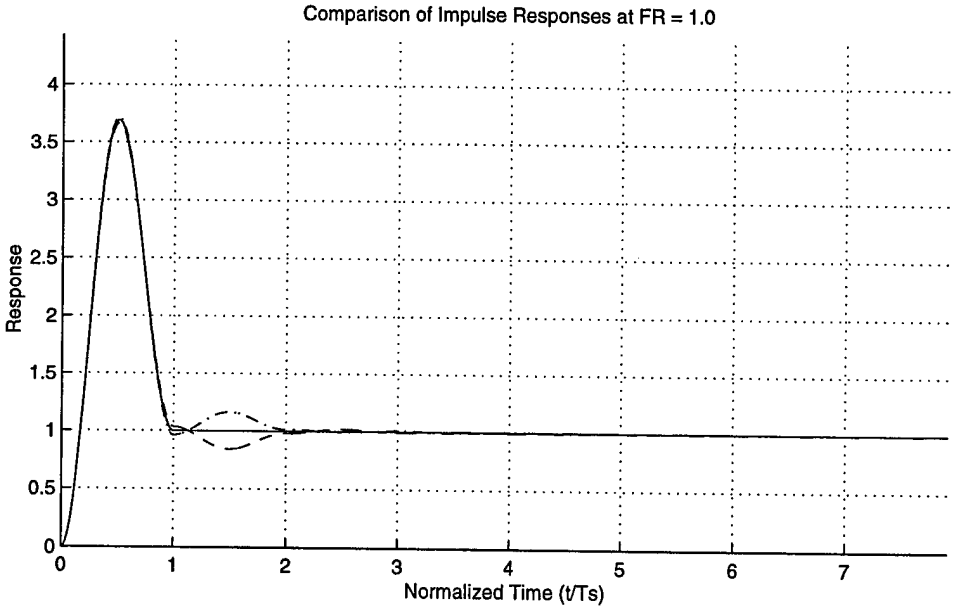

Figure 4.33 Robustness Comparisons for Change in Damping, $K_i = 1.0$

these plots correspond closely to those of the system controlled by proportional gain only. Since K_i has a constant value for the optimal response, no plots for changes in K_i are shown. Here, again, the changes caused by a change in natural frequency of the system are greatest. Recall the dual dependence on natural frequency—correctly identifying the sampling frequency for a frequency ratio of $FR = 1.0$ and correctly calculating the proportional gain K_p.

4.3 Disturbance Rejection of Proportional-Integral Controller

One concern about a controller design is its ability to reject disturbances. An examination of this controller's disturbance rejection capability will now follow. The disturbances to be introduced are a step disturbance and a normally distributed random disturbance.

Figure 4.34 shows the impulse and step responses of proportional-integral (PI) with a unit step disturbance at a normalized time of $\frac{t}{T_s} = 5.0$, or following five sampling periods. Here the disturbance is introduced at the sampling instant. Hence, the controller, shown as the dashed line, does not yet recognize the disturbance. One can see, however, that as soon as the disturbance is recognized, the controller rejects the disturbance, and does so within one sample period.

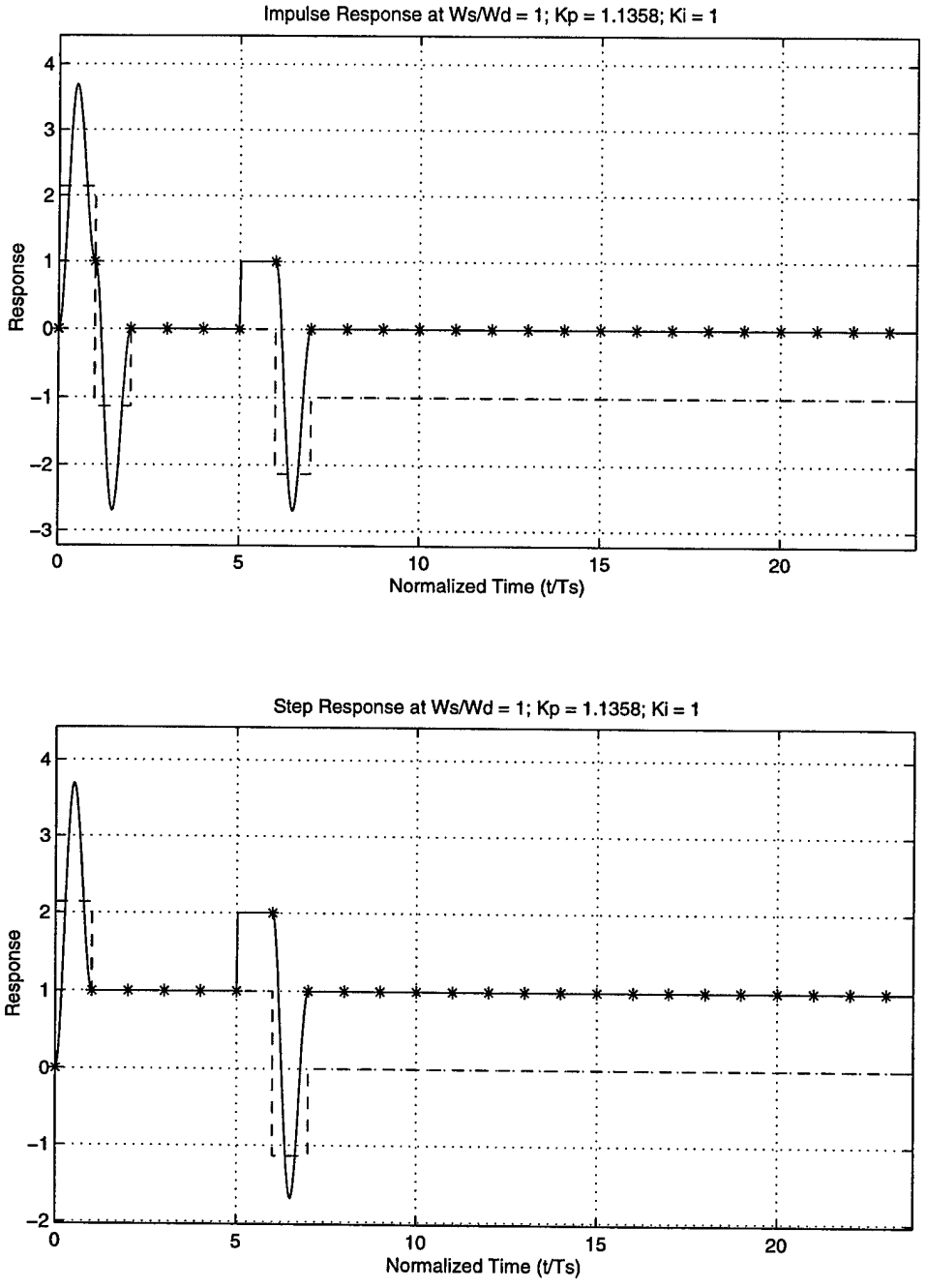

Figure 4.34 Unit Step Disturbance Rejection – Disturbance at Sample Point

Figure 4.35 shows the result when the disturbance is between sample periods—here 65% of the discrete sample period has passed. Again the controller rejects the disturbance once it "realizes" it is there, and does so within one sample period.

Figure 4.36 shows the same disturbance rejection for a greater magnitude of the step disturbance. Notice that overshoot of the continuous response increases, but this is to be expected.

Finally, Figure 4.37 shows the disturbance rejection when the step is in the negative direction. Examination of Figures 4.34 through 4.37 shows that this system has excellent step disturbance rejection capabilities. This can be expected since the step is basically a zero-frequency disturbance, and the controller handles input at frequencies lower than the sampling frequency with ease.

The controller's ability to reject a broadband disturbance will now be examined. The disturbance to be introduced next will be a normalized random input, with vector values of the disturbance vector generated by Matlab's "RANDN" command [49]. The resulting pseudo-random numbers are normally distributed with zero mean and a variance equal to one. The random number generator is reset for each run, meaning the random input for each of the following figures is the same.

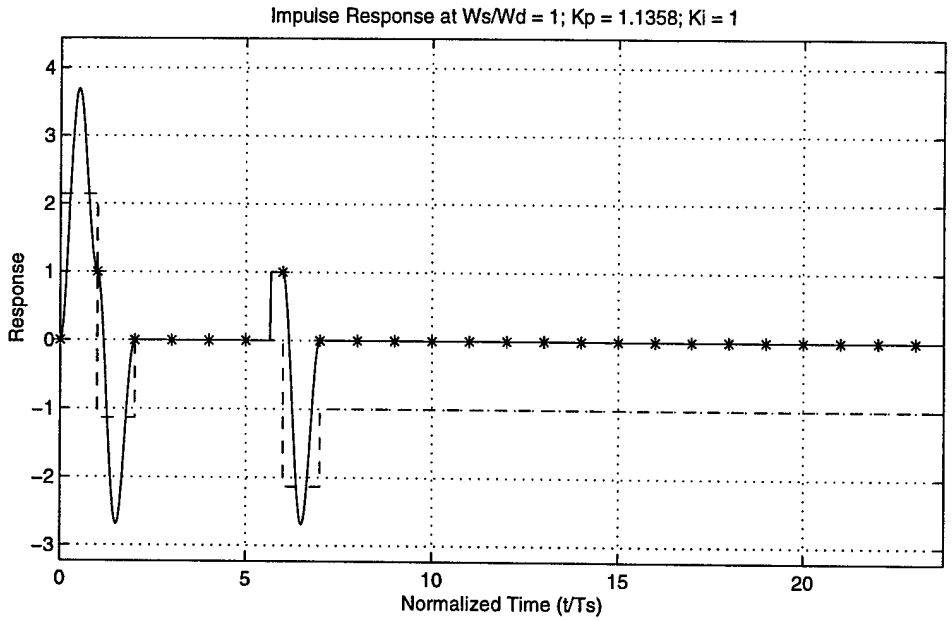

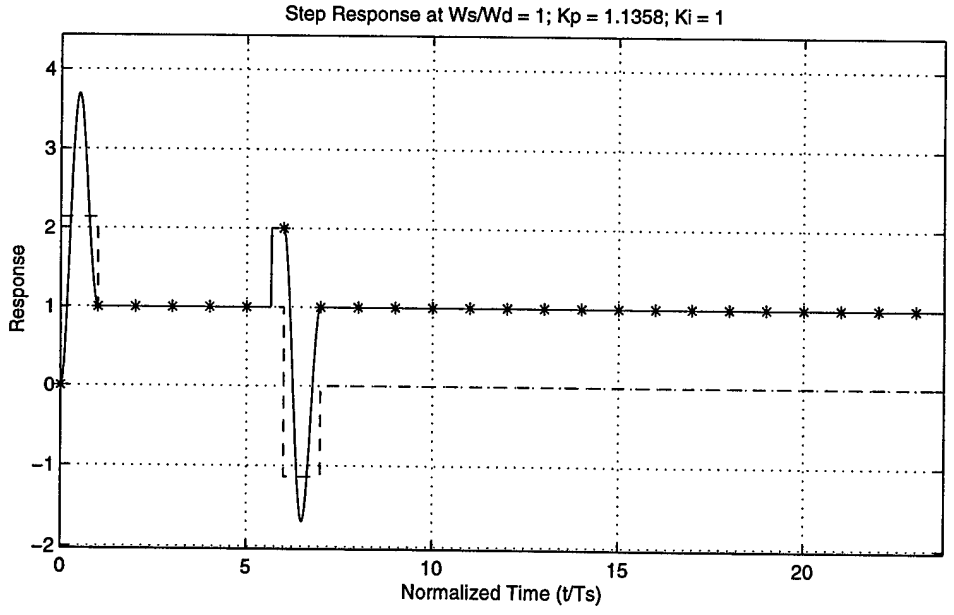

Figure 4.35 Unit Step Disturbance Rejection
Disturbance 65% of Sample Period Past Sample Point

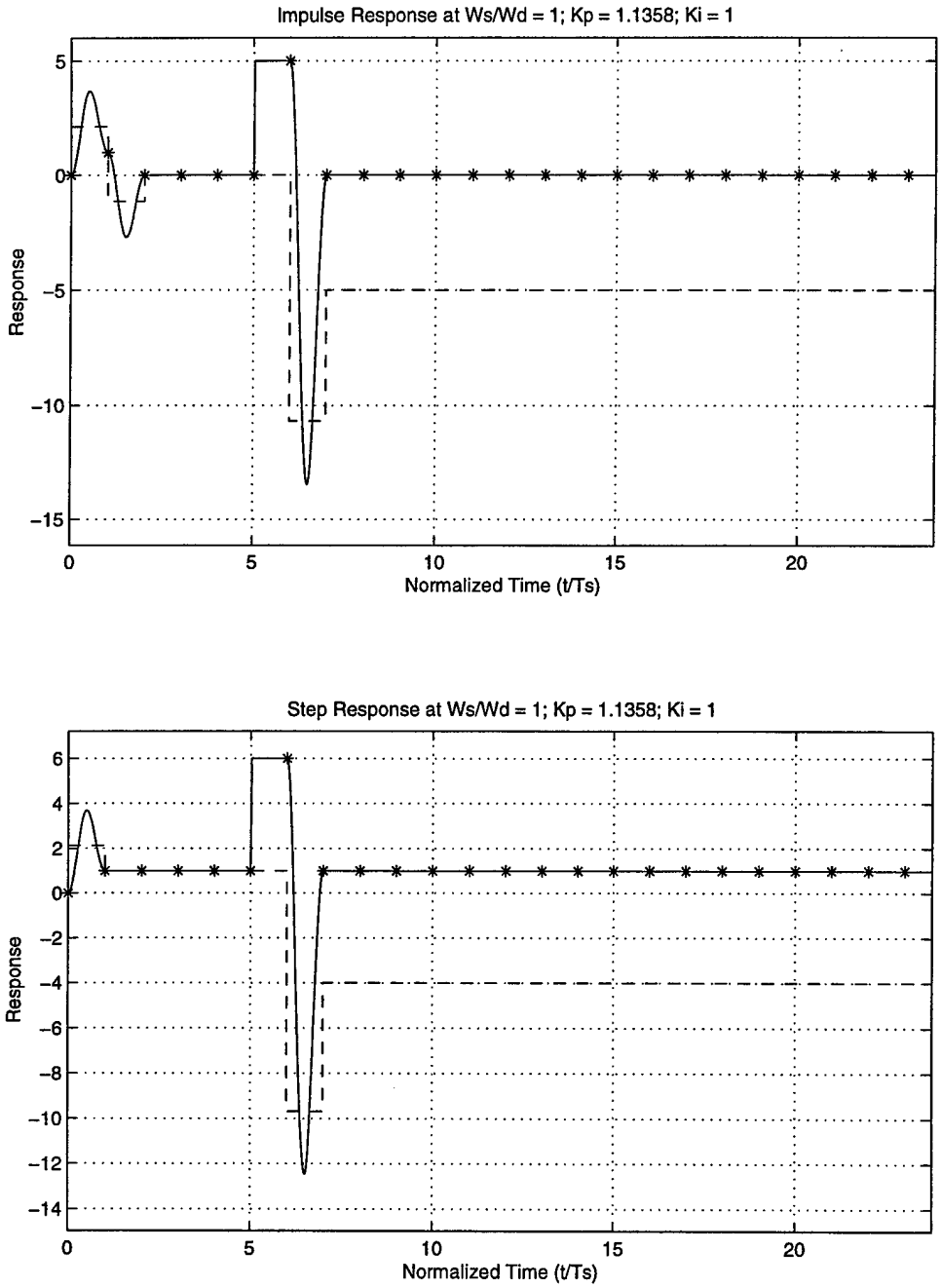

Figure 4.36 Step Disturbance Rejection – Step Size = 5.0

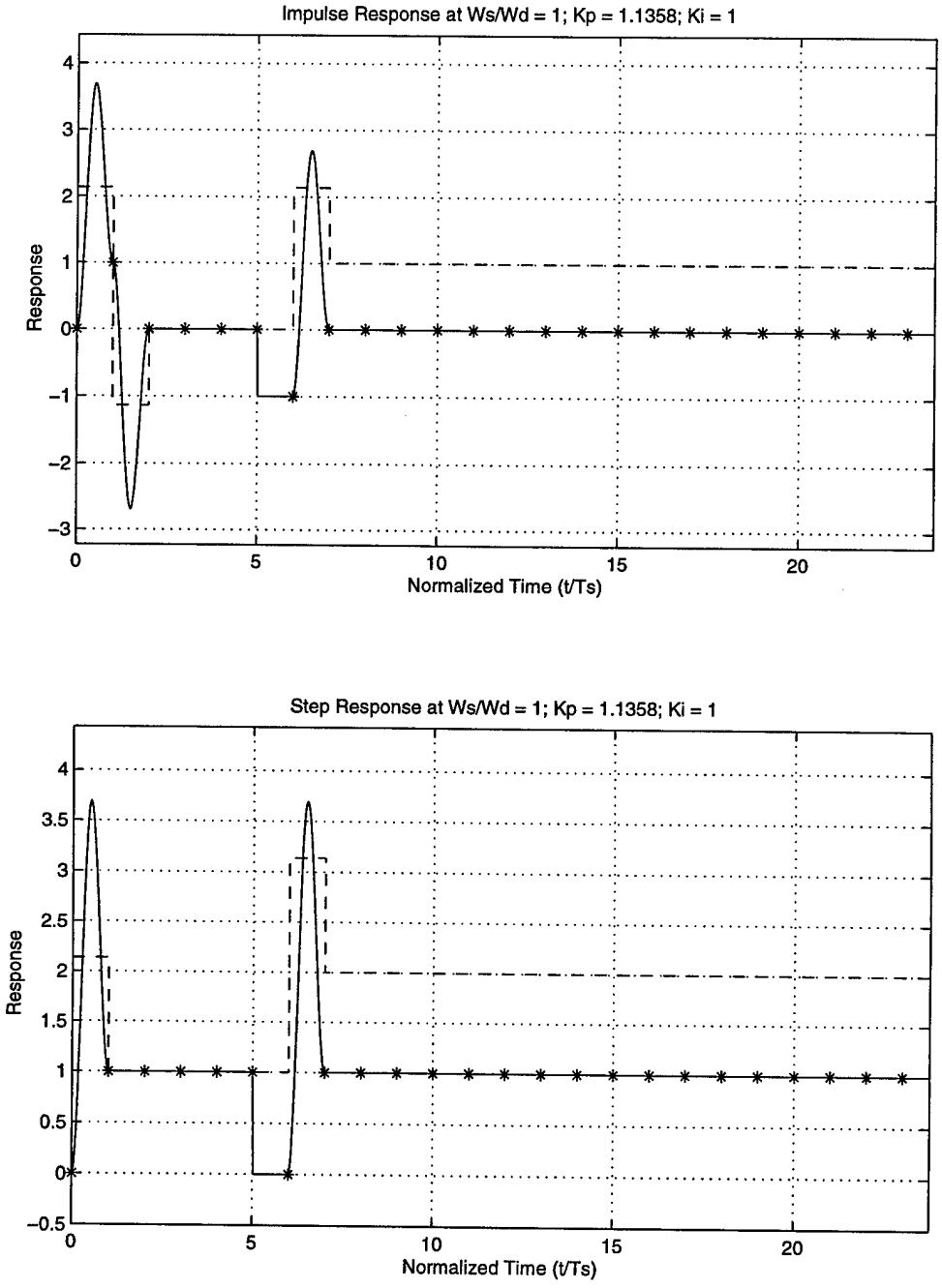

Figure 4.37 Negative Unit Step Disturbance Rejection – Disturbance at Sample Point

Figure 4.38 shows the system with the random noise input starting just after the fifth sample period and continuing until just before the seventh sample period. Again, the control effort is shown as the dashed line. During the random disturbance, the controller can only control for the point it "saw" at the sample point. Thus, little if any control is accomplished. Following the disturbance, however, within one sample period the system returns to the correct steady-state values.

Figure 4.39 shows similar results for the disturbance beginning between sample periods. Here, one can see that the location of the start of the random disturbance affects the response.

The ability of this system to control a disturbance with a broadband frequency range is poor, at best. This again follows what was found from the system's ability to follow a sinusoidal input – good for frequencies below the sampling frequency, but poor for frequencies on the order of or greater than the sampling frequency.

4.4 Chapter Four Summary

In chapter four we examined the design of a proportional-integral (PI) controller for a system in which aliasing is allowed. The chapter began with an examination of the integral controller alone. Similar trends were seen as in chapter three. With the PI-controller, the deadbeat response was obtained with zero steady-state error and

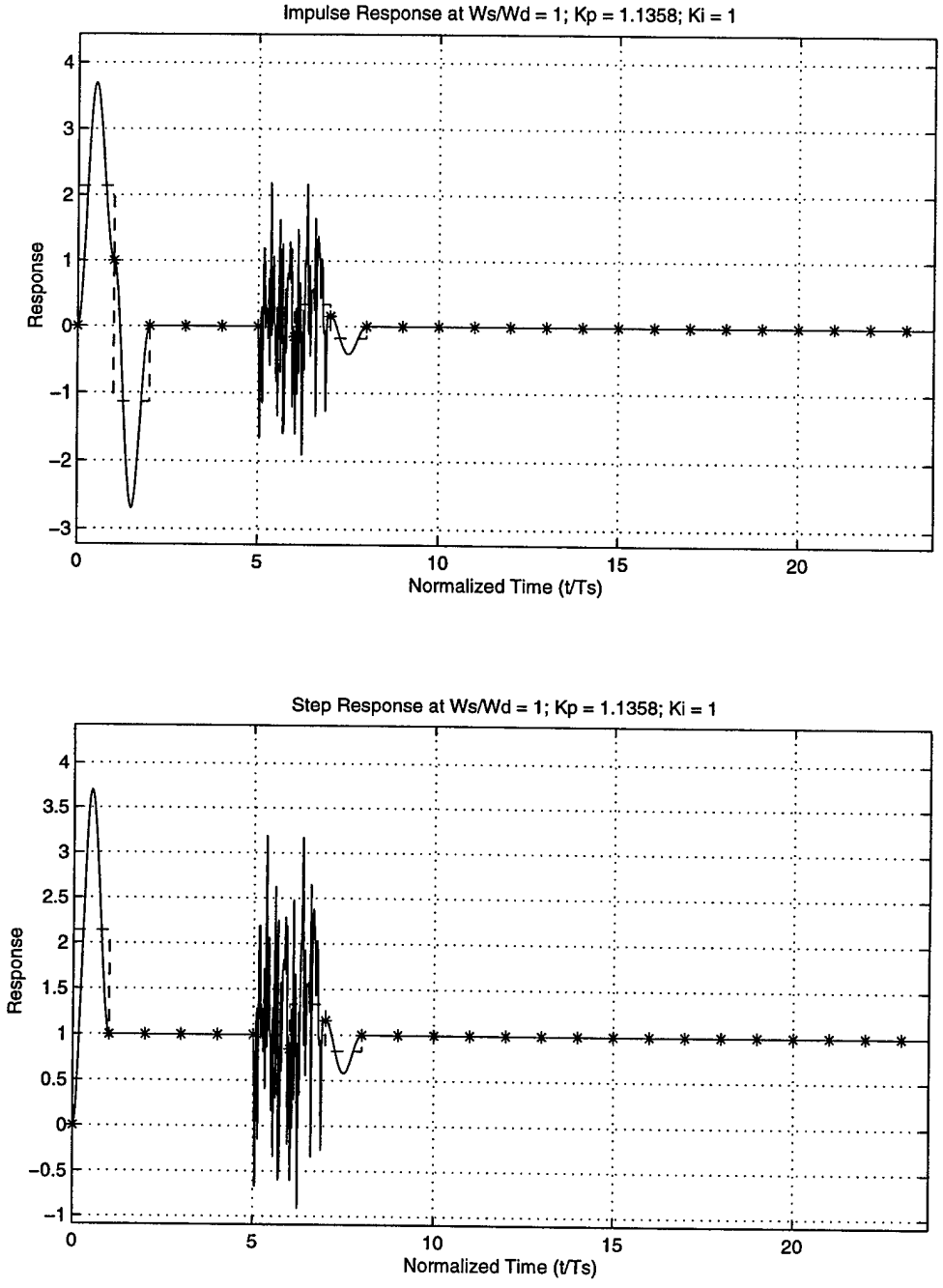

Figure 4.38 Random Disturbance Rejection – Disturbance Beginning at Sample Point

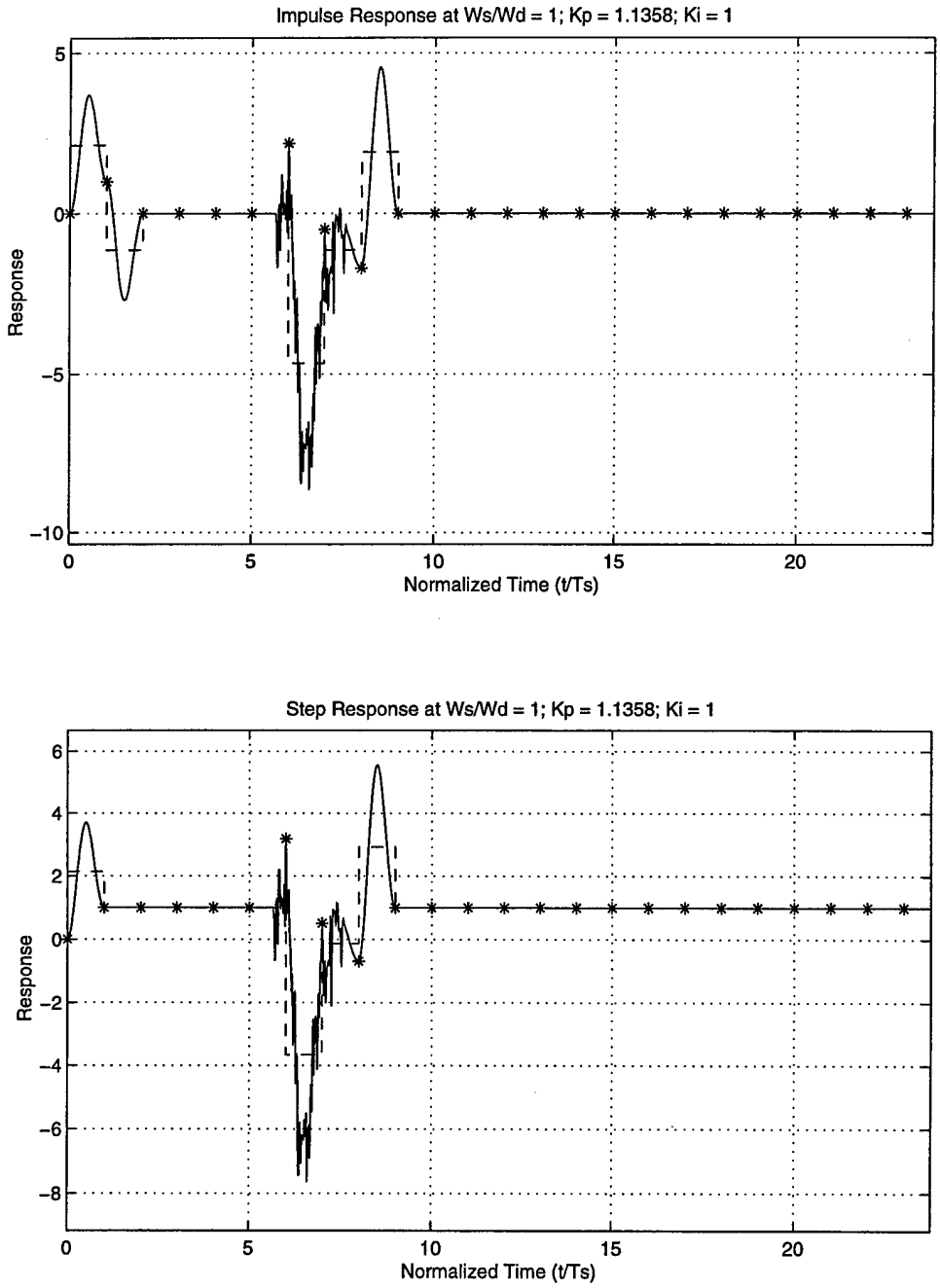

Figure 4.39 Random Disturbance Rejection
Disturbance Beginning Between Sample Points

reasonable control effort. The disturbance rejection of this controller is good when the frequency of the disturbance is less than the order of the frequency of the sampler. Finally, robustness characteristics for this PI-controller were found to be adequate.

CHAPTER FIVE. FOURTH-ORDER SYSTEM DESIGN WITH ALIASING

5.0 INTRODUCTION

With the success of implementing aliasing as a design tool found in chapters three and four of this dissertation one may ask if the theory can be extended to higher-order systems, and if this extension will be of any benefit. Therefore, a limited analysis of a fourth-order system follows, demonstrating the applicability of sample period as a design parameter to higher-order systems is completed in this chapter. We start by examining the simple fourth-order system with two sets of complex-conjugate poles and no zeros. Sample frequency ratios are such that the high frequency mode is aliased, and a determination of "good" frequency ratios is made. A design of a controller for the low-frequency mode is performed, since, by selecting the correct sampling rate, the high-frequency mode can be virtually eliminated from the response. Finally, disturbance rejection is again examined.

5.1 THE FOURTH-ORDER PLANT

Consider a plant, consisting of two second-order systems found in series with each other. This plant may be written as

$$G_p(s) = \frac{\omega_{n1}^{\ 2}\omega_{n2}^{\ 2}}{(s^2 + 2\zeta_1\omega_{n1}s + \omega_{n1}^{\ 2})(s^2 + 2\zeta_2\omega_{n2}s + \omega_{n2}^{\ 2})} \quad , \qquad [5.1]$$

where ζ_1 and ζ_2 are the damping ratios, and ω_{n1} and ω_{n2} are the natural frequencies of the two modes of the fourth-order plant. Locations of the poles of this plant may be found using Equation 3.1, and the fourth-order system can be divided by s, and expanded by partial fractions to enable its z-transform:

$$\frac{G_p(s)}{s} = \omega_{n1}^{\ 2}\omega_{n2}^{\ 2}\left(\frac{a_0}{s} + \frac{a_1}{s+p_1} + \frac{a_2}{s+p_2} + \frac{a_3}{s+p_3} + \frac{a_4}{s+p_4}\right) \quad , \qquad [5.2]$$

where the constants of the numerator terms can be found from a series of algebraic manipulations of the poles using the following constants:

$$p_5 = p_1p_2 + p_1p_3 + p_1p_4 + p_2p_3 + p_2p_4 + p_3p_4 \quad , \qquad [5.3]$$

$$p_6 = p_2p_3 + p_2p_4 + p_3p_4 \quad , \qquad [5.4]$$

$$p_7 = p_1p_3 + p_1p_4 + p_3p_4 \quad , \qquad [5.5]$$

$$p_8 = p_1p_2 + p_1p_4 + p_2p_4 \quad , \qquad [5.6]$$

$$p_9 = p_1p_2 + p_1p_3 + p_2p_3 \quad , \qquad [5.7]$$

$$p_{10} = p_1p_2p_3 + p_1p_2p_4 + p_1p_3p_4 + p_2p_3p_4 \quad , \qquad [5.8]$$

$$p_{11} = p_2p_3p_4 \quad , \qquad [5.9]$$

$$p_{12} = p_1p_3p_4 \quad , \qquad [5.10]$$

$$p_{13} = p_1p_2p_4 \quad , \qquad [5.11]$$

$$p_{14} = p_1p_2p_3 \quad , \qquad [5.12]$$

$$d_0 = \frac{1}{p_1p_2p_3p_4} \qquad [5.13]$$

$$d_1 = \frac{-d_0p_1}{p_1 - p_2} \quad , \qquad [5.14]$$

$$d_2 = \frac{p_3 - p_1}{p_1 - p_2} \quad , \qquad [5.15]$$

$$d_3 = \frac{p_4 - p_1}{p_1 - p_2} \quad , \qquad [5.16]$$

$$d_4 = -d_0 - d_1 \quad , \qquad [5.17]$$

$$d_5 = 1 + d_2 \quad , \qquad [5.18]$$

$$d_6 = 1 + d_3 \quad , \qquad [5.19]$$

$$d_7 = d_0p_5 + d_1p_7 + d_4p_6 \quad , \qquad [5.20]$$

$$d_8 = p_8 + d_2p_7 + d_5p_6 \quad , \qquad [5.21]$$

$$d_9 = p_9 + d_3p_7 + d_6p_6 \quad , \qquad [5.22]$$

$$d_{10} = \frac{-d_7}{d_8} \quad , \qquad [5.23]$$

$$d_{11} = \frac{-d_9}{d_8} \quad , \qquad [5.24]$$

$$d_{12} = d_4 - d_5 d_{10} \quad , \qquad [5.25]$$

$$d_{13} = -d_6 - d_5 d_{11} \quad , \qquad [5.26]$$

$$d_{14} = d_1 + d_2 d_{10} \quad , \text{and} \qquad [5.27]$$

$$d_{15} = d_3 + d_2 d_{11} \quad . \qquad [5.28]$$

With these constants defined, the constants of Equation 5.2 can be defined as

$$a_0 = d_0 \quad , \qquad [5.29]$$

$$a_1 = d_{12} + d_{13} a_4 \quad , \qquad [5.30]$$

$$a_2 = d_{14} + d_{15} a_4 \quad , \qquad [5.31]$$

$$a_3 = d_{10} + d_{11} a_4 \quad , \text{and} \qquad [5.32]$$

$$a_4 = \frac{-d_o p_{10} - d_{10} p_{13} - d_{12} p_{11} - d_{14} p_{12}}{p_{14} + d_{11} p_{13} + d_{13} p_{11} + d_{15} p_{12}} \quad . \qquad [5.33]$$

Taking the z-transform of Equation 5.2, applying the zero-order hold, gives

$$H(z)=\frac{\omega_{n1}{}^2\omega_{n2}{}^2(f_3z^3+f_2z^2+f_1z+f_0)}{(z+b_1)(z+b_2)(z+b_3)(z+b_4)} \quad , \qquad [5.34]$$

where

$$b_n=-e^{-p_nT_s} \quad , \qquad [5.35]$$

$$f_0=a_0b_1b_2b_3b_4-a_1b_2b_3b_4-a_2b_1b_3b_4-a_3b_1b_2b_4-a_4b_1b_2b_3 \quad , \qquad [5.36]$$

$$\begin{aligned} f_1=&a_0(b_1b_2b_3+b_1b_2b_4+b_1b_3b_4+b_2b_3b_4)\\ &+a_1(b_2b_3b_4-b_2b_3-b_2b_4-b_3b_4)+a_2(b_1b_3b_4-b_1b_3-b_1b_4-b_3b_4) \quad ,\\ &+a_3(b_1b_2b_4-b_1b_2-b_1b_4-b_2b_4)+a_4(b_1b_2b_3-b_1b_2-b_1b_3-b_2b_3) \end{aligned}$$

[5.37]

$$\begin{aligned} f_2=&a_0(bb+bb+bb+bb+bb+bb)\\ &+a_1(b_2b_3+b_2b_4+b_3b_4-b_2-b_3-b_4)+a_2(b_1b_3+b_1b_4+b_3b_4-b_1-b_3-b_4) \quad ,\\ &+a_3(b_1b_2+b_1b_4+b_2b_4-b_1-b_2-b_4)+a_4(b_1b_2+b_1b_3+b_2b_3-b_1-b_2-b_3) \end{aligned}$$

[5.38]

$$\begin{aligned} f_3=&a_0(b_1+b_2+b_3+b_4)+a_1(b_2+b_3+b_4-1)+a_2(b_1+b_3+b_4-1)\\ &+a_3(b_1+b_2+b_4-1)+a_3(b_1+b_2+b_3-1) \end{aligned} \quad . \qquad [5.39]$$

5.2 Design of Proportional Controller For Fourth-Order System In Which One Mode is Aliased

One of the concerns in designing systems in which aliasing is present is the effect of aliasing on only part of the system's modes. Suppose a system exists with two modes, the fourth-order system, and that only one of these modes is aliased. In other words, sampling is done such that one mode is aliased, but the other is not. The following examines the effect of aliasing on such a system.

Begin by allowing the controller to be proportional control only. Solving for $F(z)$ from Equation 3.3:

$$F(z) = \frac{K_p(z+b_1)(z+b_2)(z+b_3)(z+b_4)}{z^4 + (K_g f_3 + b_5)z^3 + (K_g f_2 + b_6)z^2 + (K_g f_1 + b_7)z + K_g f_0 + b_8} \quad , \qquad [5.40]$$

where

$$b_5 = b_1 + b_2 + b_3 + b_4 \quad , \qquad [5.41]$$

$$b_6 = b_1 b_2 + b_1 b_3 + b_1 b_4 + b_2 b_3 + b_2 b_4 + b_2 b_4 \quad , \qquad [5.42]$$

$$b_7 = b_1 b_2 b_3 + b_1 b_2 b_4 + b_1 b_3 b_4 + b_2 b_3 b_4 \quad , \qquad [5.43]$$

$$b_8 = b_1 b_2 b_3 b_4 \quad \text{, and} \qquad [5.44]$$

$$K_g = K_p \omega_{n1}{}^2 \omega_{n2}{}^2 \quad . \qquad [5.45]$$

From Equation 5.40, the root loci (z-plane and s*-plane) of a fourth-order system in which one mode is aliased can be constructed. Additionally, the magnitude and phase of the frequency response functions and the impulse and step responses will be plotted for the fourth-order plant of Equation 5.1 combined with the mixed controller function of Equation 5.40. Parameters for the fourth-order system are

$$\omega_{n1} = 1.0 \text{ Hz}$$

$$\zeta_1 = 0.5$$

$$\omega_{n2} = 10.0 \text{ Hz}$$

$$\zeta_2 = 0.01 \qquad [5.46]$$

Sampling period will be such that the second mode is aliased but the first mode is not. For comparison purposes, Figures 5.1 through 5.3 show the root loci, frequency response function plots, and impulse and step responses, respectively, when the frequency ratio is $FR = 100$—a frequency ratio for which little or no aliasing is present for either mode.

Symbols on the root loci plots are as follows. Diamonds and pluses (+) represent the zeros and poles of the plant, respectively. Realize again that these zeros and poles do not

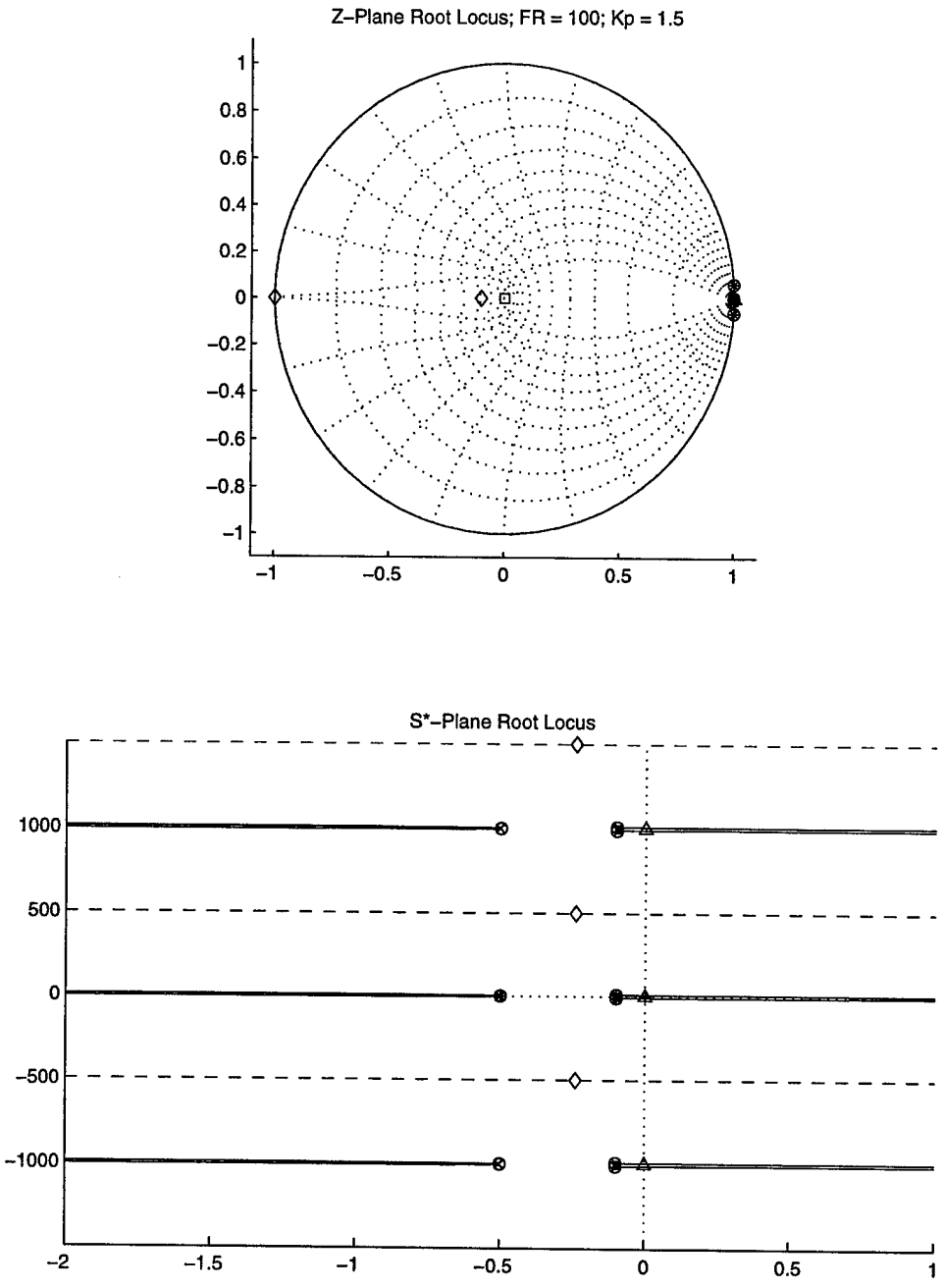

Figure 5.1 Fourth-Order Root Loci; FR = 100, $K_p = 1.5$

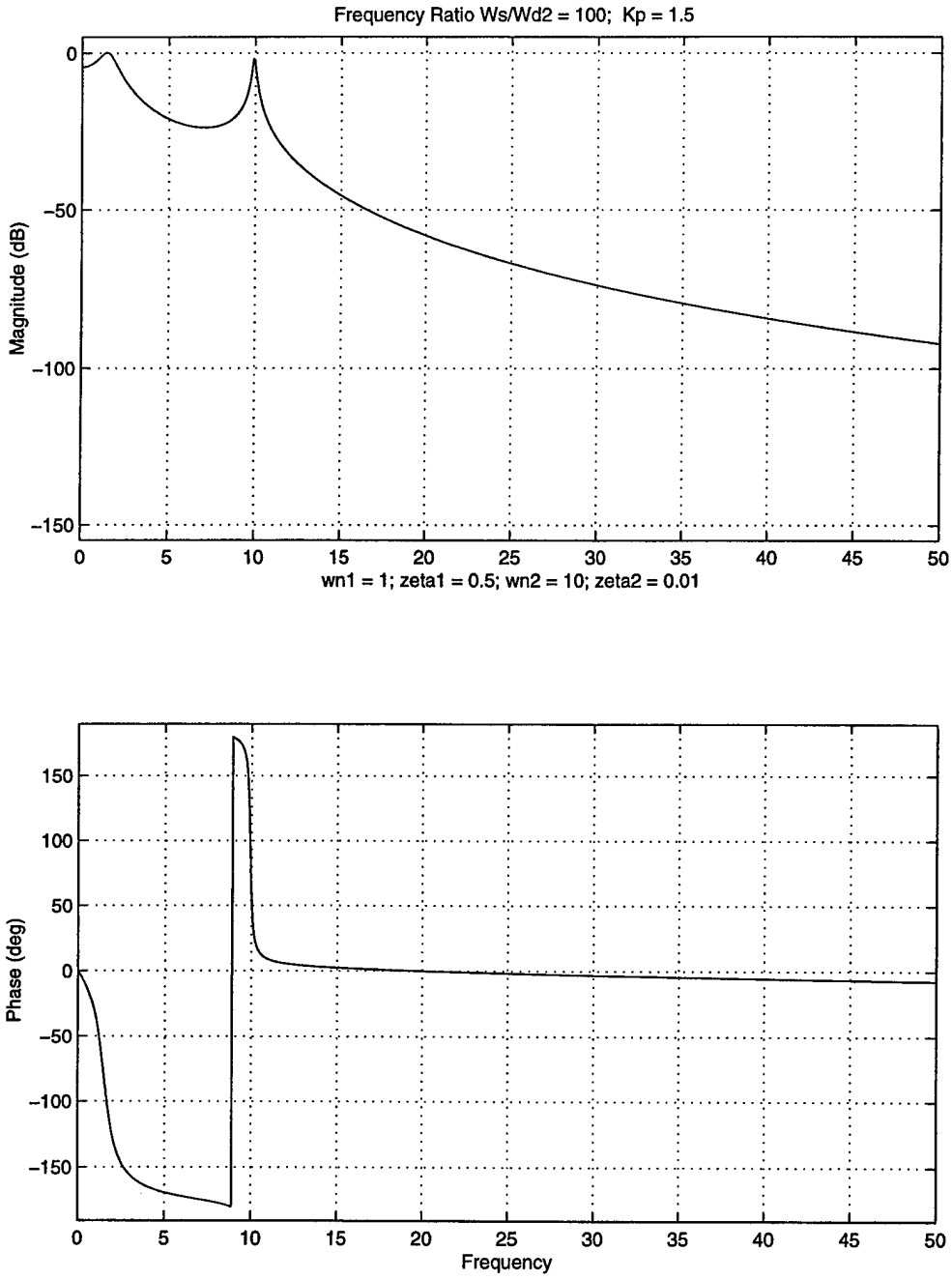

Figure 5.2 Fourth-Order Frequency Response Function Plot; FR = 100, K_p = 1.5

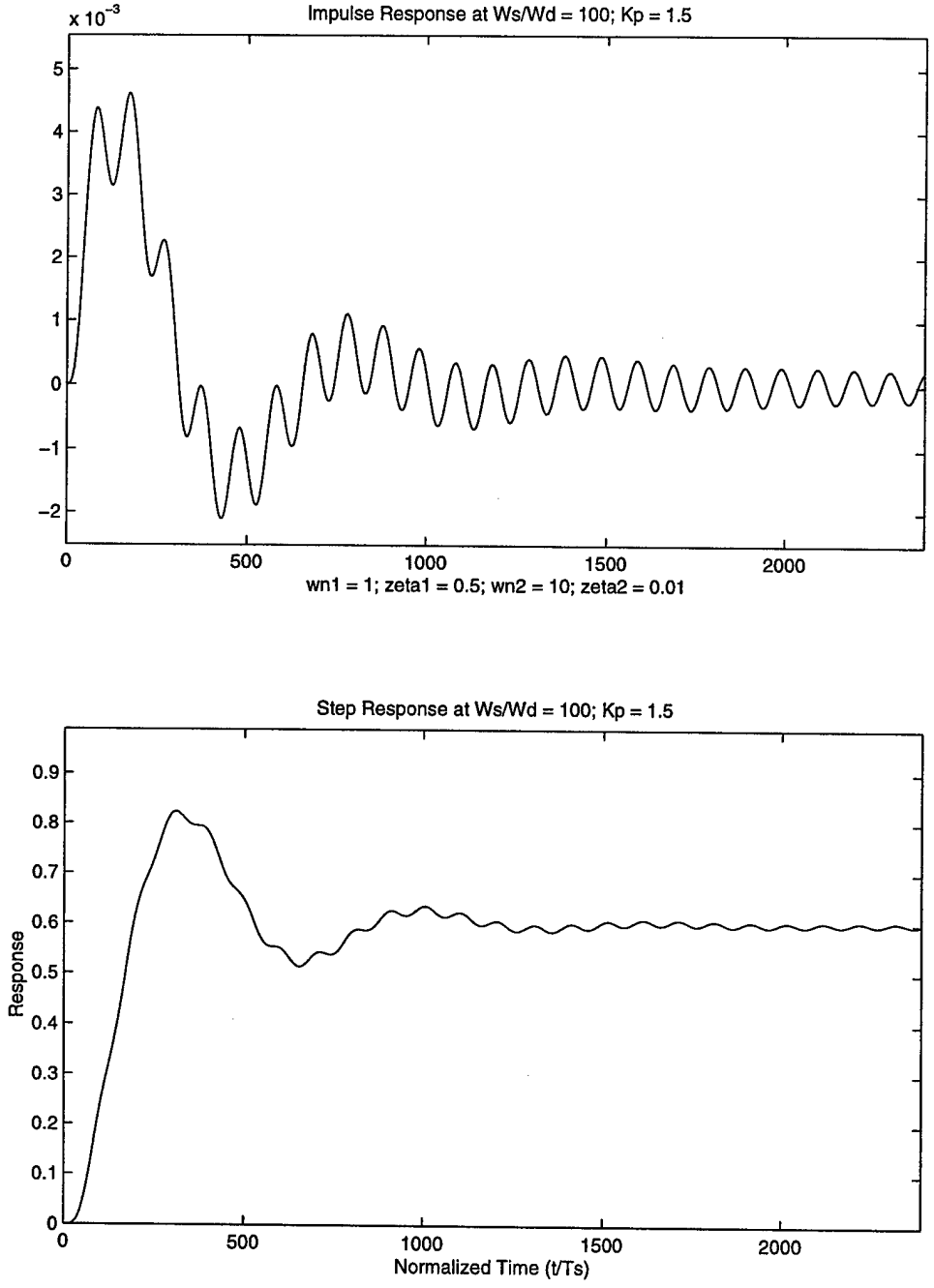

Figure 5.3 Fourth-Order Impulse and Step Responses; FR = 100, $K_p = 1.5$

really exist in the z-plane—they are merely shown for a more complete understanding of the system. Circles and "x's" represent the zeros and poles of the mixed term, $F(z)$, respectively. Finally, triangles and asterisks (*) represent the zero-order hold terms.

Examination of Figure 5.1 shows the effects of sampling very rapidly with respect to natural frequencies of the system. The poles and zeros of the discrete portion of the root locus lie very close to $z=1$. Figure 5.2 shows the classical frequency response function plot of a fourth-order system. The lightly damped poles at $\omega_{n2} =$ 10.0 Hz show up as the sharp peak with the 180^0 phase shift, and the slower poles at $\omega_{n1} =$ 1.0 Hz show up with a less sharp peak and phase passing through -90^0. The effect of the higher frequency poles is clearly visible in the impulse and step responses of Figure 5.3.

Now, allowing aliasing of the second (or faster) poles select the sampling frequency with respect to the damped natural frequency of these poles:

$$\omega_s = \omega_{d2} = \omega_{n2}\sqrt{1-\zeta_2^{\,2}} \quad . \qquad [5.47]$$

Here, we will only examine frequency ratios of $FR = 2.0$ and $FR = 1.0$, taking advantage of the lessons learned with the second-order system designs. These frequency ratios should show the two "extremes" of aliased design. If the design of the fourth-order system with one aliased mode follows that of the second-order system, the poles and zeros of the aliased mode should lie on the real axis in the z-plane.

Figures 5.4 and 5.5 show this is indeed the case—at these frequency ratios the aliased poles lie on the real axis. When $FR = 2.0$ the poles and zeros lie on the negative real axis, and when $FR = 1.0$ they lie on the positive real axis. Notice the poles will move toward the zeros of the plant, represented by the diamonds. Again, in both cases, one pole remains fixed at the location of one zero of $F(z)$, which is the same location as one of the zeros of $H(z)$, while the other moves toward another zero of $H(z)$. The remaining poles of $F(z)$, those not aliased, move in a large circular path toward their meeting point on the negative real axis, where one will then move toward negative infinity and the other will move toward the remaining zero of $H(z)$.

Notice that as the frequency ratio decreases (sample period increases) the non-aliased poles move away from the point $z = 1$. Again, this is as expected. The same relationships between frequency ratio and locations in the s*-plane exist for the aliased poles as were found in chapter four: at $FR = 2.0$ the aliased poles lie on the band boundaries and at $FR = 1.0$ they lie on the mid-band lines. Another thing to note is the pole aliasing of the non-aliased poles—i.e., the non-aliased poles are repeated in each band infinitely in the s*-plane.

At a frequency ratio of $FR = 1.0$ the poles and zeros of the aliased mode lie on the positive real axis of the z-plane, and it appears they are clustered together at the same point. This also appears to be the case in the s*-plane. A closer examination shows there is some separation, as Figure 5.6 shows. This appears, however, to be very nearly a pole-zero cancellation, a fact whose significance will become apparent soon.

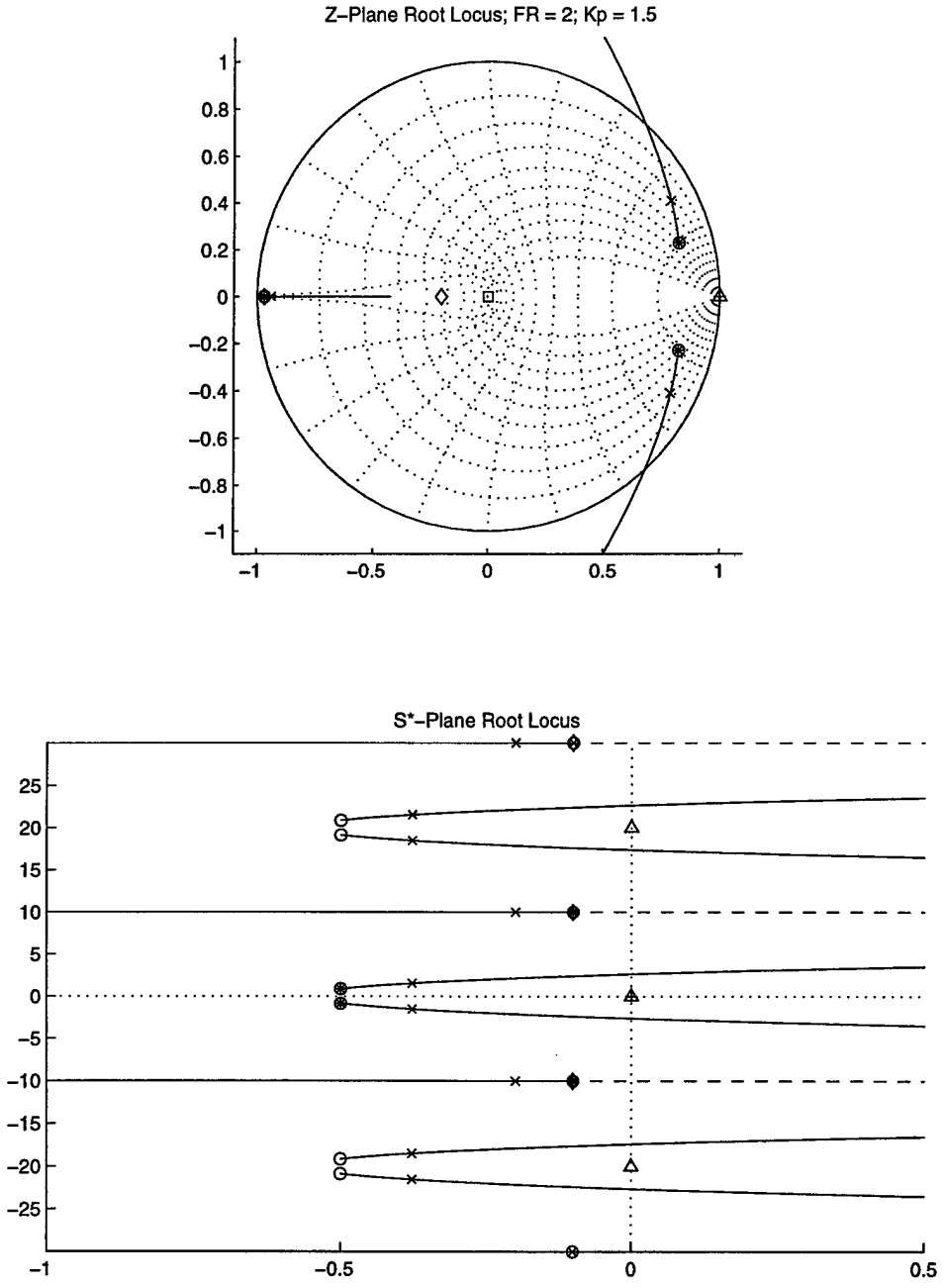

Figure 5.4 Root Loci of Fourth-Order System with One Aliased Mode
FR = 2.0, $K_p = 1.5$

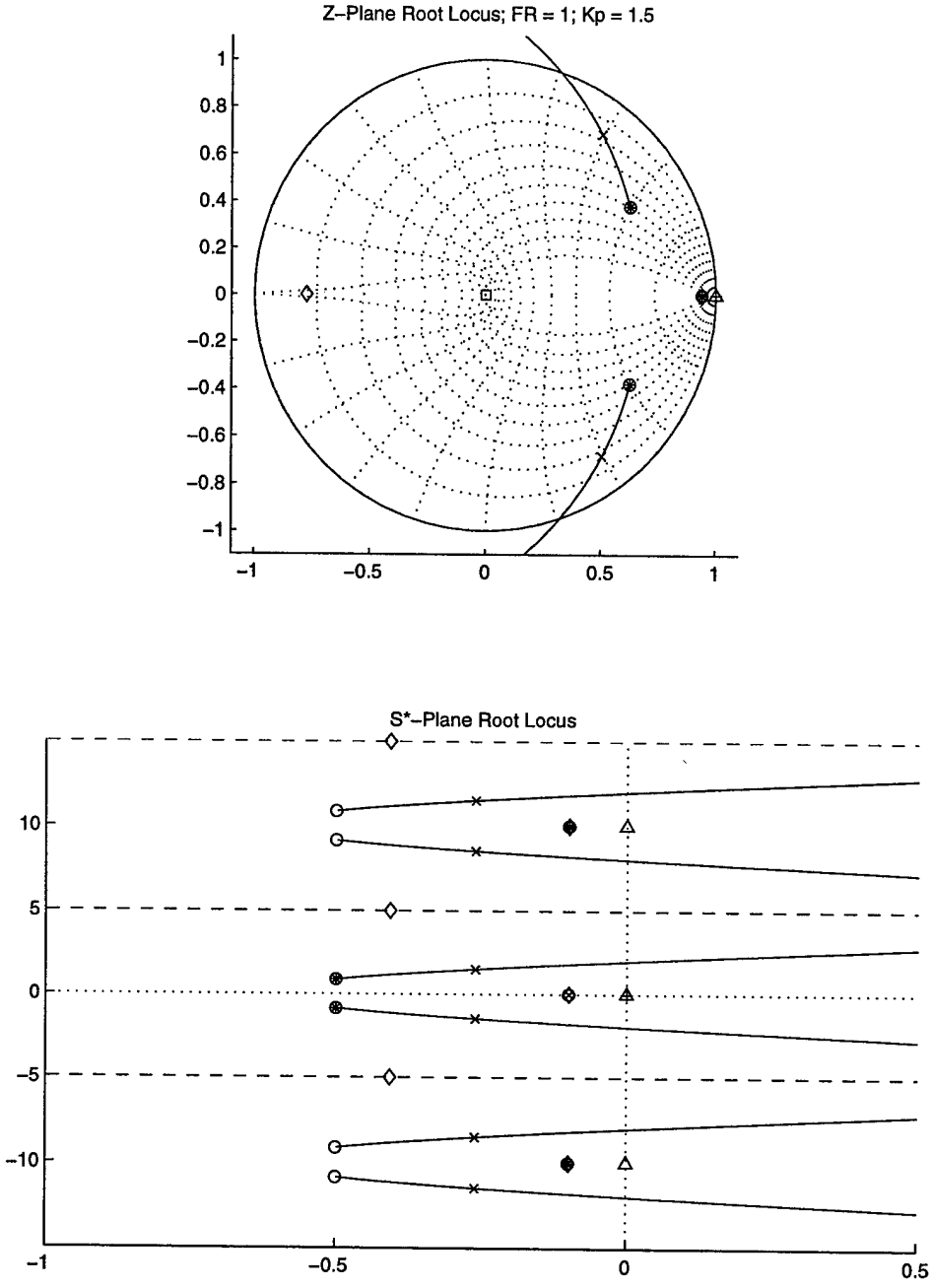

Figure 5.5 Root Loci of Fourth-Order System with One Aliased Mode
FR = 1.0, K_p = 1.5

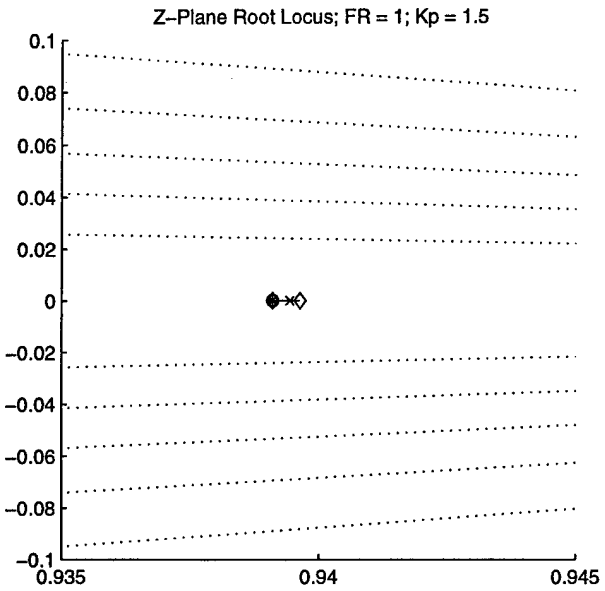

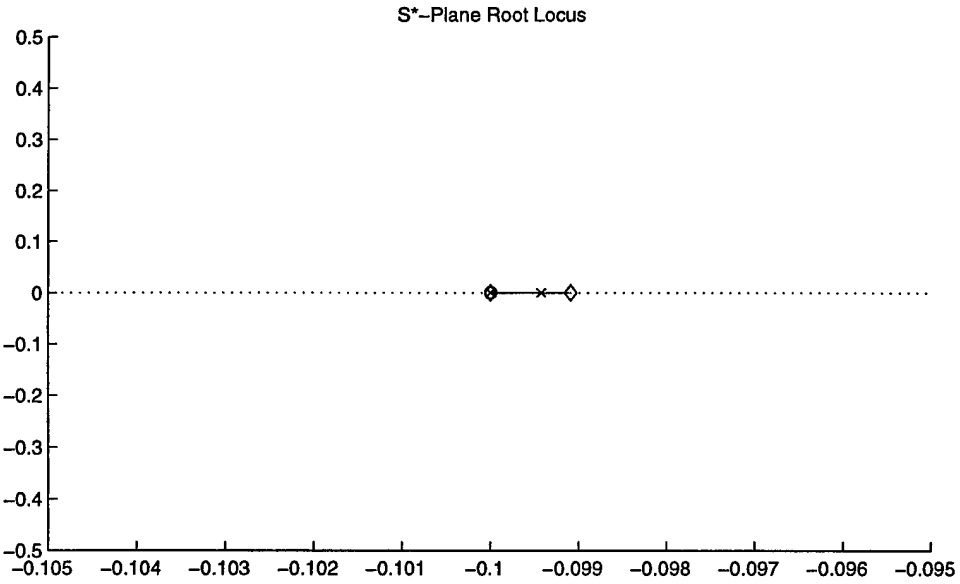

Figure 5.6 Close-Up of Aliased Pole and Zero Locations for FR = 1.0

Figures 5.7 and 5.8 show the magnitude and phase plots of the discrete-to-continuous frequency response functions for frequency ratios of $FR = 2.0$ and $FR = 1.0$, respectively. At a frequency ratio of $FR = 2.0$, the second mode sits right at the folding frequency. Thus, its effect is seen in the magnitude plot as a sharp peak with a magnitude somewhat reduced from that of when it was not aliased (Figure 5.2). For a frequency ratio of $FR = 1.0$, however, the sampling frequency is equal to the damped natural frequency of the second mode, and the effects of the zero-order hold cancel this mode. Notice the pole aliasing of the low frequency mode as it is "folded" above the folding frequency to 9.0 Hz and repeated in the other frequency bands.

Figures 5.9 and 5.10 show the impulse and step responses of the fourth-order system with one aliased mode. Here, the effect of allowing more aliasing is clearly seen when compared to the impulse and step responses of Figure 5.3. At a frequency ratio of $FR = 2.0$, seen in Figure 5.9, both the impulse and step responses show improvement over their counterparts in Figure 5.3. The magnitudes of the higher-order oscillations are less and the oscillations themselves seem to settle sooner, although the overall magnitudes of both responses are larger than for the continuous case.

Figure 5.10 shows these responses for a frequency ratio of $FR = 1.0$. As predicted by both the root loci plots and the Frequency Response Function plots, the effects of the high frequency mode are practically invisible. The responses of Figure 5.10 appear to be those of a second-order system only, although closer examination shows some of the higher-

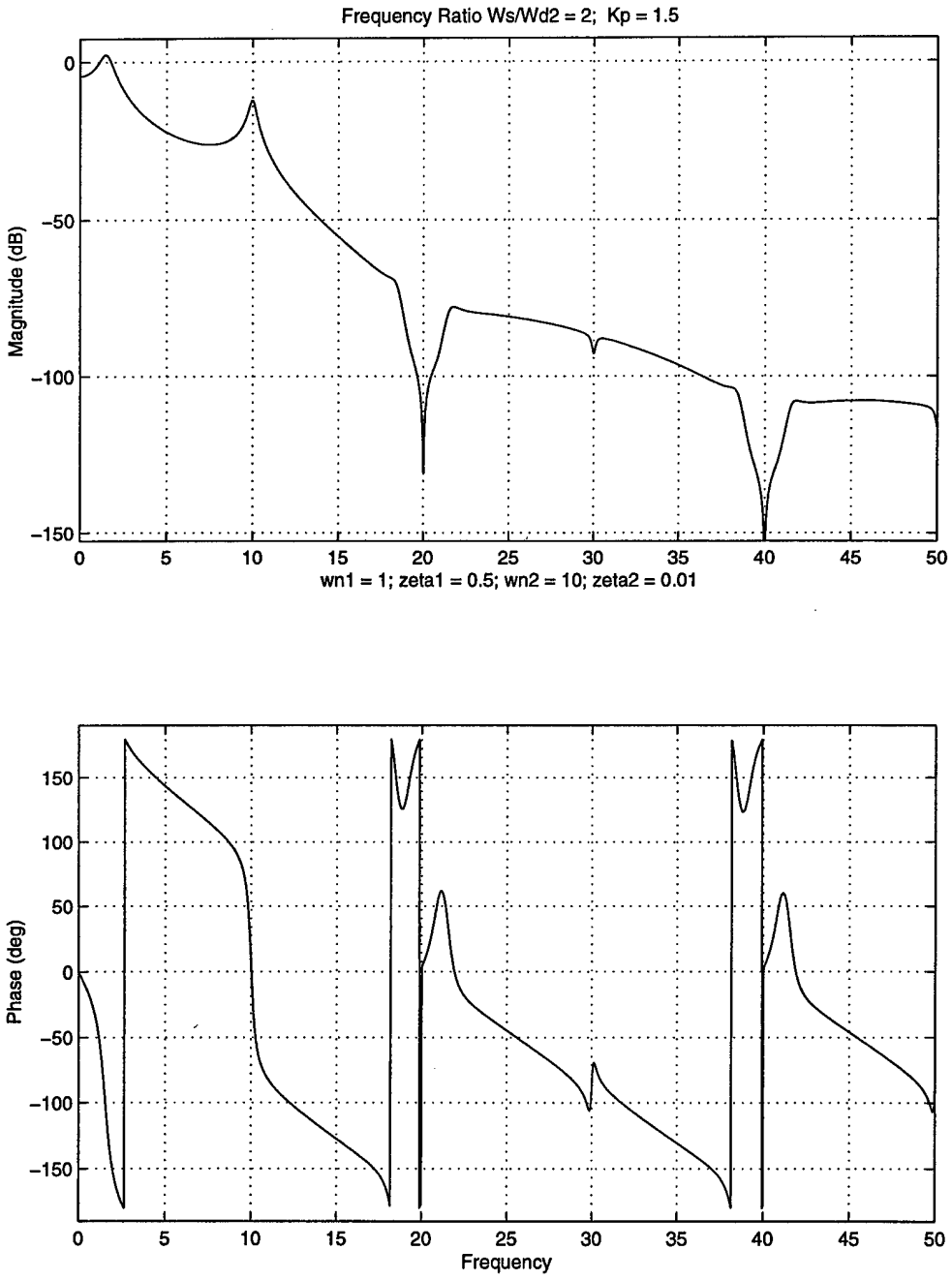

Figure 5.7 Frequency Response Function Plot of Fourth-Order System with One Aliased Mode – FR = 2.0, $K_p = 1.5$

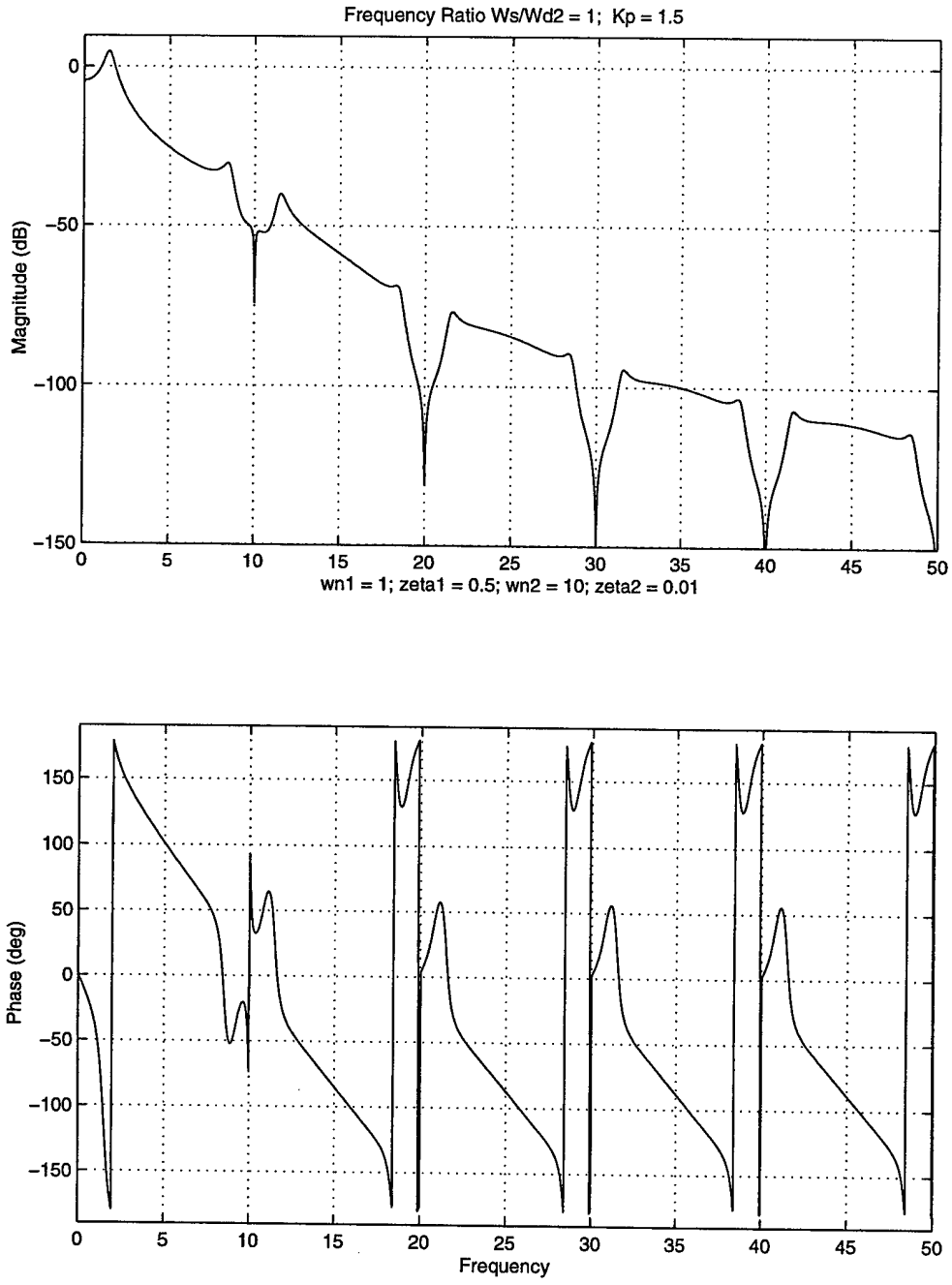

Figure 5.8 Frequency Response Function Plot of Fourth-Order System with One Aliased Mode – FR = 1.0, $K_p = 1.5$

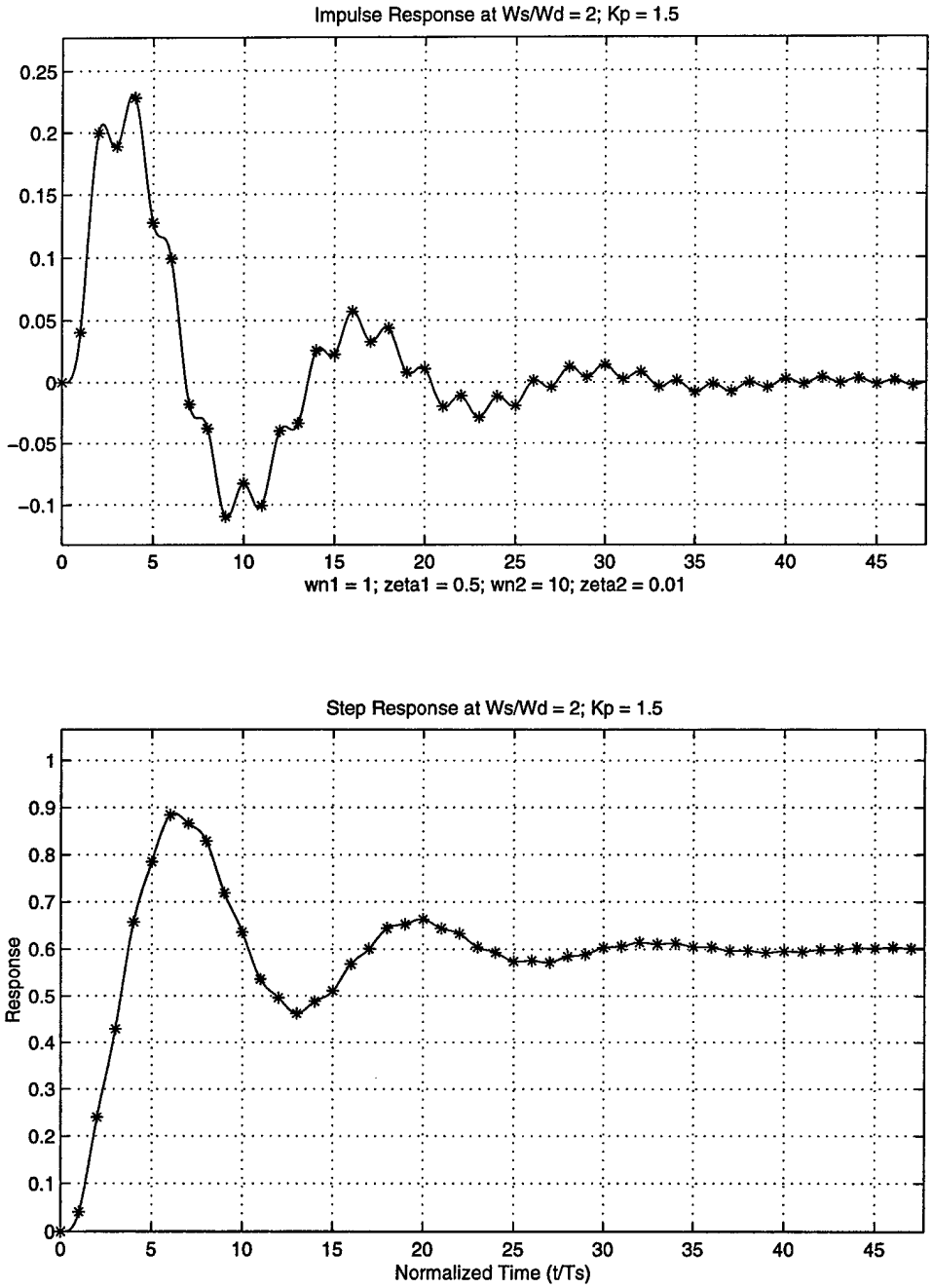

Figure 5.9 Impulse and Step Responses of Fourth-Order System with One Aliased Mode; FR = 2.0, $K_p = 1.5$

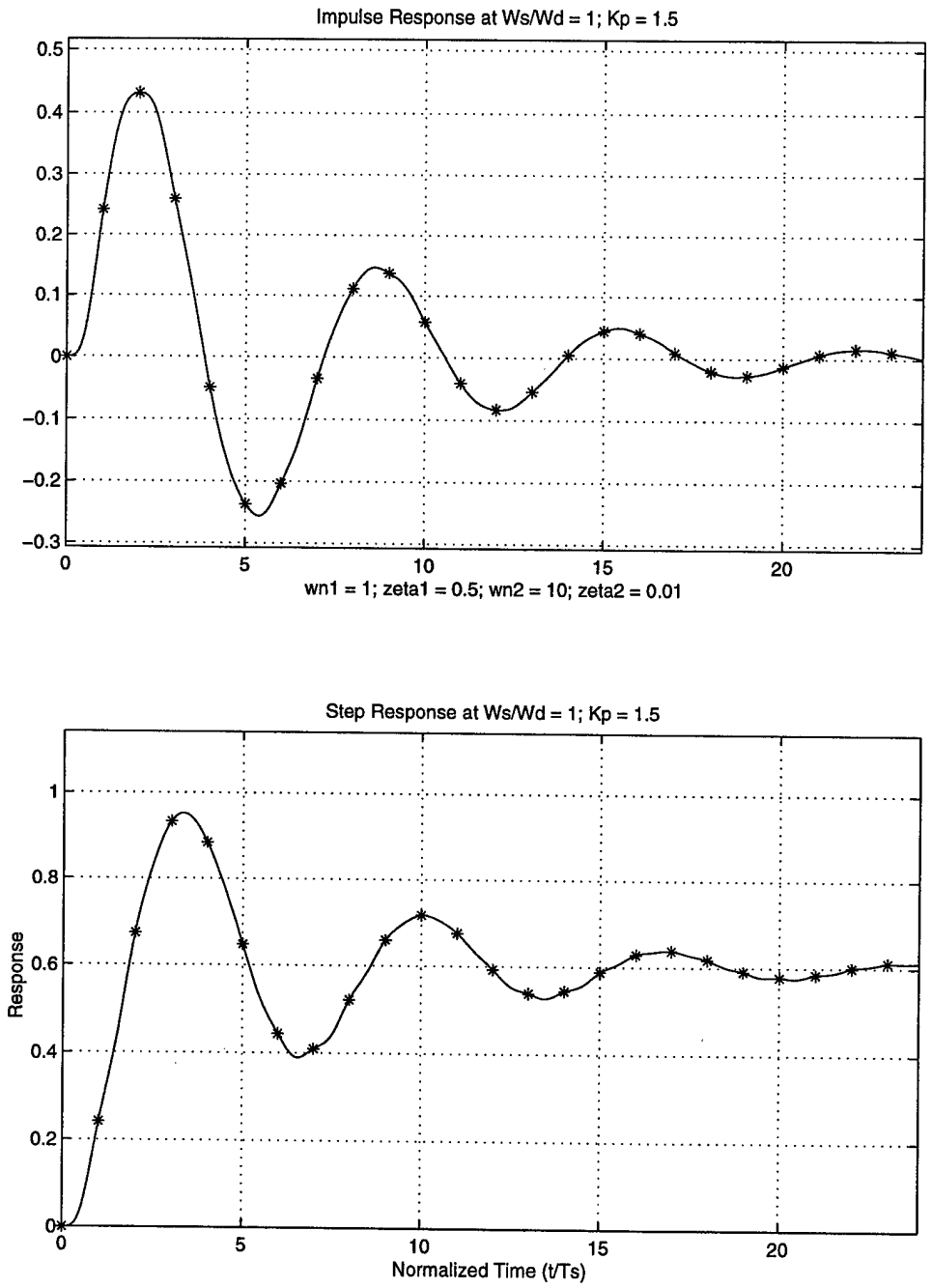

Figure 5.10 Impulse and Step Responses of Fourth-Order System with One Aliased Mode; FR = 1.0, $K_p = 1.5$

order mode effects are still present. However, the responses of Figure 5.10 are clearly superior to those of Figures 5.3 and 5.9.

Again, by allowing aliasing the system's stability has actually increased, and in the case of the fourth-order system the high frequency mode has been rendered virtually ineffective. This leads to the question of designing a controller for the remaining second-order response. Will design of a controller for this system in which the higher-order mode is aliased to the point that it no longer affects the response be possible?

5.3 Design of Proportional-Integral-Derivative Controller For Fourth-Order System In Which One Mode is Aliased

With the higher-order mode aliased as developed above ($FR = 1.0$) design of a controller for the remaining second-order response will be examined. The design will be a simple proportional-integral-derivative (PID) controller, designed in the z-plane, to improve that response.

The equation for a PID controller in the z-plane is defined as

$$G_c(z) = K_p + K_i \frac{z}{z-1} + K_d \frac{z-1}{z} = \frac{K_1 z^2 + K_2 z + K_d}{z(z-1)} \quad , \qquad [5.48]$$

where

$$K_1 = K_p + K_i + K_d \quad \text{, and} \qquad [5.49]$$

$$K_2 = -K_p - 2K_d \quad . \qquad [5.50]$$

Equation 3.3 becomes

$$F(z) = \frac{(K_1 z^2 + K_2 z + K_d)(z+b_1)(z+b_2)(z+b_3)(z+b_4)}{z^6 + g_5 z^5 + g_4 z^4 + g_3 z^3 + g_2 z^2 + g_1 z + g_0} \quad , \qquad [5.51]$$

where, recalling Equations 5.35 through 5.39 and Equations 5.41 through 5.45,

$$g_0 = K_d K_g f_0 \quad , \qquad [5.52]$$

$$g_1 = K_g (K_2 f_0 + K_d f_1) - b_8 \quad , \qquad [5.53]$$

$$g_2 = K_g (K_1 f_0 + K_2 f_1 + K_d f_2) + b_8 - b_7 \quad , \qquad [5.54]$$

$$g_3 = K_g (K_1 f_1 + K_2 f_2 + K_d f_3) + b_7 - b_6 \quad , \qquad [5.55]$$

$$g_4 = K_g (K_1 f_2 + K_2 f_3) + b_6 - b_5 \quad \text{, and} \qquad [5.56]$$

$$g_5 = K_g K_1 f_3 + b_5 \quad . \qquad [5.57]$$

Using these equations a PID controller was designed for the fourth-order system in which the high-frequency mode was aliased by setting the frequency ratio to $FR = 1.0$. The results of this design are shown in Figures 5.11 and 5.12. Figure 5.11 shows the root loci for this system. The added poles and zeros from the controller are visible, and their effect on the "fixed" poles and zeros of the aliased mode is inconsequential. Figure 5.12 shows the impulse and step responses of the system with the aliased mode. Here the effect of aliasing on the higher-order mode is clearly visible, as its contribution to the responses is nearly negligible. Very little of the effects are visible in the impulse response, as well as in the step response, although this high-order response is visible at the response settles to the final desired value.

With the design of the PID-controller for the fourth-order system accomplished, an examination of the controller's ability to reject disturbances in again in order. Figure 5.13 shows the system's responses to a step disturbance at the sample point. Again, the system is able to reject the disturbance once the controller "sees" it at the following sample point. The settling of the system to the correct steady-state value can be seen quite clearly.

Figure 5.14 shows the same characteristic for the system when the step disturbance begins between sample periods. Finally, Figure 5.15 shows the system's responses to a

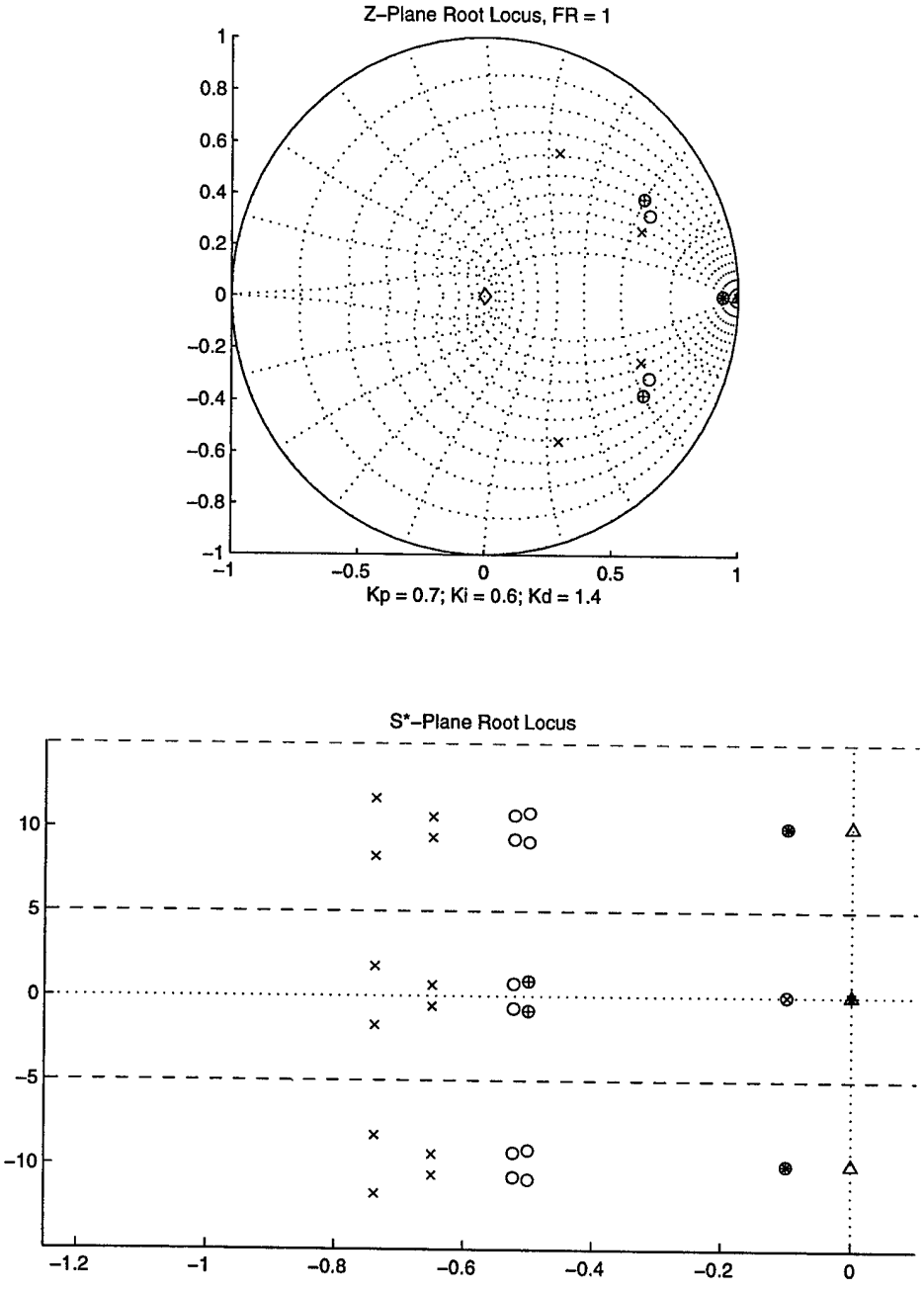

Figure 5.11 Root Loci of Fourth-Order System with One Aliased Mode

$FR = 1.0, K_p = 0.7, K_i = 0.6, K_d = 1.4$

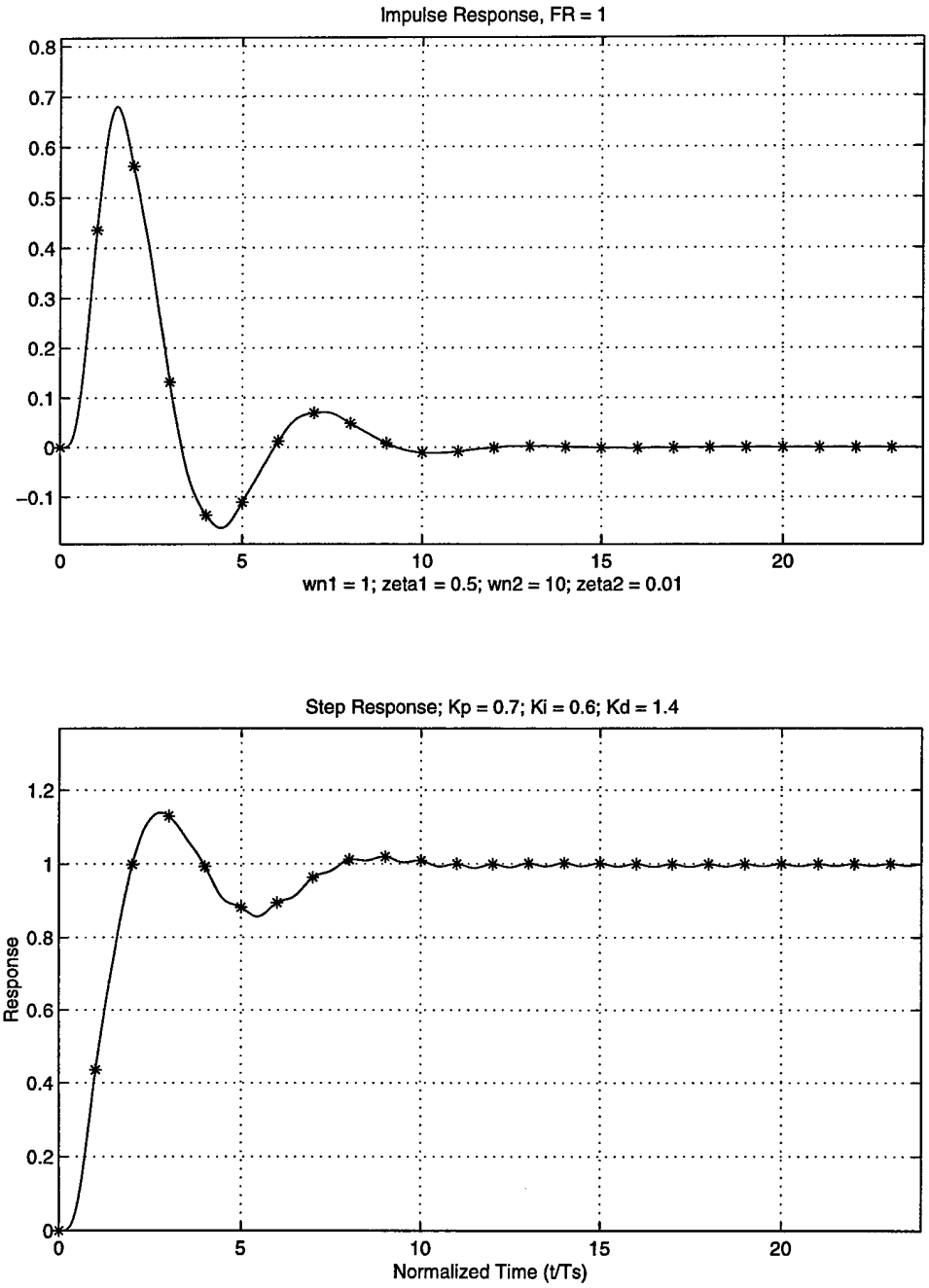

Figure 5.12 Impulse and Step Responses of Fourth-Order System with One Aliased Mode; FR = 1.0, $K_p = 0.7$, $K_i = 0.6$, $K_d = 1.4$

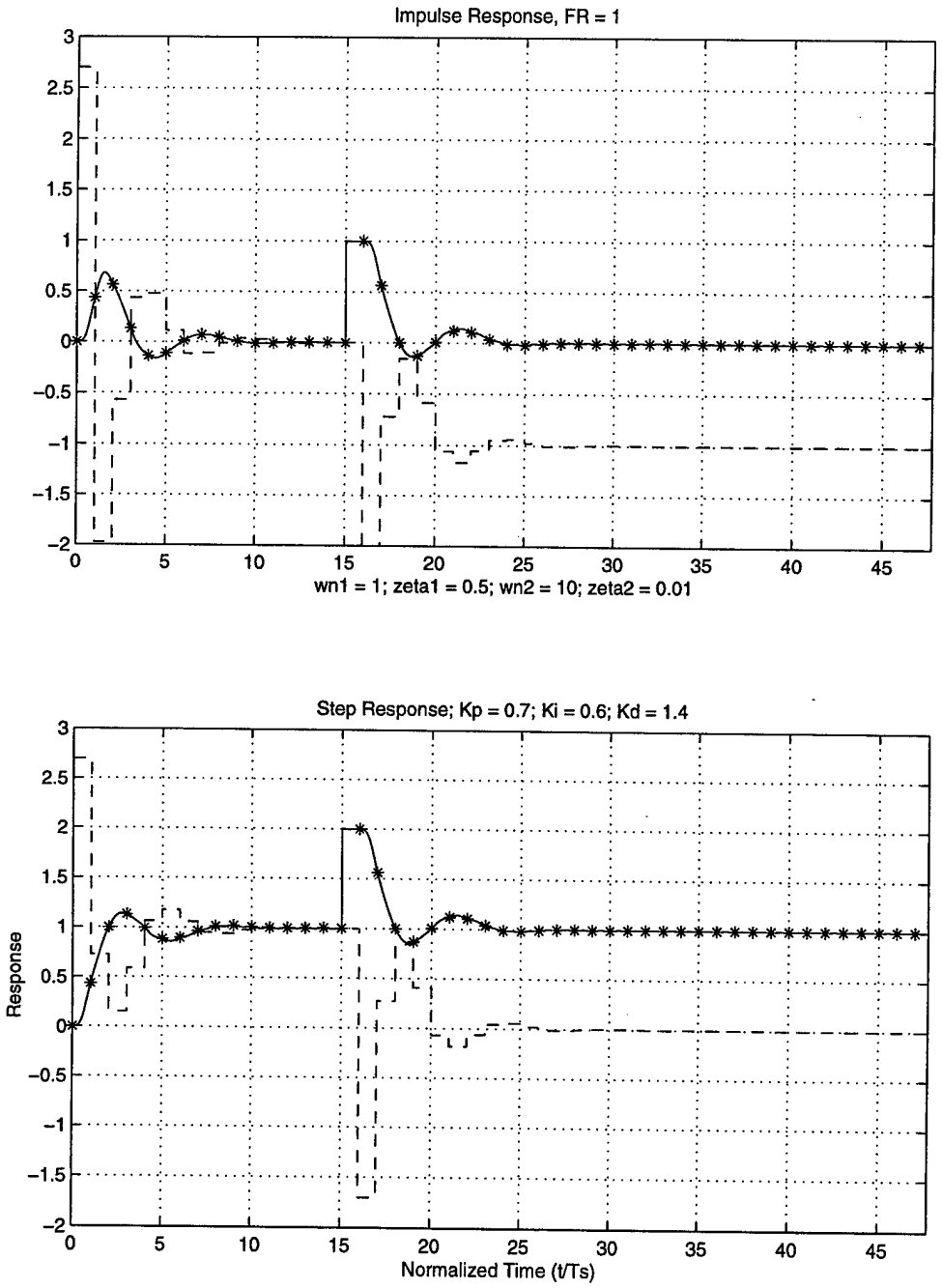

Figure 5.13 Fourth-Order System Unit Step Disturbance Rejection Disturbance at the Sample Point

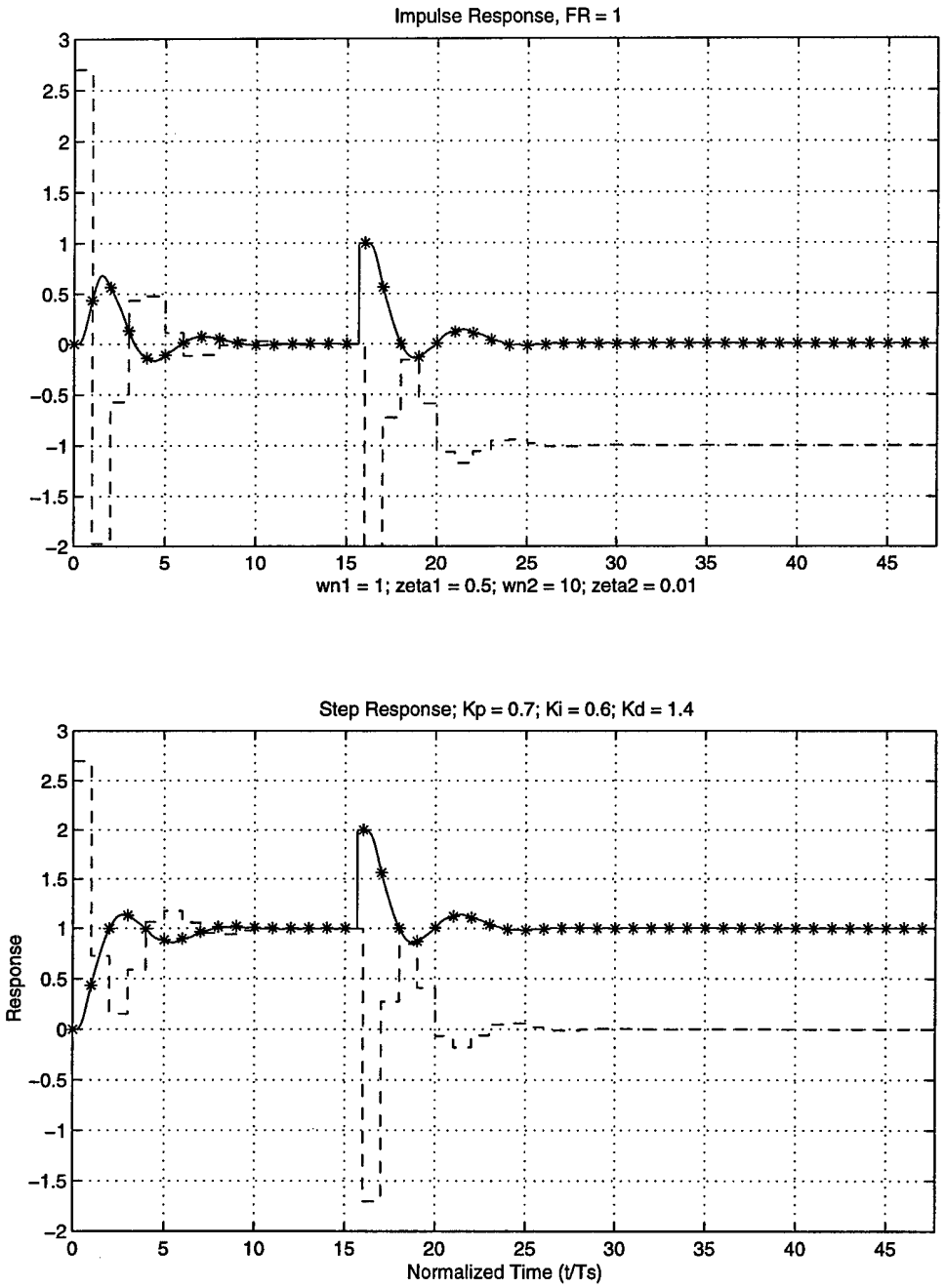

Figure 5.14 Fourth-Order System Unit Step Disturbance Rejection Disturbance Between Sample Points

random disturbance. Again, the inability of this design to control anything changing faster than the sampler's sample rate is evident. Following the disturbance, however, the system returns to the desired steady-state value as required.

Design, then, for a system in which one mode is aliased can be accomplished using traditional methods for the remaining un-aliased modes, with the aliased mode's effects being negated simply by selecting the correct sampling frequency. This selection is done such that the ratio of the sampling frequency to the damped natural frequency of the high frequency mode is equal to one. By so doing, the designer may effectively eliminate the response of that mode.

5.4 Chapter Five Summary

In this chapter the design of a controller for a fourth order system in which the high-frequency mode is aliased was designed. Once again, the frequency ratio of $FR = 1.0$ was found to have favorable effects on the control of the aliased mode. In this case, the mode was basically suppressed, and design for the low-frequency mode was accomplished using traditional design methods with little response resulting from the aliased high-frequency mode. Disturbance rejection for this controller is as was found for the other designs in which aliasing was allowed: good for disturbances whose frequencies are below the sampling frequency and poor for broadband disturbances.

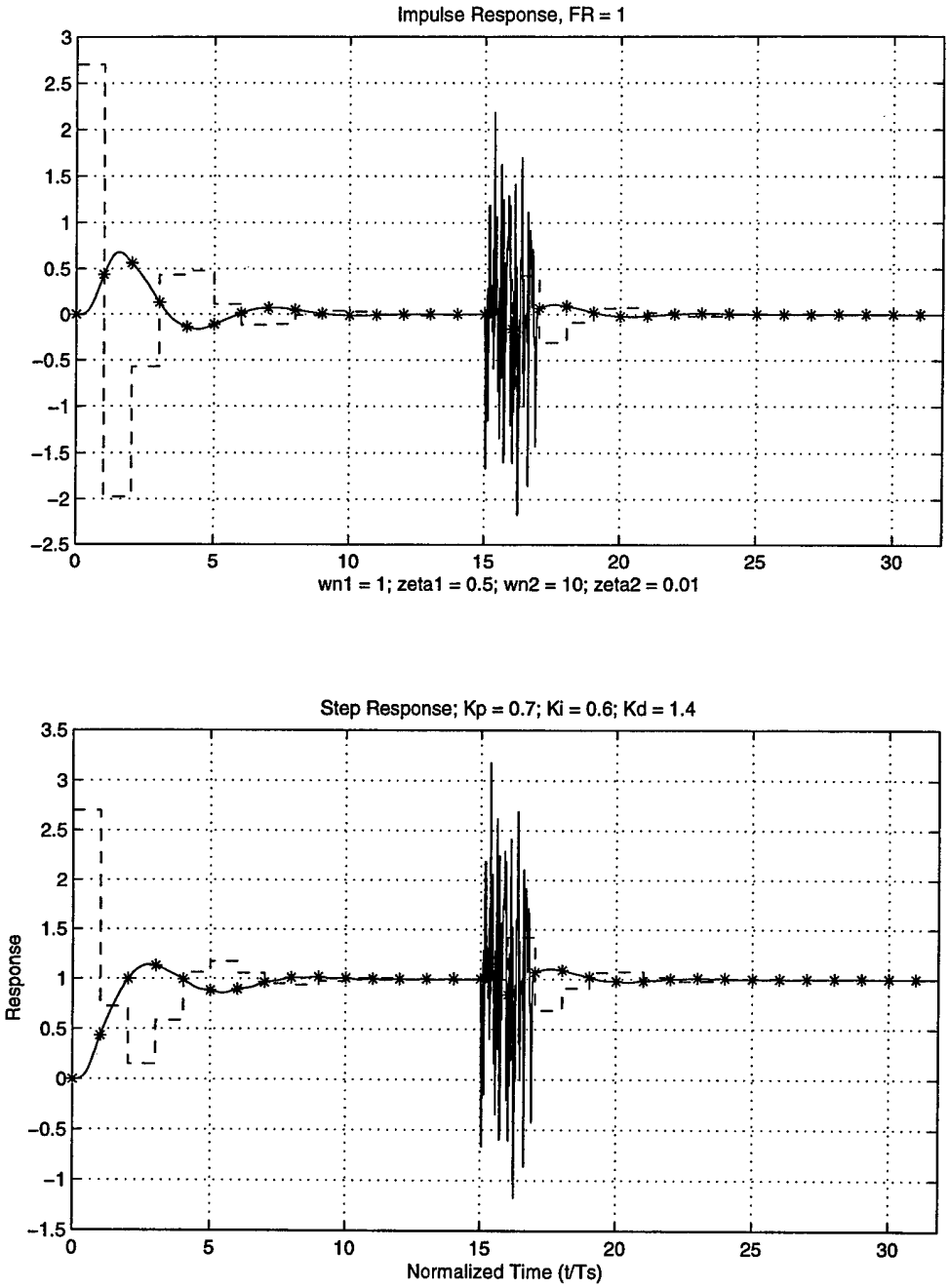

Figure 5.15 Fourth-Order System Random Input Disturbance Rejection

CHAPTER SIX. EXPERIMENTAL VERIFICATION

6.0 INTRODUCTION

Given the tools and processes developed theoretically in chapters three through five, it becomes important to verify these design methods experimentally. Experimental verification will be accomplished through applying the concepts of design to simple electronic circuits. The comparisons of experimental results to theoretical model results are excellent.

6.1 SECOND-ORDER CIRCUIT

To demonstrate the accuracy of the design method developed in chapters four and five the circuit show in figure 6.1 was constructed. This, then, becomes the plant for the discrete-to-continuous system. Given the values of resistance and capacitance seen in

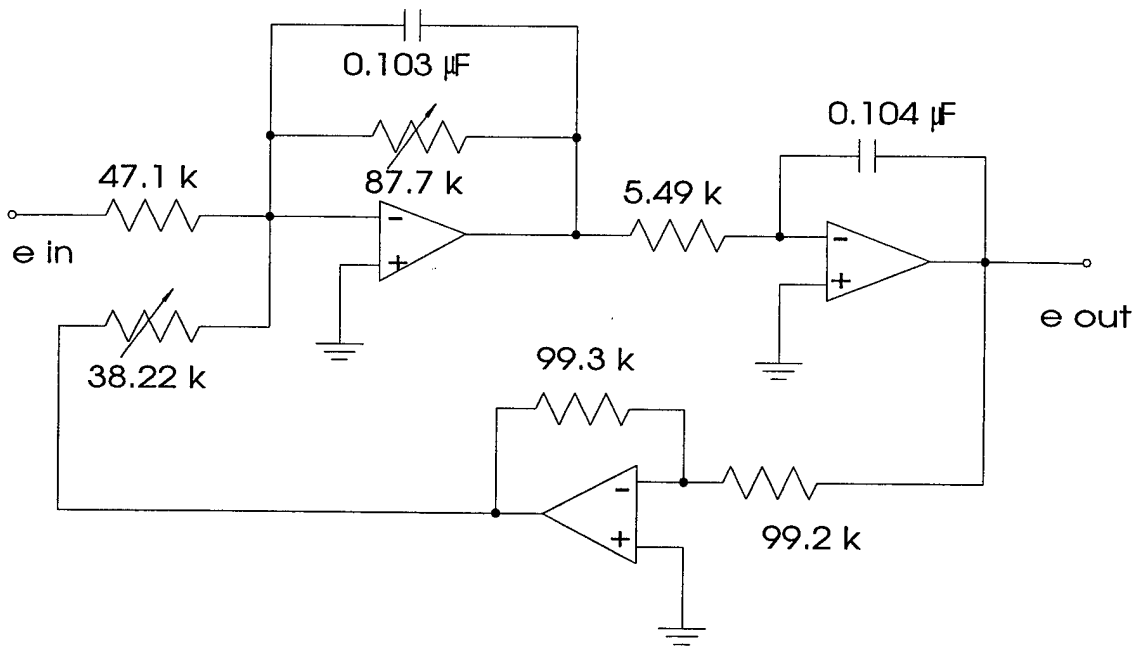

Figure 7.1 Second-Order System Circuit Diagram

figure 6.1 the natural frequency, system damping and system gain values are as found in table 6.1.

Table 6.1 Second-Order System Parameters From Calculations

System Parameter	Value
Natural Frequency	$\omega_n = 106.2116$ Hz
Damping Ratio	$\zeta = 0.08294$
System Gain	$K = 0.8106$

With the circuit built, a swept sine wave was introduced into the circuit. The sample rate was set at 4000 Hz and a Hamming window was applied to both the input and output.

The number of data points was 16,384 samples, with 30 averages of the resulting input and output auto spectra taken. Coherence over the range of interest, 0.1 to 200 Hz, was essentially equal to one, with the lowest value at a single point equal to 0.982. The values of magnitude and phase from the resulting frequency response function were saved to file.

Using Matlab, a least squares error fit between the experimental data and model parameters was accomplished to determine experimental natural frequency, damping ratio, and system gain. The results of this curve fit are shown in figure 6.2, the solid line representing the experimental data and the dashed line representing results of the curve fit—the frequency response function using model values from the curve fit. Values found from this curve fit are as found in table 6.2.

Table 6.2 Second-Order System Parameters From Curve Fit

System Parameter	Value
Natural Frequency	$\omega_n = 98.562$ Hz
Damping Ratio	$\zeta = 0.1188$
System Gain	$K = 0.8085$

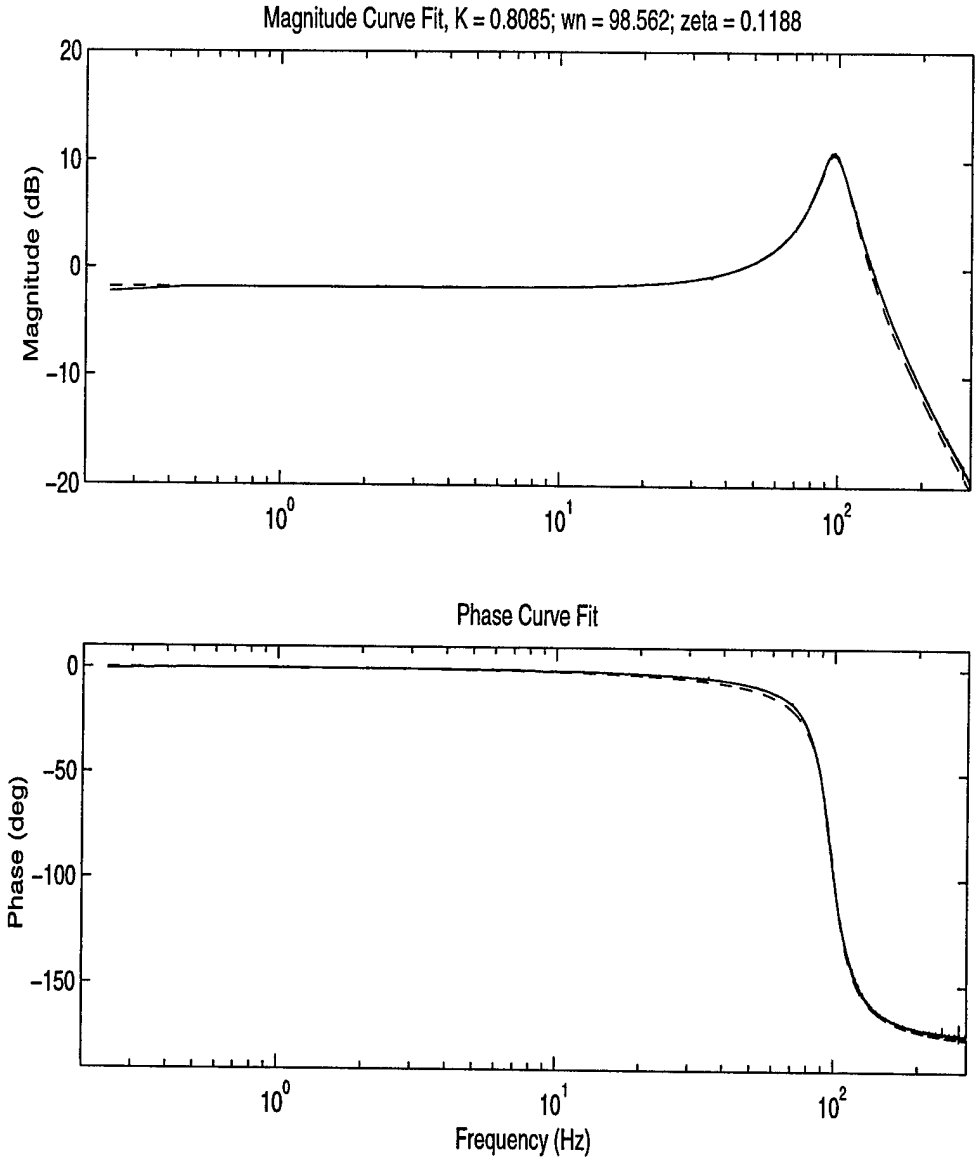

Figure 6.2 Least Squares Error Curve Fit of Model to Experimental Data

Finally, an impulse was applied to the system and 10 averages were taken. From the impulse responses, the natural frequency and damping ratio, using logarithmic decrement, were calculated. Results are listed in table 6.3.

Table 6.3 Second-Order System Parameters From Impulse Responses

System Parameter	Value
Natural Frequency	$\omega_n = 92.7803$ Hz
Damping Ratio	$\zeta = 0.1045$
System Gain	N/A

The values in tables 6.2 and 6.3 vary from those of table 6.1 because of differences in theoretical and actual systems. Physical systems, although close, rarely exhibit exact calculated values. For the experimental verification to follow values found from the impulse response will be used.

6.2 Experimental Verification of Second-Order System with Proportional and Proportional-Integral Control

With the second-order system parameters experimentally determined, the validity of the model developed in chapters three and four can now be determined. Using the same model of chapter three, values for the sampling frequency ($\omega_s = \omega_n\sqrt{1-\zeta^2}$) and the proportional gain K_p were calculated and used in the program for the digital controller. The A/D card used for data acquisition was simple with limited options and a maximum sample rate of 2000 Hz. Sample rate was "infinitely" variable, with a change of sample period possible to the ninth decimal place. Because of the magnitude of the system natural frequency and the limitations of the A/D sample rate, however, only 20

"continuous" points were taken between the sample points sent to the controller. Even so, this is a sufficient number of points to map the continuous response of the sampled data system.

The results of the first series of runs are seen in figure 6.3. Only proportional control was employed. An average of five data sets was used to eliminate noise from individual runs of the system. The match between the model results, the solid line, and the continuous output of the system, the dashed line, are not very good, indicating a problem with the model parameters. Examination of the sample points, the asterisks on figure 6.3, shows a difference between the sampling frequency and the damped natural frequency of the system with the experimental frequency being lower. Damping of the model also appears to be greater than that of the experimental system. Decreasing the natural frequency found from the impulse response by 0.51% and increasing the damping ratio by 15.88% gives the results of figure 6.4. Here, the correspondence between experimental and model data is much improved, and one can see that with even further changes made, an exact match between the model and experimental data could be obtained.

Using these same values of $\omega_n = 92.31$ Hz. and $\zeta = 0.1211$ in the proportional-integral controller, the resulting figure is shown in figure 6.5. One can see again the good match between the model and the experimental data.

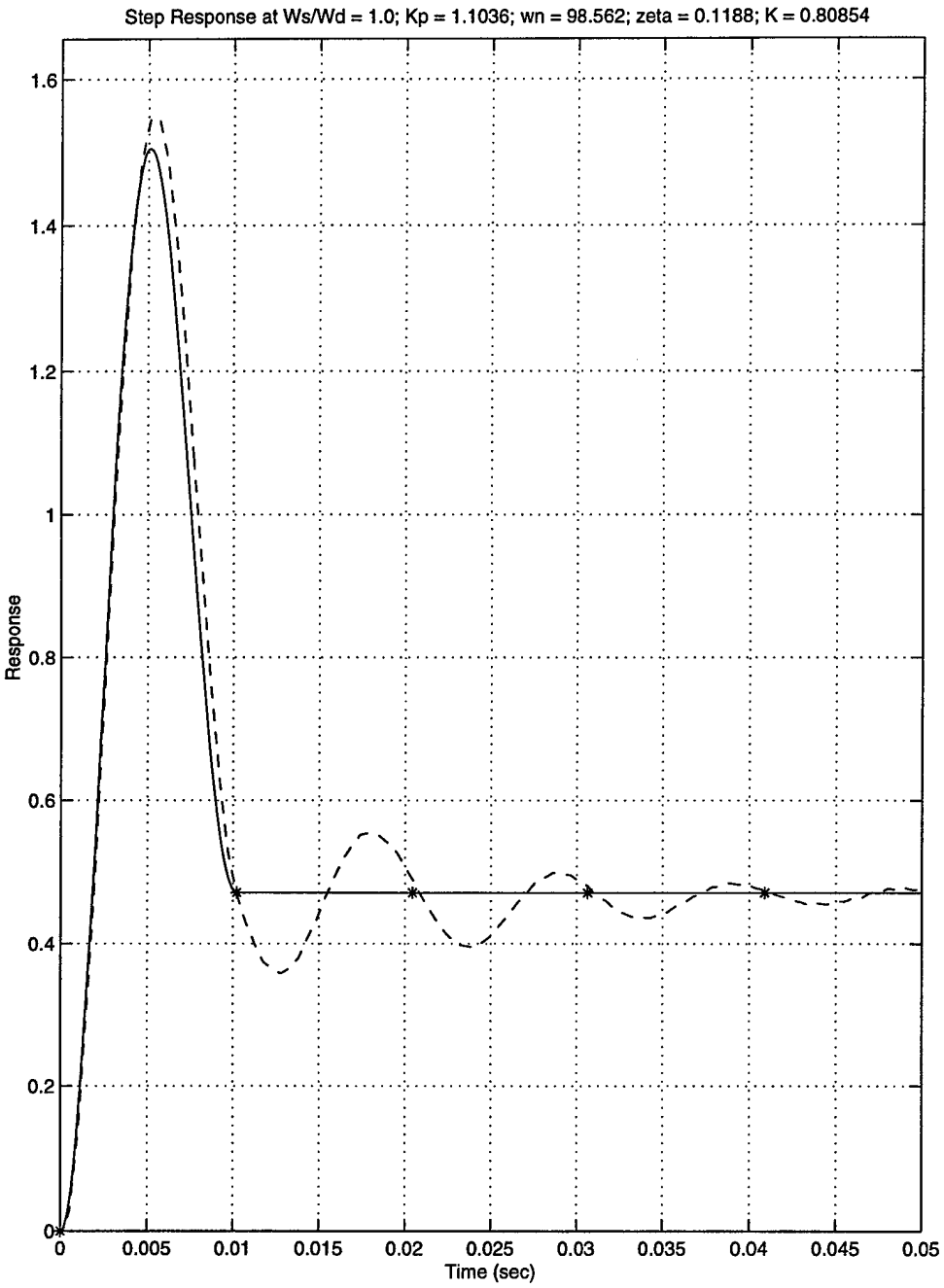

Figure 6.3 P-Controller Experimental Step Response
FR = 1.0, $\omega_n = 98.562$ Hz, $\zeta = 0.1188$, $K = 0.8085, K_p = 1.1036$

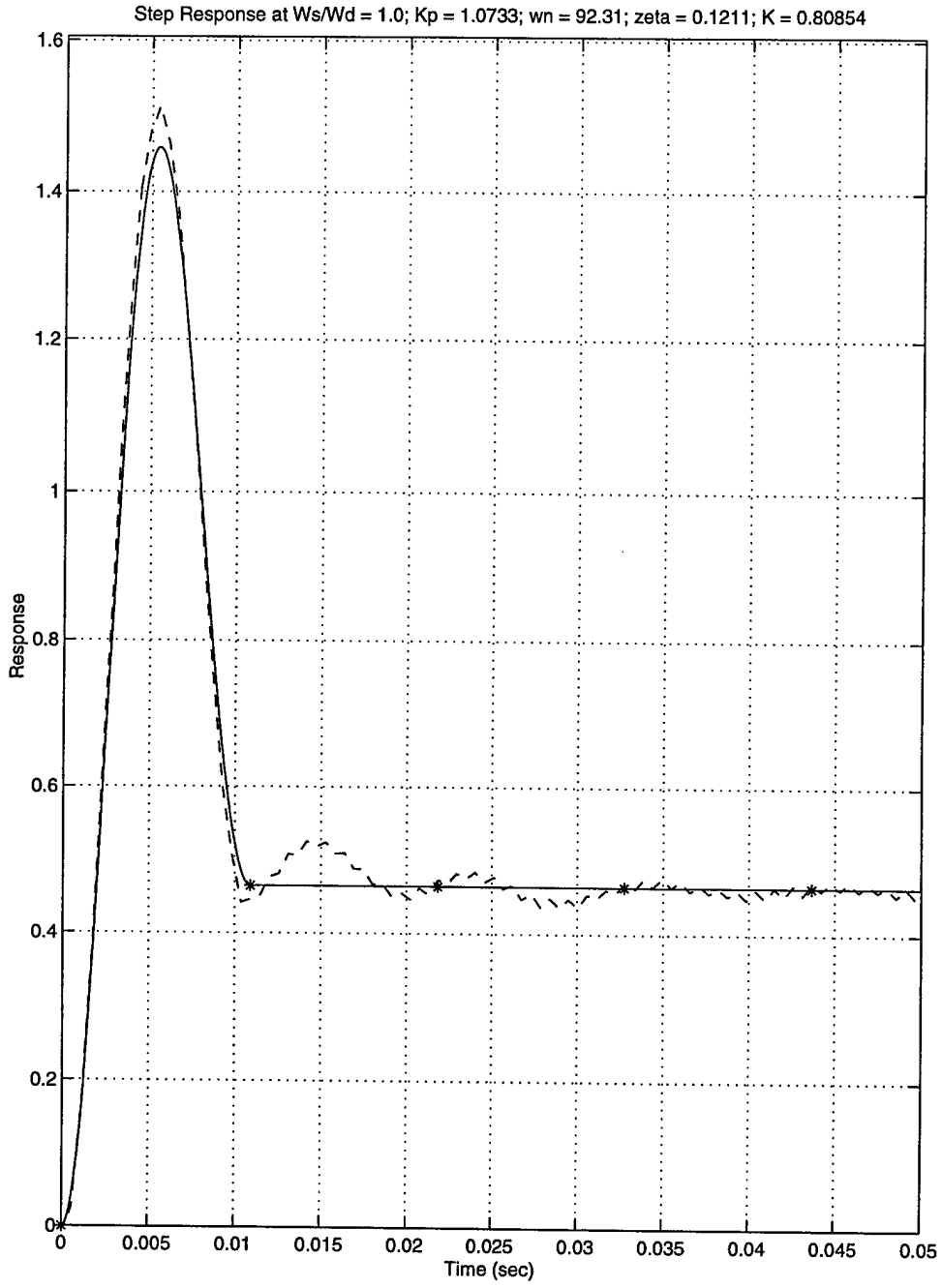

Figure 6.4 P-Controller Experimental Step Response
FR = 1.0, $\omega_n = 92.31$ Hz, $\zeta = 0.1211$, $K = 0.8085, K_p = 1.0733$

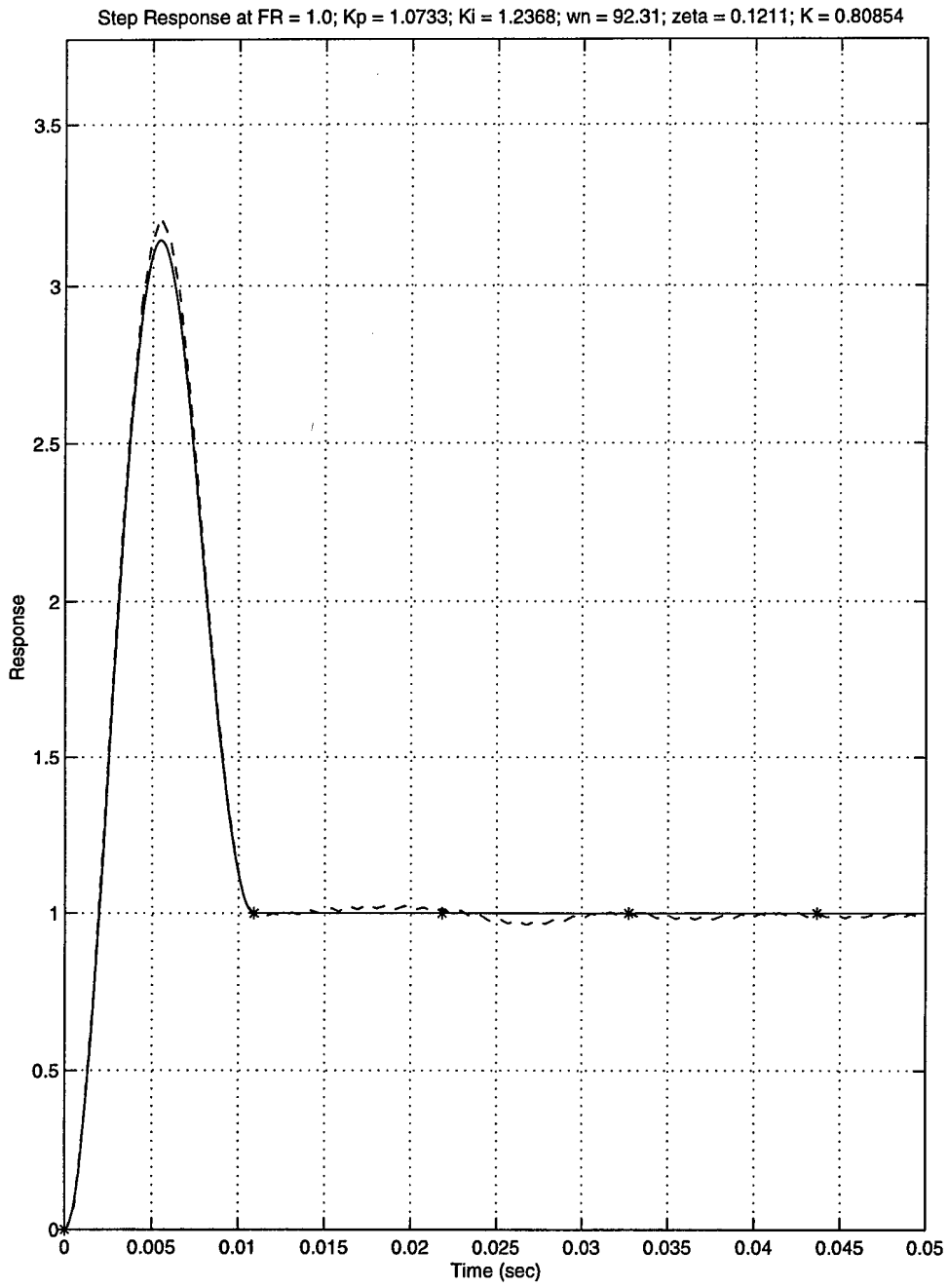

Figure 6.5 PI-Controller Experimental Step Response
FR = 1.0, $\omega_n = 92.31$ Hz, $\zeta = 0.1211$, $K = 0.8085, K_p = 1.0733$, $K_i = 1.2368$

Examination of figures 6.4 and 6.5 show that, indeed, the experimental method matches the mathematical model developed in chapters three and four. It also shows the difficulty in pole placement, as small changes in the natural frequency or damping ratio causes the system to respond differently than predicted. This can, however, be predicted using the model.

6.3 FOURTH-ORDER CIRCUIT

To demonstrate the accuracy of the model of the fourth-order system developed in chapter five, the circuit shown in figure 6.6 was constructed. The fourth-order system consists of two second-order circuits similar to that of section 6.1. To get the fourth order system, the signal of e_{out} from the top system of figure 6.6 is input as e_{in} to the bottom system of figure 6.6. Given the values of measured resistance and capacitance seen in figure 6.6, the natural frequency, system damping, and system gain values were calculated. These calculated values are shown in table 6.4, below. These values were selected such that one mode was easily aliased to the frequency range of the other. Also the aliased mode's damping ratio is such that it is very small in comparison to that of the non-aliased mode so that it's effect might be easily observed in the experimental data.

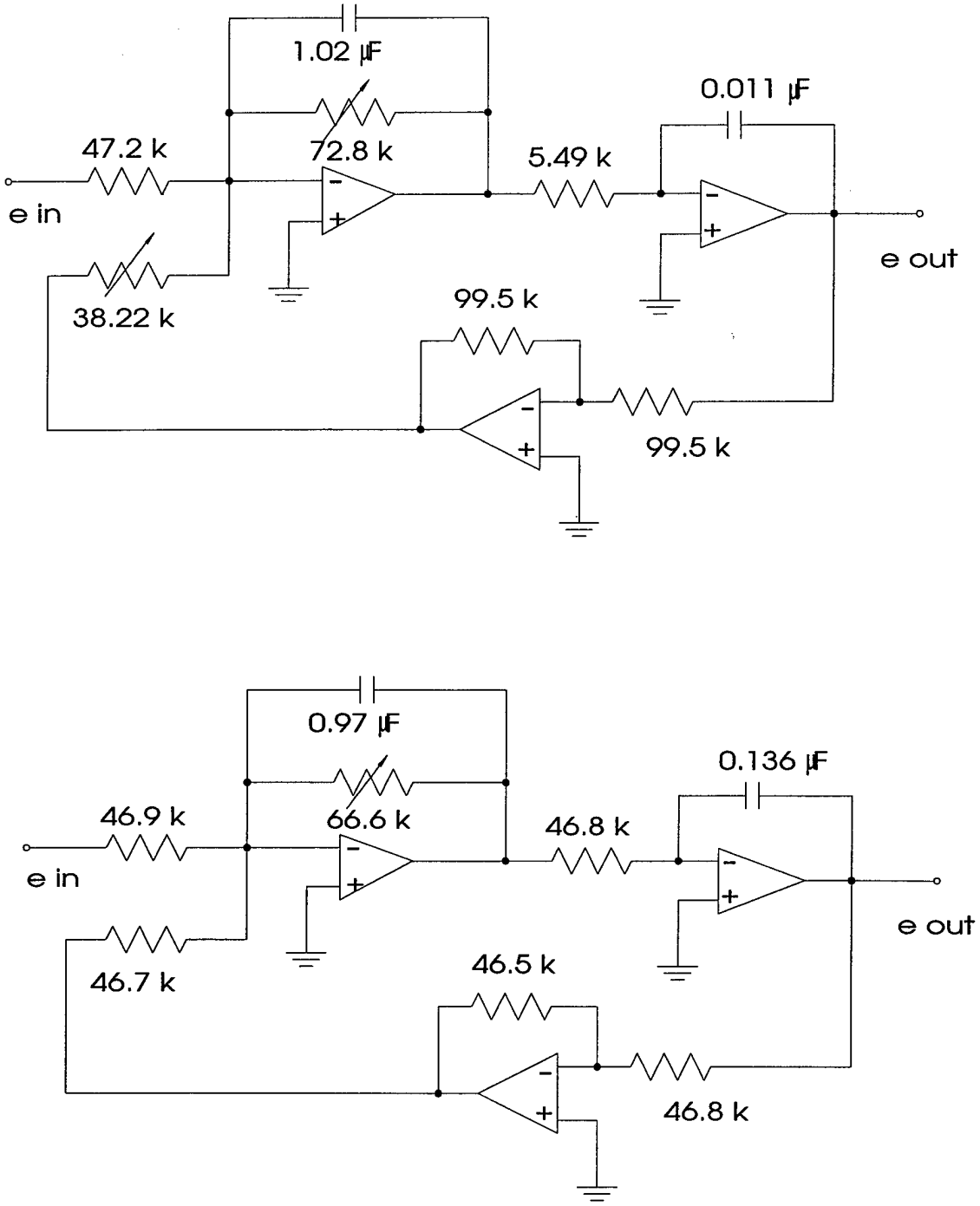

Figure 6.6 Fourth-Order System Circuit Diagram

Table 6.4 Fourth-Order System Parameters From Calculations

System Parameter	Value	
Natural Frequency	$\omega_{n1} = 106.21$ Hz	$\omega_{n2} = 9.343$ Hz
Damping Ratio	$\zeta_1 = 0.00999$	$\zeta_1 = 0.1318$
System Gain	$K = 0.8097$	$K = 1.0022$

With the two second-order circuits built, a digital impulse was introduced into each and the natural frequencies and damping ratios of each of the circuits were determined using the logarithmic decrement method. The results of these experiments are shown in table 6.5 below. Again, the physical parameters fairly closely match the calculated parameters.

Table 6.5 Fourth-Order System Parameters From Impulse Response

System Parameter	Value	
Natural Frequency	$\omega_{n1} = 108.71$ Hz	$\omega_{n2} = 10.10$ Hz
Damping Ratio	$\zeta_1 = 0.01498$	$\zeta_1 = 0.1330$

Using these values in the experimental setup, the fourth-order system was tested with a digital proportional-integral-derivative (PID) controller. The results, shown in figure 6.7 show excellent agreement of experimental data, the dashed line, to model data, the solid line. The fourth-order model accurately predicts experimental results. Close examination shows the response of the aliased mode, as well, although because of the prudent selection of sampling rate the aliased mode introduces very little response.

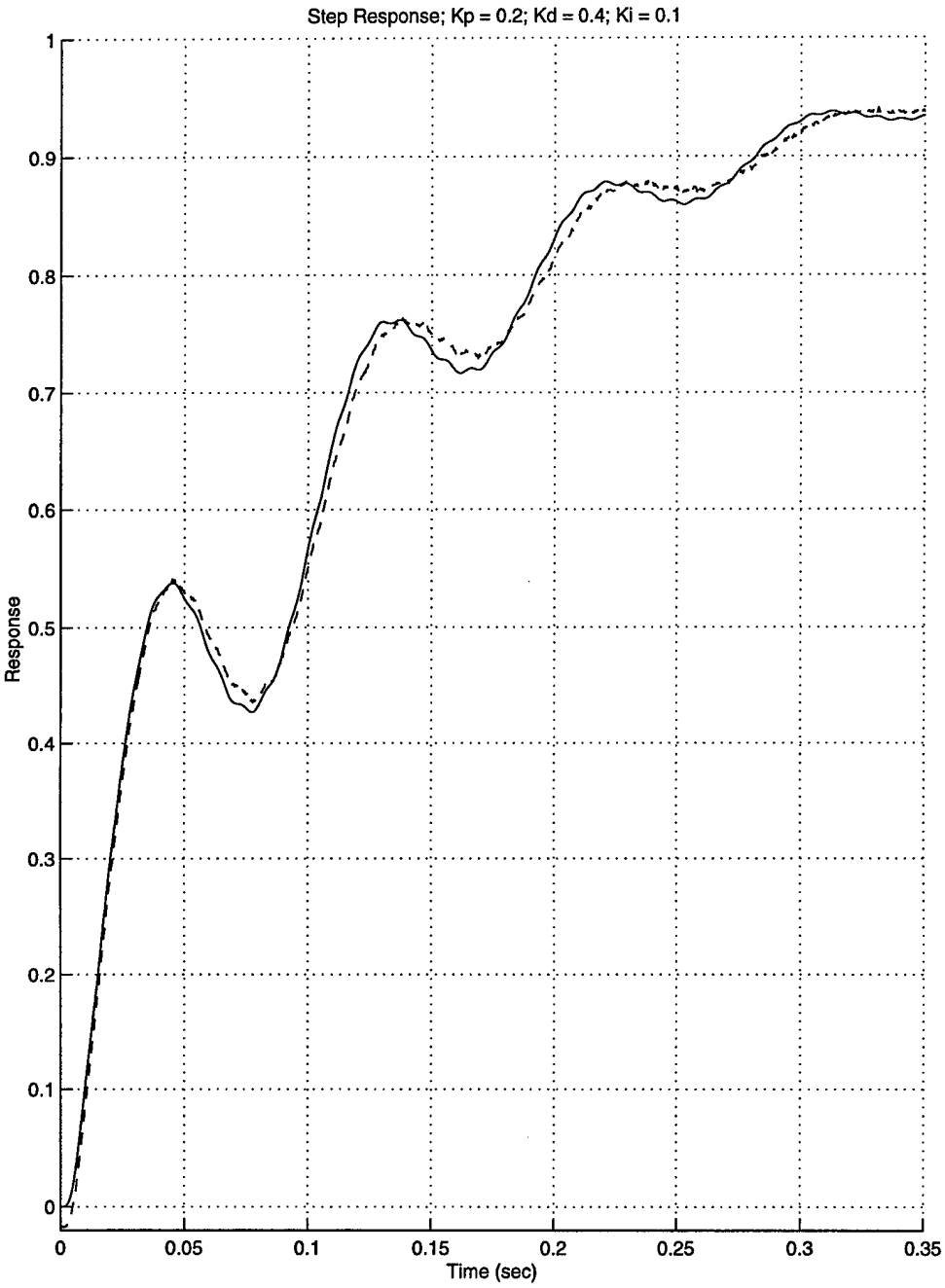

Figure 6.7 PID-Controller Experimental Step Response
$K_p = 0.2$, $K_d = 0.4$, $K_i = 0.1$

To show the effects of designing for the lower order mode, and how this will not affect the effects of the aliased mode on the response, different values for the gains were selected. The result is shown in figure 6.8. Again, experimental response matches closely to that predicted by the model. Moreover, the aliased mode has very little effect on the design of control for the non-aliased mode.

6.4 Chapter Six Summary

Experimental verification of the model developed in this dissertation was accomplished in this chapter. Experimental results show excellent agreement with the model. They also show the sensitivity of the controller's response to accurate modeling of the plant's dynamics.

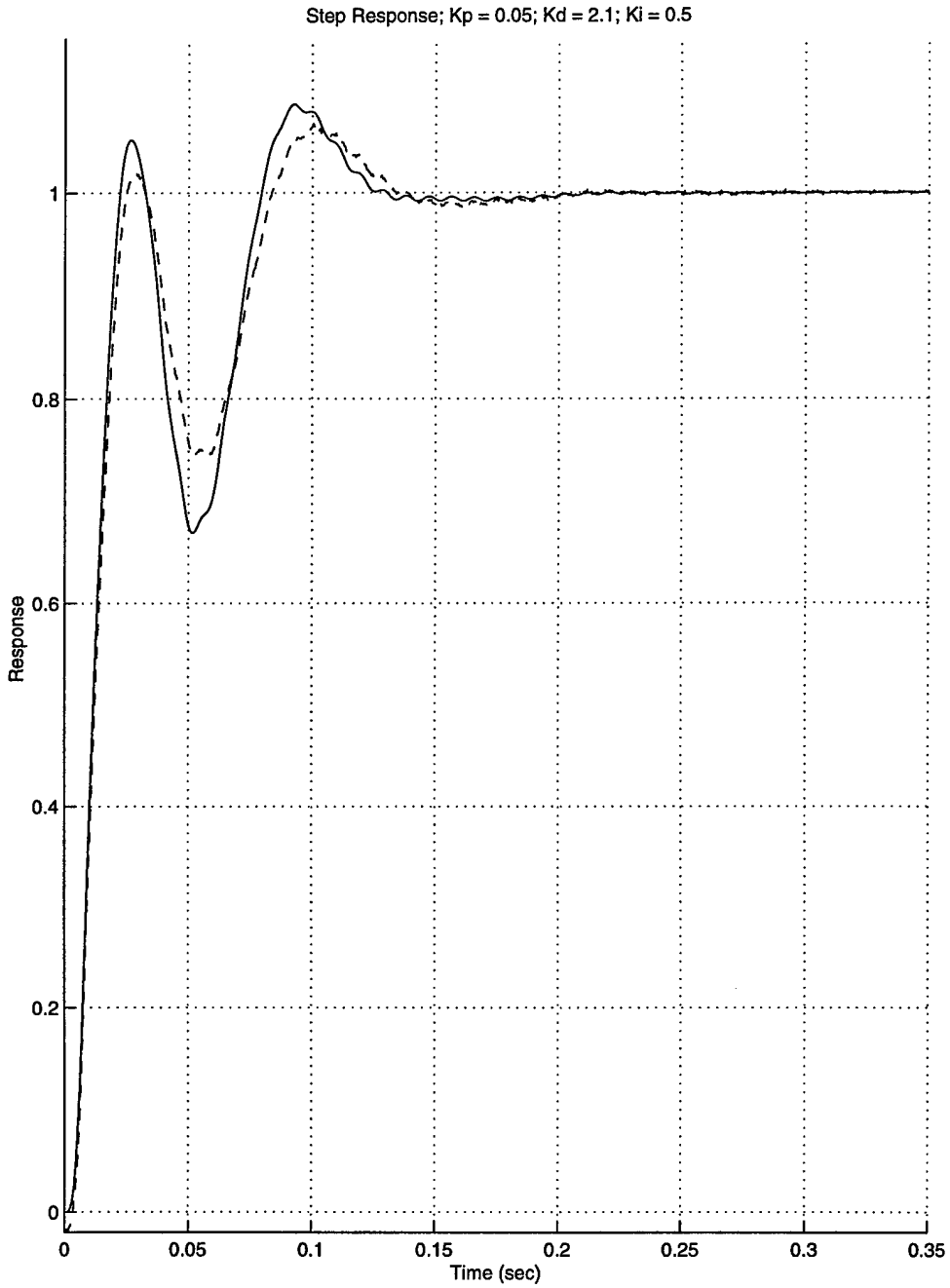

Figure 6.8 PID-Controller Experimental Step Response
$K_p = 0.05$, $K_d = 2.1$, $K_i = 0.5$

CHAPTER SEVEN. CONCLUSIONS AND RECOMMENDATIONS

7.0 CONCLUSIONS

This research effort begins by developing a model in which aliasing is allowed. The model developed includes both discrete and continuous sections of the system. Unlike the traditional sampled-data systems in which analysis is completed in either the discrete or continuous domains, this model allows analysis for systems in which both discrete and continuous models exist concurrently. The resulting transfer function is called a discrete-to-continuous transfer function.

In the limit, as the sample period of the discrete portion of the model goes to zero, the model becomes a continuous model, as would be expected. To mathematically obtain this limit, however, the system must be physically realizable, or the order of the numerator of the system must be equal to or less than the order of the denominator of the system. This condition holds true for all physical systems. The limit, as the sample period increases to infinity, is zero, signifying a system in which no feedback is ever

seen. Again, this is the expected result, since as the sample period goes to infinity in a discrete system no feedback occurs. The discrete-to-continuous model, then, accurately models both continuous and discrete systems in the limit as the sample periods go to zero and infinity, respectively.

To aid in analysis, a "new" plane was introduced—the s*-plane. This is the plane in which the continuous poles and zeros exist, and to which the poles and zeros from the discrete portion of the system are transformed, repeating infinitely through all bands. It is the plane in which the only appropriate controller function can be designed. This unique controller function $F^*(s)$ is the only function representing the unique time function $f^*(t)$ that excites the plant only at the sample points. The time function $f^*(t)$ is modeled as a series of impulses at the sample points and zero everywhere else.

The s*-plane allows one to examine the effects of aliased poles and zeros—poles and zeros located in bands outside the primary band—and their effects on the response of the discrete-to-continuous system. This definition of aliased poles (and zeros) in the s*-plane is perhaps different than the traditional view of aliasing.

In the s*-plane, a set of zeros from the discrete controller will always cancel the poles from the continuous plant. These zeros, however, are repeated in each of the infinite bands, other than the band in which the continuous poles are located, and as a result, the continuous system's response between sample periods is that of the open-loop damped natural frequency of the plant given a step input and the initial conditions found at each

sample point. This continuous response between samples cannot be completely controlled. It can, however, be used in designing an optimal control of the system.

Examination of the responses of the system shows the discrete response follows that which would be expected based on the pole placement in the z-plane. When the poles of the controller term are located on the negative real axis, the discrete response is an exponentially decaying oscillation. Likewise, when located on the positive real axis, the response is exponentially decaying with no oscillation.

Because of the discrete-to-continuous nature of the developed model, the sample rate or sample period becomes a design parameter. Allowing aliasing, or slowing the sample rate such that aliasing occurs, has a stabilizing effect on a second-order plant. This stabilizing effect is seen in the increased gain margins at certain frequency ratios, as well as in improved impulse and step responses. The frequency ratio is defined as the ratio of the sampling frequency to the damped natural frequency of the aliased mode.

Sample rates were found such that the entire root locus of a second-order system with proportional control lies on the real axis in the z-plane. These sample rates correspond to frequency ratios of

$$FR = \frac{2}{n}, \qquad n = \text{integer}. \qquad [7.1]$$

At these frequency ratios, two of the controller zeros collapse to a single point in both the z- and s*-planes, causing one of the controller poles to remain at the same point, no matter the controller gain. At this frequency ratio, the second pole of this pair, the stationary pole's "mate," travels only along the real axis in the z-plane as the controller gain is increased.

When n = odd is used in the frequency ratio, part of the root locus lies on the positive real axis and part on the negative real axis of the z-plane. This corresponds to part lying on the band boundaries and part lying on the mid-band lines in the s*-plane. The impulse and step responses seen at these frequency ratios show the most desired characteristics of the aliased responses. Selecting a frequency ratio of $FR = 1.0$ gives the best response of this class of responses, giving only one complete cycle of the damped natural response of the open-loop plant.

Additionally, when the frequency ratio is set to one, placement of the non-stationary pole mentioned above can be such that it lies at the origin of the z-plane, which corresponds to negative infinity in the s*-plane. With the controller designed such that the pole is located here, a deadbeat response results. Using a simple proportional-integral (PI) controller, the perfect deadbeat response is obtained with very little problem: within one sample period, the step response is at its final desired value. For this response, the proportional gain, K_p, is a function only of the damping and the integral gain, K_i, is always equal to one. Experimentation shows the model to produce accurate results, with

experimental data matching the response predicted by the model. This deadbeat response, then, is obtainable in physical systems.

The deadbeat response of the discrete-to-continuous system is different than conventional deadbeat responses in that here, with aliasing, we are taking advantage of the system's natural response, phasing the control such that the response is exactly cancelled following one sample period. It does not force response beyond the system's own natural response.

The second-order system with proportional integral control has excellent disturbance rejection capability, if the frequency of the disturbance is lower than the frequency of the controller. The opposite is also true—this controller has poor disturbance rejection when the disturbance's frequency is broadband.

Robustness of the system is examined and the system is found to be fairly robust. Although the deadbeat response is lost, and this was to be expected, the system settles to final values within six sample periods given a 5% change in natural frequency or damping of the plant. Clearly, the plant to be controlled here must be well-identified and modeled.

One of the drawbacks of this system is the great overshoot present in the deadbeat response. Another is its poor following of non-stationary input signals. The response of the discrete-to-continuous system to sinusoidal inputs is poor, at best, unless the input sinusoid has a very low frequency relative to the sampling frequency. This type of

control, then, would not be appropriate for rapidly changing systems with respect to the sampling frequency.

The power of this type of control can be seen when considering systems in which accurate position is required, with minimum time, and with little care for overshoot of the system. Such systems might include the positioning of a crane or a disk drive head in a minimum amount of time. These systems need accurate positioning, have allowances for overshoot, and require low settling times. The aliased discrete-to-continuous system developed in this dissertation will meet these requirements.

The fourth-order system in which one of the modes is aliased was examined. It was seen that by selecting the sample rate such that the frequency ratio was $FR = 1.0$, with respect to the natural frequency of the mode to be aliased, the effects of the aliased mode are minimized. In fact, the response of this aliased mode is almost not seen. Control for the non-aliased mode can be accomplished using traditional methods, with the resulting controller affecting the aliased mode very little. Again, disturbance rejection is good for disturbances with frequencies below that of the sampler. This, then, becomes an effective means for controlling aliased modes—simply select the sampling rate to be equal to that of the aliased mode.

7.1 RECOMMENDATIONS FOR FUTURE STUDY

To further improve the design methods found in this research, additional studies should be performed with respect to physical systems. This effort examined only electric circuits to verify the theoretical model. Systems for which this method would be useful should be explored and implemented.

The further effects of zero placement in the s*-plane need to be researched as well. Zero-placement was not a parameter of the design in the theoretical modeling. The researcher simply selected zero locations for ease of experimental verification. Such zero-placement may in some manner aid or detract from the ideal designs examined here.

Further research should also aim to tie this theory for higher-order systems into state-space domain, so that the powerful techniques available there could be employed in the design of aliased controllers as well.

Another area of further research should be the examination of the effects of time delays in systems in which aliasing is allowed. Are the time delays detrimental as conventional theory would suggest, or will they aid in stabilization as was the case with aliasing only of this research effort? Richard Lyman [13] demonstrated time delays can sometimes stabilize the system.

One of the first assumptions in performing this research was that of an ideal sampler—one in which the period required to sample the signal is very much smaller than the sample period of the sampler. Another avenue of study would be examination of the effects of relaxing this assumption. As the sampler takes a more significant amount of time compared to the sample period, the ideal sampler degenerates to a step-on, step-off mechanism, causing some phase delay and smaller magnitude in the frequency response function (FRF) as the frequency increases. The results become the multiplication of the FRF by a sinc function—similar to multiplying one more zero-order hold times the entire FRF.

Additionally, the effects of optimizing the parameters found for the controllers could be examined. Will optimization techniques work? And what are their effects on the aliased modes, either the deadbeat response found for the second order system or the aliased mode found for the fourth-order system?

REFERENCES

1. Franklin, Gene F., Powell, J. David, & Workman, Michael. Digital Control of Dynamic Systems. Menlo Park, California: Addison Wesley Longman, Inc., 1998

2. Shannon, C. E., "Communication in the Presence of Noise." Proceedings of the IRE, January 1949, pp: 10-21

3. Nyquist, H., "Certain Factors Affecting Telegraph Speed." Bell Systems Technical Journal, Vol. 3, April 1924: pg. 324

4. Figliola, Richard S., & Beasely, Donald E., Theory and Design for Mechanical Measurements, New York, New York: John Wiley & Sons, Inc., 1995

5. Thornhill, R. Joe, & Smith, Craig C., Fourier and Spectral Analysis in Dynamic Systems, Short Course Notes, 1994

6. Durney, Alan N., "Using On-Board Robot Controller Hardware and Robot Sensors to Identify a Robot Plant for Control Law Design." Masters Thesis, Department of Mechanical Engineering, Brigham Young University, August 1993

7. Kuo, Benjamin C., Discrete-Data Control Systems. Englewood Cliffs, New Jersey: Prentice-Hall, Inc., 1970

8. Ehrlich, Rick, Taussig, Carl, & Abramovitch, Daniel, "Identification of Sampled Data Systems at Frequencies Beyond the Nyquist Rate." Proceedings of the 1989 IEEE Conference on Decision and Control. Tampa, Florida, December 1989.

9. Kang, M. S. & Yang B., "Discrete Time Noncolocated Control of Flexible Mechanical Systems Using Time Delay." ASME Journal of Dynamic Systems, Measurement and Control, vol. 116, June 1994: pp. 216-222

10. Yang, Bingen, & Hu, Jwu-Sheng, "Can Aliased Modes of a Flexible System Be Controlled by a Digital Controller of a Low Sampling Rate." ASME Symposium on Mechatronics. DSC-Vol. 50, American Society of Mechanical Engineers, November 1993

11. Sims, Jay R., "Identification and Control of Dynamic Systems with Frequency Aliasing." Masters Thesis, Department of Mechanical Engineering, Brigham Young University, December 1995

12. Dormido, S., Lopez-Rodriguez, I., Fdez-Marron, J. L., & Aranda, J., "Design of Digital Control System Using the Sampling Period as a Compensator." Proceedings of MELECON, Vol. 9, 1991: pp. 812-815

13. Lyman, Richard J., Jr., "Root Loci based on Sampling Period and Time Delay: Design Tools for Controllers of Sampled-Data Systems." Masters Thesis, Department of Mechanical Engineering, Brigham Young University, August 1995

14. Wang, C. H., Wang, W. Y., & Lee, T. T., "Sampling Time Effects of Higher-Order Digitisations and Their Applications in Digital Redesign," IEE Proceedings: Control Theory and Applications, Vol. 141, No. 2, March 1994, pp. 83-92

15. Wang, C. H., Lin, M. Y., & Teng, C. C., "On the Nature of the Boxer-Thaler and Madwed Integrators and Their Applications to Digitising a Continuous-Time System," IEEE Transactions, 1990, pp. 1163-1167

16. Diduch, C. P. & Doraiswami, R., "Role of Sample Period in Transients, Robustness and Sensitivity in Optimally Designed Digital Control Systems," International Journal of Systems Science, Vol 19, No. 6, 1988, pp. 921-934

17. Hirata, Hidetoshi & Powell, J. David, "Sample Rate Effects on Disturbance Rejection for Digital Control Systems," Proceedings of the 1990 American Control Conference, Vol. 2, 1990, pp. 1137-1144

18. Hirata, Hidetoshi, "Sample Rate Effects on Disturbance Rejection for Digital Control Systems," Doctoral Dissertation, Department of Aeronautics and Astronautics, Stanford University, October 1989

19. Kranc, George A., "Input-Output Analysis of Multirate Feedback Systems," IRE Transactions on Automatic Control, November 1957, pp.21-28

20. Tornero, Josep, Gu, Yuping, & Tomizuka, Masayoshi, "Analysis of Multi-rate Discrete Equivalent of Continuous Controller," Proceeding of the American Control Conference, June 1999, pp.2759-2763

21. Tangirala, Arun K., Li, Dongguang, Patwardhan, Robhit, Shah, Sirish L., & Chen, Tognwen, "Issues in Multirate Process Control," Proceedings of the American Control Conference, June 1999, pp. 2771-2775

22. Chen, T. & Francis, B., Optimal Sampled-Data Control Systems, London, England: Springer-Verlag, 1995

23. Cavicchi, Thomas J., "Phase-Root Locus and Relative Stability," IEEE Control Systems, August 1996, pp. 69-77

24. Diduch, C. P. & Doraiswami, R., "Robustness of Optimally Designed Sampled Data Control Systems," Proceedings of the 1987 American Control Conference, Vol. 2, June 1987, pp. 1247-1252

25. Braslavsky, J. H., Middleton, R. H., & Freudenberg, J. S., "Sensitivity and Robustness of Sampled-data Control Systems: A Frequency Domain Viewpoint," Proceedings of the American Control Conference, June 1995, pp. 1040-1044

26. Tsypkin, Ya. Z., "Stability of Systems with Delayed Feedback," Translation by L. Jocic and S. Kahne, Reprinted with permission from Avtomat. Telemekh, vol. 7, 1946, pp.107-129

27. Hou, Zhikun, & Ali, Mohammad S., "Stability Criteria for Active Control Systems with Time Delays," First World Conference on Structural Control, August 1994, pp. FP4-42 – FP4-50

28. Rattan, Kuldip S., "Compensating for Computational Delay in Digital Equivalent of Continuous Control Systems," IEEE Transactions on Automatic Control, Vol. 34, No. 8, August 1989, pp. 895-899

29. Ovaska, Seppo J. & Vainio, Olli, "Predictive Compensation of Time-Varying Computing Delay on Real-Time Control Systems," IEEE Transactions on Control Systems Technology, Vol. 5, No. 5, September 1997, pp. 523-526

30. Hara, S., Kondo, R., & Katori, H., "Properties of Zeros in Digital Control Systems with Computational Time Delay," International Journal of Control, Vol, 49, No. 2, 1989, pp. 493-511

31. Jury, E. I., Theory and Application of the Z-Transform Method, New York, New York: John Wiley & Sons, Inc., 1964

32. Ragazzini, J. R., & Zadeh, L. A., "The Analysis of Sampled-Data Systems." AIEE Transactions, vol. 71, November 1952: pp. 225-234

33. Ogata, Katsuhiko, Discrete-Time Control Systems, Englewood Cliffs, New Jersey: Prentice-Hall, Inc., 1987

34. Philips, Charles L. & Nagle, H. Troy, Digital Control System Analysis and Design, Englewood Cliffs, New Jersey: Prentice Hall, 1990

35. Zill, Dennis G., & Cullen, Michael R., Advanced Engineering Mathematics, Boston, Massachusetts: PWS Publishing Company, 1992

36. Dorf, Richard C. & Bishop, Robert H., Modern Control Systems, Reading, Massachusetts: Addison Wesley, 1998

37. Dutton, Ken, Thompson, Steve, & Barraclough, Bill, The Art of Control Engineering, Reading, Massachusetts: Addison Wesley, 1997

38. Astrom, Karl J. & Wittenmark, Bjorn, Computer Controlled Systems, Englewood Cliffs, New Jersey: Prentice Hall, 1990

39. Casvola, Alessandro, Mosca, Edoardo, & Zelca, Pietro, "Robust Ripple-Free Deadbeat Control Design," International Journal of Control, Vol. 72, No. 6, April 1999, pp. 564-573

40. Nesic, Dragan & Bastin, Georges, "Stabiliazability and Dead Beat Controllers for Two Classes of Wiener-Hammerstein Models," IEEE Transactions on Automatic Control, Vol. 44, No. 11, November 1999, pp. 2068-2071

41. Nesic, Dragan & Mareels, Iven M. Y., "Dead Beat Control Ability of Polynomial Systems: Symbolic Computation Approaches," IEEE Transactions on Automatic Control, Vol. 43, No. 2, February 1999, pp. 162-175

42. Verde, C., "On the Use of Sensistivity Functions to Design Dead-Beat Control Algorithm," Automatica, Vol. 35, No. 5, May 1999, pp. 945-949

43. Yamada, Manabu, Riadh, Zaier, & Funahashi, Yasuyuki, "Deadbeat Control System with Time-Varying Uncertainty: Minimization of Worst Case Steady-State Tracking Error," International Journal of Control, Vol. 72, No. 2, February 1999, pp. 141-149

44. Cutforth, Craig F. & Pao, Lucy Y., "An Analysis of Frequency-Domain Input Shaping Designs for Three-Mode Flexible Systems," Proceedings of the American Control Conference, June 1999, pp. 4388-4392

45. Cutforth, Craig F. & Pao, Lucy Y., "A Modified Method for Multiple Actuator Input Shaping," Proceedings of the American Control Conference, June 1999, pp. 66-70

46. Lim, Sungyung, Stevens, Homer D., & How, Jonathan P., "Input Shaping Design for Multi-Input Flexible Systems," Journal Of Dynamic Systems, Measurement, and Control, Vol. 121, No. 3, September 1999, pp. 448-456

47. Rhim, Sungsoo & Book, Wayne J., "Adaptive Command Shaping Using Adaptive Filter Approach in Time Domain," Proceedings of the American Control Conference, June 1999, pp. 81-85

48. Sinhose, William E. & Mills, Bart W., "Command Generation Using Specified-Negative-Amplitude Input Shapers," Proceedings of the American Control Conference, June 1999, pp. 61-65

49. Biran, Adrian & Briener, Moshe, Matlab 5 for Engineers, Reading, Massachusetts: Addison-Wesley Publishing Company, 1999

50. Kreyszig, Erwin, Advanced Engineering Mathematics, New York, New York: John Wiley & Sons, Inc., 1988

51. Franklin, Gene F., Powell, J. David, & Emami-Naeini, Abbas, Feedback Control of Dynamic Systems, Reading, Massachusetts: Addison-Wesley Publishing Company, 1994

52. Shannon, C. E., Oliver, B. M., & Pierce, J. R., "The Philosophy of Pulse Code Modulation," Proceedings of the I. R. E., Vol. 35, November 1938, pp. 1324-1331

APPENDIX A. THEORETICAL REVIEW

A.0 INTRODUCTION

This appendix will review and discuss briefly the concepts necessary to develop the model used in this research. The review will include the mathematical equations of the Laplace- and Z-transforms and the natural logarithm of a complex number, a brief explanation of root loci and frequency response function plot and their uses, the concepts behind and the assumptions made for the ideal sampler, the result of sampling on a continuous system, and a review of the zero-order hold and its affect on a continuous system.

A.1 THE LAPLACE TRANSFORM

When dealing with continuous systems for which control is to be accomplished, it is often easier to deal in the s- or Laplace domain, rather than in the time domain. The definition

of the one-sided Laplace transform is given by Zill and Cullen [35:209] as

$$\mathcal{L}\{f(t)\} = F(s) = \int_0^{\infty} e^{-st} f(t)dt = \lim_{b\to\infty} \int_0^{b} e^{-st} f(t)dt \quad . \qquad [A.1]$$

The one-sided Laplace transform given in Equation A.1 assumes that $f(t)$ is zero for all time less than zero.

The inverse Laplace transform simply returns the original time signal [35:217]:

$$\mathcal{L}^{-1}\{F(s)\} = f(t) \quad . \qquad [A.2]$$

The inverse Laplace transform of a function may not be unique. However, if f_1 and f_2 are continuous on $[0,\infty)$ and

$$\mathcal{L}\{f_1(t)\} = \mathcal{L}\{f_2(t)\} \quad , \qquad [A.3]$$

then $f_1 = f_2$ on that interval.

Tables of Laplace transforms for many time functions can be found in any advanced mathematics text [35:inside front cover], [50:299-300]. The Laplace domain is also known as the frequency domain.

A.2 THE Z-TRANSFORM

When working with sampled-data systems, a transformation between the sampled-time domain and z-domain aids in analysis. The definition of the one-sided z-transform is given by Jury [31:2] as

$$\mathcal{Z}\{f(nT_s)\} = F(z) = \sum_{n=0}^{\infty} f(nT_s)z^{-n} \quad . \qquad [A.4]$$

Again, tables of z-transforms are available to aid in this calculation [1:inside front cover], [31:278-296], [32], [33:49-50]. The inverse z-transform gives:

$$\mathcal{Z}^{-1}\{F(z)\} = \hat{f}(nT_s) \quad . \qquad [A.5]$$

However, with the inverse z-transform one must be careful as to its interpretation. Ogata [33:69] states, "...only the time sequence at the sampling instants is obtained from the inverse z-transform. Thus, the inverse z-transform of $X(z)$ yields a unique $x(k)$, but

does not yield a unique $x(t)$." Hence, the "hat" notation on $\hat{f}(nT_s)$—a reminder that it represents any one of an infinite number of continuous time functions, $f(t)$, with equivalent values at the sample instants.

Since both the s- and z-transformations are representations of a function of time one may question whether there is any relation between the two. Indeed, there is. Franklin, Powell, and Workman [1:127] explain that the discrete system can be found from the continuous system by mapping the s-plane poles into the z-plane using the relation

$$z = e^{sT_s} \quad . \qquad \text{[A.6]}$$

One must be careful not to map zeros using this same relationship, as the result is incorrect. To map a system with poles and zeros, one must use the partial fraction expansion of the system, expanding the ratio of polynomials associated with the pole-zero form into pole-residue form. Since the poles found in either the pole-residue form or the pole-zero form are identical, they map correctly either way. The zeros, however, do not. This will be further explored as the theory for this research effort is developed.

A.3 NATURAL LOGARITHM OF A COMPLEX NUMBER

The natural logarithm of a complex number, z, is defined as [35:962-963]

$$\ln(z) = \ln|z| + j(\theta + 2n\pi) \qquad n = 0, \pm 1, \pm 2, \ldots \ , \qquad [A.7]$$

where θ is the argument of z [35:937]:

$$\theta = \arg(z) = \tan^{-1}\left(\frac{y}{x}\right) \ , \qquad [A.8]$$

given that

$$z = x + jy \ . \qquad [A.9]$$

Because of the nature of the tangent function, the principal value of the argument of z is defined to lie in the interval $(-\pi, \pi]$.

A.4 Root Loci

Given a system or plant, $G_p(s)$, the plot of the locus of its closed-loop pole locations in the s-plane as a parameter K changes gives what is known as the *root locus* of the system. It is the graph of all possible roots, assuming single-loop negative feedback of a system, of

$$1+KG_c(s)G_p(s)=0 \qquad \text{[A.10]}$$

as K changes [51:244-246]. Here the gain K is shown as the varying parameter, and $G_c(s)$ is the continuous controller. The root locus can be used to design feedback characteristics of a system in either the continuous or discrete domains. The equation for a discrete domain root locus is given [1:227-234] as

$$1+KG_c(z)G_p(z)=0, \qquad \text{[A.11]}$$

where $G_c(z)$ is the discrete or digital controller and $G_p(z)$ is the discrete representation of the plant. Again, K, here a proportional gain, is the parameter of interest that will be varied to develop the root locus plot.

Stability in the continuous domain corresponds to pole locations located in the left-half of the s-plane ($s \leq 0$), with the jω axis being the stability boundary. In the discrete (or digital) domain the unit circle, $|z| \leq 1$, is the stability boundary. Discrete roots located within the unit circle indicate a stable system.

A.5 FREQUENCY RESPONSE FUNCTIONS

The frequency response function (FRF) is another means of observing characteristics of dynamic systems. Given a system, $G_p(s)$, the FRF consists of a magnitude and phase, often plotted in Bode form, where the magnitude is found by

$$\begin{aligned} magnitude &= \left|G_p(s)\right|_{s=j\omega} = \left|G_p(j\omega)\right| \\ &= \sqrt{\{\mathrm{Re}[G_p(j\omega)]\}^2 + \{\mathrm{Im}[G_p(j\omega)]\}^2} \end{aligned} \quad , \qquad [A.12]$$

and the phase is found by

$$phase = \angle G_p(j\omega) = \tan^{-1}\left\{\frac{\mathrm{Im}[G_p(j\omega)]}{\mathrm{Re}[G_p(j\omega)]}\right\} \quad . \qquad [A.13]$$

By plotting the open-loop FRF, $G_p(s)$, with s taking on values of $j\omega$ we are basically determining the stability of the closed-loop system, since the $j\omega$ axis is the stability boundary. Two measures of stability come from the FRF—the gain and the phase margins.

The gain margin (GM) is that factor by which the gain can be increased before instability occurs [51:375]. It is found from the FRF magnitude plot by measuring the distance from the $|KG(j\omega)|$ curve and the $|KG(j\omega)|=1$ line at the frequency where $\angle G(j\omega)=-180°$ on the FRF phase plot. For stability, GM must be greater than one. The phase margin (PM) is the amount by which the phase of $G(j\omega)$ at $|KG(j\omega)|=1$ exceeds $-180°$. For stability, PM must be positive.

A.6 SAMPLING

Kuo [7:16-19] defines an ideal sampler as one in which the sampling duration is very much smaller than both the sampling period and the largest time constant of the input signal. The output of this ideal sampler is written as

$$f^*(t)=\sum_{k=0}^{\infty} f(kT_s)\delta(t-kT_s) \qquad \text{[A.14]}$$

where $f(t)$ is the input signal, T_s is the sample period, and δ is the Dirac delta function. The notation of an asterisk (*) will denote a sampled (or discrete) version of a continuous signal.

Equation A.14, the equation of a sampled signal, is just that—a mathematical model of the real system. Ogata [33:153] explains that by assuming a zero-time duration of the real sampler pulse, one can assume that the sequence of pulses output from the sampler becomes a sequence of impulses with strengths equal to the continuous-time signal at the sampling instants. This assumption, then, allows for the simple analysis of discrete-time systems. The assumption is valid if the sampling duration is very small in comparison to the time between samples and if some sort of hold is connected to the output of the sampler to drive a continuous plant with a sampled signal.

Several properties of the sampled signal, $f^*(t)$, become apparent. It is a unique function. However, because it is unique, that does not mean the function $f(t)$ sampled to produce $f^*(t)$ is unique. Any number of functions may produce $f^*(t)$, given they all equal $f^*(t)$ at the sample instants. The function $f^*(t)$ is identically equal to zero between the sample times and equal to impulses at the sample times. As such, it is a discrete representation of a continuous function, but can also be thought of as a continuous function. It is also an impulse modulator—sampling $f^*(t)$ gives simply

$f^*(t)$, which means that it is also one of the infinite continuous functions we could sample to generate $f^*(t)$.

Taking the Laplace transform of Equation A.14 gives

$$F^*(s) = \mathcal{L}\{f^*(t)\} = \sum_{k=0}^{\infty} f(kT_s)e^{-ksT_s} \quad , \qquad \text{[A.15]}$$

or alternatively,

$$F^*(s) = \frac{1}{T_s}\sum_{n=-\infty}^{\infty} F(s + jn\omega_s) \quad . \qquad \text{[A.16]}$$

The function $F^*(s)$ can be thought of as the sampled version of $F(s)$, the Laplace transform of $f(t)$. Kuo [7:22-23] and Ragazzini & Zadeh [32] define several important properties of $F^*(s)$:

1. From Equation A.16 it is easy to see that $F^*(s)$ is a periodic function with period $j\omega_s$:

$$F^*(s + jm\omega_s) = F^*(s) \quad ; \quad m \text{ integer}. \qquad \text{[A.17]}$$

Because $f^*(t)$ is sampled in time, $F^*(s)$ becomes periodic in frequency.

2. It then follows that because $F^*(s)$ is periodic, if $F^*(s)$ has a pole or a zero at $s = s_1$, then $F^*(s)$ has poles or zeros at $s = s_1 + jm\omega_s$; m integer from $-\infty$ to $+\infty$.

3. $F(s) = G(s)R^*(s)$ implies $F^*(s) = G^*(s)R^*(s)$, or mathematically:

$$[G(s)R^*(s)]^* = G^*(s)R^*(s) \quad . \qquad \text{[A.18]}$$

In other words, because $F^*(s)$ is already periodic, shifting it an integral number of periods leaves it unchanged, or sampling a sampled signal results in the same sampled signal as described above.

Taking the z-transform of Equation A.14 gives [31:2]

$$F^*(z) = \mathcal{Z}\{f^*(t)\} = \sum_{k=0}^{\infty} f(kT_s)z^{-k} \quad . \qquad \text{[A.19]}$$

Notice the similarity of Equation A.19 to Equation A.15. Indeed, as before mentioned, the Laplace transform of $f^*(t)$ is the same as the z-transform of $f^*(t)$ given that

$$z = e^{sT_s} \quad . \qquad [A.20]$$

Because of this, the mapping of $F(z)$ to $F^*(s)$ is unique, while the mapping of $F(z)$ to $F(s)$ is not. This unique form of $F^*(s)$, then, is the form we will use in our design process.

One important aspect of sampling comes from Shannon [1] [52]. Shannon states that if a signal contains no frequency content above a certain frequency, say f_N, then that signal can be completely characterized following sampling only if the sampling frequency, f_s, is greater than twice the greatest frequency contained in the signal. In other words,

$$f_s > 2f_N \quad . \qquad [A.21]$$

An example of the effects of sampling follows for a second order system with a natural frequency $\omega_n = 100$ rad/sec and a damping ratio $\xi = 0.01$. For purposes of this example, a sampling rate of $\omega_2 = 200$ rad/sec was selected. Notice, however, that by so selecting the sample rate, Shannon's criterion for sampling was not met. The effects of sampling are shown well in the frequency response function of Figure A.1. If a signal is sampled at

a rate lower than that defined by Shannon, a phenomenon known as aliasing occurs. The phenomenon is indeed observable in Figure A.1.

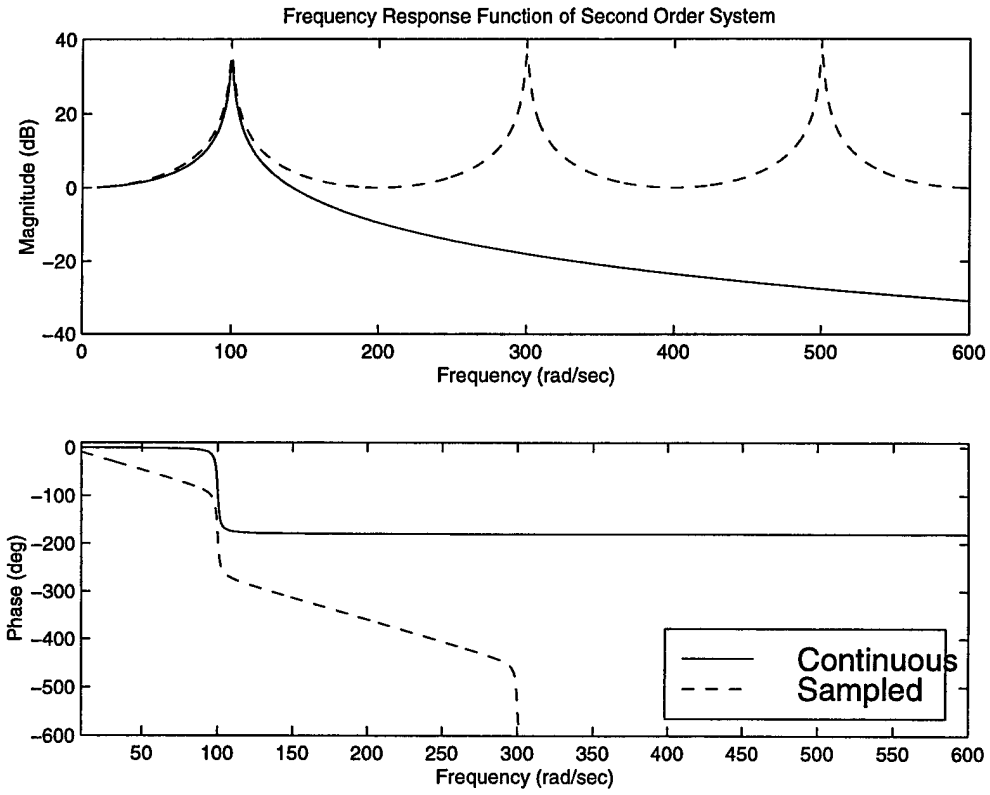

Figure A.1 The Effects of Sampling on a Second-Order System

A.7 THE ZERO-ORDER HOLD (ZOH)

Following any digital controller, the output signal must be converted to a continuous signal for input to the continuous plant. This is accomplished in the digital-to-analog converter (DAC). The DAC converts the binary output of the controller to an analog voltage. Since the output consists of values at discrete times, a method for "holding" the analog value from one discrete time to the next must be incorporated. The most common means of accomplishing this is through the Zero-Order-Hold (ZOH).

The ideal ZOH simply holds the converted output voltage constant from one time step to the next. In effect, then, the ZOH converts the series of binary impulses from the controller into a series of rectangular voltage pulses. These pulses have a height equal to the value of the binary output and a width equal to the sample period.

Assuming the binary impulse input to the ZOH is a unit impulse, the impulse response for the ZOH is given by

$$zoh(t) = u(t) - u(t - T_s) \quad , \qquad \text{[A.22]}$$

where $u(t)$ is the unit step function and T_s is the sample period. Taking the Laplace transform of Equation A.22 gives

$$ZOH(s) = \frac{1 - e^{-sT_s}}{s} \quad . \qquad [A.23]$$

Letting $s = j\omega$, and after some mathematical manipulation [1:165-166] or [7:28], we have

$$ZOH(j\omega) = T_s \operatorname{sinc}\left(\frac{\omega T_s}{2}\right) e^{-j\frac{\omega T_s}{2}} \quad , \qquad [A.24]$$

where the sinc function is defined by

$$\operatorname{sinc}(x) = \frac{\sin(x)}{x} \quad . \qquad [A.25]$$

Examination of Equation A.24 shows the ZOH effectively introduces a phase shift of $\frac{\omega T_s}{2}$ and a change in magnitude equal to $T_s \operatorname{sinc}\left(\frac{\omega T_s}{2}\right)$. Plotting the ZOH, as in Figure A.2, also shows this.

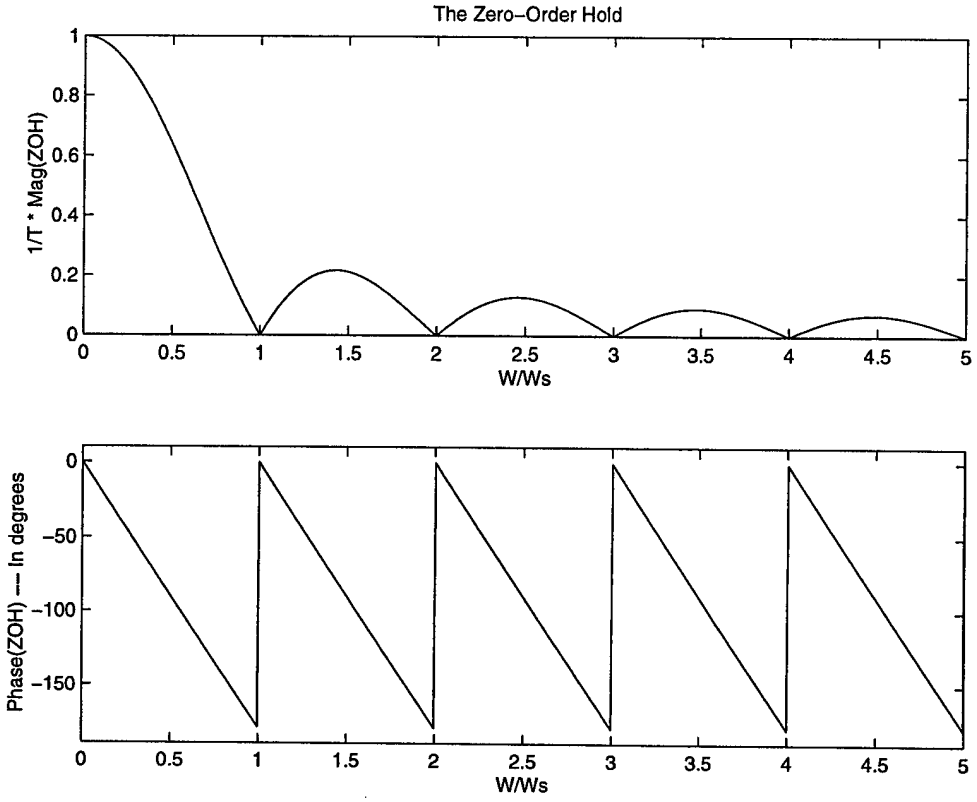

Figure A.2 The Zero-Order Hold

To show the effect of the ZOH applied to a signal, the lightly damped system from above (ω_n = 100 rad/sec, ξ = 0.01) is pre-multiplied by a ZOH. The sampling frequency is set to twice the natural frequency. The results are shown below in Figure A.3.

One thing to notice in Figure A.3 is the wrapping of the phase. This will be the case in many of the plots to follow, as it aids in a scale for the phase plots which allows closer examination of the phase relationships.

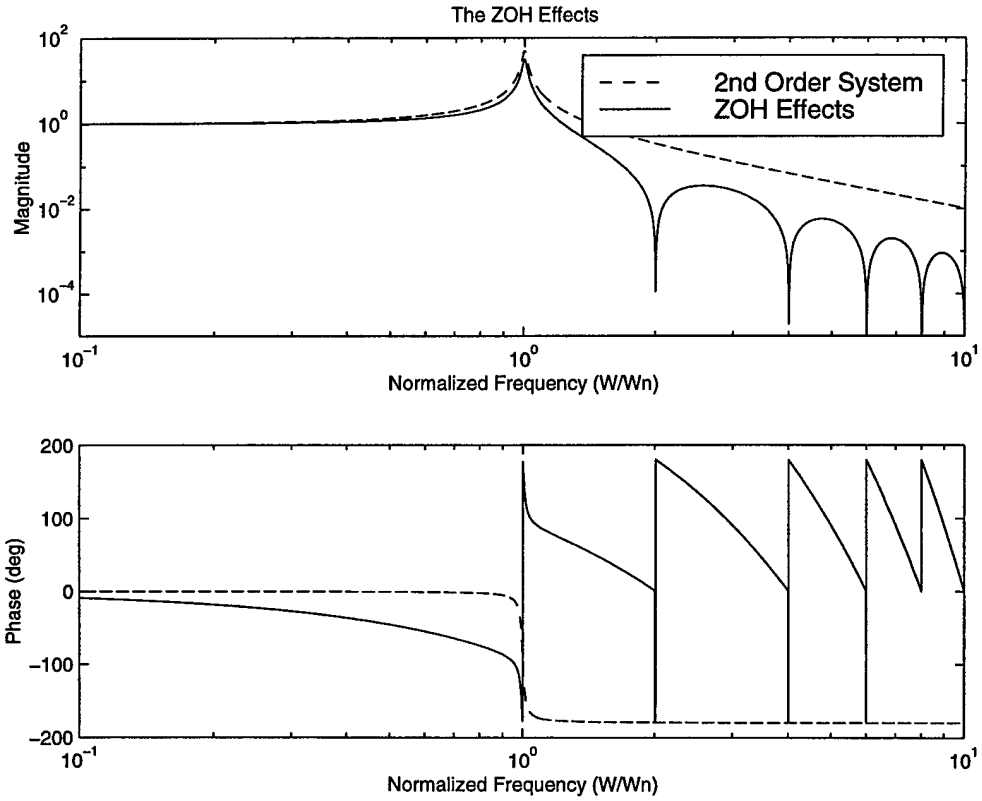

Figure A.3 Zero-Order Hold Effects on Second-Order System

A.8 APPENDIX A SUMMARY

Here, the equations for the Laplace- and Z-transforms and the natural logarithm of a complex number were introduced and reviewed. The concepts of root loci and frequency

response function plots were discussed. The definition of an ideal sampler and its mathematical model was given, and the effects of sampling were examined. Finally, the zero-order hold and its effect on a continuous system were reviewed. These results are used extensively in the development of this research.

APPENDIX B. SECOND-ORDER MODEL IMPLEMENTATION USING MATLAB (M-FILE)

```
% m101st.m -- m-file to examine design of 2nd-order discrete-to-
%  continuous system of the form:
%
%                          1
%     Gp(s) =     ---------------- ,
%                 (s + p1)(s + p2)
%
%  with proportional/integral control
%
%                     z      Kp(z - 1) + Ki*z   K*z - Kp
%  Gc(z) = Kp + Ki*-----  = ---------------- = -------- ,
%                  z - 1         z - 1            z - 1
%
%  where
%
%     K = Kp + Ki .
%
% This will plot z-plane and s*-plane root loci, bode plot, impulse and
%  step responses, and response to sine-wave inputs at two different
%  frequencies...
%
% David S. Hansen, 20 April 2000

clear all

% User defined parameters
wn = 1;                                 % natural frequency
zeta = 0.1;                             % damping ratio
wd = wn*sqrt(1 - zeta^2);               % damped natural frequency
p1 = wn*(zeta - sqrt(zeta^2 - 1));      % plant poles
p2 = conj(p1);
Kp = 0.5;                               % proportional gain
Ki = 0;                                 % Integral gain
K = Kp + Ki;
FR = 2/4;                               % frequency ratio (equal sampling
                                        %  freq. over damped nat. freq.)
ws = FR*wd;                                                % sample
frequency
Ts = (2*pi)/ws;                         % sample time
maxtime = 150;                          % Maximum time of simulation
```

```
isteps1 = 40;                          % Number of intermediate steps
                                       %  between each sample times
isteps2 = 40;
stepsize = .05;                        % size of step for root locus calcs.


% *** Plot roots and poles in both z- and s*-planes for defined Kp ***
% ====================================================================
% Find zeros and poles of H(s) = ZOH(s)*Gp(s)
pole1c = -p1;              % from Gp
pole2c = -p2;
pole3c = 0;                % from ZOH

% Using partial fraction expansion, Gp(s)/s is
%
%  Gp(s)    a0      a1        a2
%  ----- = -- + ------ + ------
%    s       s    s + p1    s + p2
%
%  where a0, a1, and a2 are:
a0 = 1/(p1*p2);
a1 = 1/(p1*(p1-p2));
a2 = -1/(p2*(p1-p2));

% Taking z-transform of H(s) gives
%
%            c1*z + c2
% H(z) = ----------------
%         (z + b1)(z + b2)
%
%  where b1, b2, c1 and c2 are:
b1 = -exp(-p1*Ts);
b2 = -exp(-p2*Ts);
c1 = real(wn^2*(a0 - a1*b1 - a2*b2));
c2 = real(wn^2*(a0*b1*b2 - a1*b2 - a2*b1));

% Continuous zeros and poles "in" z-domain:
pole1d = exp(pole1c*Ts);% plant poles from both H(z) and H(s) -> z-plane
pole2d = exp(pole2c*Ts);
zero1d = 0;                % plant zeros (2) from H(s) -> z-plane
zero2d = -c2/c1;           % plant zero from H(z)
pole3d = 1;                % ZOH pole and zero
zero3d = 1;

% Recall,
%
%              (Gcnum)(Hden)                    (K*z - Kp)(z + b1)(z + b2)
% F(z) = ------------------------------  =  ------------------------
%        (Gcnum)(Hnum) + (Gcden)(Hden)       z^3 + d1*z^2 + d2*z + d3
%
%  where
d1 = K*c1 + b1 + b2 - 1;
d2 = K*c2 - Kp*c1 + b1*b2 - b1 - b2;
d3 = -Kp*c2 - b1*b2;
```

```
poles = roots([1 d1 d2 d3]);

% Now find values for specified gains...
zero1z = -Kp/K;                          % Controller zero
zero2z = -b1;                            % Hden zeros
zero3z = -b2;
pole1z = poles(1);                       % F(z) poles
pole2z = poles(2);
pole3z = poles(3);

% Now transform to s*-plane and repeat
z1s = 1/Ts*log(zero1z);                  % Gc(z) zero
z2s = 1/Ts*log(zero2z);                  % Zeros from Hden(z)
z3s = 1/Ts*log(zero3z);
z4s = 1/Ts*log(zero2d);                  % H(z)zero
p1s = 1/Ts*log(pole1z);                  % F(z) poles
p2s = 1/Ts*log(pole2z);
p3s = 1/Ts*log(pole3z);
for loop = 1:5
   zero1s(loop) = z1s + (loop - 3)*j*ws;  % combined zeros
   zero2s(loop) = z2s + (loop - 3)*j*ws;
   zero3s(loop) = z3s + (loop - 3)*j*ws;
   zero4s(loop) = z4s + (loop - 3)*j*ws;  % "discrete" zero
   pole1s(loop) = p1s + (loop - 3)*j*ws;  % combined poles
   pole2s(loop) = p2s + (loop - 3)*j*ws;
   pole3s(loop) = p3s + (loop - 3)*j*ws;
   zero1c(loop) = j*(loop - 3)*ws;        % zeros from ZOH(s)
end

% Plot results
figure(1); clf;
% z-domain root locus
subplot(221); hold on;
plot(real(pole1d),imag(pole1d),'*');     % "continuous" poles
plot(real(pole2d),imag(pole2d),'*');
plot(real(zero1d),imag(zero1d),'s');     % "continuous" zeros
plot(real(zero2d),imag(zero2d),'d');     % discrete zero
plot(real(zero3d),imag(zero3d),'^');     % zoh zero
plot(real(pole3d),imag(pole3d),'+');     % zoh pole
plot(real(pole1z),imag(pole1z),'x');     % combined poles
plot(real(pole2z),imag(pole2z),'x');
plot(real(pole3z),imag(pole3z),'x');
plot(real(zero1z),imag(zero1z),'o');     % combined zeros
plot(real(zero2z),imag(zero2z),'o');
plot(real(zero3z),imag(zero3z),'o');
hold off; zgrid; axis square; axis([-1.1 1.1 -1.1 1.1]);
phrase = ['Z-Plane Root Locus; FR = ',num2str(FR),
      '; Kp = ',num2str(Kp),'; Ki = ',num2str(Ki)];
title(phrase)

% s*-domain root locus
vect1 = [-1.5 1];                        % vectors for plotting axes and
strip boundaries
vect2 = [-5*ws/2 -5*ws/2];
vect3 = [-3*ws/2 -3*ws/2];
```

```
vect4 = [-ws/2 -ws/2];
vect5 = [0 0];
vect6 = [-2.5 2.5];
subplot(223); hold on;
plot(real(pole1c),imag(pole1c),'*');      % plant poles
plot(real(pole2c),imag(pole2c),'*');
plot(real(pole3c),imag(pole3c),'+');      % zoh pole
for loop = 1:5
   plot(real(pole1s(loop)),imag(pole1s(loop)),'x');   % combined poles
   plot(real(pole2s(loop)),imag(pole2s(loop)),'x');
   plot(real(pole3s(loop)),imag(pole3s(loop)),'x');
   plot(real(zero1s(loop)),imag(zero1s(loop)),'o');   % combined zeros
   plot(real(zero2s(loop)),imag(zero2s(loop)),'o');
   plot(real(zero3s(loop)),imag(zero3s(loop)),'o');
   plot(real(zero4s(loop)),imag(zero4s(loop)),'d');   % "discrete" zeros
   plot(real(zero1c(loop)),imag(zero1c(loop)),'^');   % zoh zeros
end
plot(vect1,vect5,':'); plot(vect5,vect6,':');
plot(vect1,vect2,'--'); plot(vect1,vect3,'--');
plot(vect1,vect4,'--'); plot(vect1,-vect2,'--');
plot(vect1,-vect3,'--'); plot(vect1,-vect4,'--');
hold off; axis([-1.5 1 -2.5 2.5]);
phrase = ['S*-Plane Root Locus; FR = ',num2str(FR),
      '; Kp = ',num2str(Kp),'; Ki = ',num2str(Ki)];
title(phrase)


% *** Plot System Bode Plot for defined Ki ***
% ============================================
numpoints = 2000;              % Number of frequency points for FRF
num = wn^2;
den = [1 p1+p2 p1*p2];
Gps = tf(num,den);             % Continuous plant
Hz = c2d(Gps,Ts,'zoh');        % H*(z): Sampled Plant with ZOH
w = linspace(0.001,50,numpoints);   % Linearly spaced frequency vector
normw = w./wd;                 % Normalized frequency vector for plotting

% Porportional/Integral Controller
Gcznum = [K -Kp];
Gczden = [1 -1];
Gcz = tf(Gcznum,Gczden,Ts);
[magGcz,phsGcz] = bode(Gcz,w);
magGcz = reshape(magGcz,1,numpoints);
phsGcz = reshape(phsGcz,1,numpoints);
phsGcz = phsGcz*pi/180;        % Convert phase from degrees to radians.

% Continuous System
[magGps,phsGps] = bode(Gps,w);
magGps = reshape(magGps,1,numpoints);
phsGps = reshape(phsGps,1,numpoints);
phsGps = phsGps*pi/180;        % Convert phase from degrees to radians.

% Discrete System
[magHz,phsHz] = bode(Hz,w);
magHz = reshape(magHz,1,numpoints);
```

```
phsHz = reshape(phsHz,1,numpoints);
phsHz = phsHz*pi/180;          % Convert phase from degrees to radians.

% Calculate magnitude and phase at discrete frequency points
for loop = 1:numpoints
      ZOH = (1-exp(-j*w(loop)*Ts))/(j*w(loop)*Ts);
   Gps1 = magGps(loop)*exp(j*phsGps(loop));
   Gcz1 = magGcz(loop)*exp(j*phsGcz(loop));
      Hpz = magHz(loop)*exp(j*phsHz(loop));
      numcl = Gcz1*ZOH*Gps1;
      dencl = 1 + (Gcz1*Hpz);
      cltf(loop) = numcl/dencl;
end

magFRF = 20*log10(abs(cltf));        % Magnitude (in dB) of FRF
phsFRF = angle(cltf)*180/pi;         % Phase (in degrees) of FRF
a = max(magFRF);
plotmax = a + 5;
plotmin = plotmax - 100;
subplot(222);
plot(normw,magFRF); grid;
phrase = ['Frequency Ratio Ws/Wd = ',num2str(FR),
      '; Kp = ',num2str(Kp),'; Ki = ',num2str(Ki)];
title(phrase);
xlabel('Normalized Frequency (W/Wd)');
ylabel('Magnitude (dB)');
axis([0 4.5 plotmin plotmax]);
subplot(224);
plot(normw,phsFRF); grid;
axis([0 4.5 -190 190]);
xlabel('Normalized Frequency (W/Wd)');
ylabel('Phase (deg)');


% *** Plot Impulse Response for defined Ki ***
% ============================================
Tn = Ts/isteps1;                     % Intermediate time steps
[F,G,H,J] = tf2ss(num,den);
[phi,gamma] = c2d(F,G,Tn);           % Continuous approximation in
                                     %  discrete domain

% Define initial conditions
x = [0;0]; uthen = 0; errorthen = 0;
tcon = 0; ycon = 0;
tdis = 0; ydis(1) = 0;

% Step through calculations for "maxtime" seconds
for count1 = 0:round(maxtime/Ts);
   % Define unit impulse:
   if count1 == 0
      r = 1;
   else
      r = 0;
   end
   errornow = r - ydis(count1 + 1);
```

```
    u = uthen + K*errornow - Kp*errorthen;        % Control effort

    % Calculate continuous output
       for count2 = 1:isteps1;
             tcon = [tcon;(count1*isteps1 + count2)*Tn];
             x = phi*x + gamma*u;
          ycon = [ycon;(H*x + J*u)];
    end
       index = isteps1*(count1 + 1) + 1;
       tdis = [tdis;tcon(index)];
    ydis = [ydis;ycon(index)];
    uthen = u;
    errorthen = errornow;
end

% Plot Results
a = max(ycon);
b = min(ycon);
plotmax = a + 0.2*a;
plotmin = b + 0.2*b;
figure(2); clf;
subplot(221);
plot(tcon./Ts,ycon,'-',tdis./Ts,ydis,'r--',tdis./Ts,ydis,'r*'); grid;
xlabel('Normalized Time (t/Ts)'); ylabel('Response');
axis([0 maxtime/Ts plotmin plotmax]);
phrase = ['Impulse Response at Ws/Wd = ',num2str(FR),
      '; Kp = ',num2str(Kp),'; Ki = ',num2str(Ki)];
title(phrase);


% *** Plot Step Response for defined Kp ***
% ========================================
clear x uthen tcon ycon tdis ydis
% Define initial conditions
x = [0;0]; uthen = 0; errorthen = 0;
tcon = 0; ycon = 0;
tdis = 0; ydis(1) = 0;
r = 1;            % Unit step

% Step through calculations for "maxtime" seconds
for count1 = 0:round(maxtime/Ts);
   errornow = r - ydis(count1 + 1);
   u = uthen + K*errornow - Kp*errorthen;        % Control effort

   % Calculate continuous output
      for count2 = 1:isteps1;
            tcon = [tcon;(count1*isteps1 + count2)*Tn];
            x = phi*x + gamma*u;
         ycon = [ycon;(H*x + J*u)];
   end
      index = isteps1*(count1 + 1) + 1;
      tdis = [tdis;tcon(index)];
   ydis = [ydis;ycon(index)];
   uthen = u;
   errorthen = errornow;
```

```
end

% Plot Results
a = max(ycon);
b = min(ycon);
plotmax = a + 0.2*a;
plotmin = b + 0.2*b;
subplot(223);
plot(tcon./Ts,ycon,'-',tdis./Ts,ydis,'r--',tdis./Ts,ydis,'r*'); grid;
xlabel('Normalized Time (t/Ts)'); ylabel('Response');
axis([0 maxtime/Ts plotmin plotmax]);
phrase = ['Step Response at Ws/Wd = ',num2str(FR)
      ,'; Kp = ',num2str(Kp),'; Ki = ',num2str(Ki)];
title(phrase);


% *** Plot time response for sine-wave input ***
% ==============================================
clear x uthen tcon ycon tdis ydis
ww = 0.05;                              % Input sine wave frequency
maxtime = 200;                          % Maximum time for simulation (in
seconds)
Tn = Ts/isteps2;                        % Intermediate time steps

% 2nd-Order State-space System paramters
[phi,gamma] = c2d(F,G,Tn);              % Continuous approximation in
                                        %  discrete domain

% Define initial conditions
x = [0;0]; uthen = 0; errothen = 0;
tcon = 0; ycon = 0;
tdis(1) = 0; ydis(1) = 0;
index = 0; index1 = 0;

% Step through calculations until "maxtime" seconds
for count1 = 0:round(maxtime/Ts);
   % Define sinusoidal input and control as a result...
   time = count1*Ts;
   r = sin(ww*time);
   errornow = r - ydis(count1 + 1);
   u = uthen + K*errornow - Kp*errorthen;

      % Calculate continuous output
   for count2 = 1:isteps2
      index1 = index1 + 1;
      t(index1) = (count1*isteps2 + count2)*Tn;
      y(index1) = sin(ww*t(index1));
            tcon = [tcon;(count1*isteps2 + count2)*Tn];
            x = phi*x + gamma*u;
            ycon = [ycon;(H*x + J*u)];
      end
      index = isteps2*(count1 + 1) + 1;
      tdis = [tdis;tcon(index)];
   ydis = [ydis;ycon(index)];
   uthen = u;
```

```
   errothen = errornow;
end

% Plot Time Response
a = max(ycon);
b = min(ycon);
if a > 1
   plotmax = a + 0.2*a;
else
   plotmax = 1;
end
if b < -1
   plotmin = b + 0.2*b;
else
   plotmin = -1;
end
subplot(222); grid;
plot(tcon./Ts,ycon,'-',tdis./Ts,ydis,'*',t./Ts,y,'--');
xlabel('Normalized Time (t/Ts)'); ylabel('Response');
phrase = ['Response to sin(',num2str(ww),'*t) input; FR = ',
      num2str(FR),'; Kp = ',num2str(Kp),'; Ki = ',num2str(Ki)];
title(phrase);
axis([0 maxtime/Ts plotmin plotmax]);

clear x uthen tcon ycon tdis ydis
ww = 0.09;                                    % Input sine wave frequency

% Define initial conditions
x = [0;0]; uthen = 0; errorthen = 0;
tcon = 0; ycon = 0;
tdis = 0; ydis(1) = 0;
index = 0; index1 = 0;
% Step through calculations until "maxtime" seconds
for count1 = 0:round(maxtime/Ts);
   % Define sinusoidal input and control as a result...
   time = count1*Ts;
   r = sin(ww*time);
   errornow = r - ydis(count1 + 1);
   u = uthen + K*errornow - Kp*errorthen;

      % Calculate continuous output
   for count2 = 1:isteps2
      index1 = index1 + 1;
      t(index1) = (count1*isteps2 + count2)*Tn;
      y(index1) = sin(ww*t(index1));
      tcon = [tcon;(count1*isteps2 + count2)*Tn];
            x = phi*x + gamma*u;
            ycon = [ycon;(H*x + J*u)];
      end
      index = isteps2*(count1 + 1) + 1;
      tdis = [tdis;tcon(index)];
   ydis = [ydis;ycon(index)];
   uthen = u;
   errorthen = errornow;
end
```

```
% Plot Time Response
a = max(ycon);
b = min(ycon);
if a > 1
   plotmax = a + 0.2*a;
else
   plotmax = 1;
end
if b < -1
   plotmin = b + 0.2*b;
else
   plotmin = -1;
end
subplot(224); grid;
plot(tcon./Ts,ycon,'-',tdis./Ts,ydis,'*',t./Ts,y,'--');
xlabel('Normalized Time (t/Ts)'); ylabel('Response');
phrase = ['Response to sin(',num2str(ww),'*t) input; FR = ',
      num2str(FR),'; Kp = ',num2str(Kp),'; Ki = ',num2str(Ki)];
title(phrase);
axis([0 maxtime/Ts plotmin plotmax]);
```

APPENDIX C. FOURTH-ORDER MODEL IMPLEMENTATION USING MATLAB (M-FILE)

```
% fourth.m -- m-file to examine design of a 4th-order system of the
%  form:
%
%                                Kg
%     Gp(s) =      -------------------------
%                  (s+p1)(s+p2)(s+p3)(s+p4)
%
%
%           =                          K*wn1^2*wn2^2
%                  ------------------------------------------------  ,
%                  (s^2+2*zeta1*wn1*s+wn1^2)(s^2+2*zeta2*wn2*s+wn2^2)
%
%  with PID control
%
%                    z-1        z
%  Gc(z) = Kp + Kd*--- + Ki*---.
%                     z        z-1
%
% This will plot z-plane and s*-plane root loci, bode plots, and impulse
%  and step responses
%
% David S. Hansen, 17 May 2000

clear all;

% User-defined parameters
Kp = 0.7;                       % Proportional gain
Kd = 1.4;                       % Derivative gain
Ki = 0.6;                       % Integral gain
K1 = Kp + Kd + Ki;
K2 = -Kp - 2*Kd;
FR = 1;                         % Frequency ratio (ws/wd)
K = 1.0;                        % System gain
maxtime = 15;                   % maximum time for simulations
isteps1 = 100;

% Non-aliased mode
wn1 = 1.0;
zeta1 = 0.5;
p1 = wn1*(zeta1-sqrt(zeta1^2-1));
```

```
p2 = conj(p1);
wd1 = wn1*sqrt(1-zeta1^2);

% Aliased mode
wn2 = 10;
zeta2 = 0.01;
p3 = wn2*(zeta2-sqrt(zeta2^2-1));
p4 = conj(p3);
wd2 = wn2*sqrt(1-zeta2^2);

Kg = K*wn1^2*wn2^2;

% Sampling Parameters
ws = FR*wd2;
Ts = (2*pi)/ws;


% *** Plot Root Loci ***
% ======================

% Continuous Plant Poles
pole1c = -p1;
pole2c = -p2;
pole3c = -p3;
pole4c = -p4;

% Expand Gp(s)/s using partial fractions
%
%     Gp(s)   a0    a1     a2     a3     a4
%     ----- = -- + ---- + ---- + ---- + ----   (all multiplied by Kg)
%       s     s    s+p1   s+p2   s+p3   s+p4
%
%     where the constants are defined below...

p5 = (p1*p2)+(p1*p3)+(p1*p4)+(p2*p3)+(p2*p4)+(p3*p4);
p6 = (p2*p3)+(p2*p4)+(p3*p4);
p7 = (p1*p3)+(p1*p4)+(p3*p4);
p8 = (p1*p2)+(p1*p4)+(p2*p4);
p9 = (p1*p2)+(p1*p3)+(p2*p3);
p10 = (p1*p2*p3)+(p1*p2*p4)+(p1*p3*p4)+(p2*p3*p4);
p11 = p2*p3*p4;
p12 = p1*p3*p4;
p13 = p1*p2*p4;
p14 = p1*p2*p3;

d0 = 1/(p1*p2*p3*p4);
d1 = -d0*p1/(p1-p2);
d2 = (p3-p1)/(p1-p2);
d3 = (p4-p1)/(p1-p2);
d5 = -d0-d1;
d6 = 1+d2;
d7 = 1+d3;
d8 = (d0*p5)+(d5*p6)+(d1*p7);
d9 = (d2*p7)+p8-(d6*p6);
d10 = (d3*p7)+p9-(d7*p6);
```

```
d11 = -d8/d9;
d12 = -d10/d9;
d13 = d5-(d6*d11);
d14 = -d7-(d6*d12);
d15 = d1+(d2*d11);
d16 = d3+(d2*d12);

% ...aahh, here they are
a0 = d0;
a4 = -((d0*p10)+(d13*p11)+(d15*p12)+(d11*p13))
a4 = a4/((d14*p11)+(d16*p12)+(d12*p13)+p14);
a3 = d11+(d12*a4);
a2 = d15+(d16*a4);
a1 = d13+(d14*a4);

% Taking the z-transform of H(s)
%
%              Kg*(f3*z^3 + f2*z^2 + f1*z + f0)
%     H(z) = --------------------------------
%              (z + b1)(z + b2)(z + b3)(z + b4)
%
%     where
b1 = -exp(-p1*Ts);
b2 = -exp(-p2*Ts);
b3 = -exp(-p3*Ts);
b4 = -exp(-p4*Ts);
b5 = b1+b2+b3+b4;
b6 = (b1*b2)+(b1*b3)+(b1*b4)+(b2*b3)+(b2*b4)+(b3*b4);
b7 = (b1*b2*b3)+(b1*b2*b4)+(b1*b3*b4)+(b2*b3*b4);
b8 = b1*b2*b3*b4;

%  and
f0 = (a0*b8)-(a1*b2*b3*b4)-(a2*b1*b3*b4)-(a3*b1*b2*b4)-(a4*b1*b2*b3);
f1 = a0*b7;
f1 = f1+(a1*((b2*b3*b4)-(b2*b3)-(b2*b4)-(b3*b4)));
f1 = f1+(a2*((b1*b3*b4)-(b1*b3)-(b1*b4)-(b3*b4)));
f1 = f1+(a3*((b1*b2*b4)-(b1*b2)-(b1*b4)-(b2*b4)));
f1 = f1+(a4*((b1*b2*b3)-(b1*b2)-(b1*b3)-(b2*b3)));
f2 = a0*b6;
f2 = f2+(a1*((b2*b3)+(b2*b4)+(b3*b4)-b2-b3-b4));
f2 = f2+(a2*((b1*b3)+(b1*b4)+(b3*b4)-b1-b3-b4));
f2 = f2+(a3*((b1*b2)+(b1*b4)+(b2*b4)-b1-b2-b4));
f2 = f2+(a4*((b1*b2)+(b1*b3)+(b2*b3)-b1-b2-b3));
f3 = a0-(a1*b1)-(a2*b2)-(a3*b3)-(a4*b4);
f0 = real(f0);
f1 = real(f1);
f2 = real(f2);
f3 = real(f3);

% This causes the mixed term F(Z) to be
%
%              (K1*z^2 + K2*z + Kd)(z + b1)(z + b2)(z + b3)(z + b4)
%     F(z) = ---------------------------------------------------
%              Kg*(K1*z^2+K2*z+Kd)(f3*z^3+f2*z^2+f1*z+f0)
%                    + z(z-1)(z+b1)(z+b2)(z+b3)(z+b4)
```

```
%
% giving zeros from numerator and poles from denominator.

% Zeros of F(z)
zero1d = -b1;
zero2d = -b2;
zero3d = -b3;
zero4d = -b4;
zeros = roots([K1 K2 Kd]);
zero5d = zeros(1);
zero6d = zeros(2);

% Poles of F(z)
g1 = K1*Kg*f3+b5-1;
g2 = Kg*(K1*f2+K2*f3)+b6-b5;
g3 = Kg*(K1*f1+K2*f2+Kd*f3)+b7-b6;
g4 = Kg*(K1*f0+K2*f1+Kd*f2)+b8-b7;
g5 = Kg*(K2*f0+Kd*f1)-b8;
g6 = Kg*Kd*f0;
poles = roots([1 g1 g2 g3 g4 g5 g6]);
pole1d = poles(1);
pole2d = poles(2);
pole3d = poles(3);
pole4d = poles(4);
pole5d = poles(5);
pole6d = poles(6);

% Location of continuous zeros and poles if they were "in" the z-plane
zero1cd = 0;                          % 3-poles located at negative
infinity in s-plane...
pole1cd = exp(pole1c*Ts);             % Plant poles
pole2cd = exp(pole2c*Ts);
pole3cd = exp(pole3c*Ts);
pole4cd = exp(pole4c*Ts);

% Zero-order hold zero and pole
zero7d = 1;
pole7d = 1;

% Plot z-plane root locus
figure(1); clf;
subplot(211); hold on;
plot(real(zero1cd),imag(zero1cd),'d');          % Gp(s) zero
plot(real(pole1cd),imag(pole1cd),'+');          % Gp(s) poles
plot(real(pole2cd),imag(pole2cd),'+');
plot(real(pole3cd),imag(pole3cd),'+');
plot(real(pole4cd),imag(pole4cd),'+');
plot(real(zero1d),imag(zero1d),'o');            % F(z) zeros
plot(real(zero2d),imag(zero2d),'o');
plot(real(zero3d),imag(zero3d),'o');
plot(real(zero4d),imag(zero4d),'o');
plot(real(zero5d),imag(zero5d),'o');
plot(real(zero6d),imag(zero6d),'o');
plot(real(pole1d),imag(pole1d),'x');            % F(z) poles
plot(real(pole2d),imag(pole2d),'x');
```

```
plot(real(pole3d),imag(pole3d),'x');
plot(real(pole4d),imag(pole4d),'x');
plot(real(pole5d),imag(pole5d),'x');
plot(real(pole6d),imag(pole6d),'x');
plot(real(zero7d),imag(zero7d),'^');      % ZOH zero and pole
plot(real(pole7d),imag(pole7d),'*');
hold off; zgrid; axis square; axis([-1 1 -1 1]);
phrase = ['Z-Plane Root Locus, FR = ',num2str(FR)];
title(phrase);
phrase = ['Kp = ',num2str(Kp),'; Ki = ',num2str(Ki),';
            Kd = ',num2str(Kd)];
xlabel(phrase);



% Now convert to and plot in the s*-plane...
z1dc = 1/Ts*log(zero1d);
z2dc = 1/Ts*log(zero2d);
z3dc = 1/Ts*log(zero3d);
z4dc = 1/Ts*log(zero4d);
z5dc = 1/Ts*log(zero5d);
z6dc = 1/Ts*log(zero6d);
z7dc = 1/Ts*log(zero7d);
p1dc = 1/Ts*log(pole1d);
p2dc = 1/Ts*log(pole2d);
p3dc = 1/Ts*log(pole3d);
p4dc = 1/Ts*log(pole4d);
p5dc = 1/Ts*log(pole5d);
p6dc = 1/Ts*log(pole6d);
for loop = 1:4,
   zero1dc(loop) = z1dc + (loop - 2)*j*ws;
   zero2dc(loop) = z2dc + (loop - 2)*j*ws;
   zero3dc(loop) = z3dc + (loop - 2)*j*ws;
   zero4dc(loop) = z4dc + (loop - 2)*j*ws;
   zero5dc(loop) = z5dc + (loop - 2)*j*ws;
   zero6dc(loop) = z6dc + (loop - 2)*j*ws;
   zero7dc(loop) = z7dc + (loop - 2)*j*ws;
   pole1dc(loop) = p1dc + (loop - 2)*j*ws;
   pole2dc(loop) = p2dc + (loop - 2)*j*ws;
   pole3dc(loop) = p3dc + (loop - 2)*j*ws;
   pole4dc(loop) = p4dc + (loop - 2)*j*ws;
   pole5dc(loop) = p5dc + (loop - 2)*j*ws;
   pole6dc(loop) = p6dc + (loop - 2)*j*ws;
end;
pole7dc = 1/Ts*log(pole7d);
vect1 = [-2 2];
vect2 = [-3*ws/2 -3*ws/2];
vect3 = [-ws/2 -ws/2];
vect4 = [0 0];
subplot(212); hold on;
plot(vect1,vect4,':',vect4,[-3*ws/2 3*ws/2],':');
plot(vect1,vect2,'--',vect1,-vect2,'--');
plot(vect1,vect3,'--',vect1,-vect3,'--');
plot(real(pole1c),imag(pole1c),'+');
plot(real(pole2c),imag(pole2c),'+');
```

```
plot(real(pole3c),imag(pole3c),'+');
plot(real(pole4c),imag(pole4c),'+');
for loop = 1:4,
   plot(real(zero1dc),imag(zero1dc),'o');
   plot(real(zero2dc),imag(zero2dc),'o');
   plot(real(zero3dc),imag(zero3dc),'o');
   plot(real(zero4dc),imag(zero4dc),'o');
   plot(real(zero5dc),imag(zero5dc),'o');
   plot(real(zero6dc),imag(zero6dc),'o');
   plot(real(zero7dc),imag(zero7dc),'^');
   plot(real(pole1dc),imag(pole1dc),'x');
   plot(real(pole2dc),imag(pole2dc),'x');
   plot(real(pole3dc),imag(pole3dc),'x');
   plot(real(pole4dc),imag(pole4dc),'x');
   plot(real(pole5dc),imag(pole5dc),'x');
   plot(real(pole6dc),imag(pole6dc),'x');
end;
plot(real(pole7dc),imag(pole7dc),'*');
hold off; axis([-1.25 0.1 -3*ws/2 3*ws/2]);
title('S*-Plane Root Locus');

print -deps -tiff fig611



% *** Plot System Bode Plot for defined Kp ***
% ============================================
numpoints = 2000;              % Number of frequency points for FRF
num = K*wn1^2*wn2^2;
den1 = [1 2*zeta1*wn1 wn1^2];
den2 = [1 2*zeta2*wn2 wn2^2];
den = conv(den1,den2);

Gps = tf(num,den);             % Continuous plant
Hz = c2d(Gps,Ts,'zoh');        % H*(z): Sampled Plant with ZOH
w = linspace(0.001,50,numpoints);   % Linearly spaced frequency vector
normw = w./wd2;                % Normalized frequency vector for plotting

% PID Controller
Gcznum = [Kp+Ki+Kd -Kp-2*Kd Kd];
Gczden = [1 -1 0];
Gcz = tf(Gcznum,Gczden);
[magGcz,phsGcz] = bode(Gcz,w);
magGcz = reshape(magGcz,1,numpoints);
phsGcz = reshape(phsGcz,1,numpoints);
phsGcz = phsGcz*pi/180;        % Convert phase from degrees to radians.

% Continuous System
[magGps,phsGps] = bode(Gps,w);
magGps = reshape(magGps,1,numpoints);
phsGps = reshape(phsGps,1,numpoints);
phsGps = phsGps*pi/180;        % Convert phase from degrees to radians.

% Discrete System
[magHz,phsHz] = bode(Hz,w);
```

```
magHz = reshape(magHz,1,numpoints);
phsHz = reshape(phsHz,1,numpoints);
phsHz = phsHz*pi/180;   % Convert phase from degrees to radians.

% Calculate magnitude and phase at discrete frequency points
for count = 1:numpoints
      ZOH = (1-exp(-j*w(count)*Ts))/(j*w(count)*Ts);
   Gps1 = magGps(count)*exp(j*phsGps(count));
   Gcz1 = magGcz(count)*exp(j*phsGcz(count));
      Hpz = magHz(count)*exp(j*phsHz(count));
      numcl = Gcz1*ZOH*Gps1;
      dencl = 1 + (Gcz1*Hpz);
      cltf(count) = numcl/dencl;
end

magFRF = 20*log10(abs(cltf));       % Magnitude (in dB) of FRF
phsFRF = angle(cltf)*180/pi;        % Phase (in degrees) of FRF

a = max(magFRF);
plotmax = a + 5;
plotmin = plotmax - 160;

figure(2); clf;
subplot(211);
plot(w,magFRF); grid;
phrase = ['Kp = ',num2str(Kp),'; Ki = ',num2str(Ki),';
            Kd = ',num2str(Kd)];
title(phrase);
phrase = ['wn1 = ',num2str(wn1),'; zeta1 = ',num2str(zeta1),';
            wn2 = ',num2str(wn2),'; zeta2 = ',num2str(zeta2)];
xlabel(phrase);
ylabel('Magnitude (dB)');
axis([0 50 plotmin plotmax]);
subplot(212);
plot(w,phsFRF); grid;
axis([0 50 -190 190]);
xlabel('Frequency');
ylabel('Phase (deg)');

%print -deps -tiff fig68



[F,G,H,J]=tf2ss(num,den);

% *** Plot Impulse Response for defined Kp ***
% ============================================
Tn = Ts/isteps1;            % Intermediate time steps
[phi,gamma] = c2d(F,G,Tn); % Continuous approximation in discrete domain

% Define initial conditions
x = [0;0;0;0];
tcon = 0; ycon = 0;
tdis = 0; ydis = 0;
uthen = 0; ethen = 0; ethen2 = 0;
```

```
% Step through calculations for "maxtime" seconds
for count1 = 0:round(maxtime/Ts);
   % Define unit impulse:
   if count1 == 0
      r = 1;
   else
      r = 0;
   end
   enow = r - ydis(count1 + 1);
   u = uthen + K1*enow + K2*ethen + Kd*ethen2;  % Control effort

   % Calculate continuous output
      for count2 = 1:isteps1;
            tcon = [tcon;(count1*isteps1 + count2)*Tn];
      x = phi*x + gamma*u;
      ycon = [ycon;real(H*x + J*u)];
   end
      index = isteps1*(count1 + 1) + 1;
      tdis = [tdis;tcon(index)];
   ydis = [ydis;ycon(index)];
   % Age data
   uthen = u;
   ethen2 = ethen;
   ethen = enow;
end

a = max(ycon);
b = min(ycon);
plotmax = a + 0.2*a;
plotmin = b + 0.2*b;

% Plot Results
figure(3); clf;
subplot(211);
plot(tcon./Ts,ycon,'-',tdis./Ts,ydis,'r--',tdis./Ts,ydis,'r*'); grid;
%plot(tdis./Ts,ydis,'-');
phrase = ['wn1 = ',num2str(wn1),'; zeta1 = ',num2str(zeta1),';
          wn2 = ',num2str(wn2),'; zeta2 = ',num2str(zeta2)];
xlabel(phrase);
axis([0 maxtime/Ts plotmin plotmax]);
phrase = ['Impulse Response, FR = ',num2str(FR)];
title(phrase);


% *** Plot Step Response for defined Kp ***
% ========================================
% Define initial conditions
x = [0;0;0;0];
tcon = 0; ycon = 0;
tdis = 0; ydis = 0;
uthen = 0; ethen = 0; ethen2 = 0;

r = 1;            % Unit step
```

```
% Step through calculations for "maxtime" seconds
for count1 = 0:round(maxtime/Ts);
   enow = r - ydis(count1 + 1);
   u = uthen + K1*enow + K2*ethen + Kd*ethen2;  % Control effort

   % Calculate continuous output
      for count2 = 1:isteps1;
            tcon = [tcon;(count1*isteps1 + count2)*Tn];
      x = phi*x + gamma*u;
      ycon = [ycon;real(H*x + J*u)];
   end
      index = isteps1*(count1 + 1) + 1;
      tdis = [tdis;tcon(index)];
      ydis = [ydis;ycon(index)];
   % Age data
   uthen = u;
   ethen2 = ethen;
   ethen = enow;
end

a = max(ycon);
b = min(ycon);
plotmax = a + 0.2*a;
plotmin = b + 0.2*b;

% Plot Results
subplot(212);
plot(tcon./Ts,ycon,'-',tdis./Ts,ydis,'r--',tdis./Ts,ydis,'r*'); grid;
%plot(tdis./Ts,ydis,'-');
xlabel('Normalized Time (t/Ts)'); ylabel('Response');
axis([0 maxtime/Ts plotmin plotmax]);
phrase = ['Step Response; Kp = ',num2str(Kp),'; Ki = ',num2str(Ki),';
            Kd = ',num2str(Kd)];
title(phrase);

print -deps -tiff fig612
```